BINDING SERVICES
Tel +44 (0)29 2087 4949
Fax +44 (0)29 20371921
e-mail bindery@cardiff.ac.uk

Numerical Simulation of Cracking using Embedded Surfaces in a Three Dimensional Constitutive Model for Concrete

Siew Chang Hee

B.Eng. (Hons), M.Sc.

Thesis submitted to the University of Wales in candidature

for the degree of Doctor of Philosophy

February 2006

School of Engineering

University of Wales, Cardiff

ProQuest LLC
789 East Eisenhower Parkway
P.O. Box 1346
Ann Arbor, MI 48106-1346

Abstract

This thesis presents three new three-dimensional constitutive models for cementitious materials. All three models use embedded damage planes and adopt the theory of contact mechanics to describe the characteristic behaviour of cracks formed in concrete and other cementitious materials.

The first of these is a smooth frictional contact model which incorporates a simplified Mohr-Coulomb yield surface to capture plastic slip planes in concrete. The aim of the model is to accurately represent the behaviour of smooth construction joints in large concrete structures. The second proposed model is the dual-surface contact model. The model employs two contact surfaces, each of which nominally represents a different component of concrete composite, i.e. coarse aggregate particles and mortar.

The third model is the 'embedded planes with local plasticity contact' model (EPLPC). The model adopts a yield surface, which is similar to the damage surface in strain space, to capture plastic embedment on crack surfaces. This model, as with the dual-surface contact model, is developed to simulate crack opening-closing, as well as the behaviour of aggregate interlock. The models are integrated with a hardening/softening frictional plasticity component that uses a smoothed triaxial plastic yield surface developed from that used by Lubliner *et al.* (1989).

Each of the proposed models is implemented with a consistent tangent stiffness operator and return mapping algorithm, similar to that of the Closest Point Projection algorithm. The models are coded in Fortran77 and implemented in a constitutive driver program, and also a finite element software package LUSAS.

The models are assessed using a series of stress/strain paths at the constitutive level, and also validated against a range of experimental data. These include data from uniaxial and multiaxial compressive tests, uniaxial tensile tests with and without unloading-reloading cycles, and also tests in which shear load is applied on open cracks.

Acknowledgements

I would first like to thank my supervisors Dr. Tony Jefferson and Prof. Bhushan Karihaloo for giving me this opportunity to carry out this research, and for their invaluable help, support and guidance throughout the duration of this study.

My special thanks also go to Dr. Terry Bennett for providing guidance and advice in my research works.

I would also like to express my sincere gratitude and appreciation to the Overseas Research Students Awards Scheme and the Engineering department of Cardiff University for the financial support provided.

I would like to extend my thanks to my family, friends and colleagues for their encouragement and moral support throughout my academic development.

Last but not least, I would like to thank my parents for their tremendous love and support throughout my life. Without you, this would not have been possible and I thank you from the bottom of my heart.

Contents

Notation

a	yield surface shape parameter
a_c	hardening/softening curve parameter
a_c, a_t	model parameter for damage criterion in compression and tension (Chapter 2)
a_m	continuous softening curve parameter
a_p	parameter in the softening function to control the level of damage
a_t	proportion of peak tensile strength at which damage starts
a_κ	defined in equation (4.34)
a_κ	defined in equation (5.41)
a_κ	defined in equation (7.26)
A	undamaged cross-sectional area
$\boldsymbol{A}$	defined in equation (4.42)
$\boldsymbol{A}$	defined in equation (5.49)
$\boldsymbol{A}_c$	defined in equation (6.17)
$\boldsymbol{A}_{c\Delta}$	defined in equation (4.51)
$\boldsymbol{A}_{c\Delta}$	defined in equation (5.58)
$\boldsymbol{A}_{c\Delta}$	defined in equation (6.38)
$\boldsymbol{A}_{c\Delta}$	defined in equation (7.48)
A_d	total area of microcracks
$\boldsymbol{A}_e$	defined in equation (7.37)
A_r	smoothing function
$\overline{a}$	standard nodal degrees of freedom
$\overline{A}$	effective cross-sectional area
$\widetilde{a}_{ij}$	additional degrees of freedom associated with node i and enrichment function j
b_c, b_t	model parameter for damage criterion in compression and tension
b_m	continuous softening curve parameter
b_r	biaxial/uniaxial strength ratio

$\boldsymbol{B}_c$	defined in equation (6.17)
$\boldsymbol{B}_E$	defined in equation (4.44)
$\boldsymbol{B}_E$	defined in equation (5.51)
$\boldsymbol{B}_E$	defined in equation (6.26)
$\boldsymbol{B}_E$	defined in equation (7.40)
$\boldsymbol{B}_\gamma$	defined in equation (6.27)
$\boldsymbol{B}_\lambda$	defined in equation (4.43)
$\boldsymbol{B}_\lambda$	defined in equation (5.50)
$\boldsymbol{B}_\lambda$	defined in equation (7.38)
$\boldsymbol{B}_\mu$	defined in equation (7.39)
c	yield function shape parameter
c_1	softening curve factor
c_c, c_t	compressive and tensile cohesions
c_{c1}	hardening/softening curve parameter
c_{c2}	constant governing initial plastic slope of smooth hardening curve
c_g	contact function constant
c_m	continuous softening curve parameter
c_κ	defined in equation (4.34)
c_κ	defined in equation (5.41)
c_κ	defined in equation (7.26)
$\boldsymbol{C}_{ca}$	defined in equation (6.40)
$\boldsymbol{C}_{cc}$	defined in equation (6.41)
$\boldsymbol{C}_{cg}$	defined in equation (6.41)
$\boldsymbol{C}_{cs}$	defined in equation (6.36)
$\boldsymbol{C}_{cu}$	defined in equation (6.44)
$\boldsymbol{C}_{c\phi}$	defined in equation (6.44)
$\boldsymbol{C}_{c\gamma}$	defined in equation (6.36)
$\boldsymbol{C}_{lsf}$	local compliance matrix
$\boldsymbol{C}_{ltf}$	defined in equation (4.47)
$\boldsymbol{C}_{ltf}$	defined in equation (5.54)

$\boldsymbol{C}_{ltf}$	defined in equation (7.43)
$\boldsymbol{C}_L$	inverse matrix of the local elastic constitutive matrix
D	damage parameter
D_c, D_t	damage measure in compression and tension
$\boldsymbol{D}_e$	elastic stiffness matrix
$\boldsymbol{D}_{ep}$	consistent tangent stiffness matrix
$\boldsymbol{D}_{lp}$	defined in equation (7.33)
$\boldsymbol{D}_{ls}$	defined in equation (4.11)
$\boldsymbol{D}_{ls}$	defined in equation (5.18)
$\boldsymbol{D}_{ls}$	defined in equation (7.1)
$\boldsymbol{D}_{lt}$	defined in equation (4.38)
$\boldsymbol{D}_{lt}$	defined in equation (5.45)
$\boldsymbol{D}_{lt}$	defined in equation (7.33)
$\boldsymbol{D}_{l\kappa}$	defined in equation (4.38)
$\boldsymbol{D}_{l\kappa}$	defined in equation (5.45)
$\boldsymbol{D}_{l\kappa}$	defined in equation (7.33)
$\boldsymbol{D}_l$	secant elastic-damage constitutive matrix
$\boldsymbol{D}_L$	local elastic constitutive matrix
e	eccentricity parameter
$\boldsymbol{e}$	local effective strain
e_{bg}	relative normal displacement at start of contact loss in interlock state
$\boldsymbol{e}_a$	inelastic local strain on crack plane
$\boldsymbol{e}_e$	local elastic strain vector
e_{ful}	strain beyond which contact is minimum
e_{fulc}, e_{fulf}	strain beyond which contact is minimum for coarse and fine components
e_g	crack opening parameter
e_{gc}, e_{gf}	crack opening parameter for coarse and fine components
e_{hi}	strain at end of first section of shear contact function
$\boldsymbol{e}_p$	local plastic strain vector
e_r, e_s, e_t	local strain components

$\boldsymbol{e}_{rec}$	recoverable strain vector
$\boldsymbol{e}_s$	local plastic slip strain
E	Young's modulus
$\overline{E}$	effective elasticity modulus
f	loading function (Chapter 2)
f	damage loading function (Chapter 3)
f_c	uniaxial compressive strength
f_e	local yield function
f_{es}	local plastic slip function
$\boldsymbol{f}_{e\kappa}$	defined in equation (7.31)
f_h	contact function parameter
$\boldsymbol{f}_n$	defined in equation (7.54)
f_s	fracture stress parameter
f_t	uniaxial tensile strength
f_{ti}	stress at first damage
$\boldsymbol{f}_\kappa$	defined in equation (4.36)
$\boldsymbol{f}_\kappa$	defined in equation (5.43)
$\boldsymbol{f}_\kappa$	defined in equation (7.29)
$\boldsymbol{f}_{\kappa e}$	defined in equation (7.54)
F	yield function
F_d	damage loading function
$\boldsymbol{F}_e$	total-local function
F_p	yield function
$\boldsymbol{F}_E$	defined in equation (4.44)
$\boldsymbol{F}_E$	defined in equation (5.51)
$\boldsymbol{F}_E$	defined in equation (6.26)
$\boldsymbol{F}_E$	defined in equation (7.40)
F_λ	defined in equation (4.43)
F_λ	defined in equation (5.50)
F_λ	defined in equation (7.38)

F_γ	defined in equation (6.27)
F_μ	defined in equation (7.39)
$\boldsymbol{g}$	embedment strain
$\boldsymbol{g}_c, \boldsymbol{g}_f$	embedment strain for coarse and fine components
g_e	local plastic potential function
$\boldsymbol{g}_m$	defined in equation (4.53)
$\boldsymbol{g}_m$	defined in equation (5.60)
$\boldsymbol{g}_m$	defined in equation (7.48)
$\boldsymbol{g}_{\varepsilon m}$	defined in equation (5.49)
G	plastic potential function
G_f	fracture energy
h_c, h_t	isotropic hardening-softening function in compression and tension
h_κ	defined in equation (4.36)
h_κ	defined in equation (5.43)
h_κ	defined in equation (7.29)
h_ω	defined in equation (6.3)
H	hardening parameter
H_c	proportion of undamaged material
H_f	contact function
H_{fc}, H_{ff}	contact function for fine and coarse components
H_g	function for smooth transition to closed and interlock states
H_{gc}, H_{gf}	function for smooth transition to closed and interlock states for coarse and fine components
H_m	contact function constant
$\boldsymbol{I}$	identity matrix
I_1	first stress invariant
$\boldsymbol{I}_{c\Delta}$	defined in equation (6.38)
$\boldsymbol{I}_{dc}$	defined in equation (6.46)
$\boldsymbol{I}_e$	defined in equation (6.46)
$\boldsymbol{I}_N$	defined in equation (4.53)

$\boldsymbol{I}_N$	defined in equation (5.60)
$\boldsymbol{I}_{\Delta N}$	defined in equation (7.48)
$\boldsymbol{J}$	fourth-order symmetrical tensor
J_2	second stress invariant
J_3	third stress invariant
k	bar stiffness (Chapter 3)
k	Drucker-Prager cohesion parameter (Chapter 2)
k_c, k_t	model parameter for damage criterion in compression and tension
$\boldsymbol{k}_\sigma$	defined in equation (4.34)
$\boldsymbol{k}_\sigma$	defined in equation (5.41)
$\boldsymbol{k}_\sigma$	defined in equation (7.26)
K	softening parameter
K_0	undamaged bulk modulus (Chapter 2)
K_0	initial value of softening parameter (Chapter 3)
K_c, K_t	hardening-softening parameter in the loading function of damage in compression and tension
L	length of bars
m	number of parallel bars (Chapter 3)
m	continuous softening curve parameter
m_c, m_t	plastic participation factors in damage force
m_{ful}	factor for shear contact limiting strain
m_{fulc}, m_{fulf}	factor for shear contact limiting strain for coarse and fine components
m_g	gradient of the interlock surface
m_{gc}, m_{gf}	interlock surface parameter for coarse and fine components
m_{hi}	factor for end of first section of shear contact function
m_{hic}, m_{hif}	factor for end of first section of shear contact function for coarse and fine components
$\boldsymbol{M}_\kappa$	defined in equation (4.47)
$\boldsymbol{M}_\kappa$	defined in equation (5.54)
$\boldsymbol{M}_\kappa$	defined in equation (7.43)

M_λ	defined in equation (4.43)
M_λ	defined in equation (5.50)
M_λ	defined in equation (7.38)
M_μ	defined in equation (7.39)
$\boldsymbol{m}'_c$	defined in equation (6.22)
$\boldsymbol{m}'_p$	differential of $\boldsymbol{M}_x$ with respect to local recoverable strain
$\boldsymbol{m}'_x$	differential of $\boldsymbol{M}_x$ with respect to local strain
$\boldsymbol{m}'_\kappa$	differential of $\boldsymbol{M}_x$ with respect to hardening parameter
$\boldsymbol{M}_p$	defined in equation (7.43)
$\boldsymbol{M}_x$	defined in equation (4.11)
$\boldsymbol{M}_x$	defined in equation (5.18)
$\boldsymbol{M}_x$	defined in equation (7.1)
$\boldsymbol{M}_E$	defined in equation (4.44)
$\boldsymbol{M}_E$	defined in equation (5.51)
$\boldsymbol{M}_E$	defined in equation (7.40)
n	number of nodes
n	number of broken bars (Chapter 3)
n_{max}	maximum number of PODs permitted to form
n_p	number of damage plane
N	shape function
$\boldsymbol{N}$	stress transformation matrix
$\boldsymbol{N}_e$	defined in equation (7.33)
$\boldsymbol{N}_\Delta$	defined in equation (4.38)
$\boldsymbol{N}_\Delta$	defined in equation (5.45)
$\boldsymbol{N}_\Phi$	defined in equation (7.54)
p	softening curve constant
P	total force
P_γ	defined in equation (6.27)
P_λ	defined in equation (7.38)
P_μ	defined in equation (7.39)

$\boldsymbol{P}_E$	defined in equation (6.26)
$\boldsymbol{P}_E$	defined in equation (7.40)
q	softening curve parameter
r	elliptic function
r_c	residual strength factor
r_d	energy resistance function
r_d, s_d, t_d	unit vectors of crack plane
r_e	factor in damage loading function
r_{es}	defined in equation (6.7)
r_f	contact function constant
r_ε	strain ratio, defined in equation (5.29)
r_μ	parameter in the local yield function
r_σ	cohesion to tensile strength ratio
r_ζ	relative shear strain intercept
$\boldsymbol{R}_{ep}$	error measure for local plastic strain
$\boldsymbol{R}_{es}$	error measure for local plastic slip strain
$\boldsymbol{R}_\varepsilon$	error measure for plastic strain
$\boldsymbol{R}_{\varepsilon m}$	defined in equation (5.49)
$\boldsymbol{R}_{\varepsilon\kappa p}$	defined in equation (7.37)
R_κ	error measure for hardening parameter
$\boldsymbol{s}_d$	local stress vector for fully debonded slip component
$\boldsymbol{s}_f$	local stress vector
$\boldsymbol{s}_{fc}, \boldsymbol{s}_{ff}$	local stress vector for coarse and fine components
$\boldsymbol{s}_u$	local stress vector for undamaged material
u	enriched displacement approximation (Chapter 2)
u	displacement (Chapter 3)
w_c	fracture process zone width
x_k	defined in equation (5.28)
y_d^c	compressive damage criteria

y_d^t	tensile damage criteria
Y_c, Y_t	damage energy release rate in compression and tension
Y_v	volumetric thermodynamic conjugate force for damage
z_1, z_2, z_3	softening curve contants
α	model parameter for compressive damage criterion (Chapter 2)
α	yield surface shape parameter
α_1	elastic constitutive matrix factor
α_2	elastic constitutive matrix factor
α_c	proportion of coarse particles in a representative volume of the fully debonded component
α_p	Drucker-Prager friction parameter
α_β	yield surface shape parameter
β	yield surface shape parameter
β_d	dilatation parameter
χ	parameter for enhancement factor
X	enhancement factor in work hardening/softening plastic evolution function
X_1	constant for enhancement factor
$\delta \boldsymbol{e}_a$	iterative local added strain
$\delta \boldsymbol{e}_p$	iterative local plastic strain
$\delta \boldsymbol{e}_s$	iterative local plastic slip strain
$\delta \boldsymbol{s}_d$	iterative local stress for fully debonded slip component
$\delta \boldsymbol{s}_f$	iterative local stress
$\delta \boldsymbol{\varepsilon}$	iterative strain
$\delta \boldsymbol{\varepsilon}_p$	iterative plastic strain
$\delta\gamma$	iterative local plastic slip parameter
$\delta\kappa$	iterative hardening parameter
$\delta\lambda$	plastic multiplier increment
$\delta\mu$	incremental local plastic parameter increment
$\delta \boldsymbol{\sigma}$	iterative stress

$\delta\omega$	softening parameter increment
$\Delta \boldsymbol{e}_p$	incremental local plastic strain
$\Delta \boldsymbol{e}_s$	local plastic slip strain increment
$\Delta \boldsymbol{\varepsilon}$	strain increment
$\Delta \boldsymbol{\varepsilon}_p$	plastic strain increment
$\Delta\lambda$	incremental plastic parameter
$\Delta\kappa$	incremental hardening parameter
$\Delta\gamma$	incremental local plastic slip parameter
$\Delta\mu$	incremental local plastic parameter
$\Delta \boldsymbol{\sigma}$	out of balance stress
$\Delta \boldsymbol{\sigma}_a$	applied stress increment
$\Delta \boldsymbol{\sigma}_{rc}$	'reaction' stress increment
ε	uniaxial strain
$\boldsymbol{\varepsilon}$	Cartesian strain vector
ε_0	strain at end of softening curve
$\boldsymbol{\varepsilon}_a$	sum of the transformed inelastic local strain vector on all crack planes
ε_c	uniaxial compressive strain
$\boldsymbol{\varepsilon}_e$	elastic strain
ε_t	elastic strain at peak uniaxial stress
ε_{ti}	strain at first damage
ε_{tol}	strain tolerance
ε_v^e	elastic volumetric strain
ε_v^p	plastic volumetric strain
$\bar{\varepsilon}_p$	equivalent deviatoric plastic strain
$\tilde{\varepsilon}$	equivalent strain
ϕ	damage function
ϕ_{cl}	closure function
ϕ_{clc}, ϕ_{clf}	closure function for coarse and fine components
ϕ_{int}	interlock function
ϕ_{intc}, ϕ_{intf}	interlock function for coarse and fine components

ϕ_s	local plastic slip potential function
$\boldsymbol{\Phi}_d$	transformation matrix
$\boldsymbol{\Phi}_{dc}$, $\boldsymbol{\Phi}_{df}$	transformation matrix for coarse and fine components
$\boldsymbol{\Phi}_{gc}$, $\boldsymbol{\Phi}_{gf}$	defined in equation (5.16)
γ	local plastic multiplier
γ_p	yield surface shape parameter
$\boldsymbol{\Gamma}$	defined in equation (6.44)
$\boldsymbol{\Gamma}$	defined in equation (7.54)
$\boldsymbol{\Gamma}_e$	defined in equation (6.49)
η	ratio between work hardening and work hardening limit
η	defined in equation (5.18)
η_0, η_1	contact function parameters
φ	parameter governing the crack 'floating' stage
κ	hardening parameter
κ_c, κ_t	damage variable for compression and tension
κ_p	hardening parameter limit
$\dot{\lambda}$	plastic multiplier
μ_{es}	coefficient of friction
μ_ε	equivalent friction factor in strain terms
μ_σ	residual friction factor
ν	Poisson's ratio
θ	lode angle
ρ	deviatoric stress invariant (Chapter 2)
ρ	eccentricity parameter
ρ_c	yield surface smoothing function parameter
ρ_{f1}, ρ_{f2}	contact function constants
σ	uniaxial stress
$\boldsymbol{\sigma}$	stress tensor
σ_1	principal stress
σ_m	mean nominal stress

$\boldsymbol{\sigma}_{new}$	new converged stress
$\boldsymbol{\sigma}_{old}$	last converged stress
$\boldsymbol{\sigma}_{rec}$	recorded last converged stress
$\boldsymbol{\sigma}_t$	total stress
σ_{tol}	stress tolerance
$\boldsymbol{\sigma}_{tr}$	trial stress
σ_y	yield stress
$\boldsymbol{\sigma}_1$	trial stress based on the secant elastic-damage constitutive matrix
$\boldsymbol{\sigma}^+ / \boldsymbol{\sigma}^-$	positive/negative stress tensor
$\bar{\sigma}$	effective uniaxial stress
$\hat{\sigma}_{\max}$	maximum principal stress
ϖ	relative error
ω	damage variable
$\boldsymbol{\Omega}$	defined in equation (6.44)
$\boldsymbol{\Omega}$	defined in equation (7.54)
$\boldsymbol{\Omega}_e$	defined in equation (6.49)
ξ	hydrostatic stress invariant
$\boldsymbol{\Xi}$	defined in equation (6.45)
$\boldsymbol{\Xi}$	defined in equation (7.56)
ψ	dilatancy parameter
ψ	thermodynamic potential (Chapter 2)
Ψ	global enrichment function
$\boldsymbol{\Psi}$	defined in equation (6.50)
$\boldsymbol{\Psi}$	defined in equation (7.55)
ζ	damage strain parameter
ζ_k	damage strain at peak of tensile curve
Z_0	initial position of yield function
Z	friction hardening/softening function
∂_{ij}	Kronecker delta
$\circ$	contraction with respect to the 'in-plane' components of a 3rd order matrix

Chapter One

Introduction

1.1 Cracking – Effect and modelling

Cracks are always present within concrete structures, even at early age before the application of any mechanical load. Although they are often just microcracks, they grow stably under external loading, coalesce with other microcracks and eventually form large macrocracks which can lead to complete loss of structural strength. The modelling of crack initiation and propagation is one of the most essential aspects in the failure analysis of concrete structures.

Many constitutive formulations for concrete cracking have been established over the years. The theory of plasticity and continuum damage mechanics are the most commonly used by researchers to describe the compressive and tensile behaviour of concrete. Other more powerful models include those of plastic-damage and microplane models. The way in which these models capture the behaviour of cracks differ from one another.

One of the important characteristics governing the behaviour of cracked concrete is aggregate interlock, which according to experimental evidence, can provide a significant contribution to the total shear resistance of concrete beams. Also, when cracked concrete is subjected to cyclic loads, the ability of numerical models to simulate crack opening and closing is important. Constitutive crack models should be able to simulate the above behavioural characteristics, and include the gradual reduction of material stiffness on unloading, and the regaining of stiffness when crack faces regain contact.

The work described in this thesis employs the theories of plasticity, damage mechanics and contact mechanics in order to develop a comprehensive constitutive model suitable for the simulation of cracked concrete. The plastic-damage-contact model (Craft) by Jefferson (2003a, b) was used as a basis for the construction of the constitutive model. The Craft model has a fairly basic damage-contact component, which is used to describe the behavioural characteristics of cracks in concrete. Hence, the work presented in this thesis is dedicated to the improvement of the local embedded plane model.

1.2 Study objectives

The primary objective of the current study was to develop different and improved interface models that can be coupled into the plastic-damage-contact framework. This was fulfilled with the development of three different contact models as follows

- Dual-surface contact model
- Smooth frictional contact model
- Embedded planes with local plasticity contact model

Each of the above can be further subdivided into a series of steps required to realise their development

- Develop governing equations
- Derive the return mapping algorithm and consistent tangent stiffness operator
- Verify the consistent algorithm via a Mathcad implementation
- Develop a computer code in Fortran77 to numerically implement the proposed theoretical models in both a constitutive driver program and a finite element program
- Verify that both the dual contact and embedded planes with plasticity contact model correctly predict the behaviour of cracked concrete when compared to standard tests for compressive, tensile and combined loading paths
- Verify that the smooth frictional contact model correctly predicts the behaviour of construction joints for compressive, tensile and combined loading paths

1.3 Summary of contents

Chapter two presents a brief review on the behaviour of concrete and also a review on published literature relating to experimental investigation on the behaviour of aggregate

interlock on cracked concrete. Attention then turns to published literature on the various constitutive models available for modelling concrete. Emphasis here is placed on the four main types of model that are currently the subject of extensive research. This is followed by the various approaches used to model cracking.

Chapter three outlines the fundamental theories which form the basis of the theories used to develop the models in this study. A brief description of the derivation of the tangent stiffness matrix and stress recovery algorithm is given.

Chapter four details the theoretical formulation of the plastic-damage-contact model, which is used as a basis of the contact models developed in this study. Detailed descriptions of the local damage-contact component and plasticity component of the model are presented. The stress recovery algorithm and derivation of the consistent tangent matrix are documented.

Chapter five presents the theoretical formulation of the proposed dual-surface contact model. The decomposition of local stress in the damaged component is explored. The way in which the contact model parameters are obtained is discussed. Full derivations of the consistent tangent matrix and stress recovery algorithm are given. The implementation of the constitutive model is verified by comparisons with previously published data.

Chapter six concerns the theoretical formulation of the proposed smooth frictional contact model. The introduction of the local slip function is discussed. Full derivations of the consistent tangent operator and return mapping algorithm are presented. The numerical implementation of the theoretical formulation using Mathcad is fully documented. The implementation of the proposed model is verified using a variety of loading paths.

Chapter seven details the theoretical formulation of the proposed 'embedded planes with local plasticity contact' model (EPLPC). The inclusion of the local plasticity function is discussed, and modification to the softening function is suggested. Complete derivations of the consistent tangent stiffness matrix and return mapping algorithm are documented, followed by the verification procedure of the consistent algorithm. The implementation of the model is verified by comparisons with previously published results, using a variety of loading paths. Predictions made using the proposed model are discussed.

Chapter eight summarises the conclusions given for each of the proposed model. The overall conclusions of the work are discussed and further research is suggested.

Chapter Two

Literature Review

2.1 Introduction

A vast number of numerical models for concrete have been developed over the last 30 years. These developments have been accompanied by the various experiments carried out which provide better insight into the complexity of concrete behaviour. Under uniaxial compression, concrete exhibits considerable ductility and non-linearity prior to reaching its peak stress, whereas in tension, the behaviour is far more brittle. Upon reaching its compressive limit, concrete losses strength in all directions. In contrast, under tensile loading, strength degradation is confined to the direction normal to the crack plane (Jefferson 1989). In biaxial compression, experimental evidence has shown that the maximum strength of concrete increases by up to 125% of the uniaxial strength (Kupfer *et al.* 1969). In triaxial compression tests, the strength and ductility of concrete has also been found to increase significantly under high confinement (Li and Ansari 1999; Sfer *et al.* 2002).

Under uniaxial loading, concrete generally exhibits linearly elastic behaviour as long as the uniaxial compressive stress does not exceed 45–50% of the peak compressive strength f_c of the material, and it exhibits nonlinear strain-hardening behaviour when the compressive stress varies between $0.5f_c$ and f_c. Concrete demonstrates a strain-softening behaviour after its peak strength f_c has been reached.

On the other hand, concrete has a much lower strength in tension. The material behaves almost entirely elastically up until 70% of the peak tensile strength f_t, after which nonlinearity takes place and strain softening occurs. In the post-peak regime, microcracks are developed in an area known as the fracture process zone (Karihaloo 1995), which results in a continual decrease of the strength of concrete together with an increase in deformation. These microcracks eventually bridge and coalesce into macrocracks. At this point, the presence of major cracks jeopardises the integrity of the material.

This chapter gives a review of the type of existing concrete models that are present in today's software packages. The first section presents literature relating to experimental investigations undertaken on concrete specimens. This is followed by outlines of the various constitutive models that have been developed over the years to describe the behaviour of concrete material. The last section presents descriptions of the different approaches available to simulate cracks in concrete.

2.2 Crack opening-closing and aggregate interlock

When a crack is formed within a concrete material, the crack surfaces are generally rough and irregular. This is largely due to the coarse aggregate particles, which remain embedded in one or the other of the crack faces, as shown in Figure 2.1. Parallel movement between these faces along the crack plane causes projecting particles from one face of the crack to come into contact with the matrix of the other face. Shear forces can be transmitted across the crack interface subjected to simultaneous shear and normal compression. This phenomenon is known as aggregate interlock (also termed interface shear).

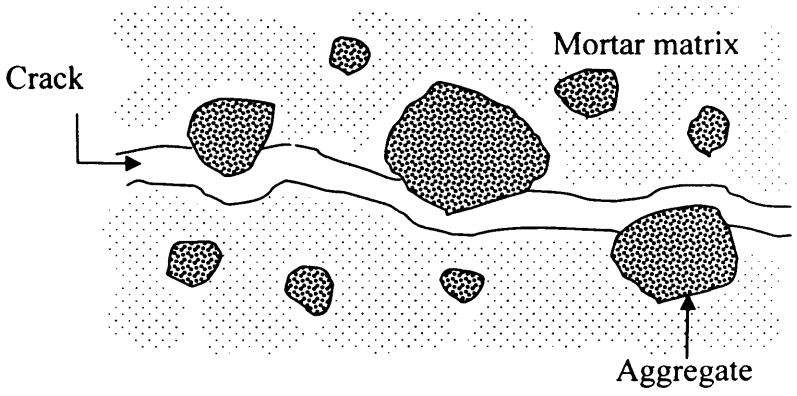

Figure 2.1. Irregular crack surface

When shear is applied to an initially cracked surface, relative slip (shear displacement) between the faces is accompanied by the separation of the surfaces (dilation) owing to rough asperities of aggregate and mortar tips projecting across the sliding path. In cases where reinforcement is present across the crack, the separation of the surfaces generates

tensile stress in the reinforcement (Ali and White 1999). For equilibrium, elongation of the reinforcement produces compression forces on the interface. Thus, shear is transferred across the crack by the action of aggregate interlock, as well as by friction due to asperities of the aggregates and the surrounding matrix. For the case of reinforced material, dowel action of reinforcement crossing the crack surface also contributes to the shear transfer mechanism (Ali and White 1999).

Aggregate interlock has been found to provide a significant contribution to the total shear resistance of concrete beams (Fenwick and Paulay 1968). A number of authors have studied the resistance to shear displacement of concrete interfaces in various ways. However, hardly any attention has been given to the phenomenon of wedging action which provides the link between normal and shear stresses, on the one hand and crack opening and shear displacement on the other hand. As far as the mechanism of shear transfer across cracks is concerned, it cannot be simply described using merely a relationship between shear stress and shear displacement. A more realistic description of the mechanism would have to include not only shear stress and shear displacement, but also normal stress and crack opening (Divakar *et al.* 1987).

The results obtained from experiments with concrete specimens subjected to normal-shear loading provide evidence that there is a gradual build up of shear and compressive stresses, up to a certain limit and then plateau or reduce, when a crack is first opened in tension and subsequently sheared (Hassanzadeh 1991; Nooru-Mohamed 1992). However, the level of stresses decreases with increasing crack opening, up to some limit,

after which no further contact can be regained in shear (Walraven and Reinhardt 1981).

When a material is subjected to alternated loads, the effects of crack closure are of importance. During load cycles, microcracks close progressively and the material stiffness increases while the degree of damage remains unchanged. The real unloading-reloading response of a cracked concrete is highly non-linear, and is neither the elastic response of plasticity nor the secant response of damage theory. Results obtained from experiments with concrete specimen subjected to pure tension show that the slopes of unloading curves vary continuously between secant and almost initial stiffness, and intersect the zero-stress axis with considerable residual opening. Under normal-shear loading condition, the unloading stiffness gets closer to the initial stiffness due to a higher degree of contact between the crack faces.

The simulation of these phenomena is one of the main topics of this thesis. The following presents a review of current existing numerical models for concrete that can be found in the literature.

2.3 Constitutive models for concrete

2.3.1 Damage models

The application of continuum damage mechanics theory to concrete dates from the late 1970s. The concept of effective stress was originated by Kachanov (1980) to describe the

rupture process of metals. The theory is based on the thermodynamics of irreversible process. The underlying assumption of the theory is that the constitutive properties of the fracturing materials depend upon a damage variable, which can be a scalar, vectorial or tensorial quantity.

Isotropic damage models have been widely used because of their simplicity, numerical implementation and parameter identification (Burlion *et al.* 2000). Among the various scalar damage models that have been developed over the years are those of Simo and Ju (1987), Ju (1989) and Oliver *et al.* (1990). The use of a scalar damage variable implies that the material is assumed to be isotropic, i.e. independent of the crack orientation.

From experimental observations, it has been confirmed that damage is in fact not isotropic but has preferential directions. The initially assumed isotropic material becomes gradually anisotropic. Fichant *et al.* (1999) undertook a comparative study to assess the limitation of scalar damage models in describing the response of concrete subjected to different loading conditions. They found out that the scalar model is capable of predicting failure mainly due to uniaxial tension. For multi-axial tension problems, a damage model that accounts for damage-induced anisotropy in concrete is preferable.

A number of anisotropic damage models have been developed for quasi-brittle materials. These models differ from one another mainly in the order of the damage tensors employed to describe the progressive deterioration of the material, for example, Krajcinovic and Fonseka (1981) used damage vectors, Mazars and Pijaudier-Cabot

(1989) used a second-order tensor and Carol *et al.* (1994), Ortiz (1985) and Yazdani and Schreyer (1990) employed a fourth-order tensor.

The development of microcracks causes progressive degradation of the elastic stiffness. Under cycling loading, microcracks which have initially opened may close during load reversal. This causes restoration of the material rigidity, known as the unilateral effect. This directional phenomenon can be observed in a beam subjected to cycling loading. Several numerical models, in the context of isotropic and anisotropic damage, have been established with the incorporation of the effect of microcrack closure (Brencich and Gambarotta 2001; Dragon *et al.* 2000; Ju 1989; Thionnet and Renard 1999).

Separate damage criteria have been employed to capture the different responses of concrete under tension and compression (Comi and Perego 2001; Mazars and Pijaudier-Cabot 1989). For example, in Comi and Perego (2001), the two damage criteria used to model tensile and compressive behaviour, respectively, are expressed as follows

$$y_d^t(\boldsymbol{\sigma}) = J_2 - a_t I_1^{\,2} + b_t h_t(D_t) I_1 - (1-\alpha D_c) k_t h_t(D_t)^2 \tag{2.1}$$

$$y_d^c(\boldsymbol{\sigma}) = J_2 + a_c I_1^{\,2} + b_c h_c(D_c) I_1 - k_c h_c^{\,2}(D_c) \tag{2.2}$$

in which I_1 is the first invariant of the stress tensor and J_2 is the second invariant of the deviator stress. a_i , b_i , k_i (i = t or c) and α are non-negative model parameters determined based on the experimental failure envelope and properties of the material. h_t

and h_c are isotropic hardening-softening functions to control the evolution of the two failure surfaces. D_c and D_t are the compressive and tensile damage variable respectively. In equation (2.1), the presence of the term D_c in the tensile damage function is to take into account the effect of compressive damage on the tensile strength of the material.

The concept of positive and negative projections of stress and strain tensors has also been adopted by several researchers (Ortiz 1985; Simo and Ju 1987; Hansen and Schreyer 1995). Mazars and Pijaudier-Cabot (1989) developed a composite damage surface which was expressed as a double criterion using two thermodynamic forces associated with the tensile and compressive damage variables, as follows

$$y_d^c = Y_c - K_c(D_c) \tag{2.3}$$

$$y_d^t = Y_t - K_t(D_t) \tag{2.4}$$

where

$$Y_t = \frac{\partial \psi}{\partial D_t} = \frac{1}{2E(1-D_t)^2}\left[(1+\nu)(\boldsymbol{\sigma}^{+T}\boldsymbol{\sigma}^{+}) - \nu\left[(tr\boldsymbol{\sigma})^{+}\right]^2\right]$$

$$Y_c = \frac{\partial \psi}{\partial D_c} = \frac{1}{2E(1-D_c)^2}\left[(1+\nu)(\boldsymbol{\sigma}^{-T}\boldsymbol{\sigma}^{-}) - \nu\left[(tr\boldsymbol{\sigma})^{-}\right]^2\right]$$

$$\psi = \frac{1}{2}\left\{\frac{1}{E(1-D_t)}\left[(1+\nu)(\boldsymbol{\sigma}^{+T}\boldsymbol{\sigma}^{+}) - \nu\left[(tr\boldsymbol{\sigma})^{+}\right]^2\right] + \ldots\right.$$

$$\left. \ldots \frac{1}{E(1-D_c)}\left[(1+\nu)(\boldsymbol{\sigma}^{-T}\boldsymbol{\sigma}^{-}) - \nu\left[(tr\boldsymbol{\sigma})^{-}\right]^2\right]\right\}$$

E and ν are Young's modulus and Poisson's ratio respectively, and ψ denotes the thermodynamic potential energy. K_t and K_c are two separate hardening-softening functions for tension and compression, respectively.

In the model developed by Ortiz (1985), concrete is treated as a composite material, in which both mortar and aggregate are modelled separately. The resulting governing equations for the two-phase material are derived using the theory of mixtures, with the assumptions that the total stresses are the sum of a scalar multiple of the stresses in each of the two phases. Ortiz (1985) employed a rate-independent damage model to describe the behaviour of the mortar phase. In contrast to most of the available damage models in the literature, the model uses the elastic compliances as the damage variables. The damage surface, as shown in Figure 2.2, uses the sum of the square of the positive and negative principal stresses.

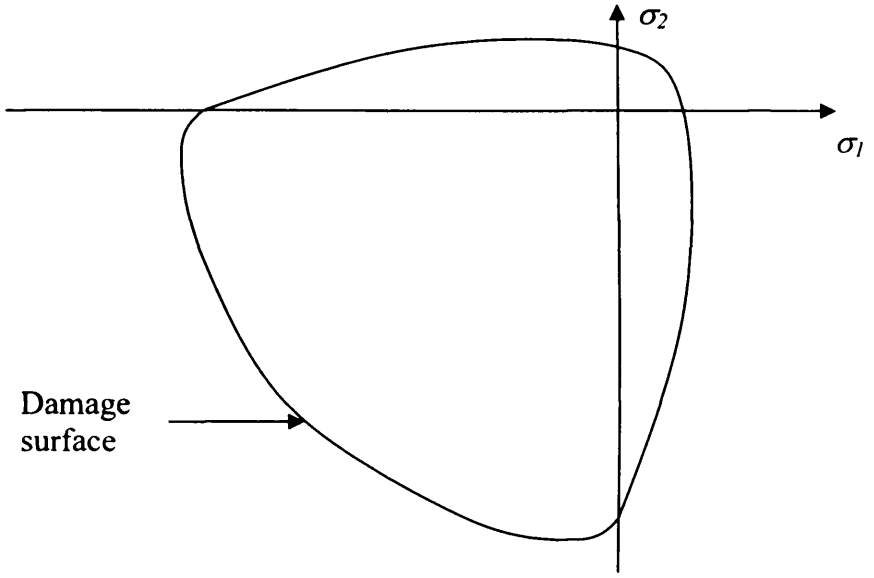

Figure 2.2. Damage surface in Ortiz's composite damage model

The square of the negative compressive stresses is multiplied by a constant, which is considerably less than unity. The softening law is an expression that matches the uniaxial tensile softening curve of concrete. The mortar damage model also allows for some plastic deformation by the use of the assumption that a proportion of the inelastic strain increments are plastic. As for the plasticity model, Ortiz (1985) utilised the standard Drucker-Prager yield function with a non-associated flow rule to model the aggregate phase. The plastic potential function is also a Drucker-Prager surface, but it has a different slope from that of the yield function.

In contrast to the basic approach by Ortiz (1985), which was a stress-based formulation, Stevens and Liu (1992) refined the model to simulate concrete inelasticity using a strain-based formulation. The original model by Ortiz has been further developed by several researchers to capture the response of brittle solids under proportional and

non-proportional load paths (Karnawat and Yazdani 2001), and to model softening and localisation phenomena (Schreyer and Neilsen 1996).

Labadi and Hannachi (2005) developed a damage surface similar to the yield function in the conventional theory of plasticity. The loading function was defined in the strain space and depends on the equivalent strain $\tilde{\varepsilon}$ and damage parameter as follows

$$f = \tilde{\varepsilon} - K = \left[\frac{1 + r_e(\frac{f_c}{f_t} - 1)}{\frac{f_c}{f_t}} \right] \sqrt{\frac{1}{2} \boldsymbol{\varepsilon}^T \boldsymbol{J} \boldsymbol{\varepsilon}} - K \tag{2.5}$$

where

$$r_e = \begin{cases} 0 & \text{if} \quad \sum_{i=1}^{3} |\varepsilon_i| = 0 \\ \dfrac{\sum_{i=1}^{3} \langle \varepsilon_i \rangle}{\sum_{i=1}^{3} |\varepsilon_i|} & \text{if} \quad \sum_{i=1}^{3} |\varepsilon_i| > 0 \end{cases}$$

$\boldsymbol{J}$ is a fourth-order symmetrical tensor and K is the softening function. The equivalent strain was defined, taking into account the asymmetric behaviour of concrete in tension and compression.

Tao and Phillips (2005) presented a simplified isotropic damage model capable of simulating concrete under biaxial stress states. Two damage variables were employed to capture the different damage criteria under tension and compression. A weighted damage variable was also introduced to prevent conflict occurring when both tensile and compressive damage are activated under biaxial or reverse cyclic loading. Under uniaxial loading, damage is solely governed by the associated damage parameter, whereas under biaxial loading, both tensile and compressive damage parameters contribute to the induced damage.

It has been acknowledged that care has to be taken when generating damage functions for quasi-brittle materials. Yazdani *et al.* (2002) reported that an apparent snapback was observed in the post-peak regime of a uniaxial loading path. This is due to an internal contradiction developed in the damage model itself, in which snapback is predicted even though the theory was not structured to model this behaviour. Cope *et al.* (2005) proved that by establishing a set of functions with certain characteristics, the formulation could lead to the construction of a well behaved response in the stress-strain space.

2.3.2 Plasticity models

The largest group of continuum models, for the simulation of concrete, is the group based on the theory of plasticity. Constitutive models that are based on conventional plasticity always require an elastic constitutive relationship, the assumption of total strain decomposition, the definition of a yield surface with an evolution rule, and a flow rule.

There have been a number of yield surfaces developed over the years. These surfaces differ from one another by the shape of the yield envelope in principal stress space and by the number of model parameters employed to define the yield function. The Von Mises and Tresca criteria are examples of one-parameter yield surfaces, while the Mohr-Coulomb and Drucker-Prager criteria form the basis of two-parameter plasticity models. Among the various yield surfaces, the Drucker-Prager yield criterion, in particular, has been employed and modified by a number of researchers for the constitutive modelling of concrete (Addessi *et al.* 2002; Feenstra and de Borst 1996; Kang and Willam 1999; Salari *et al.* 2004; Willam and Warnke 1974). Figure 2.3 shows a comparison of yield surfaces for plain concrete.

The complex behaviour of concrete under multiaxial load has led to the development of biaxial and triaxial models using the theory of plasticity. Among the various biaxial models developed, Chen and Chen (1975) presented a yield surface which is used to capture both the compressive and tensile behaviour of concrete. The biaxial envelope, as indicated in Figure 2.4, consists of corners at the compression-compression and compression-tension boundaries, which leads to numerical instabilities (de Borst 1987). In addition, the use of plasticity theory to describe the tensile behaviour of concrete has been found inappropriate since concrete in uniaxial and biaxial tension remains almost purely elastic up to its fracture limit and does not maintain its original stiffness upon unloading after the limit, as predicted by the theory of plasticity.

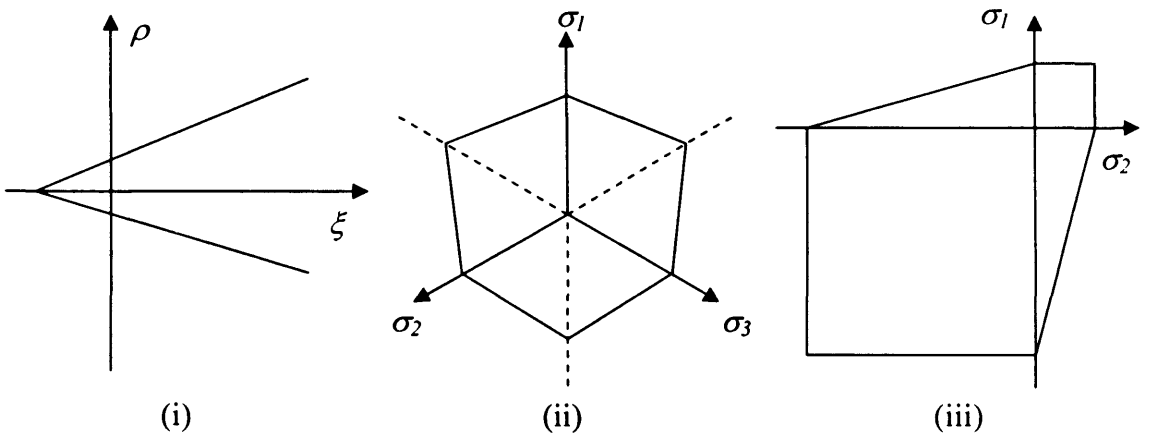

(a) Mohr-Coulomb

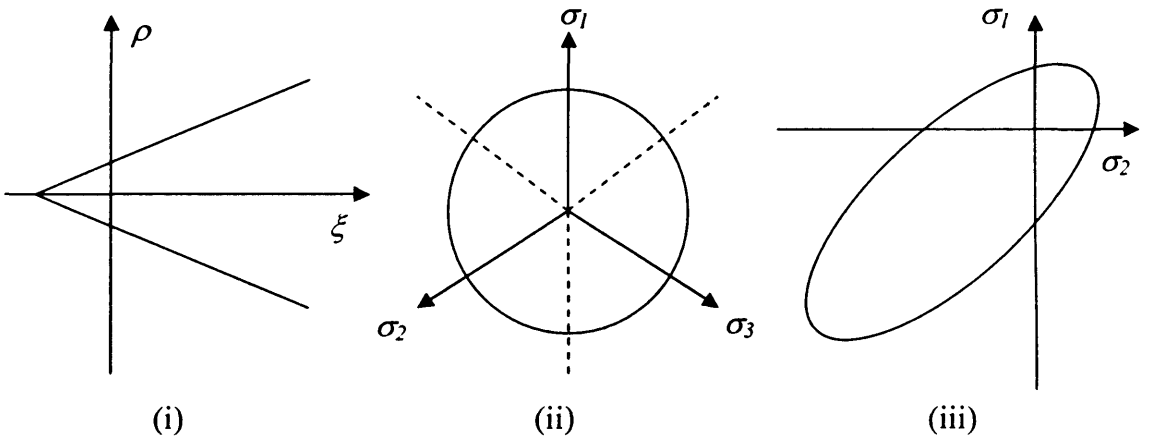

(b) Drucker-Prager

Figure 2.3. Comparison of yield surfaces for plain concrete; (i) meridian section, (ii) deviatoric section, (iii) plane stress section

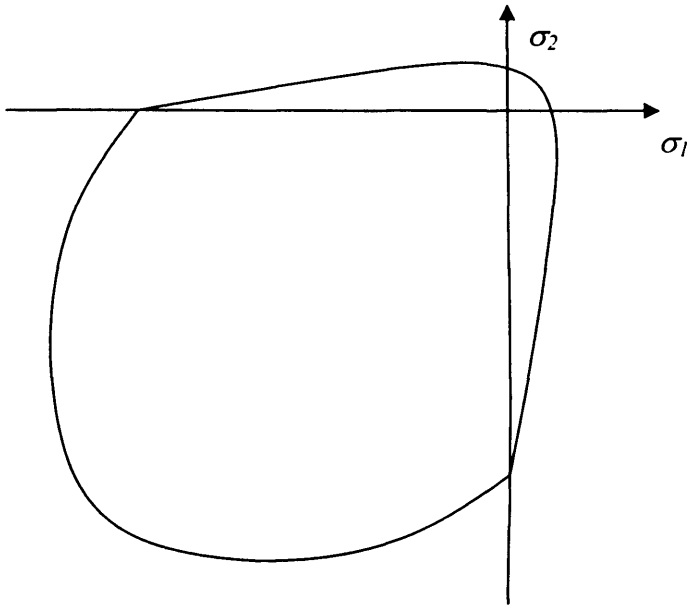

Figure 2.4. Chen and Chen yield surface in biaxial principal stress space

Buyukozturk (1977) presented a smooth continuous yield envelope which provides a good fit to biaxial test data in the compression-compression region. However, the yield surface is incapable of capturing the behaviour of concrete in the compression-tension region. Concrete is assumed to behave linearly elastic in the tension-tension region up to its tensile limit, after which cracking is assumed to occur. Yielding in the compression-tension region will result in a discontinuity between the compression-tension and tension-tension regions.

In the 1980s, more attempts were made in the development of plasticity models to simulate the complex triaxial behaviour of concrete. These included the work by Hsieh *et al.* (1982) in which a four parameter yield surface, similar to that of Ottosen (1979), was employed to capture the characteristic behaviour of concrete. The model uses a fracture surface to limit the tensile strength, as well as introducing a crushing coefficient to control

the amount of cracking and crushing. The addition of the coefficient which relates to the amount of crushing helps to alleviate the difficulties presented due to the inclusion of a fracturing criterion into a plasticity model.

Este and Willam (1994) developed a plasticity model named the Extended Leon Model (ELM), which is characterised by an elliptic loading surface in the deviatoric plane. The model utilises an elliptic function $r(\theta)$, similar to that used by William and Warnke (1974), in which an eccentricity parameter e was introduced to generate a continuous failure surface, as shown in Figure 2.5.

$$r(\theta,e)=\frac{4(1-e^2)\cos^2\theta+(2e-1)^2}{2(1-e^2)\cos\theta+(2e-1)\sqrt{4(1-e^2)\cos^2\theta+5e^2-4e}} \tag{2.6}$$

In the ELM model, an isotropic hardening rule was used to describe the inelastic behaviour of concrete in the pre-peak regime. The model employs a non-associated plastic flow rule to control the inelastic dilatant behaviour of concrete. The performance of the model had been assessed by means of numerical analyses of concrete specimens subjected to mixed-mode loading. The model was found to provide good prediction of crack patterns (Pivonka *et al.* 2004).

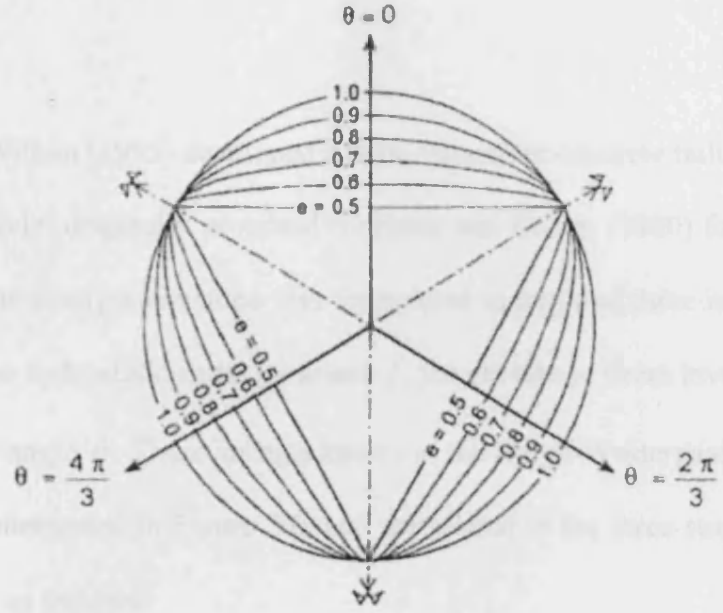

Figure 2.5. Elliptic function

Feenstra and de Borst (1996) developed a composite yield function for the numerical analysis of concrete structures, either plain or reinforced, which are predominantly in tension compression biaxial stress states. The model uses a Rankine (principal stress) yield criterion to limit the in-plane tensile stresses and a Drucker-Prager yield contour for the compressive-compressive regime in biaxial stress. The composite yield contour closely matches the classical Kupfer and Gerstle (1973) data.

The plasticity-based approach has experienced difficulties in modelling stiffness degradation due to progressive damage. However, it has been shown from experimental evidence that stiffness degradation due to tensile cracking is excessive only when tensile cracking has fully developed (Willam *et al.* 1987; Hordijk 1991). Stiffness degradation due to compressive loading is even less pronounced than stiffness degradation due to

tensile loading.

Menétrey and Willam (1995) developed a three-parameter concrete failure criteria that is based on the model originally proposed by Hoek and Brown (1980) for the analysis of rock masses. The strength envelope was formulated in terms of three independent stress invariants i.e. the hydrostatic stress invariant ξ, the deviatoric stress invariant ρ, and the deviatoric polar angle θ. These are also known as the Haigh-Westergaard coordinates, as geometrically interpreted in Figure 2.6, and are related to the three stress invariants i.e. I_1, J_2 and J_3, as follows

$$\xi = \frac{I_1}{\sqrt{3}}, \qquad \rho = \sqrt{2J_2} \qquad \text{and} \qquad \cos 3\theta = \frac{3\sqrt{3}}{2}\frac{J_3}{J_2^{3/2}} \tag{2.7}$$

The failure criterion has a smooth and convex surface in stress space, in addition to parabolic meridians which intersect the hydrostatic axis at the point of equitriaxial tension. The deviatoric section changes from triangular shapes at low confinement to almost circular shapes at high confinement. The failure function was derived such that it can be generalised to incorporate other strength criteria, for instance the Huber-Mises, Drucker-Prager, Rankine, and Mohr-Coulomb criteria. An elliptic function after William and Warnke (1974) was adopted to counter for the presence of sharp corners in the deviatoric plane.

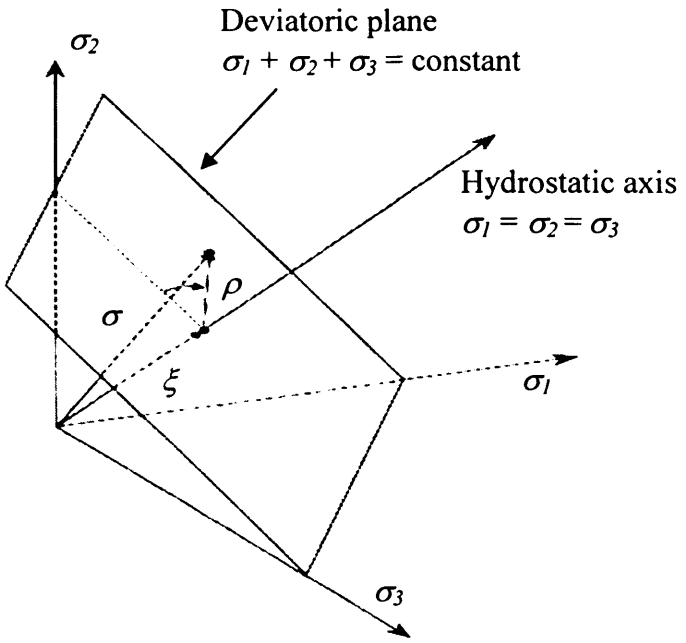

Figure 2.6. Haigh-Westergaard stress space

Imran and Pantazopoulou (2001) developed a constitutive model for concrete based on non-associative, non-linear strain hardening plasticity theory. Volumetric strain was used as the state variable, which provides measurement of the extent and intensity of damage in the material. It is possible to determine the degree of stiffness and strength degradation as well as the ductility for any stress state. In contrast to most conventional plasticity models, the failure envelope used in this model is allowed to expand (hardening) or contract (softening) with respect to the deformation of plastic strains. This is due to the failure being controlled by a continuous damage-drive process rather than a distinct event.

Grassl *et al.* (2002) developed a hardening law and combined it with a three-parameter yield surface developed by Menétrey and Willam (1995), as depicted in Figure 2.7, to

describe the behaviour of plain concrete in triaxial compression. The hardening law differs from those in other plasticity theories by using the volumetric component of the plastic strain increment as the hardening parameter. The overall formulation is simplified and can be easily implemented by means of an implicit backward-Euler algorithm.

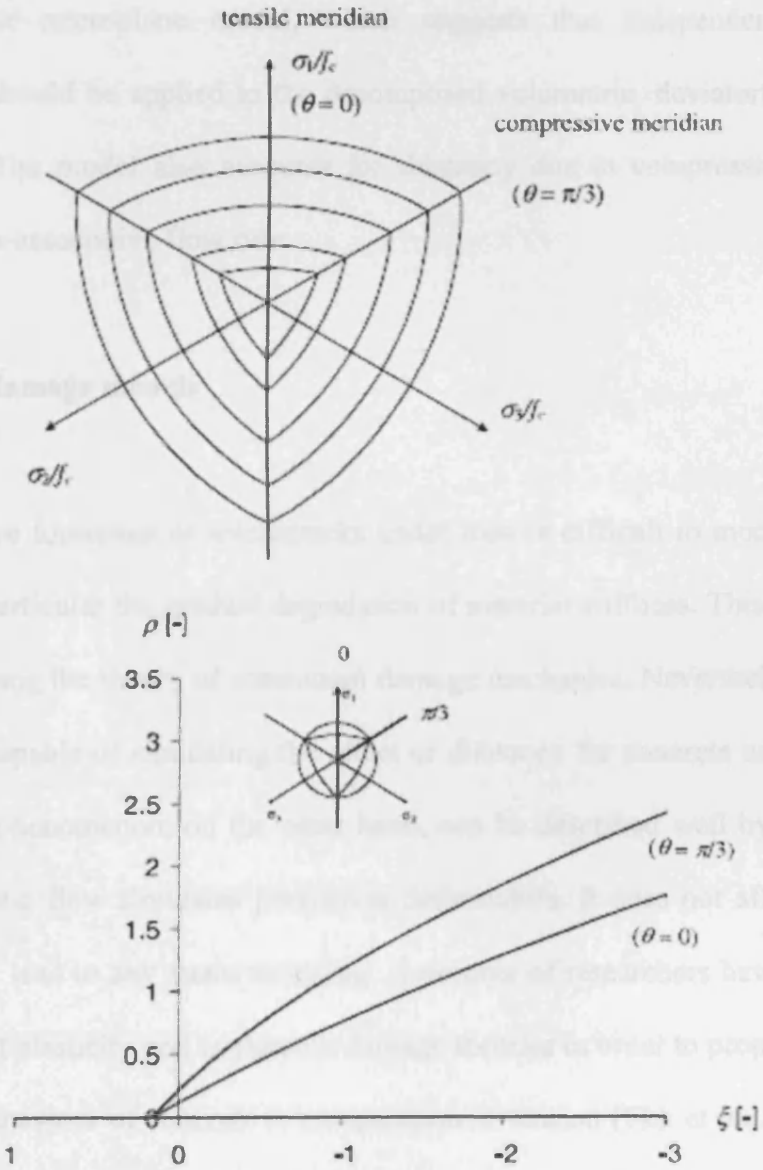

Figure 2.7. Deviatoric and meridian sections of the yield surface by Grassl *et al.* (2002)

More recently, Park and Kim (2005) developed a plasticity model that uses three independent failure surfaces to simulate more accurately the behavioural characteristics of concrete in various stress states. These failure surfaces correspond to the three orthogonal stress components, which are the volumetric and deviatoric stress components respectively. The idea behind the development of the model is merely based on the success of the microplane model, which suggests that independent stress-strain relationships should be applied to the decomposed volumetric, deviatoric, and tangent components. The model also accounts for dilatancy due to compressive damage by adopting a non-associative flow rule.

2.3.3 Plastic-damage models

The progressive formation of microcracks under load is difficult to model by classical plasticity, in particular the gradual degradation of material stiffness. This behaviour can be captured using the theory of continuum damage mechanics. Nevertheless, the theory by itself is incapable of simulating the effect of dilatancy for concrete under multiaxial loading. This phenomenon, on the other hand, can be described well by the theory of plasticity. Plastic flow simulates permanent deformation. It does not affect the elastic properties, nor lead to any strain softening. A number of researchers have explored the combination of plasticity and continuum damage theories in order to properly model the constitutive behaviour of concrete in compression or tension (Ekh *et al.* 2003; Lubliner 1989; Luccioni and Rougier 2005).

Experimental evidence has shown that concrete exhibits a certain degree of ductility before failure under compressive loading with confining pressure. This observation is represented in Figure 2.8. In tensile and low confining pressure regimes, the damage surface dominates, and brittle behaviour is simulated. As the confining pressure increases, the behaviour becomes ductile due to the activity of the plasticity surface. However, the amount of ductility is limited as the stress is prevented from reaching the plasticity surface by the damage state. As the confining pressure increases further, the material becomes more ductile with no strain softening. The plasticity surface dominates and prevents the stress from reaching the damage surface (Yazdani and Schreyer 1990).

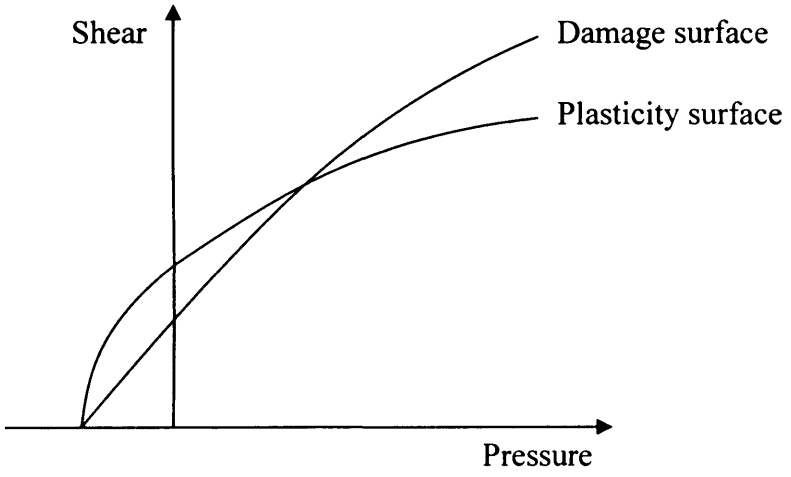

Figure 2.8. Representation of plasticity and damage surfaces

One of the plasticity-based damage models is the so-called Barcelona model, developed by Lubliner *et al.* (1989). The model employs a fracture energy based scalar damage variable to represent all damage states. Two other variables, i.e. elastic and plastic degradation variables, were also introduced to simulate stiffness degradation. These

variables are coupled with the plastic deformation in the constitutive relations to facilitate calibration of the parameters with experimental results. The model employs a Drucker-Prager typed yield criterion, as depicted in Figure 2.9, and a Mohr-Coulomb plastic potential function for non-associated deformation.

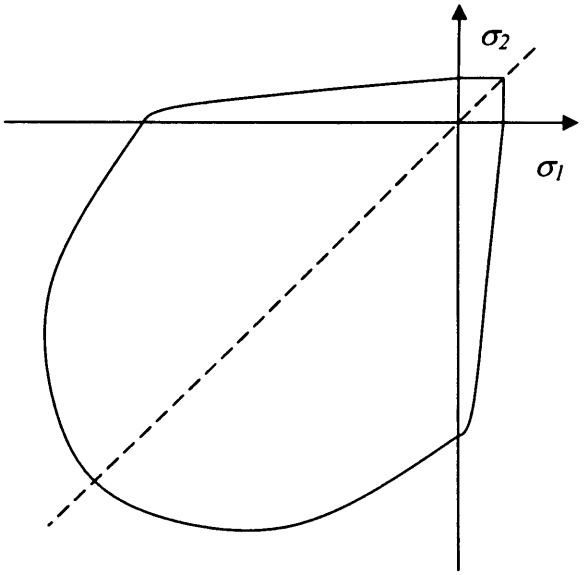

Figure 2.9. Yield envelope in plane stress space by Lubliner *et al.* (1989)

Luccioni *et al.* (1996) adopted the same plasticity model developed by Lubliner *et al.* (1989) and employed the concept of effective stress in developing the damage model. The evolutions of both plastic strains and stiffness degradation were obtained by solving simultaneous equations formed using the consistency conditions. By relating the hardening variables to the energy dissipation in each problem, correct energy dissipation of the whole problem was attained.

Lee and Fenves (1998) developed a similar plastic-damage model to that of Lubliner *et al.* (1989) to characterise the cyclic behaviour of concrete. The model employs the same concepts of fracture-energy based damage, but with two damage variables to describe the different damage processes under tensile and compressive loading. The original yield function used in the Barcelona model was modified by including multiple hardening variables. In the Barcelona model, the dimensionless constant β, which is used to define the yield surface, is derived using the initial tensile and compressive strengths of the material. Lee and Fenves (1998) modified the yield function F, as expressed below, by redefining β in terms of the current tensile and compressive strengths of the materials, both of which are a function of the respective damage variables, κ_t and κ_c.

$$F(\sigma,\kappa)=\frac{1}{1-\alpha_\beta}\left[\alpha_\beta I_1+\sqrt{3J_2}+\beta(\kappa)\langle\hat{\sigma}_{\max}\rangle\right]-c_c(\kappa) \tag{2.8}$$

where

$$\beta(\kappa)=\frac{c_c(\kappa)}{c_t(\kappa)}(1-\alpha_\beta)-(1+\alpha_\beta)$$

$c_t(\kappa)$ and $c_c(\kappa)$ are the tensile and compressive cohesions respectively. $\hat{\sigma}_{\max}$ denotes the maximum principal stress and α_β is a constant parameter. The evolution of the yield surface is governed by the damage variables, which in turn are functions of the equivalent plastic strain.

In the plastic-damage model, the uniaxial strength functions are factored into two parts corresponding to the effective stress and stiffness degradation. The constitutive relations for the elastoplastic response are separated from the degradation damage response. The model also introduces a simple thermodynamically consistent damage model which is capable of simulating the effect of damage on elastic stiffness and also its recovery during crack opening and closing.

Yazdani and Schreyer (1990) presented a combined plastic-damage model for plain concrete. The model was developed within the general framework of the internal variable theory of thermodynamics. The pressure dependent damage model, with both hardening and softening features, is capable of simulating both cleavage and compressive cracking due to the combination of shear sliding and crack opening. The anisotropic damage model, together with a classical von Mises plasticity model with strain hardening, is able to describe the characteristics of concrete such as dilation with shear and enhanced ductility with increased confining pressure. Another advantage of the model is its suitability for computer implementation. Figure 2.10 shows schematic diagrams of the combined plastic-damage model.

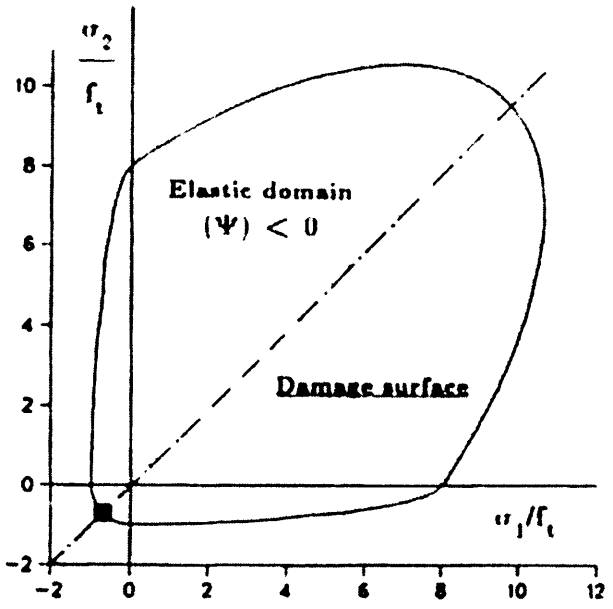

(a) Yield envelope

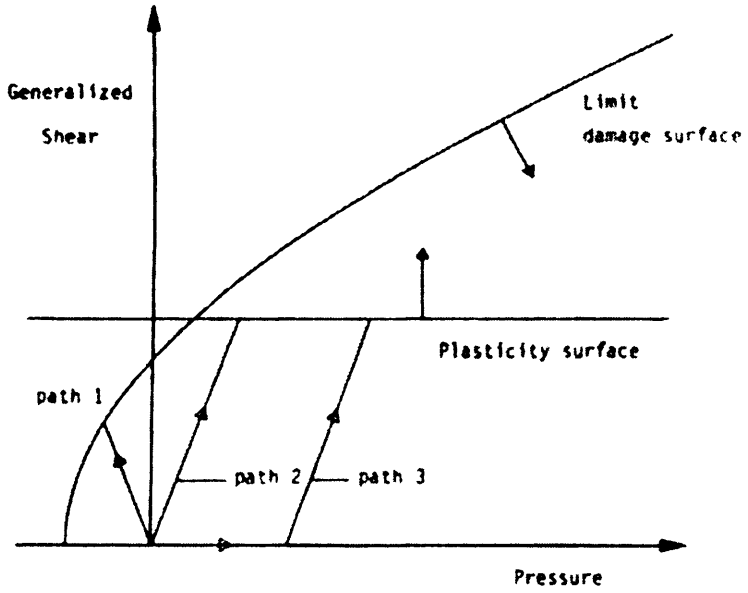

(b) Plastic-damage surface

Figure 2.10. Combined plastic-damage model by Yazdani and Schreyer (1990)

Another significant contribution to the development of plastic-damage model can be found in the work by Meshke *et al.* (1998). A multi-surface elastoplastic damage model was developed to simulate plastic deformations as well as stiffness degradation. The model employs the maximum tensile stress criterion to control cracking. To simulate the postcracking characteristics of concrete, a hyperbolic softening law was introduced, which can be easily calibrated to the fracture energy release rate. The model uses a hardening/softening Drucker-Prager yield surface to capture the behaviour of plain concrete under mixed tensile-compressive and multiaxial compressive stress states.

Hansen *et al.* (2001) combined the theories of plasticity and damage mechanics to develop a multi-surface anisotropic plastic-damage model for plain concrete. A parabolic extension of the classic two-invariant Drucker-Prager plasticity model was adopted to capture the degradation of frictional strength of concrete, as well as the dilatation of materials under shear. The model employs a Rankine-type anisotropic damage model which was introduced by Carol *et al.* (2001). A second-order damage tensor was used to describe anisotropic damage. The model is capable of modelling stiffness recovery due to the closing of microcracks.

Shen *et al.* (2004) presented a fully coupled plastic-damage model to simulate the history-dependent plastic-damage behaviour of massive structural concrete under confinement. The model employs a Drucker-Prager yield criterion based on the work by Menétrey and Willam (1995), with a non-associated plastic flow rule. In this model, the damage evolution is coupled with the increase of plastic strain. The model is capable of

simulating accurately both uniaxial tension and compression cases, as well as multiaxial compression with hydrostatic confinement stresses.

Salari *et al.* (2004) developed a fully coupled plastic-damage model for concrete, in which the decrement of the plasticity threshold is associated with the change of a scalar damage variable. The model controls plastic behaviour using a pressure-dependent Drucker-Prager yield criterion as follows

$$F_p(\boldsymbol{\sigma}, \bar{\varepsilon}_p, D) = \alpha_p I_1 + \sqrt{J_2} - (1-D)k \tag{2.9}$$

in which α_p and k are the Drucker-Prager friction and cohesion parameters, respectively. D denotes the scalar-valued damage parameter. A non-associated flow rule was employed, which requires a plastic potential function of the form

$$G(\boldsymbol{\sigma}, \bar{\varepsilon}_p) = \beta_d I_1 + \sqrt{J_2} \tag{2.10}$$

where β_d is a dilatation parameter used to control inelastic volume expansion. The damage loading function used in the model was derived as follows

$$F_d(Y_v, D) = Y_v - r_d(D) \tag{2.11}$$

in which

$$Y_v = \frac{1}{2} K_0 \left\langle \varepsilon_v^e \right\rangle^2 + m \int_0^{\varepsilon_v^p} |\sigma_m| \left\langle d\varepsilon_v^p \right\rangle$$

$$m = m_t \text{ for } \varepsilon_v^e > 0 \quad \text{and} \quad m = m_c \text{ for } \varepsilon_v^e < 0$$

Y_v is the volumetric thermodynamic conjugate force for damage. K_0 and σ_m denote the undamaged bulk modulus of the intact material and mean nominal stress, respectively. ε_v^e and ε_v^p are the volumetric parts of the elastic and plastic strain, respectively and r_d is the energy resistance function. m_t and m_c are model parameters, which were introduced in the damage function to capture the tensile and compressive behaviour of quasi-brittle materials separately. The use of a single scalar damage indicator hinders the model to be used for cases where load reversal takes place.

2.3.4 Microplane models

The development of microplane formulations dates back to the year 1938, when Taylor (1938) came up with a brilliant idea of characterising the constitutive behaviour of polycrystalline metals by relations between stress-strain vectors acting on planes of various orientations within the material. Using Taylor's idea as the starting point, Batdorf and Budianski (1949) successfully formulated the theory, famously known as the 'slip theory of plasticity' and developed a realistic model for plastic-hardening metals. The slip theory is based on the assumption that the stress vectors acting on the various slip planes

in the material are the projection of the macroscopic stress tensor, or in other words, statically constrained. This constraint creates material instability when a strain-softening constitutive law is introduced, and thus, lacks of the ability to model damage in quasi-brittle materials (Bažant 1984).

This led to the emergence of the microplane model, later labelled M1, which was first devised to describe tensile failure of concrete (Bažant 1984; Bažant and Oh 1985; Bažant and Gambarova 1984). The microplanes can be interpreted as weak links between aggregate particles and the cement matrix. The microplane theory differs from the slip theory in that instead of the static constraint, the kinematic constraint is introduced in the microplane theory. The strain vectors on each plane are now assumed to be the projection of the macroscopic strain tensor, as shown in Figure 2.11. Despite satisfactory results predicted in tension and shear, the formulation is incapable of capturing the volumetric-deviatoric interaction observed under compressive stresses for concrete.

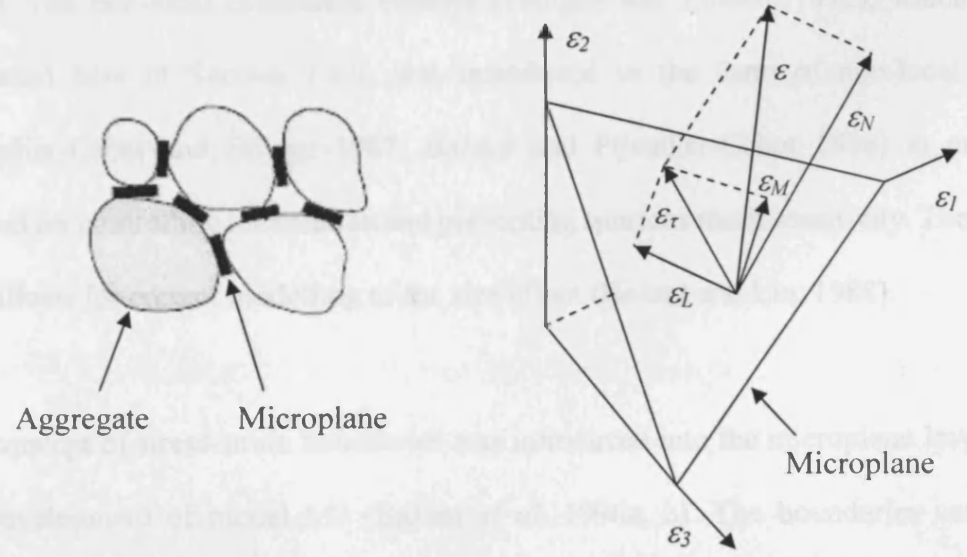

Figure 2.11. Decomposition of macroscopic strain tensor on the microplane

Bažant and Prat (1988a,b) extended Model M1 to describe the behaviour of postpeak softening damage in both compression and tension. The model, labelled Model M2, introduces a volumetric-deviatoric split of the normal stresses and strains on the microplanes. This allows for the simulation of high inelastic deviatoric strain on the microplanes parallel to the direction of compression or by slip on inclined microplanes. However, it was found that the separation of normal strains into the volumetric and deviatoric parts led to excessively large positive lateral strains being developed in the tail of softening under unixaxial tensile stress (Jirásek 1993). This is due to the localisation of tensile strain softening into the volumetric strain, while the deviatoric strains on the strain softening microplanes undergo unloading.

The microplane model of Bažant and Prat (1988a,b) was further improved by the inclusion of the non-local continuum concept, which enables the new model to describe cyclic loading, rate effect, cracking and nonlinear triaxial behaviour (Ožbolt and Bažant, 1992). The non-local continuum concept (Eringen and Edelen, 1972), which will be discussed later in Section 2.4.2, was introduced in the form of non-local damage (Pijaudier-Cabot and Bažant 1987; Bažant and Pijaudier-Cabot 1988) to provide a method for controlling localisation and preventing spurious mesh sensitivity. The concept also allows for correct modelling of the size effect (Bažant and Lin, 1988).

The concept of stress-strain boundaries was introduced into the microplane level within the development of model M3 (Bažant *et al.* 1996a, b). The boundaries and elastic behaviour are defined as functions of different strain components. This facilitates the

simultaneous modeling of tensile, compressive and shear softening behaviours of the material. A strain-independent linear frictional-cohesive yield surface was introduced, which relates the normal and shear stress components on the microplane. To remedy the drawback encountered in model M2, an additional softening tensile stress-strain boundary was employed, which is defined in terms of the total normal strains.

An alternative solution for the pathological behaviour of the microplane M3 model was introduced by Ožbolt *et al.* (2001). The improved model preserves the conceptual simplicity of the model formulation based on the kinematic constraint approach, however, the kinematic constraint is relaxed at the microplane level. This was achieved by splitting the microplane strain component into the effective and relaxed part using the discontinuity function, which is related to the volumetric stress-strain relationship.

Further development on the microplane model has been made, within which a work-conjugate volumetric-deviatoric split was introduced (Bažant *et al.* 2000a). The microplane model M4 also presents strain independent horizontal boundaries for the normal and deviatoric stresses on the microplanes. These boundaries enable the model to capture the yield capacity due to the smooth roundness of stress peaks in unconfined compression and tension. In this model, the linear frictional yield function presented in model M3 was replaced with a frictional non-linear boundary. This is to remedy the incorrect prediction of high stresses with very high hydrostatic pressures. The way in which the material parameters are identified was explored with a new fitting procedure introduced. A method to control the steepness and tail length of post-peak softening was

presented along with damage modeling with a reduction of unloading stiffness and crack-closing boundary. The performance of model M4 was further improved by developing the model within a thermodynamically consistent framework (Carol *et al.* 2001; Kuhl *et al.* 2001).

Most of the microplane models described so far were developed for small strains, except for model M3, which has been generalised to finite strain. Bažant *et al.* (2000b) modified the microplane M4 model by introducing the back-rotated Cauchy (true) tensor as the stress measure. Green's Lagrangian tensor was introduced due to the strain tensor conjugate to the back-rotated Cauchy (or Kirchoff) stress tensor being unsuitable because of its path dependency.

In the latest microplane model M5, Bažant and Caner (2005a,b) employed hybrid constraints, i.e. static and kinematic constraints, to better simulate the tensile cohesive fracture by removing the incorrectly predicted excessive lateral contraction or expansion and stress locking at very large postpeak tensile strains. The kinematic constraint was used to describe hardening nonlinear triaxial behaviour, and coupled with the static constraint which is responsible for the simulation of cohesive tensile fracture. A new iterative algorithm was introduced to facilitate the coupling procedure and thus, overall convergence properties. The cohesive softening stiffness matrix, which is based on the fracture energy of concrete and the effective crack spacing, was used as the predictor and the hardening stiffness matrix as the corrector that returns the current stress point to the stress-strain boundaries. This method is in contrast to the classical iterative return

mapping algorithm for hardening elasto-plastic behaviour, in which the roles of predictor and corrector are interchanged.

2.4 Computational modelling

Tensile failure in heterogeneous materials like concrete involves the initiation of microcracks, after which the softening processes continue with crack growth, branching and coalescence into a dominant crack which separates the material. Numerous numerical tools have been developed to simulate cracking in concrete. The discrete and smeared crack concepts are traditionally the two most popular methods adopted by researchers to simulate the behaviour of cracked concrete.

2.4.1 Approaches to modelling cracking

In the discrete crack approach, a crack is introduced as a discontinuity in the geometry of the structure (Ngo and Scordelis 1967). In this approach, the crack is formed when the nodal force at the node ahead of the crack tip exceeded a tensile strength criterion. Crack propagation is simulated by splitting the node into two and assuming the tip of the crack to propagate to the next node. The procedure is repeated when the tensile strength criterion is violated at this node. One of the advantages of discrete models is their applicability to relatively coarse finite element meshes. In addition, discrete models can reproduce anisotropy that arises naturally in a cracked material.

However, there are also a few drawbacks which limit their applicability to model cracking. Among these is the mesh-induced directional bias in crack representation which is inevitable if the crack path is not known a priori. Another drawback of the discrete crack approach is the continuous change in topology during the propagation of cracks. This process requires the application of intensive remeshing techniques, which are computationally expensive especially in three-dimensional finite element analysis. The efficiency of the approach is also greatly reduced in the case of multiple crack situations.

In the smeared crack approach, fracture is represented in a smeared manner, in which an infinite number of parallel cracks with small opening are distributed over the finite element. The idea is based on experimental observation, whereby small cracks are formed within a heterogeneous material, and linked up at the later stage of the loading process to form dominant cracks. The smeared crack approach is preferable to the discrete as it does not involve remeshing techniques and continuous change of mesh topology. The deterioration process of the material is captured using a non-linear constitutive relation with strain softening. The propagation of cracks in the volume that is attributed to an integration point is simulated by a deterioration of the stiffness and strength at that integration point. The weakness of smeared crack models is their proneness to mesh sensitivities. There exist two types of mesh sensitivities, i.e. mesh sensitivity with respect to the shape of the finite elements, and mesh sensitivity with respect to the size of the elements (Petrangeli and Ožbolt 1996).

Probably the earliest smeared crack model for concrete cracking was by Rashid (1968). In this approach, a crack is assumed to form when the maximum tensile stress in the element exceeds a critical value. The constitutive equation is then modified such that the stress normal to the crack plane becomes zero. This representation of a complete loss of stiffness at the onset of failure leads to numerical difficulties. The crack model also exhibits pathological sensitivity to the mesh size.

The inclusion of the shear retention factor improves the capability of fixed smeared crack models by taking into account the interaction between tensile and shear components of the tractions. It can be regarded as a representation of some effects of aggregate interlocking and friction within the crack. Traditional smeared crack models for concrete fracture suffer from stress locking, i.e. by spurious stress transfer across a widely open crack. For fixed crack models with a nonzero retention factor, locking is mainly due to shear stresses generated by a rotation of the principal strain axes after the crack initiation. Later improvements treated the retention factor as a function of the crack opening, decaying to zero as the crack opens wide.

In the rotating crack model (Rots 1988), the crack is always orientated in a direction normal to the principal stress. This prevents the build up of spurious stresses tangential to the crack. The use of the shear retention factor is also omitted because the shear stiffness coefficient is uniquely defined by the assumption that the axes of principal stress and strain coincide. However, stress locking is still observed due to the poor kinematic representation of the discontinuous displacement field around a macroscopic crack.

2.4.2 Regularisation techniques

Upon closer observation of a fracture, it appears that it is often preceded by the formation of a process zone in which damage and other inelastic effects accumulate. This phenomenon is commonly known as strain localisation, or localisation of deformation. Strain localisation occurs in the form of the localised accumulation of microcracks in concrete under low confining pressures. The inadequacy of conventional continuum models to simulate the behaviour of softening materials has been recognised since the mid 1970s. Among the various problems encountered are the ill-posedness of boundary value problems, excessive damage localisation on refined mesh and pathological spurious mesh sensitivity. In the continuum approach, non-local and gradient enhanced models have been shown to be effective in overcoming such a problem i.e. mesh dependency.

Non-local continuum models, in general, consider the interaction of particles. Within a non-local continuum, the stress at a point depends not only on the strain at that point but also on the strain field in the neighbourhood of that point. The approach consists of replacing a certain variable by its non-local counterpart obtained by weighted averaging over a spatial neighbourhood of each point under consideration. These spatial averaged state variables are introduced into the classical constitutive relations. The non-local continuum models preserve material stability by avoiding localisation. They also produce solutions that are free from mesh sensitivities. Bažant (1984) and Bažant *et al.* (1984) introduced the concept of non-local averaging to strain-softening materials. The method was later improved by Pijaudier-Cabot and Bažant (1987) who developed a non-local

damage theory. Other constitutive models include the non-local smeared crack model (Bažant and Lin 1988a), the plasticity-based model with softening yield limit (Bažant and Lin 1988b) and the non-local microplane model (Bažant and Ožbolt 1990; Ožbolt and Bažant 1992).

Despite the success of non-local continuum models in generating mesh-objective solutions, the regularisation technique has not been without its drawbacks. In particular, for integral models, the difficulty encountered when dealing with a complex shaped structure, the need to change existing computing codes due to the implementation of a consistent numerical solution procedure, the presence of inconsistent tangent operators which dramatically degrades convergence characteristics, have all limited their usefulness (Peerlings *et al.* 1996).

Addessi *et al.* (2002) developed an elasto-plastic non-local damage model to simulate the mechanical behaviour of cementitious materials. The local damage model is regularised by the introduction of the Laplacian damage variable in the loading function, which is related to the material characteristic length that controls the size of the localisation zone. The fact that the damage evolution process is now governed by the differential equation makes the evaluation of the tangent constitutive matrix more difficult to perform.

Enhanced gradient models have been developed in recent years to overcome the limitations of classical continuum models for softening problems through the inclusion of higher-order gradient terms and an internal length scale related to the specific material (de

Borst 2001; Askes and Metrikine 2005; Peerlings *et al.* 1996). One of the basic features of higher-order models is the need to generate fine meshes in the localisation zone for capturing high strain gradients. Hence, prior knowledge of the failure zone is necessary. This hinders the applicability of higher order models for large-scale three-dimensional problems due to the high computational costs involved.

Despite the success of both non-local and gradient-enhanced continuum models in generating mesh-objective solutions, it has been found that the use of a non-local dissipation-driving state variable results in an incorrect prediction of damage initiation away from the crack tip in mode-I problems. Also, the approach was found to produce wrong failure pattern in certain cases of shear band problems (Simone *et al.* 2004).

The concept of strain or displacement discontinuities embedded into standard finite elements has been explored by several researchers as a method of overcoming the mesh dependency of classical continuum models and the dependency of discrete models on mesh alignment, when separation is only possible at element interfaces. The choice of an appropriate constitutive model suitable for implementation in an element with an embedded discontinuity is governed by the type of the discontinuity, i.e. weak (strain) and strong (displacement) discontinuity (Mosler and Meshke 2003; Oliver *et al.* 2004).

For models incorporating weak discontinuities, it is sufficient to postulate a continuum stress-strain law (Sluys and Berends 1998). Two discontinuity lines are incorporated into the strain field to form a localisation band. This approach avoids the need to deal with

unbounded strains as a result of a displacement jump, but the ability of such an approach to overcome mesh-alignment dependence and to reproduce full mode-I crack opening is questionable since elements are not kinematically enhanced.

Models with strong discontinuities, in addition to a stress-strain law for the material, also require a traction-separation law governing the behaviour of the embedded crack (Larsson and Runesson 1996). The embedded crack is represented by a single discontinuity line in the displacement field. The embedment of discontinuities within elements allows the use of relatively large elements compared to the width of the localisation zone, making the method suitable for three-dimensional and large scale applications (Simo *et al.* 1993).

Stress locking that appears in smeared crack models can be eliminated by improving the kinematic representation of highly localized fracture. According to Jirásek (2000), the techniques of incorporating a discontinuity (of strain or displacements) into the interior of a finite element can be classified into three different groups, i.e. statically optimal symmetric (SOS), kinematically optimal symmetric (KOS), and statically and kinematically optimal non-symmetric (SKON). The SOS formulation works with a natural stress continuity condition, but it does not properly reflect the kinematics of a completely open crack. On the other hand, the KOS formulation describes the kinematic aspects satisfactorily, but it leads to an awkward relationship between the stress in the bulk of the element and the tractions across the discontinuity line. The SKON formulation deals with a very natural stress continuity condition and is capable of properly

representing complete separation at late stages of the fracturing process, without any locking effects (spurious stress transfer).

Conventional embedded crack approaches have been found to predict incorrectly the direction of the displacement discontinuity at the onset of cracking (Jirásek and Zimmerman 2001a,b). It has been suggested that diffuse damage at early stages of material degradation is adequately captured by a model dealing with inelastic strain, while highly localised fracture is better represented by a displacement discontinuity. In order to simulate such a cracking process, Jirásek and Zimmerman (2001a,b) developed a delayed embedded crack model (DEC), which may be described as a smeared crack model with transition to an embedded crack.

The DEC model employs the smeared crack approach immediately at the onset of cracking to describe the displacement discontinuity, and activates an embedded crack at later stages when the crack has reached a certain critical crack opening. At every material point, the crack is smeared until it reaches a critical opening value, after which a displacement discontinuity is introduced into the respective finite element. The DEC model is capable of producing results free from stress locking. However, the use of the smeared crack approach results in the formation of a cracking band which is biased by the orientation of finite element mesh. This problem can be alleviated if the smeared part of the model is reformulated as non-local.

Sukumar *et al.* (2000) employed the extended finite element method (X-FEM) to alleviate shortcomings associated with meshing of the crack surfaces in existing methods. The finite element approximation was enriched by additional functions through the notion of partition of unity (Babuška and Melenk 1997) to model the presence of cracks, voids or inhomogeneities. The enriched displacement approximation can be written in the form

$$u = \sum_{i=1}^{n} N_i \left(\bar{a}_i + \sum_{j=1}^{m} \Psi_j \tilde{a}_{ij} \right) \tag{2.12}$$

where n denotes the number of nodes of the finite element model; N_i ($i = 1, 2 .. n$) are the standard shape functions; $\bar{a}_i$ ($i = 1, 2 .. n$) are the standard displacement degrees of freedom; Ψ_j ($j = 1, 2 .. m$) are the global enrichment functions; and $\tilde{a}_{ij}$ are the additional degrees of freedom associated with node i and enrichment function j.

In the model, a discontinuous function was used to model the interior of the crack surface, and functions from the two-dimensional asymptotic crack-tip displacement fields were added for the crack front enrichment. The method provides a robust and versatile numerical tool to solve crack problems in complex structural components without the need to explicitly align the mesh with the crack.

The superior kinematic properties and numerical robustness provided by extended finite elements based on the partition of unity have made the technique more preferable than traditional elements with embedded discontinuities based on incompatible discontinuous

modes (Daux *et al.* 2000; Dolbow *et al.* 2001). However, this regularisation technique requires relatively complicated implementation and also the need to add new global degrees of freedom during the simulation, as well as to refine integration scheme in the enriched area around the crack (Jirásek and Belytschko 2002). Figure 2.12 shows comparisons of characteristics between the standard finite element (smeared), element with embedded discontinuity and extended finite element in a separation test.

Another method, which has also been successful in solving a certain class of finite element problems, has been explored by several researchers in recent years. The meshless, or mesh-free methods, which is based on node analysis, demonstrates flexibility in modelling complex discontinuities, as well as avoids the distortion of mesh when extreme large deformation is encountered. The method also provides an efficient means for addressing high gradient problems such as that occurred in strain localisation.

Belytschko and Black (1999) developed a minimal remeshing finite element method for crack growth. Cracks and crack growth can be modelled by finite elements with no remeshing. The essential idea in this method is to add enrichment functions to the approximation which contains a discontinuous displacement field by means of the partition of unity finite element method. This allows for the solving of most crack growth problems without any remeshing. However, some remeshing near the crack root is still necessary in order to capture severely curved cracks. This method also allows crack tips to be represented inside an element.

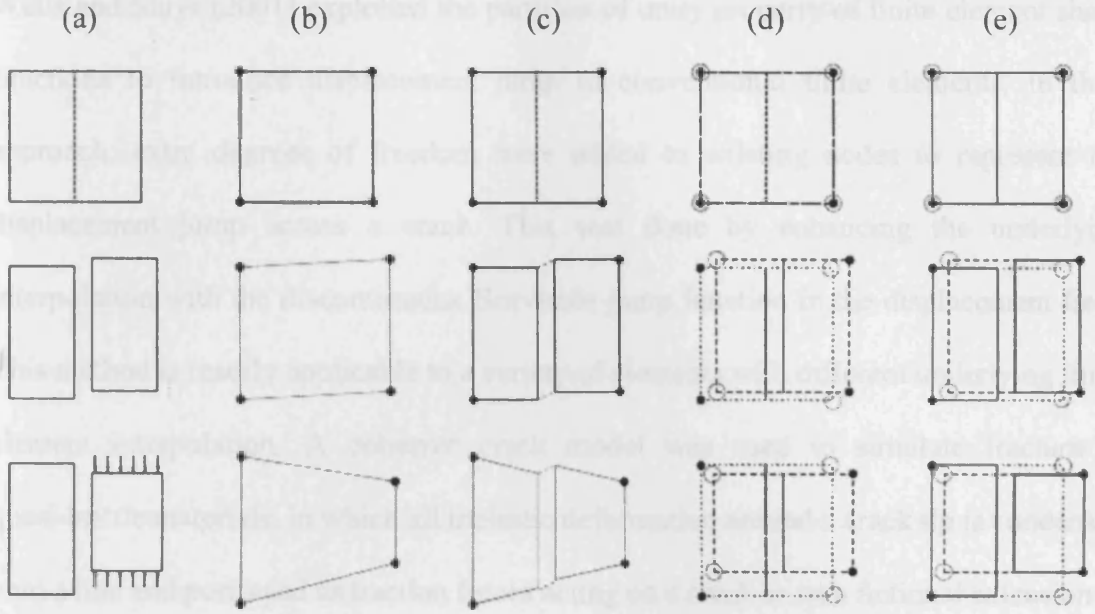

Figure 2.12. Separation test: (a) real body, (b) standard finite element (smeared), (c) element with embedded discontinuity, (d-e) extended finite element

In the aforementioned remeshing technique, curved cracks were treated by mapping the straight crack enriched field. This is not readily applicable to long cracks or three dimensions. Möes *et al.* (1999) improved the method by incorporating a discontinuous field across the crack faces away from the crack tip by means of the generalised Heaviside function. The technique also exploits the partition of unity property of finite elements, in which a standard approximation is enriched in a region of interest by the local functions in conjunction with additional degrees of freedom. The enrichment functions were the near-tip asymptotic fields and a discontinuous function to represent the jump in displacement across the crack line. The only drawback of the method is the need for a variable number of degrees of freedom per node.

Wells and Sluys (2001) exploited the partition of unity property of finite element shape functions to introduce displacement jump to conventional finite elements. In their approach, extra degrees of freedom were added to existing nodes to represent the displacement jump across a crack. This was done by enhancing the underlying interpolation with the discontinuous Heaviside jump function in the displacement field. This method is readily applicable to a variety of elements with different underlying finite element interpolation. A cohesive crack model was used to simulate fracture in quasi-brittle materials, in which all inelastic deformation around a crack tip is condensed onto a line and portrayed as traction forces acting on a crack or on a fictional extension of a crack. The bulk of the material away from the discontinuity was treated to be elastic.

The results obtained were insensitive to the mesh structure and also element size. The model is also capable of modelling curved crack, which has proved difficult with other models. A crucial advantage over conventional interface elements is that deformations at the discontinuity are purely inelastic. This bypasses the reliability of a 'dummy' elastic stiffness to achieve numerical stability. Numerical examples showed that the model is capable of giving excellent results with relatively coarse meshes, though it is still necessary to use fine meshes in regions with high stress gradients in order to accurately evaluate the normal vector to the discontinuity path.

de Borst *et al.* (2004) developed a crack model based on the cohesive-segment method for heterogeneous materials. The model is capable of describing the heterogeneity characteristic of concrete, including the processes of crack initiation, growth, coalescence

and branching. These processes are mainly due to the presence of particles with different sizes and stiffnesses within the matrix. The model employs a decohesion constitutive relation, which specifies the conditions for crack nucleation and also the direction of crack propagation.

A cohesive segment was introduced to represent the discontinuity when the criterion for crack initiation is met. The cohesive segment was inserted through the integration point and orientated such that it is orthogonal to the direction of the major principal stress. The magnitude of the displacement jump was determined by a set of additional degrees of freedom which were added to all nodes whose support is crossed by the cohesive segment. This was done by exploiting the partition of unity property of finite element shape functions. The resulting model, which exhibits the advantages of both the discrete and smeared crack approaches, is capable of capturing the transition from distributed micro-cracking to a dominant crack.

2.5 Conclusions

In recent years, considerable effort has been made and good progress achieved in developing material models for concrete. Technology advances have allowed for the establishment of more rigorous models for the constitutive modelling of concrete. The ease of computational effort provides more accurate predictions of the behaviour of concrete under different loading conditions. This can be seen from the increased number of constitutive models developed over the years, ranging from the more common

plasticity and damage models, to models which are considered more complex and powerful such as the microplane models, and those developed using the combined theory of plasticity and continuum damage mechanics.

The consideration of softening related problems, such as strain localisation, play a crucial role in the development of constitutive models for concrete. Various regularisation techniques have been established to deal with the significant post-peak softening behaviour of concrete, the behaviour of which cannot be correctly captured by conventional continuum models.

The type of approach chosen for the proposed models presented in the following chapters of this thesis is the smeared crack concept. In addition, the constitutive models employ the plastic-damage concept to capture the behavioural characteristics of concrete in various stress states. This is because plasticity theory is well established and suitably proven to describe the behaviour of concrete when coupled with the theory of damage mechanics.

Chapter Three

Fundamental Theories

3.1 Introduction

This chapter serves to aid the understanding of the plastic-damage-contact models proposed later in this thesis. A brief description of the development of a classical plasticity model will be first presented, followed by the introduction of the theory of continuum damage mechanics.

3.2 Plasticity theory

The theory of plasticity deals with the calculation of stresses and strains in a deformed body, within which part or all of the body has yielded. Johnson and Mellor (1978) state that the most difficult problems to solve analytically in plasticity are those of constrained plastic flow, where part of the body has yielded and part is still elastic. It is difficult to handle the compatibility equations and the stress-strain relations, and very few complete solutions have been obtained to such problems. It is vital to consider the change in dimensions of the body, especially for cases where the plastic strains are large compared

with the elastic strains.

A general plasticity theory consists of four basic ingredients

- Elastic stress-strain relationship prior to plastic yielding
- Yield criterion which indicates the onset of plastic straining
- Flow rule which describes the direction of plastic strains
- Hardening law which indicates the change of yield stress during the course of plastic flow

Prior to introducing the development of the plasticity component of the crack model, the author feels that it is necessary to describe briefly the fundamental theory behind the overall development of the constitutive model.

3.2.1 Elastic stress-strain relationship

The overall strain vector ε is assumed to be the sum of both elastic, ε_e and inelastic, ε_p strain components

$$\varepsilon = \varepsilon_e + \varepsilon_p \tag{3.1}$$

A relationship between the elastic stress σ and strain can then be expressed by means of the elastic stiffness matrix as

$$\boldsymbol{\sigma} = \boldsymbol{D}_e(\boldsymbol{\varepsilon} - \boldsymbol{\varepsilon}_p) \tag{3.2}$$

where

$$\boldsymbol{D}_e = E\frac{1-\nu}{(1+\nu)(1-2\nu)}\begin{bmatrix} 1 & \alpha_1 & \alpha_1 & 0 & 0 & 0 \\ \alpha_1 & 1 & \alpha_1 & 0 & 0 & 0 \\ \alpha_1 & \alpha_1 & 1 & 0 & 0 & 0 \\ 0 & 0 & 0 & \alpha_2 & 0 & 0 \\ 0 & 0 & 0 & 0 & \alpha_2 & 0 \\ 0 & 0 & 0 & 0 & 0 & \alpha_2 \end{bmatrix}, \quad \alpha_1 = \frac{\nu}{1-\nu}, \quad \alpha_2 = \frac{1-2\nu}{2(1-\nu)}$$

$$\boldsymbol{\sigma} = \begin{bmatrix} \sigma_{xx} & \sigma_{yy} & \sigma_{zz} & \tau_{xy} & \tau_{yz} & \tau_{xz} \end{bmatrix}^T, \quad \boldsymbol{\varepsilon} = \begin{bmatrix} \varepsilon_{xx} & \varepsilon_{yy} & \varepsilon_{zz} & \gamma_{xy} & \gamma_{yz} & \gamma_{xz} \end{bmatrix}^T$$

$\boldsymbol{D}_e$ denotes the isotropic elastic constitutive matrix, and E and ν are Young's modulus and Poisson's ratio respectively. It should be borne in mind that matrices and vectors are represented by bold letters. Figure 3.1 shows a uniaxial stress-strain relationship of an ideally plastic material.

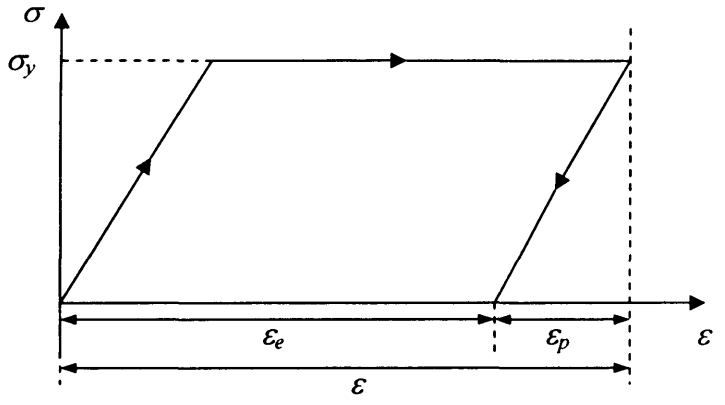

Figure 3.1. Uniaxial stress-strain relationship

3.2.2 Yield criteria

For a randomly selected stress loading path, the stress remains elastic providing the yield criterion has not been violated. The criterion introduces a stress limit at which any stresses that reach or pass the limit will become irrecoverable, or in order words, some of the strain becomes permanent plastic strain. In a one-dimensional problem, the limit is simply a scalar value termed the yield stress σ_y, whilst in a three-dimensional problem, the scalar value controls the size of the yield surface. A convex yield surface allows separation of the regions of purely elastic and plastic response in stress space. The following conditions determine the state of a material.

$F(\sigma,\kappa) < 0$ material is elastic, with the current stress state within the current yield surface

$F(\sigma,\kappa) = 0$ material has yielded, with the current stress state on the yield surface

The yield function, F is derived based on the stress state σ and a hardening parameter κ.

3.2.3 Flow rule

For situations where a material has yielded, both the direction and size of the plastic strain increment can be obtained via the introduction of a flow rule, which can exist in either associated or non-associated form. Figure 3.2 illustrates the difference between associated and non-associated flow rules. Owen and Hinton (1980) state that there exists

a direct proportional relationship between the plastic strain increment and the stress gradient of a function known as the plastic potential G such that

$$\delta\boldsymbol{\varepsilon}_p = \delta\lambda \frac{\partial G}{\partial \boldsymbol{\sigma}} \tag{3.3}$$

where λ is a proportionality constant, and is termed the plastic multiplier. The direction of the plastic strain increment is normal to the surface of the plastic potential, as indicated by the above equation. The plastic potential function can be defined in a manner similar to that of the yield function, i.e. in terms of the stress vector $\boldsymbol{\sigma}$ and hardening parameter κ.

$$G = G(\boldsymbol{\sigma}, \kappa) \tag{3.4}$$

Equation (3.3) shows a typical expression of a non-associated flow rule. Vermeer and de Borst (1984) suggest that for highly isotropic materials, it may be reasonable to assume both the yield function and the plastic potential function to be the same. This leads to an associated flow rule that can be defined as

$$\delta\boldsymbol{\varepsilon}_p = \delta\lambda \frac{\partial F}{\partial \boldsymbol{\sigma}} \tag{3.5}$$

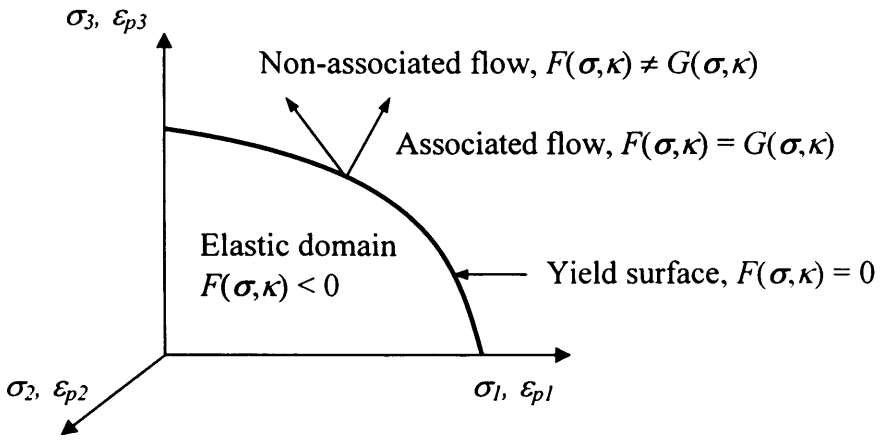

Figure 3.2. Associated and non-associated flow rule

3.2.4 Hardening rule

Once initial yielding has occurred, the stress level at which further plastic deformation will occur depends upon the current level of plastic straining. This suggests that the evolution of the yield surface is governed by the form of hardening law adopted (Owen and Hinton 1980). The relationship between the hardening parameter κ and the plastic strain increment can be expressed as

$$\kappa = \kappa(\varepsilon_p) \tag{3.6}$$

In general, there exist two plastic hardening rules that have been widely used in plasticity models. These are

- *Isotropic hardening* – yield surface is allowed to expand or contract uniformly in all directions, as depicted in Figure 3.3(a)
- *Kinematic hardening* – the yield domain remains unchanged, but the surface is allowed to move in stress space, as shown in Figure 3.3(b)

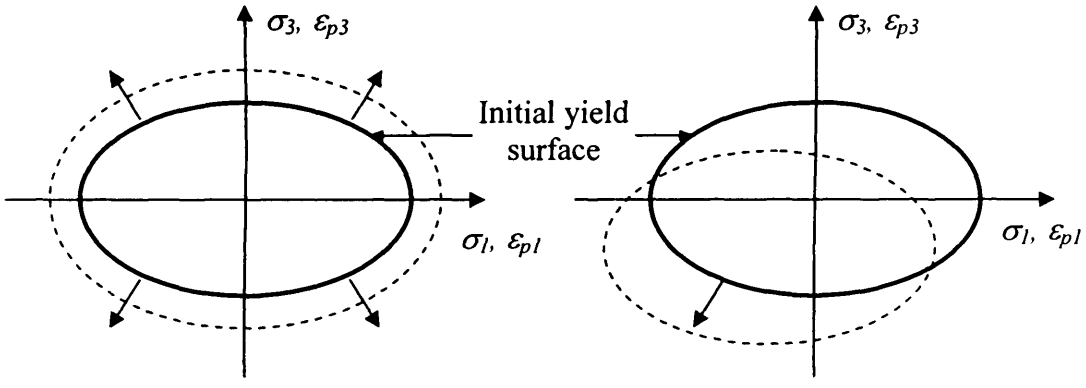

(a) Isotropic (b) Kinematic

Figure 3.3. Plastic hardening rules

3.2.5 Elasto-plastic constitutive matrix

Once the yield function has a value greater than zero the standard elasticity matrix is no longer valid and a new matrix must be developed. One of the conditions to be satisfied upon developing a plasticity model is for the stress to remain on the yield surface throughout the process of plastic straining. This can be explained mathematically by the following expression

$$F(\boldsymbol{\sigma}, \kappa) = 0 \tag{3.7}$$

If the yield surface is hardening, due to the applied loading, the following expression must also be satisfied.

$$\delta F(\boldsymbol{\sigma}, \kappa) = 0 \tag{3.8}$$

Expanding (3.8) yields the consistency condition as

$$\frac{\partial F}{\partial \boldsymbol{\sigma}}^T \delta\boldsymbol{\sigma} + \frac{\partial F}{\partial \kappa}\delta\kappa = 0 \tag{3.9}$$

Having considered the basic parts of a classical plasticity model it is now possible to define the elasto-plastic incremental stress-strain relationship.

Utilising equations (3.2), (3.3) and (3.6) in (3.9), and collecting terms yields

$$\delta\lambda = \frac{\frac{\partial F}{\partial \boldsymbol{\sigma}}^T \boldsymbol{D}_e}{H + \frac{\partial F}{\partial \boldsymbol{\sigma}}^T \boldsymbol{D}_e \frac{\partial G}{\partial \boldsymbol{\sigma}}}\delta\boldsymbol{\varepsilon} \tag{3.10}$$

where

$$H = -\frac{\partial F}{\partial \kappa}\frac{\partial \kappa}{\partial \varepsilon_p}^T \frac{\partial G}{\partial \boldsymbol{\sigma}}$$

Substituting (3.10) into the elastic stress-strain relationship gives

$$\delta\boldsymbol{\sigma} = \boldsymbol{D}_{ep}\delta\boldsymbol{\varepsilon} \tag{3.11}$$

where

$$\boldsymbol{D}_{ep} = \boldsymbol{D}_e - \frac{\boldsymbol{D}_e \dfrac{\partial G}{\partial \boldsymbol{\sigma}} \dfrac{\partial F}{\partial \boldsymbol{\sigma}}^T \boldsymbol{D}_e}{H + \dfrac{\partial F}{\partial \boldsymbol{\sigma}}^T \boldsymbol{D}_e \dfrac{\partial G}{\partial \boldsymbol{\sigma}}}$$

$\boldsymbol{D}_{ep}$ is the iterative elasto-plastic constitutive matrix and H denotes the hardening parameter.

3.2.6 Stress recovery algorithm

During plastic straining, the process of 'pushing' the yield surface to the new stress point is governed by a stress recovery algorithm. The following describes the stress recovery algorithm as proposed by Ortiz and Simo (1986) using a 'tangent cutting' formulation. The return mapping algorithm can be defined based upon the elastic-plastic split in the strain increment by first integrating the elastic equations to obtain an elastic predictor. The initial elastically predicted stress is then relaxed until the yield surface satisfying the elasto-plastic state is reached. Figure 3.4 shows the 'steepest descent return path' for the case of isotropic hardening.

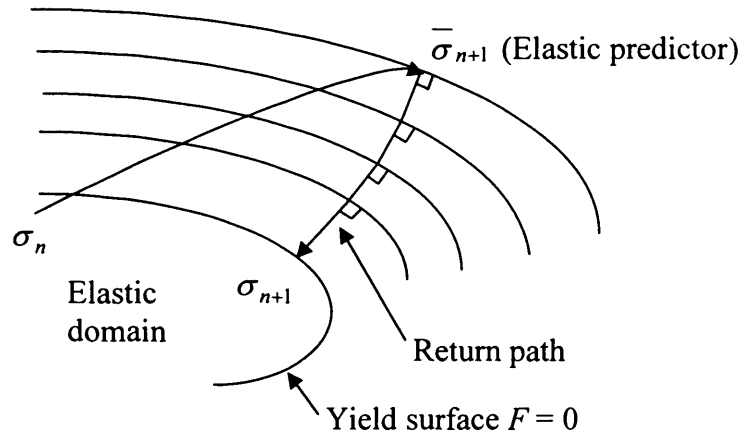

Figure 3.4. Steepest descent return path for the case of isotropic hardening

- Calculate the trial stress $\boldsymbol{\sigma}_{tr}$. This is the 'elastic predictor' referred to by Ortiz and Simo (1986) and can be defined as

$$\boldsymbol{\sigma}_{tr} = \boldsymbol{\sigma}_{old} + \boldsymbol{D}_e \delta\boldsymbol{\varepsilon} \tag{3.12}$$

- Evaluate the yield function F at $\boldsymbol{\sigma}_{tr}$. If the yield function is less than zero then the material has not yielded for the current applied load increment. At this stage the material is assumed to behave elastically and thus the stress recovery procedure is completed. If the material has yielded, i.e. $F > 0$, then,
  - Evaluate the yield function gradient $\dfrac{\partial F}{\partial \boldsymbol{\sigma}}$ and the plastic potential function gradient $\dfrac{\partial G}{\partial \boldsymbol{\sigma}}$
  - Evaluate the hardening parameter H

- Compute the plastic multiplier $\delta\lambda$

$$\delta\lambda = \frac{F}{H + \frac{\partial F}{\partial \boldsymbol{\sigma}}^T \boldsymbol{D}_e \frac{\partial G}{\partial \boldsymbol{\sigma}}} \tag{3.13}$$

- Update the trial stress $\boldsymbol{\sigma}_{tr}$

$$\boldsymbol{\sigma}_{tr} = \boldsymbol{\sigma}_{old} - \boldsymbol{D}_e \frac{\partial G}{\partial \boldsymbol{\sigma}} \delta\lambda \tag{3.14}$$

- Update the state variables i.e. λ, κ, ε_p
- Re-evaluate the yield function at the new trial stress
- If converged to within the specified tolerance, exit the stress recovery loop, otherwise return to the start of the stress recovery loop

- End stress recovery procedure

Figure 3.5 shows diagrammatically the stress recovery algorithm. Implementation of the aforementioned algorithm in finite element codes has posed difficulties in obtaining solutions for problems that involve large time steps in particular. This is due to the loss of the asymptotic rate of quadratic convergence characteristics of Newton's methods. Simo and Taylor (1986) suggested that a consistent tangent operator should be used instead, along with the implicit stress recovery algorithm, in order to optimise the overall computational cost.

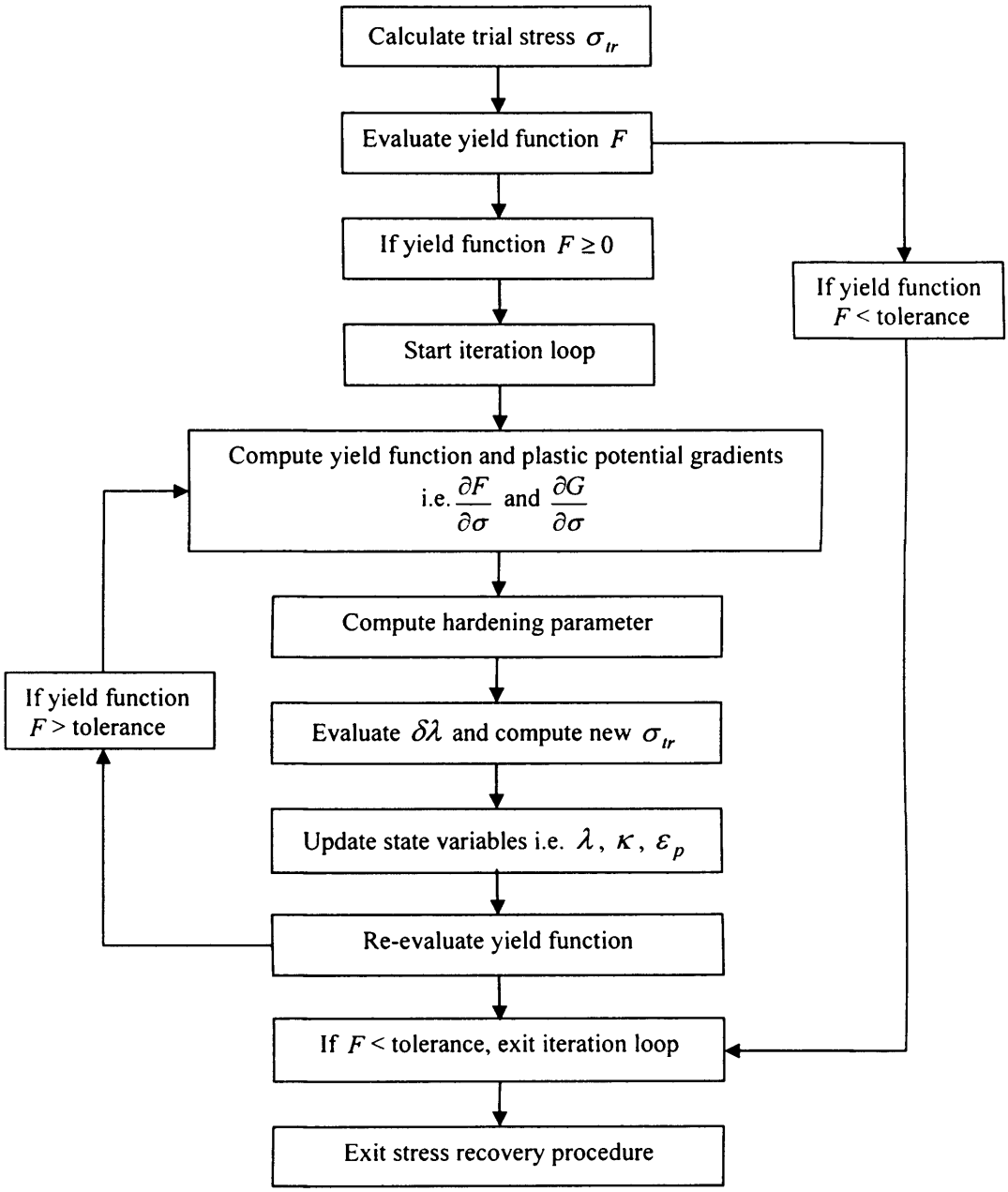

Figure 3.5. Stress recovery algorithm

3.3 Continuum damage mechanics

3.3.1 Concepts of damage mechanics

The concept of effective stress is based on considering a fictitious undamaged configuration of a body and comparing it with the actual damaged configuration. The concept can be explained with the aid from Figure 3.6.

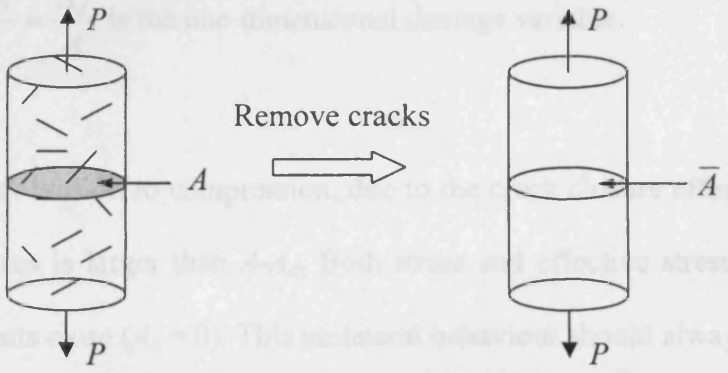

(a) Damaged body (b) Effective undamaged body

Figure 3.6. Cylindrical bar subjected to uniaxial tension

Consider the case of uniaxial tension with a scalar damage variable D. The bar is subjected to a uniaxial tensile load P. As a result of damage the virgin cross-sectional area A is reduced and becomes the effective cross-sectional area $\overline{A}=A-A_d$, with A_d being the total area of microcracks. The uniaxial tensile force P acting on the bar, as shown in Figure 3.6(a), is easily expressed using the formula $P=\sigma A$. Consider now a fictitious undamaged bar as shown in Figure 3.6(b). In this configuration, all damage is removed

from the bar. Given that both bars are subjected to the same tensile force, the uniaxial tensile force acting on the undamaged bar is expressed as $P = \bar{\sigma}\bar{A}$, where $\bar{\sigma}$ is the effective uniaxial stress. Equating the two expressions for P, the following expression for the effective uniaxial stress $\bar{\sigma}$ is derived

$$\bar{\sigma} = \frac{\sigma}{1-D} \tag{3.15}$$

where $D = \frac{A-\bar{A}}{A} = \frac{A_d}{A}$ is the one-dimensional damage variable.

In unloading from tension to compression, due to the crack closure effect, the effective cross-sectional area is larger than A-A_d. Both stress and effective stress become equal when all the defects close ($A_d = 0$). This unilateral behaviour should always be accounted for in the constitutive modelling of concrete materials.

The principle of strain equivalence follows directly the effective stress concept, as schematically explained in Figure 3.7. The hypothesis states (Lemaitre 1992):

"*Any strain constitutive equation for a damaged material may be derived in the same way as for a virgin material except that the usual stress is replaced by the effective stress*".

Application of the strain equivalence hypothesis results in the state of coupling between damage and elasticity, which, for a uniaxial case, can be expressed as

$$\sigma = \overline{E}\varepsilon \tag{3.16}$$

where $\overline{E} = (1 - D)E$ is the effective elasticity modulus.

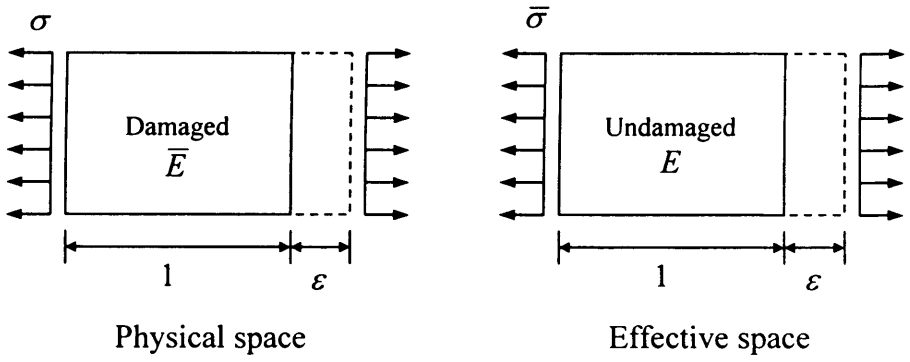

Figure 3.7. Hypothesis of strain equivalence

Similar to conventional plasticity models, damage models can also be developed within two alternative frameworks. In a strain-based formulation, damage is characterised through the effective stress concept along with the hypothesis of strain equivalence. On the contrary, in a stress-based formulation, the hypothesis of stress equivalence is used and damage is described through the effective strain concept. The hypothesis states (Simo and Ju 1987):

"*The stress associated with a damaged state under the applied strain is equivalent to the stress associated with its undamaged state under the effective strain*".

Figure 3.8 shows a schematic representation of the stress equivalence hypothesis.

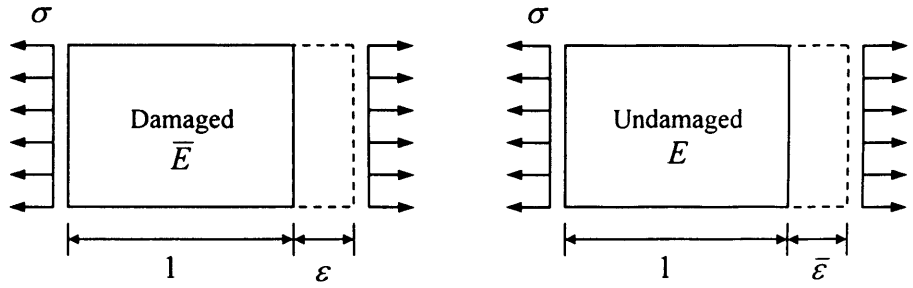

Figure 3.8. Hypothesis of stress equivalence

3.3.2 Elementary damage model

Consider the case of uniaxial tension with scalar damage variable. Figure 3.9 shows a system of m parallel bars with the same stiffness k. After the tensile strength in a particular bar is exceeded, a perfectly brittle behaviour is assumed, in which the stress drops to zero with no additional straining. Assuming that for a given displacement u, n bars are broken. The total force that is transmitted is equal to

$$P = \sum_{i=1}^{m-n} ku = (m-n)ku = (1-\frac{n}{m})EA\frac{u}{L} \tag{3.17}$$

in which E is the total stiffness of the system, and A and L denote the total cross-sectional area and the length of the bars respectively.

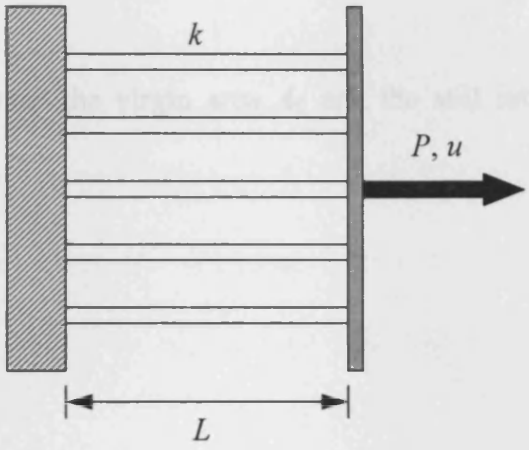

Figure 3.9. System of m parallel elastic-perfectly brittle bars

In going from a discrete to a continuum model, the macroscopically observed stress can be defined as

$$\sigma = \frac{P}{A} = (1-\omega)E\varepsilon \tag{3.18}$$

in which $\omega = n/m$ is the fraction of broken bars ranging from 0 to 1, and $\varepsilon = u/L$ denotes the strain in the bars. Utilising the concept of effective stress, the effective stress $\bar{\sigma}$ is related to area of unbroken bars as

$$\bar{\sigma} = \frac{P}{\bar{A}} = (1-\omega)\frac{EA\varepsilon}{\bar{A}} \tag{3.19}$$

For each individual bar, the following relation must hold

$$\bar{\sigma} = E\varepsilon \tag{3.20}$$

The relationships between the virgin area A_0 and the still intact area A can then be expressed as

$$\bar{A} = (1-\omega)A \tag{3.21}$$

Generalising (3.18) to three dimensions yields

$$\boldsymbol{\sigma} = (1-\omega)\boldsymbol{D}_e\boldsymbol{\varepsilon} \tag{3.22}$$

where $\boldsymbol{D}_e$ is the isotropic elastic stiffness matrix, either expressed in terms of Young's modulus and Poisson's ratio or in terms of shear and bulk moduli. As in plasticity, it is necessary to define a damage loading function. One relatively simple form being

$$f(\tilde{\varepsilon},\kappa) = \tilde{\varepsilon} - K \tag{3.23}$$

in which the equivalent strain $\tilde{\varepsilon}$ can generally be defined using the elastic energy.

$$\tilde{\varepsilon} = \frac{1}{2}\boldsymbol{\varepsilon}^T\boldsymbol{D}_e\boldsymbol{\varepsilon} \tag{3.24}$$

Alternatively, $\tilde{\varepsilon}$ can also be a function of the principal strains

$$\tilde{\varepsilon} = \sqrt{\sum_{i=1}^{3} \langle \varepsilon_i \rangle^2} \tag{3.25}$$

where ε_i are the tensile principal strains, and $\langle \varepsilon_i \rangle = \varepsilon_i$ if $\varepsilon_i > 0$ and $\langle \varepsilon_i \rangle = 0$ otherwise. K is a history dependent parameter, which takes an initial value K_0. During the loading history, K increases by taking the largest value ever attained of the equivalent strain.

Similar to plasticity models, an evolution law is also required for the damage variable ω, which is here defined as a function of K.

$$\omega = \omega(K) \tag{3.26}$$

A tangent operator for the constitutive relationships can be obtained by first differentiating equation (3.22)

$$\delta\boldsymbol{\sigma} = (1-\omega)\boldsymbol{D}_e\delta\boldsymbol{\varepsilon} - \delta\omega\boldsymbol{D}_e\boldsymbol{\varepsilon} \tag{3.27}$$

Given that $\omega = \omega(K)$, $K = K(\tilde{\varepsilon})$ and $\tilde{\varepsilon} = \tilde{\varepsilon}(\boldsymbol{\varepsilon})$ yields

$$\delta\omega = \frac{\partial\omega}{\partial K}\frac{\partial K}{\partial\tilde{\varepsilon}}\frac{\partial\tilde{\varepsilon}}{\partial\boldsymbol{\varepsilon}}^T \delta\boldsymbol{\varepsilon} \tag{3.28}$$

where $\frac{\partial K}{\partial \tilde{\varepsilon}} = 1$ Loading

$\frac{\partial K}{\partial \tilde{\varepsilon}} = 0$ Unloading

Substituting (3.28) in (3.27) yields the tangential stiffness relation for an isotropic elastic-damaging material

$$\delta\boldsymbol{\sigma} = \left[(1-\omega)\boldsymbol{D}_e - \frac{\partial \omega}{\partial K}\frac{\partial K}{\partial \tilde{\varepsilon}}\boldsymbol{D}_e\boldsymbol{\varepsilon}\frac{\partial \tilde{\varepsilon}}{\partial \boldsymbol{\varepsilon}}^T \right]\delta\boldsymbol{\varepsilon} \tag{3.29}$$

Noting that on unloading, the second term in the above equation becomes zero. Thus the tangent stiffness matrix takes the form of the secant stiffness matrix for unloading. This makes the damage theory different from standard plasticity theories, where unloading is according to the original elastic stiffness. Figures 3.10 and 3.11 show typical uniaxial stress-strain curves for both plasticity and damage models for concrete materials subjected to compressive and tensile loadings respectively.

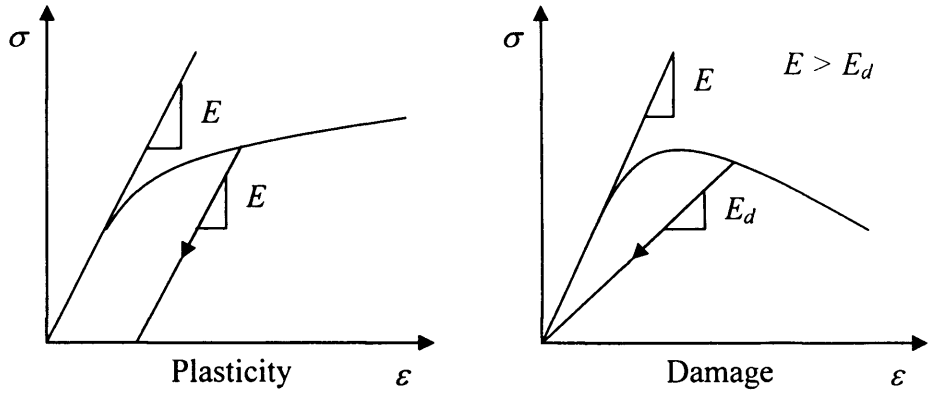

Figure 3.10. Uniaxial compressive stress-strain curves for plasticity and damage models

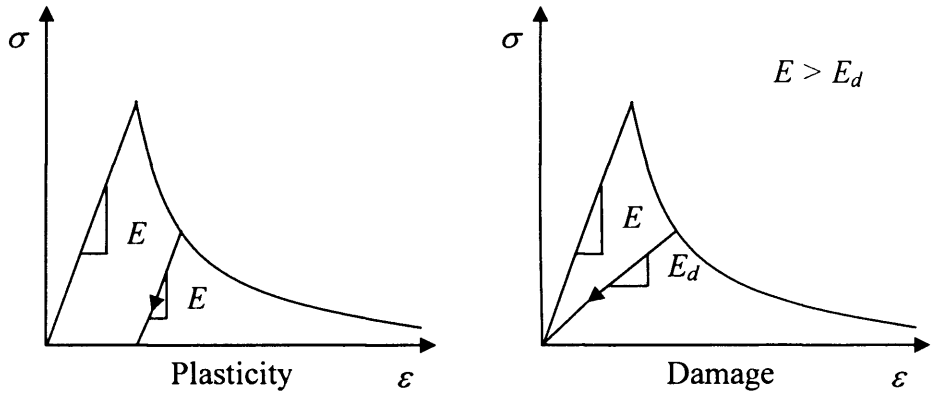

Figure 3.11. Uniaxial tensile stress-strain curves for plasticity and damage models

3.4 Conclusions

The development of microcracks in concrete results in the degradation of material stiffness, the behaviour of which can be well captured by the theory of continuum damage mechanics. This is reflected by the use of the secant stiffness on unloading path. On the other hand, the theory of plasticity simulates plastic flow, which leads to permanent deformation. The theory can also capture the effect of dilatancy in concrete under

multiaxial loading. Both phenomena do not however affect the stiffness of the material. This is reflected by the use of an elastic stiffness on both loading and unloading paths. Hence, in order to capture both tensile and compressive behaviour of concrete, models developed based on the combination of both theories, i.e. plastic-damage models, seem to be a better option for constitutive modelling of concrete.

Chapter Four

Plastic-Damage-Contact Model

4.1 Introduction

The plastic-damage-contact model, also known as Craft, was originally developed by Jefferson (2003a, b) to simulate both tensile and compressive behaviour of concrete, and in particular the post-cracking behaviour of cracked concrete. The model employs the concept of embedded contact surfaces to simulate micro and macro crack opening and closing behaviour, including shear contact (aggregate interlock), in which open crack faces can regain contact under applied shear and normal compressive loadings (Jefferson 2002a).

The model employs plasticity, damage and contact theory in the formulation and thus has been classified 'plastic-damage-contact' rather than the more commonly used classification of plastic-damage.

The essential elements of the models are

- a triaxial plasticity component to simulate frictional behaviour and the increase in strength with triaxial confinement
- a plastic-work damage function for simulating loss of tensile strength with compressive damage
- a local stress-strain relationship, which is based on damage-contact theory
- a total-local function, such that the local and global constitutive relationships are both satisfied
- a thermodynamically consistent global stress-strain relationship

4.2 Plasticity component

4.2.1 Yield function

The model has a fully integrated plasticity component which uses the same straight compressive meridians as those developed by Lubliner *et al.* (1989). An illustration of the yield surface on the π-plane is shown in Figure 4.1. A smoothing function presented by Willam and Warnke (1974) is employed to blunt sharp edges of the yield surface as observed in the π-plane.

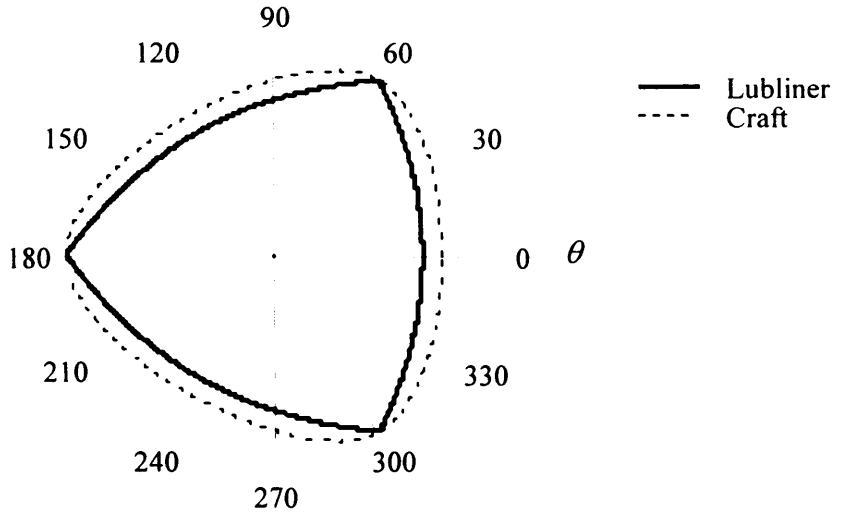

Figure 4.1. Yield surface on the π-plane

The yield function is derived as follows

$$F(\sigma, Z(\kappa)) = \sqrt{J_2} A_r(\theta) + \left(\alpha + \frac{\gamma_p}{3}\right) I_1 Z - f_c Z(1-\alpha) \tag{4.1}$$

where

$$A_r(\theta) = \rho_c \left(\frac{2\cos(\theta)^2 + b^2}{\cos(\theta) + b\sqrt{2\cos(\theta)^2 + c}} \right) \tag{4.2}$$

f_c, I_1 and J_2 are the uniaxial compressive strength, the first stress invariant and the second deviatoric stress invariant respectively. θ is the Lode angle with range 0° to 60° and Z denotes the friction hardening factor, which varies with the work hardening

parameter κ. The initial value of the friction hardening factor Z_0 governs the yield surface starting position. Z varies from a possible value of 0, at which the yield surface forms a line on the hydrostatic axis, up to 1 at which the yield surface reaches its peak position.

The model constants b, c, α, γ_p and ρ_c in both (4.1) and (4.2) are computed as follows (Lubliner *et al.* 1989)

$$\alpha = \frac{b_r - 1}{2b_r - 1},\quad b = \sqrt{2} - 1,\quad c = \frac{5}{2} - 2\sqrt{2},\quad \rho = 1/\sqrt{2},\quad \gamma_p = \frac{1-\rho}{2\rho - 1},\quad \rho_c = \sqrt{3} + \frac{\gamma_p}{\sqrt{3}}$$

in which ρ denotes the eccentricity parameter and b_r is the ratio between the biaxial and uniaxial strengths, which is generally in the range 1.05 to 1.3 (Kupfer *et al.* 1969; van Mier 1997). It is noted that the smoothing function in (4.2) is a simplified version of that developed by Willam and Warnke (1974) by setting ρ to a constant value of $1/\sqrt{2}$. The complete version, as expressed below, was adopted in the proposed models presented in the following chapters of this thesis.

$$A_r(\theta,\rho) = \rho_c\left(\frac{4(1-\rho^2)\cos^2\theta + (2\rho-1)^2}{2(1-\rho^2)\cos\theta + (2\rho-1)\sqrt{4(1-\rho^2)\cos^2\theta + 5\rho^2 - 4\rho}}\right) \tag{4.3}$$

4.2.2 Plastic potential and flow rule

The plastic potential function used in this model is of a similar form to the yield function presented earlier, but with an additional parameter ψ that controls the degree of dilatancy. If ψ is set to unity, the potential takes the same form as the yield function and the plastic flow is associated, whereas if it is set to zero, the model predicts zero dilatancy. The values of ψ in the range of -0.1 to -0.3 were found to produce good match with experimental data (Jefferson 2003a).

$$G(\sigma, Z(\kappa)) = \sqrt{J_2} A_r(\theta) + \left(\alpha + \frac{\gamma}{3}\right) I_1 Z\psi - f_c Z\psi(1-\alpha) \tag{4.4}$$

The non-associative flow rule is given by

$$\delta\varepsilon_p = \frac{\partial G}{\partial \sigma}\delta\lambda \tag{4.5}$$

where λ denotes the plastic multiplier, which obeys the condition $\delta\lambda \geq 0$.

4.2.3 Hardening/softening relationships

The model employs a frictional work hardening and softening plastic evolution function to account for pre- and post-peak non-linear behaviour. It is assumed that the amount of work to reach peak stress increases with a parameter X, which is a function of the mean

stress. This parameter performs the same role as the ductility parameter found in the model by Este and Willam (1994). The work hardening parameter is derived as

$$\delta\kappa = X(\sigma)\sigma^T \delta\varepsilon_p \tag{4.6}$$

The expression used for the enhancement factor X is as follows

$$X = e^{\chi} + e^{\chi-1} + X_I \tag{4.7}$$

where

$$\chi = \frac{I_1}{f_c * 0.9} + 0.55 \quad \text{and} \quad X_I = 0.0022$$

It should be noted that the enhancement factor is only required for compressive stress states i.e. when I_1 is negative.

A single friction hardening/softening function, as illustrated in Figure 4.2, is presented for Z to give a smooth transition from pre- to post-peak behaviour, as follows

$$Z = Z_0 + \frac{1 - Z_0}{a_c} e^{-c_{c1}\eta}(1 - e^{-c_{c2}\eta}) \tag{4.8}$$

where $\eta = \kappa/\kappa_p$, and κ_p is the value of κ at the peak yield surface position. In order to ensure that the peak occurs at $Z = 1$, the constants in equation (4.8) must satisfy the following relationships

$$c_{c1} = \frac{c_{c2}\, e^{-c_{c2}}}{1 - e^{-c_{c2}}} \qquad \text{and} \qquad a_c = e^{-c_{c1}}(1 - e^{-c_{c2}}) \tag{4.9}$$

in which $c_{c2} = 5$, $c_{c1} = 0.0339182745$ and $a_c = 0.9601372615$.

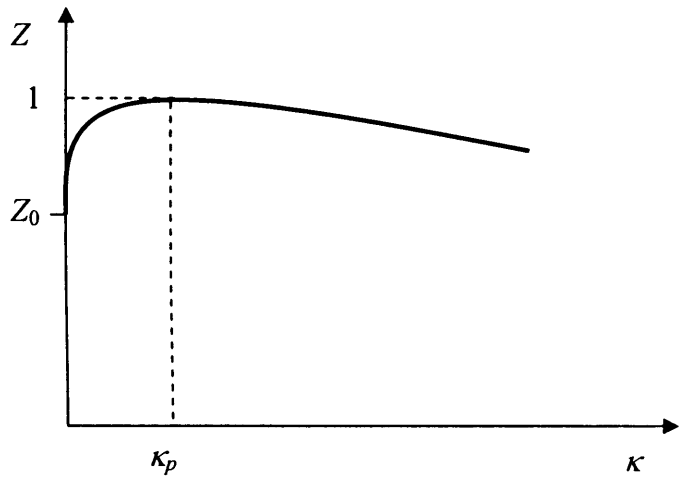

Figure 4.2. Friction hardening/softening function

The expression for κ_p was derived by integrating Saenz's (1964) equation over a uniaxial compressive stress-strain curve and then removing the elastic component, using data typical for structural concrete as follows

$$\kappa_p = f_c\left(0.72\varepsilon_c - \frac{f_c}{2E}\right) \tag{4.10}$$

where ε_c denotes the uniaxial compressive strain at the peak uniaxial compressive stress f_c.

4.3 Local damage-contact component

The damage-contact component of the model employs a simplified version of the effective crack plane model developed by Jefferson (2002b) to describe the local stress-effective strain relationship. In the crack plane model, the local stress for a damage plane *i*, is assumed to be the sum of the stresses contributed by the undamaged component and damage-contact component, as follows

$$\boldsymbol{s}_{f_i} = \boldsymbol{D}_L(H_{ci}\boldsymbol{e}_i + H_{f_i}\omega_i\boldsymbol{g}_i) = \boldsymbol{D}_L(H_{ci}\boldsymbol{I} + H_{f_i}\omega_i\boldsymbol{\Phi}_{d_i})\boldsymbol{e}_i = \boldsymbol{D}_L\boldsymbol{M}_{x_i}\boldsymbol{e}_i = \boldsymbol{D}_{ls_i}\boldsymbol{e}_i \tag{4.11}$$

where $\boldsymbol{e}_i$, $\boldsymbol{D}_L$ and $\boldsymbol{I}$ are the local effective strain, local elastic constitutive matrix and identity matrix respectively. The effective local strains $\boldsymbol{e}_i$ are those that apply to a fracture process zone of an effective crack plane. They are taken as equal to the relative displacements across the process zone divided by the width of the effective zone w_c. The reason for choosing the local effective strains as the basis of the model is that these local strains can be obtained directly from tests. $\boldsymbol{g}_i$ is the embedment strain relative to a contact

surface, and is related to the local effective strain by a transformation matrix $\boldsymbol{\Phi}_{d_i}$. Figure 4.3 shows a schematic diagram of the contact surface.

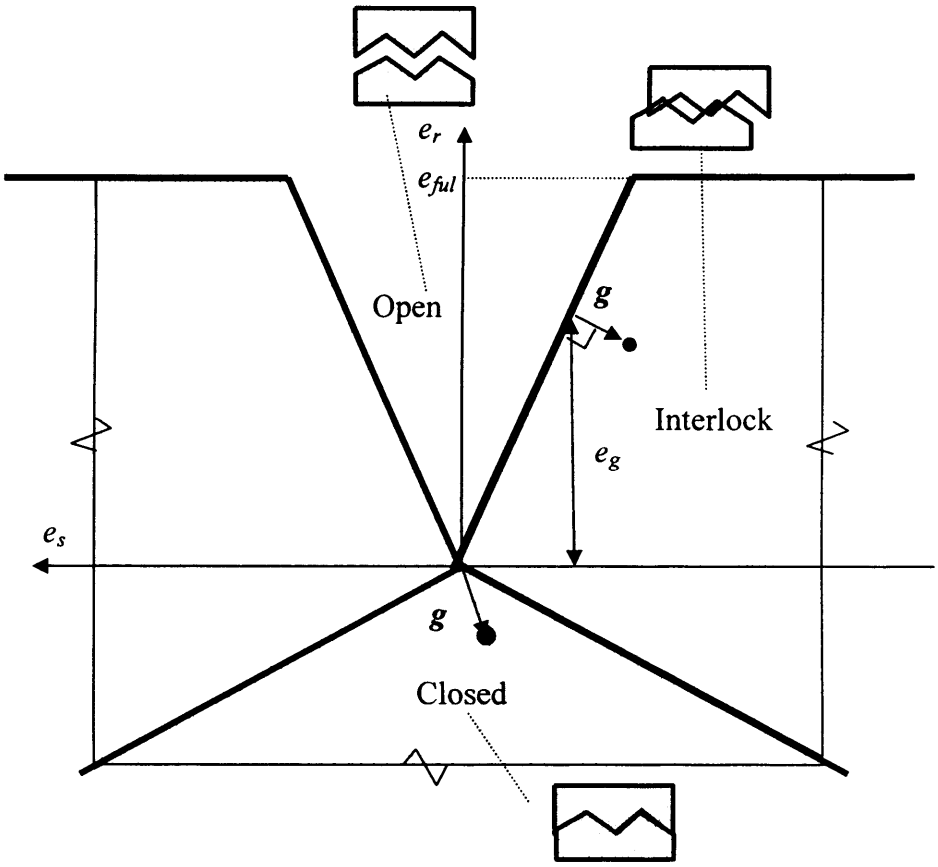

Figure 4.3. Contact surface (Jefferson 2003a)

H_c denotes the proportion of undamaged material and can be expressed as

$$H_{c_i} = (1 - \omega_i) \tag{4.12}$$

in which ω_i is a damage variable that lies in the range 0 to 1, and depends upon a local strain parameter ζ_i.

With reference to equation (4.11), the local stress in the damaged component is a function of H_f, where H_f denotes the proportion of fully debonded material on a crack plane that is in contact. The H_f function, as given below, is included to simulate the observed behaviour that the amount of shear stress that can develop with increasing shear strain reduces with increasing crack opening.

$$H_f = H_m \quad \text{if} \quad e_r < e_{bg} \tag{4.13}$$

$$H_f = H_m H_g \left[r_f e^{-\rho_{f1}\left(\frac{e_g-\varepsilon_t}{\varepsilon_0}\right)^2} + (1-r_f) e^{-\rho_{f2}\left(\frac{e_g-\varepsilon_t}{m_{ful}\varepsilon_0}\right)^2} \right] \tag{4.14}$$

where

$$H_g = 1 - e^{-c_g \frac{g}{e_g+2\varepsilon_t}}$$

g denotes the embedment, as shown in Figure 4.3, and $r_f = 0.95$, $\rho_{f1} = 4$, $\rho_{f2} = 1.5$, $c_g = 3$, $H_m = 0.995$ and $e_{bg} = 1.1\varepsilon_t$. The H_g function provides a smooth but rapid transition to closed and interlock states. The H_f function varies from 1 to effectively 0 when the

crack opening parameter e_g reaches a value at which no further shear contact is possible, as shown in Figure 4.4. This value is defined as a multiple of the strain value at the end of the softening curve i.e. $m_{ful}\varepsilon_0$.

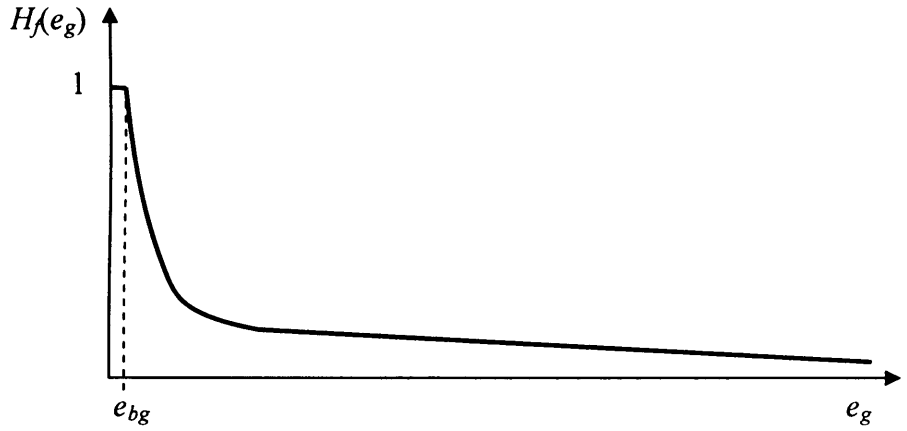

Figure 4.4. Contact proportion function

The model employs both interlock $\phi_{\text{int}}(e)$ and closed $\phi_{cl}(e)$ functions to identify the state of contact. These functions are derived based upon experimental data from tests in which cracked concrete specimens are subjected to normal-shear loadings. With reference to Figure 4.3, e_{ful} represents the crack opening strain beyond which no further contact can be gained in shear.

A crack plane is assumed to form when the major principal stress reaches the fracture stress. The POD is orientated such that its direction is orthogonal to the major principal axis. It is assumed that damage on the plane can occur with both shear and normal strains. The model employs a damage surface similar to that used by Kroplin and Weihe (1997).

The damage function is asymptotic to an equivalent strain friction surface and is orthogonal to normal strain axis at its intercept with that axis. Figure 4.5 shows a schematic diagram of the damage surface in strain space. The damage function is derived as follows

$$\phi(e,\zeta) = \frac{e_r}{2}\left[1+\left(\frac{\mu_\varepsilon}{r_\zeta}\right)^2\right]+\frac{1}{2r_\zeta{}^2}\sqrt{\left(r_\zeta{}^2-\mu_\varepsilon{}^2\right)^2 e_r{}^2+4r_\zeta{}^2\left(e_s{}^2+e_t{}^2\right)}-\zeta=0 \qquad (4.15)$$

The material constants r_ζ and μ_ε are the relative shear strain intercept and the asymptotic shear friction factor respectively. These are the strain equivalents of the relative shear stress intercept r_σ and the asymptotic friction factor μ_σ.

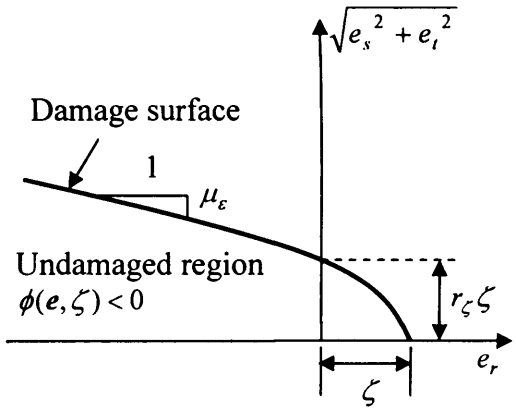

Figure 4.5. Damage surface

In this original Craft model, a single term exponential softening curve was used for the damaged evolution function. This function was derived in terms of the fracture stress f_s

and the strain parameter ζ, and has the uniaxial strength f_t, the strain at peak stress ε_t and the strain at the effective end of the curve ε_0, as control parameters. The basic function, as illustrated in Figure 4.6, is as follows

$$f_s = (1-\omega(\zeta))E\zeta \tag{4.16}$$

in which

$$\omega = 1 - r_c\frac{\varepsilon_t}{\zeta} - \left[(1-r_c)\frac{\varepsilon_t}{\zeta}e^{-c_1\frac{\zeta-\varepsilon_t}{\varepsilon_0-\varepsilon_t}}\right]e^{-2\frac{\kappa}{\kappa_p}}$$

The constant c_1 was set to fixed value of 5. The term r_c was included in the above expression to provide residual damage strength that is essential for stabilising numerical calculations and maintaining a residual damage stress.

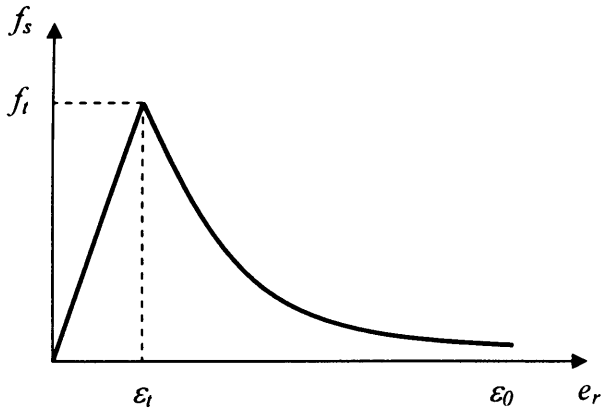

Figure 4.6. Damage evolution function

4.4 Overall stress-strain relationship

The overall relationship between the total stresses $\boldsymbol{\sigma}$ and strains is given by

$$\boldsymbol{\sigma} = \boldsymbol{D}_e(\boldsymbol{\varepsilon} - \boldsymbol{\varepsilon}_p - \boldsymbol{\varepsilon}_a) = \boldsymbol{D}_e\left(\boldsymbol{\varepsilon} - \boldsymbol{\varepsilon}_p - \sum_{j=1}^{n_p} \boldsymbol{N}_j{}^T \boldsymbol{e}_{aj}\right) \tag{4.17}$$

in which n_p denotes the number of crack planes. $\boldsymbol{D}_e$ is the elastic constitutive matrix and $\boldsymbol{\varepsilon}$ is the total strain tensor. $\boldsymbol{\varepsilon}_a$ is the sum of the transformed inelastic local strain vector $\boldsymbol{e}_a$ on all crack planes. Utilising equation (4.11), $\boldsymbol{e}_a$ is related to the effective strain vector as follows

$$\boldsymbol{e}_{ai} = \boldsymbol{e}_i - \boldsymbol{C}_L \boldsymbol{s}_{f_i} = (\boldsymbol{I} - \boldsymbol{M}_{xi})\boldsymbol{e}_i \tag{4.18}$$

The local stresses $\boldsymbol{s}_f$ on each of the PODs can be related to the global stress tensor $\boldsymbol{\sigma}$ via a transformation matrix as follows

$$\boldsymbol{s}_{f_i} = \boldsymbol{N}_i \boldsymbol{\sigma} \tag{4.19}$$

where

$$\boldsymbol{s}_f = \begin{bmatrix} s_{f_r} & s_{f_s} & s_{f_t} \end{bmatrix}^T \quad , \quad \boldsymbol{\sigma} = \begin{bmatrix} \sigma_{xx} & \sigma_{yy} & \sigma_{zz} & \sigma_{xy} & \sigma_{yz} & \sigma_{xz} \end{bmatrix}^T \quad \text{and}$$

$$N = \begin{bmatrix} r_{d1}^2 & r_{d2}^2 & r_{d3}^2 & 2r_{d1}r_{d2} & 2r_{d2}r_{d3} & 2r_{d1}r_{d3} \\ s_{d1}^2 & s_{d2}^2 & s_{d3}^2 & 2s_{d1}s_{d2} & 2s_{d2}s_{d3} & 2s_{d1}s_{d3} \\ t_{d1}^2 & t_{d2}^2 & t_{d3}^2 & 2t_{d1}t_{d2} & 2t_{d2}t_{d3} & 2t_{d1}t_{d3} \end{bmatrix}$$

r_{d1}, r_{d2}, r_{d3} are the x, y, z components of the unit vector r_d normal to the POD surface, and s_d and t_d are the corresponding in-plane vectors. s_d is generated such that its directions are perpendicular to r_d and to each of the reference axes in turn (Hasegawa 1995). t_d is then made orthogonal to both the r and s components. Figure 4.7 shows the local and global coordinate systems of a POD.

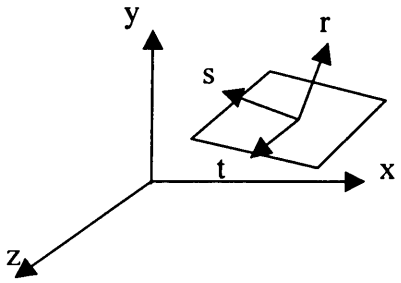

Figure 4.7. POD local and global coordinate systems

By using equations (4.11), (4.17), (4.18) and (4.19), the secant stress recoverable-strain relationship may be obtained as

$$\sigma = \left[I + D_e \sum_{j=1}^{n_p} N_j{}^T \left(M_{xj}{}^{-1} - I \right) C_L N_j \right]^{-1} D_e \left(\varepsilon - \varepsilon_p \right) \tag{4.20}$$

where $C_L = D_L{}^{-1}$.

4.5 Total-local function

The role of the total-local function is to ensure that both local and global relationship, as well as the stress transformation in equation (4.19), are simultaneously satisfied for multiple crack planes. The function allows all damage surfaces to be fully coupled. The function gives measurement of the error between the transformed global stresses computed from (4.20) and the local stresses computed from equation (4.11).

$$F_{ei} = N_i \sigma - s_{f_i} = N_i D_e \left[\varepsilon - \varepsilon_p - \sum_{j=1}^{n_p} N_j{}^T \left(I - M_{xj} \right) e_j \right] - D_L M_{xi} e_i = 0 \tag{4.21}$$

By equating the total-local function to zero, the equation can then be solved for the unknown local effective strain e. This equation may be rewritten as follows

$$\begin{bmatrix} \boldsymbol{N}_1\boldsymbol{D}_e\boldsymbol{N}_1^T\left(\boldsymbol{I}-\boldsymbol{M}_{x1}\right)+\boldsymbol{D}_L\boldsymbol{M}_{x1} & \boldsymbol{N}_1\boldsymbol{D}_e\boldsymbol{N}_2^T\left(\boldsymbol{I}-\boldsymbol{M}_{x2}\right) \\ \boldsymbol{N}_2\boldsymbol{D}_e\boldsymbol{N}_1^T\left(\boldsymbol{I}-\boldsymbol{M}_{x1}\right) & \boldsymbol{N}_2\boldsymbol{D}_e\boldsymbol{N}_2^T\left(\boldsymbol{I}-\boldsymbol{M}_{x2}\right)+\boldsymbol{D}_L\boldsymbol{M}_{x2} \end{bmatrix} \begin{bmatrix} \boldsymbol{e}_1 \\ \boldsymbol{e}_2 \end{bmatrix} = \begin{bmatrix} \boldsymbol{N}_1 \\ \boldsymbol{N}_2 \end{bmatrix} \boldsymbol{D}_e\left(\boldsymbol{\varepsilon}-\boldsymbol{\varepsilon}_p\right) \tag{4.22}$$

For cases where more than one crack plane is present, a non-linear solution procedure is required for equation (4.21). Nevertheless, it has been found that very few iterations of a Newton procedure are required to achieve convergence for equation (4.21) when multiple surfaces are active (Jefferson 2003a).

4.6 Return mapping algorithm

The overall procedure of the stress recovery algorithm employed in the Craft model is to first update the local effective strains and then account for any plastic flow. The stress update is computed from the previous converged state. In this section, it is noted that the subscripts k and $k+1$ represent the values of quantities on entry to and exit from the return mapping algorithm respectively. The symbol Δ represents the overall change of any quantity from the last converged state and δ denotes the change of a quantity within the stress update iteration. The algorithm is presented with the assumptions that both yield and fracture criteria have already been violated, i.e. plastic yield is active along with the existence of one or more PODs.

The following relationships must be satisfied in order to evaluate the new stresses $\boldsymbol{\sigma}_{k+1}$ for the incremental strain $\Delta\boldsymbol{\varepsilon}$ from the previous converged stresses $\boldsymbol{\sigma}_k$.

- total constitutive relationship

$$\boldsymbol{\sigma}_{k+1} = \boldsymbol{D}_e\left(\boldsymbol{\varepsilon}_{k+1} - \boldsymbol{\varepsilon}_{pk+1} - \sum_{j=1}^{n_p} \boldsymbol{N}_j{}^T \boldsymbol{e}_{a_{j\,k+1}}\right) \tag{4.23}$$

- stress transformation

$$\boldsymbol{s}_{f_{i\,k+1}} = \boldsymbol{N}_{i\,k+1}\boldsymbol{\sigma}_{k+1} \tag{4.24}$$

- local stress-strain relationships for all PODs i

$$\boldsymbol{s}_{f_{i_{k+1}}} = \boldsymbol{D}_{ls\,i\,k+1}\boldsymbol{e}_{i_{k+1}} \tag{4.25}$$

$$\boldsymbol{e}_{a\,i\,k+1} = \boldsymbol{C}_{lsf\,i\,k+1}\boldsymbol{s}_{f\,i\,k+1} \tag{4.26}$$

where $\boldsymbol{C}_{lsf}$ is the local compliance matrix.

- flow rule and plastic parameter

$$\Delta\boldsymbol{\varepsilon}_p = \frac{\partial G}{\partial \boldsymbol{\sigma}}_{k+1} \Delta\lambda \tag{4.27}$$

$$\Delta\kappa = X_{k+1}\Delta\lambda\boldsymbol{\sigma}_{k+1}{}^T \frac{\partial G}{\partial \boldsymbol{\sigma}}_{k+1} \tag{4.28}$$

- yield function

$$F(\boldsymbol{\sigma}_{k+1}, \kappa_{k+1}) = 0 \tag{4.29}$$

- total-local function

$$\boldsymbol{F}_{ei\,k+1} = \boldsymbol{N}_{i\,k+1}\boldsymbol{\sigma}_{k+1} - \boldsymbol{D}_{lsi\,k+1}\boldsymbol{e}_{i\,k+1} = \boldsymbol{0} \tag{4.30}$$

The model adopts an algorithm similar to that of the Closest Point Projection algorithm, which is chosen for its stability and enhanced rate of convergence (Simo and Hughes 1998). Error measures are introduced for the plastic strain and plastic parameter, which, along with the error in the yield function and total-local function, are used in a coupled Newton iterative solution procedure.

In the following, all iteration subscripts will not be included. It is assumed that all quantities on the right of an equation are those from the previous update iteration (or the values from the previous overall finite element increment for the 1st iteration).

The error measures for both plastic strain and hardening parameter are given by

$$\boldsymbol{R}_{\varepsilon} = -\Delta\boldsymbol{\varepsilon}_{p} + \frac{\partial G}{\partial \boldsymbol{\sigma}}\Delta\lambda \tag{4.31}$$

$$R_{\kappa} = -\Delta\kappa + X\Delta\lambda\boldsymbol{\sigma}^{T}\frac{\partial G}{\partial \boldsymbol{\sigma}} \tag{4.32}$$

The iterative corrections are obtained as follows

$$\delta\varepsilon_p = \boldsymbol{R}_\varepsilon + \delta\lambda \frac{\partial G}{\partial \boldsymbol{\sigma}} + \Delta\lambda \frac{\partial^2 G}{\partial \boldsymbol{\sigma}^2}\delta\boldsymbol{\sigma} \tag{4.33}$$

$$\delta\kappa = a_\kappa\left(R_\kappa + \Delta\lambda \boldsymbol{k}_\sigma{}^T \delta\boldsymbol{\sigma} + c_\kappa \delta\lambda\right) \tag{4.34}$$

where

$$a_\kappa = \left(1 - \Delta\lambda X \boldsymbol{\sigma}^T \frac{\partial G}{\partial \boldsymbol{\sigma}}\right)^{-1} \quad , \quad c_\kappa = X\boldsymbol{\sigma}^T \frac{\partial G}{\partial \boldsymbol{\sigma}} \quad \text{and}$$

$$\boldsymbol{k}_\sigma = \frac{\partial X}{\partial \boldsymbol{\sigma}}\boldsymbol{\sigma}^T \frac{\partial G}{\partial \boldsymbol{\sigma}} + X\frac{\partial^2 G}{\partial \boldsymbol{\sigma}^2}\boldsymbol{\sigma} + X\frac{\partial G}{\partial \boldsymbol{\sigma}}$$

The yield function consistency condition is as follows

$$F + \frac{\partial F}{\partial \boldsymbol{\sigma}}^T \delta\boldsymbol{\sigma} + \frac{\partial F}{\partial \kappa}\delta\kappa = 0 \tag{4.35}$$

Substituting (4.34) in (4.35) yields

$$F + \boldsymbol{f}_\kappa{}^T \delta\boldsymbol{\sigma} + \frac{\partial F}{\partial \kappa} a_\kappa R_\kappa + h_\kappa \delta\lambda = 0 \tag{4.36}$$

where

$$f_\kappa = \frac{\partial F}{\partial \sigma} + \frac{\partial F}{\partial \kappa} a_\kappa \Delta\lambda \boldsymbol{k}_\sigma \qquad \text{and} \qquad h_\kappa = \frac{\partial F}{\partial \kappa} a_\kappa c_\kappa$$

Making use of equation (4.30), the total-local consistency condition can be written as follows

$$\boldsymbol{F}_{ei} + \boldsymbol{N}_i \delta\sigma + \frac{\partial \boldsymbol{N}_i}{\partial \sigma} \circ \sigma \delta\sigma - \frac{\partial \boldsymbol{D}_{lsi}}{\partial \boldsymbol{e}_i} \circ \boldsymbol{e}_i \delta \boldsymbol{e}_i - \frac{\partial \boldsymbol{D}_{lsi}}{\partial \kappa} \boldsymbol{e}_i \delta\kappa - \boldsymbol{D}_{lsi} \delta \boldsymbol{e}_i = \boldsymbol{0} \tag{4.37}$$

in which $\circ$ denotes a contraction with respect to the 'in-plane' components of a third order matrix. The third term in the above equation is ignored here as the POD direction remains fixed during the stress update iterations. Then, substituting (4.34) in (4.37) yields

$$\boldsymbol{F}_{ei} + \boldsymbol{N}_{\Delta i} \delta\sigma - \boldsymbol{D}_{l\kappa i} a_\kappa \left(R_\kappa + c_\kappa \delta\lambda\right) - \boldsymbol{D}_{lti} \delta \boldsymbol{e}_i = \boldsymbol{0} \tag{4.38}$$

where

$$\boldsymbol{D}_{lti} = \frac{\partial \boldsymbol{D}_{lsi}}{\partial \boldsymbol{e}_i} \circ \boldsymbol{e}_i + \boldsymbol{D}_{lsi} \quad , \quad \boldsymbol{D}_{l\kappa i} = \frac{\partial \boldsymbol{D}_{lsi}}{\partial \kappa} \boldsymbol{e}_i \quad \text{and}$$

$$\boldsymbol{N}_{\Delta i} = \boldsymbol{N}_i - \boldsymbol{D}_{l\kappa i} a_\kappa \boldsymbol{k}_\sigma{}^T \Delta\lambda$$

The initial trial stress is defined as follows

$$\boldsymbol{\sigma} = \boldsymbol{D}_e\left(\boldsymbol{\varepsilon} + \Delta\boldsymbol{\varepsilon} - \boldsymbol{\varepsilon}_p - \sum_{j=1}^{n_p} \boldsymbol{N}_j{}^T \boldsymbol{e}_{aj}\right) \tag{4.39}$$

after which iterations are performed to satisfy equations (4.23) to (4.29). The total strain tensor remains unchanged during the iterations. Hence, the iterative change in the stress may be given by

$$\delta\boldsymbol{\sigma} = -\boldsymbol{D}_e\left(\delta\boldsymbol{\varepsilon}_p + \sum_{j=1}^{n_p} \boldsymbol{N}_j{}^T \delta\boldsymbol{e}_{aj}\right) \tag{4.40}$$

The iterative change in the added strain $\boldsymbol{e}_a$ is given by

$$\delta\boldsymbol{e}_{ai} = \left(\boldsymbol{I} - \boldsymbol{m}'_{xi}\right)\delta\boldsymbol{e}_i + \boldsymbol{m}'_{\kappa i}\delta\kappa \tag{4.41}$$

where

$$\boldsymbol{m}'_{xi} = \boldsymbol{M}_{xi} + \frac{\partial \boldsymbol{M}_{xi}}{\partial \boldsymbol{e}_i} \circ \boldsymbol{e}_i \qquad \text{and} \qquad \boldsymbol{m}'_{\kappa i} = \frac{\partial \boldsymbol{M}_{xi}}{\partial \kappa}\boldsymbol{e}_i$$

Substituting (4.33), (4.34) and (4.41) in (4.40) and rearranging yields

$$\delta\boldsymbol{\sigma} = -\boldsymbol{A}\left[\boldsymbol{R}_{\varepsilon} + \delta\lambda\frac{\partial G}{\partial\boldsymbol{\sigma}} + \sum_{j=1}^{n_p}\boldsymbol{N}_j{}^{T}\left[\left(\boldsymbol{I} - \boldsymbol{m}'_{x_j}\right)\delta\boldsymbol{e}_j + \boldsymbol{m}'_{\kappa_j}a_{\kappa}\left(R_{\kappa} + c_{\kappa}\delta\lambda\right)\right]\right] \tag{4.42}$$

where

$$\boldsymbol{A} = \left[\boldsymbol{I} + \boldsymbol{D}_e\left(\Delta\lambda\frac{\partial^2 G}{\partial\boldsymbol{\sigma}^2} - \sum_{j=1}^{n_p}\boldsymbol{N}_j{}^{T}\boldsymbol{m}'_{\kappa_j}a_{\kappa}\boldsymbol{k}_{\sigma}{}^{T}\Delta\lambda\right)\right]^{-1}\boldsymbol{D}_e$$

Substituting for $\delta\boldsymbol{\sigma}$ from (4.42) in (4.36) and (4.38) gives a set of coupled equations with $\delta\lambda$ and $\delta\boldsymbol{e}$ as the unknowns. These are written in the following compact form, in which i and j are indices from 1 to n_p and in which the summation of repeated indices is implied. Note i, j does not here imply differentiation with respect to the j components as it would in indicial notation.

$$F_{\lambda} = M_{\lambda}\delta\lambda + \boldsymbol{B}_{\lambda j}\delta\boldsymbol{e}_j \tag{4.43}$$

$$\boldsymbol{F}_{Ei} = \boldsymbol{M}_{Ei}\delta\lambda + \boldsymbol{B}_{Ei,j}\delta\boldsymbol{e}_j \tag{4.44}$$

in which

$$F_\lambda = F - \boldsymbol{f}_\kappa{}^T \boldsymbol{A}\left(\boldsymbol{R}_\varepsilon - \sum_{k=1}^{n_p} \boldsymbol{N}_k{}^T \boldsymbol{m}'_{\kappa k} a_\kappa R_\kappa \right) + \frac{\partial F}{\partial \kappa} a_\kappa R_\kappa$$

$$\boldsymbol{F}_{Ei} = \boldsymbol{F}_{ei} - \boldsymbol{N}_{\Delta i}\boldsymbol{A}\left(\boldsymbol{R}_\varepsilon - \sum_{k=1}^{n_p} \boldsymbol{N}_k{}^T \boldsymbol{m}'_{\kappa k} a_\kappa R_\kappa \right) - \boldsymbol{D}_{l\kappa i} a_\kappa R_\kappa$$

$$M_\lambda = \boldsymbol{f}_\kappa{}^T \boldsymbol{A}\left(\frac{\partial G}{\partial \boldsymbol{\sigma}} - \sum_{k=1}^{n_p} \boldsymbol{N}_k{}^T \boldsymbol{m}'_{\kappa k} a_\kappa c_\kappa \right) - h_\kappa$$

$$\boldsymbol{M}_{Ei} = \boldsymbol{N}_{\Delta i}\boldsymbol{A}\left(\frac{\partial G}{\partial \boldsymbol{\sigma}} - \sum_{k=1}^{n_p} \boldsymbol{N}_k{}^T \boldsymbol{m}'_{\kappa k} a_\kappa c_\kappa \right) + \boldsymbol{D}_{l\kappa i} a_\kappa c_\kappa$$

$$\boldsymbol{B}_{\lambda_j} = \boldsymbol{f}_\kappa{}^T \boldsymbol{A}\boldsymbol{N}_j{}^T \left(\boldsymbol{I} - \boldsymbol{m}'_{x_j} \right)$$

$$\boldsymbol{B}_{E_{i,j}} = \boldsymbol{N}_{\Delta i}\boldsymbol{A}\boldsymbol{N}_j{}^T \left(\boldsymbol{I} - \boldsymbol{m}'_{x_j} \right) + \boldsymbol{D}_{lti,j}\partial_{i,j}$$

where $\partial_{i,j}$ in the expression for $\boldsymbol{B}_E$ is the Kronecker delta.

The overall steps of the return mapping algorithm may now be summarised for the case when plastic yield is active and one or more POD exists.

Box 4.1. Return mapping algorithm

Step	Description
1	Initialise $\Delta\lambda = 0$ and $\Delta\kappa = 0$
2	Compute trial stress from (4.39)
3	Evaluate $F_\lambda, \boldsymbol{M}_\lambda, \boldsymbol{B}_\lambda, \boldsymbol{F}_E, \boldsymbol{M}_E, \boldsymbol{B}_E$ from (4.43) and (4.44) and solve for $\delta\lambda$ and $\delta\boldsymbol{e}_i$
4	Compute $\delta\boldsymbol{\sigma}$ from (4.42)
5	Update $\boldsymbol{e}_i$ using $\boldsymbol{e}_i = \boldsymbol{e}_i + \delta\boldsymbol{e}_i$ and update ζ_i
6	Compute $\delta\boldsymbol{\varepsilon}_p$, $\delta\kappa$ from (4.33) and (4.34) respectively
7	Update plastic terms $\boldsymbol{\varepsilon}_p = \boldsymbol{\varepsilon}_p + \delta\boldsymbol{\varepsilon}_p$, $\Delta\boldsymbol{\varepsilon}_p = \Delta\boldsymbol{\varepsilon}_p + \delta\boldsymbol{\varepsilon}_p$, $\Delta\lambda = \Delta\lambda + \delta\lambda$, $\kappa = \kappa + \delta\kappa$ and $\Delta\kappa = \Delta\kappa + \delta\kappa$
8	Compute a new trial stress from $\boldsymbol{\sigma} = \boldsymbol{D}_e\left[\boldsymbol{\varepsilon} - \boldsymbol{\varepsilon}_p - \sum_{j=1}^{n_p} \boldsymbol{N}_j^T\left(\boldsymbol{I} - \boldsymbol{M}_{xj}\right)\boldsymbol{e}_j\right]$
9	Compute F, $\boldsymbol{F}_{ei}$, $\boldsymbol{R}_\varepsilon$ and R_κ from (4.29), (4.30), (4.31) and (4.32) respectively

10	Check for convergence
	If $\lvert F\rvert \le \sigma_{tol}$, $\lvert\boldsymbol{F}_e\rvert \le \sigma_{tol}$, $\lvert\boldsymbol{R}_\varepsilon\rvert \le \varepsilon_{tol}$ and $\lvert R_\kappa\rvert \le \varepsilon_{tol}$
	Exit iteration
	Else
	Return to Step 2[1]
	End If

Note:

1. Tolerance levels are $\sigma_{tol} = f_t * 10^{-6}$ and $\varepsilon_{tol} = \varepsilon_t * 10^{-6}$

4.7 Consistent tangent constitutive relationship

In order to achieve accurate, fast convergence and stable solutions, the model employs a tangent stiffness matrix that is consistent with the stress update algorithm described in Section 4.6. The following describes the derivation of a constitutive tangent operator.

The differential form of equation (4.23) is given by

$$\delta\boldsymbol{\sigma} = \boldsymbol{D}_e\left[\delta\boldsymbol{\varepsilon} - \delta\boldsymbol{\varepsilon}_p - \sum_{j=1}^{n_p}\left(\boldsymbol{N}_j{}^T\delta\boldsymbol{e}_{a_j} + \delta\boldsymbol{N}_j{}^T\boldsymbol{e}_{a_j}\right)\right] \tag{4.45}$$

The term $\delta\boldsymbol{N}_j$ is the differential of the transformation matrix with respect to the trial stress components used for the new POD detection. The choice of this trial stress $\boldsymbol{\sigma}_I$ is discussed later in Section 4.5. Thus equation (4.45) may now be written as

$$\delta\boldsymbol{\sigma} = \boldsymbol{D}_e\left(\delta\boldsymbol{\varepsilon} - \delta\boldsymbol{\varepsilon}_p - \sum_{j=1}^{n_p}\left(\boldsymbol{N}_j{}^T\delta\boldsymbol{e}_{a_j} + \frac{\partial\boldsymbol{N}_j{}^T}{\partial\boldsymbol{\sigma}_I}\circ\boldsymbol{e}_{a_j}\boldsymbol{D}_I\delta\boldsymbol{\varepsilon}\right)\right) \tag{4.46}$$

Differentiating equation (4.26) yields

$$\delta\boldsymbol{e}_{a_i} = \boldsymbol{C}_{ltf_i}\delta\boldsymbol{s}_{f_i} - \boldsymbol{M}_{\kappa_i}\delta\kappa \tag{4.47}$$

in which

$$\boldsymbol{C}_{ltf_i} = \left(\boldsymbol{m}'^{-1}_{xi} - \boldsymbol{I}\right)\boldsymbol{C}_L \qquad \text{and} \qquad \boldsymbol{M}_{\kappa i} = \boldsymbol{m}'^{-1}_{xi}\boldsymbol{m}'_{\kappa i}$$

The following gives the differential quantities of the plastic strain, plastic parameter and the local stress vector

$$\delta\boldsymbol{\varepsilon}_p = \delta\lambda\frac{\partial G}{\partial\boldsymbol{\sigma}} + \Delta\lambda\frac{\partial^2 G}{\partial\boldsymbol{\sigma}^2}\delta\boldsymbol{\sigma} \tag{4.48}$$

$$\delta\kappa = a_\kappa\left(\Delta\lambda\boldsymbol{k}_\sigma{}^T\delta\boldsymbol{\sigma} + c_\kappa\delta\lambda\right) \tag{4.49}$$

$$\delta\boldsymbol{s}_{f_i} = \boldsymbol{N}_i\delta\boldsymbol{\sigma} + \frac{\partial\boldsymbol{N}_i}{\partial\boldsymbol{\sigma}_I}\circ\boldsymbol{\sigma}_I\boldsymbol{D}_I\delta\boldsymbol{\varepsilon} \tag{4.50}$$

Utilising equations (4.47) to (4.50) in (4.46) and collecting terms gives

$$\delta\boldsymbol{\sigma} = \boldsymbol{A}_{c\Delta}\left[\left(\boldsymbol{I} - \sum_{j=1}^{n_p}\left(\boldsymbol{N}_j{}^T\boldsymbol{C}_{ltf_j}\frac{\partial\boldsymbol{N}_j}{\partial\boldsymbol{\sigma}_I}\circ\boldsymbol{\sigma}_I\boldsymbol{D}_I + \frac{\partial\boldsymbol{N}_j{}^T}{\partial\boldsymbol{\sigma}_I}\circ\boldsymbol{e}_{a_j}\boldsymbol{D}_I\right)\right)\delta\boldsymbol{\varepsilon} - \ldots\right.$$
$$\left.\ldots\left(\frac{\partial G}{\partial\boldsymbol{\sigma}} - \sum_{j=1}^{n_p}\left(\boldsymbol{N}_j{}^T\boldsymbol{M}_{\kappa j}a_\kappa c_\kappa\right)\right)\delta\lambda\right] \tag{4.51}$$

where

$$\boldsymbol{A}_{c\Delta} = \left[\boldsymbol{I} + \boldsymbol{D}_e \left(\sum_{j=1}^{n_p} \boldsymbol{N}_j{}^T (\boldsymbol{C}_{ltf\,j} \boldsymbol{N}_j - \boldsymbol{M}_{\kappa j} a_\kappa \Delta\lambda \boldsymbol{k}_\sigma{}^T) + \Delta\lambda \frac{\partial^2 G}{\partial \boldsymbol{\sigma}^2} \right) \right]^{-1} \boldsymbol{D}_e$$

The consistency condition for the yield surface may be written as

$$\delta F = \boldsymbol{f}_\kappa{}^T \delta\boldsymbol{\sigma} + h_\kappa \delta\lambda = 0 \tag{4.52}$$

Substituting for $\delta\boldsymbol{\sigma}$ in (4.52) using (4.51) and rearranging gives

$$\delta\lambda = \frac{\boldsymbol{f}_\kappa{}^T \boldsymbol{A}_{c\Delta} \boldsymbol{I}_N}{\boldsymbol{f}_\kappa{}^T \boldsymbol{A}_{c\Delta} \boldsymbol{g}_m - h_\kappa} \delta\boldsymbol{\varepsilon} \tag{4.53}$$

in which

$$\boldsymbol{I}_N = \boldsymbol{I} - \sum_{j=1}^{n_p} \left(\boldsymbol{N}_j{}^T \boldsymbol{C}_{ltf\,j} \frac{\partial \boldsymbol{N}_j}{\partial \boldsymbol{\sigma}_I} \circ \boldsymbol{\sigma}_I \boldsymbol{D}_I + \frac{\partial \boldsymbol{N}_j{}^T}{\partial \boldsymbol{\sigma}_I} \circ \boldsymbol{e}_{a_j} \boldsymbol{D}_I \right)$$

$$\boldsymbol{g}_m = \frac{\partial G}{\partial \boldsymbol{\sigma}} - \sum_{j=1}^{n_p} \left(\boldsymbol{N}_j{}^T \boldsymbol{M}_{\kappa j} a_\kappa c_\kappa \right)$$

Substituting for $\delta\lambda$ in (4.51), and using (4.53), gives the consistent tangent relationship as follows

$$\delta\boldsymbol{\sigma} = \left[\boldsymbol{A}_{c\Delta} \boldsymbol{I}_N - \frac{\boldsymbol{A}_{c\Delta} \boldsymbol{g}_m \boldsymbol{f}_\kappa^{\,T} \boldsymbol{A}_{c\Delta} \boldsymbol{I}_N}{\boldsymbol{f}_\kappa^{\,T} \boldsymbol{A}_{c\Delta} \boldsymbol{g}_m - h_\kappa} \right] \delta\boldsymbol{\varepsilon} = \boldsymbol{D}_{ep} \delta\boldsymbol{\varepsilon} \tag{4.54}$$

where $\boldsymbol{D}_{ep}$ is the consistent tangent operator.

4.8 Stress computation procedure

Prior to entering the return mapping algorithm, checks have to be made on whether the current step will violate the yield criterion and also whether it will result in the formation of one or more new POD. These checks are carried out using the trial stress $\boldsymbol{\sigma}_I$, which is derived as follows

$$\boldsymbol{\sigma}_I = \left(\boldsymbol{I} + \boldsymbol{D}_e \sum_{j=1}^{n_p} \boldsymbol{N}_j^{\,T} \boldsymbol{C}_{lsf_j} \boldsymbol{N}_j \right)^{-1} \boldsymbol{D}_e (\boldsymbol{\varepsilon}_k + \Delta\boldsymbol{\varepsilon} - \boldsymbol{\varepsilon}_{p_k}) = \boldsymbol{D}_I (\boldsymbol{\varepsilon}_k + \Delta\boldsymbol{\varepsilon} - \boldsymbol{\varepsilon}_{p_k}) \tag{4.55}$$

where $\boldsymbol{D}_I$ is the secant elastic-damage constitutive matrix. It is suggested that the use of an elastic stress increment, as given by equation (4.39), can cause inefficiency such that it incorrectly predicts yield and POD formation (Jefferson 2003b).

The overall stress recovery procedure systematically checks for the formation of PODs one at a time. At the end of the first return mapping that is undertaken with any existing PODs and plastic flow, if required, a check is performed to detect for new POD formation. If required, one new POD is formed and the next reduction is carried out, after which a further check is performed for the next POD. The process continues until the POD formation criterion is not violated. Box 4.2 shows the algorithm for the stress recovery calculations.

Box 4.2. Overall stress calculation procedure

Step	Description
1	Record all state variables on entry
2	Compute $\boldsymbol{\sigma}_I$ (4.55)

3	If $F(\boldsymbol{\sigma}_I, \kappa) > 0$ and $I_1(\boldsymbol{\sigma}_I) < 0$ Then
	Carry out return mapping with plasticity and existing PODs to obtain new stress $\boldsymbol{\sigma}$
	If $\Delta\lambda < 0$ Then
	Reset state variables and carry out mapping without plasticity
	End If
	Else If $n_p > 0$
	Carry out return mapping with existing PODs to obtain new stress $\boldsymbol{\sigma}$
	Else
	$\boldsymbol{\sigma} = \boldsymbol{\sigma}_I$
	End If

4	For $i = 1, n_{max}$[1]
	If $\sigma_1(\boldsymbol{\sigma}) > f_t$ Then
	Form one POD[2] using principal direction of $\boldsymbol{\sigma}_I$ nearest that of $\boldsymbol{\sigma}$
	Reset all state variables and carry out return mapping with revised number of PODs to obtain new stress $\boldsymbol{\sigma}$
	Else
	No new PODs, record final stress and exit formation loop
	End If
	End For

Notes:

1. n_{max} = maximum number of PODs permitted to form
2. A POD (j) is only permitted to form if the normal satisfies $\mathbf{r}_{d_i}{}^T \mathbf{r}_{d_j} \leq 0.65$, where i = 1, n_p (with n_p being the existing number of PODs)

4.9 Numerical examples

The Craft model has been implemented into a constitutive driver program for the simulation of single point stress-strain path examples. In order to assess the effectiveness of the local damage-contact model in simulating cracked concrete material, the model was validated by comparisons with results obtained from normal-shear tests. Table 4.1 gives the material parameters used in the analyses.

Table 4.1. Material properties used for analyses

Material parameters	Example 1	Example 2
E (N/mm^2)	30000	50000
υ	0.15	0.15
f_c (N/mm^2)	29.5	40
f_t (N/mm^2)	2.7	3
ε_c	0.0022	0.0023
ε_0	0.001	-
G_f (N/mm)	-	0.1
b_r	1.15	1.15
Z_0	0.5	0.6
ψ	-0.1	-0.1
m_g	0.38	0.4
m_{ful}	20	1.3

The first example involves the normal-shear test carried out by Walraven and Reinhardt (1981). Figure 4.8 shows the test specimen, which had a shear plane of 300×120 mm^2 and were tested in a stiff testing frame with external restraint bars to control the crack opening. Different initial crack opening displacements were specified for each test. Once a crack had been formed to the required opening, the specimen was then subjected to shear loading whilst the normal and shear displacements were monitored. Figure 4.9 and 4.10 show comparisons of the results obtained for tests with initial crack opening displacements of 0.2 mm.

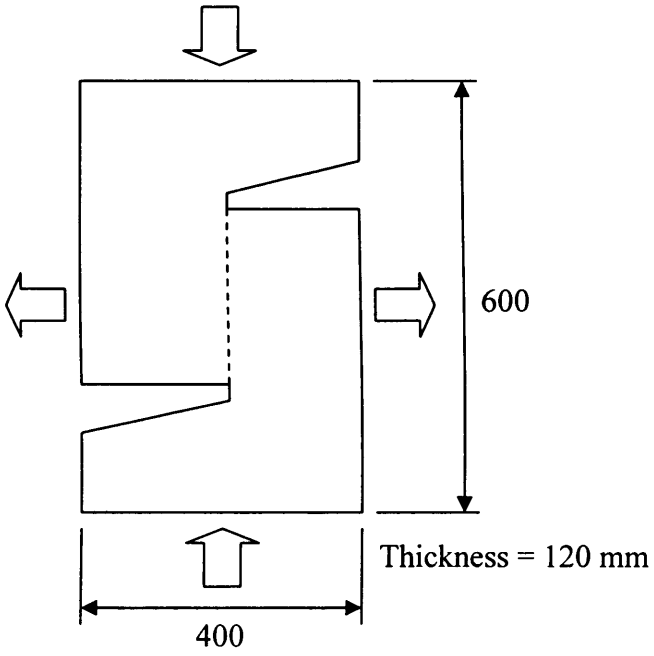

Figure 4.8. Walraven and Reinhardt's test specimen

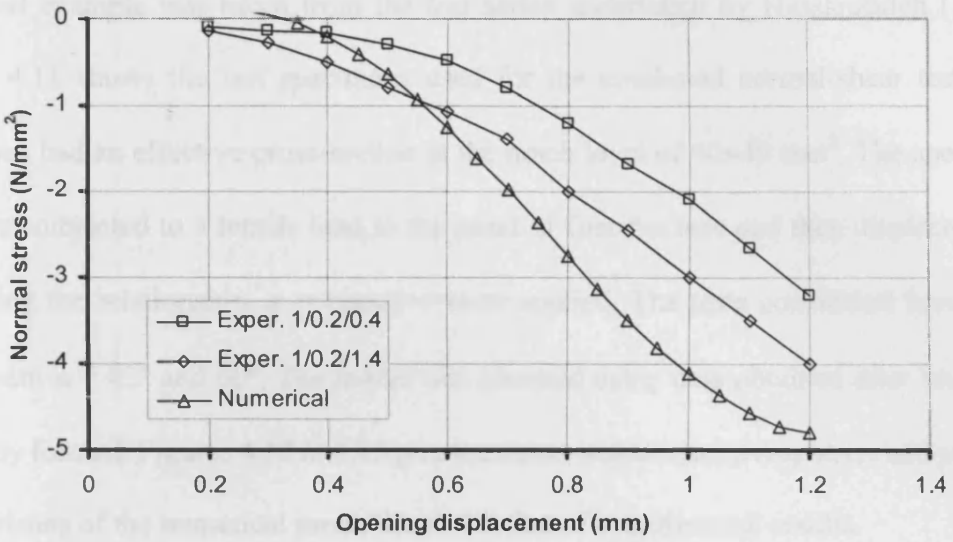

Figure 4.9. Normal stress-displacement relationship

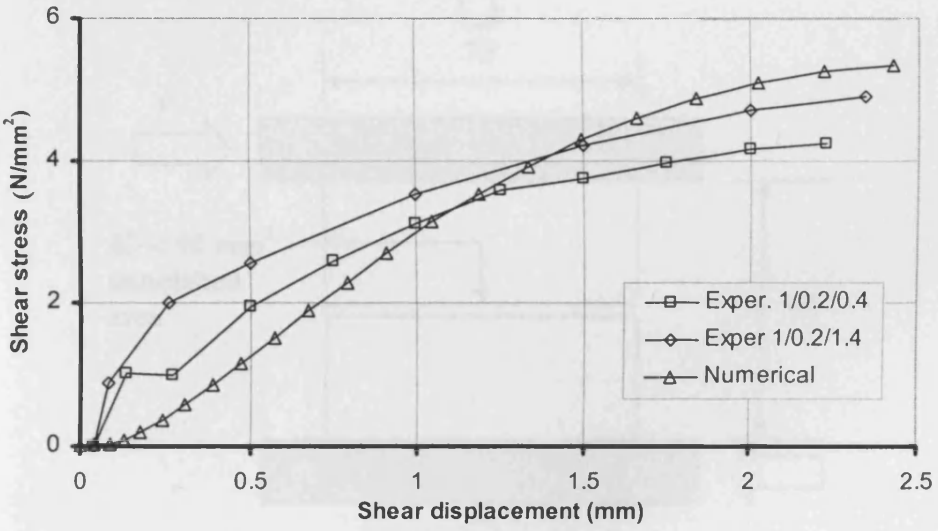

Figure 4.10. Shear stress-displacement relationship

The next example was taken from the test series undertaken by Hassanzadeh (1991). Figure 4.11 shows the test specimens used for the combined normal-shear test. The specimen had an effective cross-section at the notch level of 40×40 mm^2. The specimen was first subjected to a tensile load to the point of first fracture and then displacements according the relationship, $u = (\tan\alpha)*v$ were applied. The tests considered here were those with $\alpha = 45°$ and 60°. The model was assessed using data obtained after the crack had fully formed. Figures 4.12 to 4.15 give the stress-displacement responses and provide comparisons of the numerical predictions with that of experimental results.

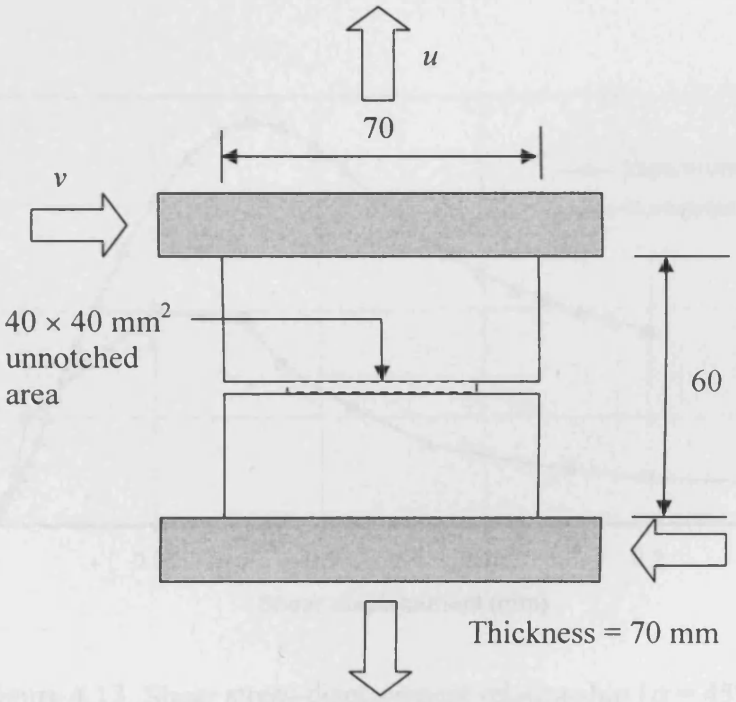

Figure 4.11. Hassanzadeh's test specimen

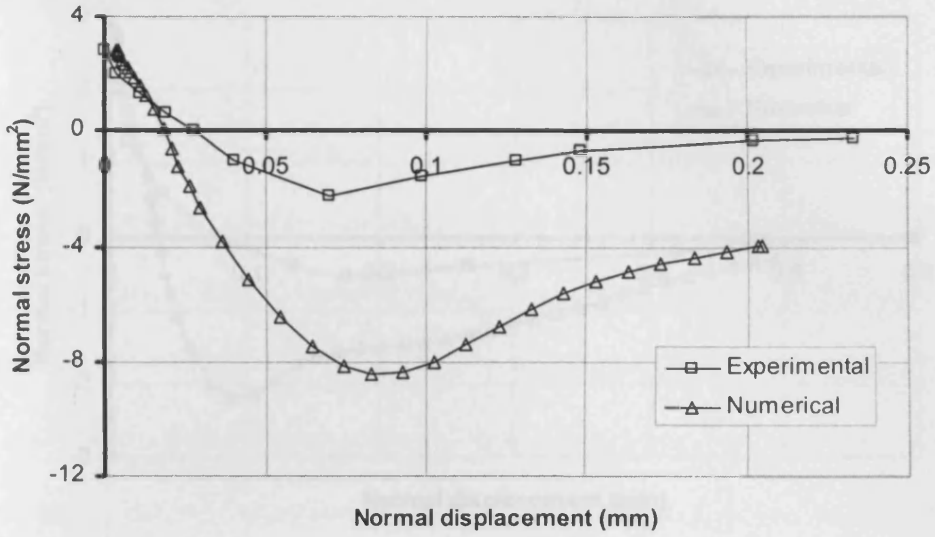

Figure 4.12. Normal stress-displacement relationship ($\alpha = 45°$)

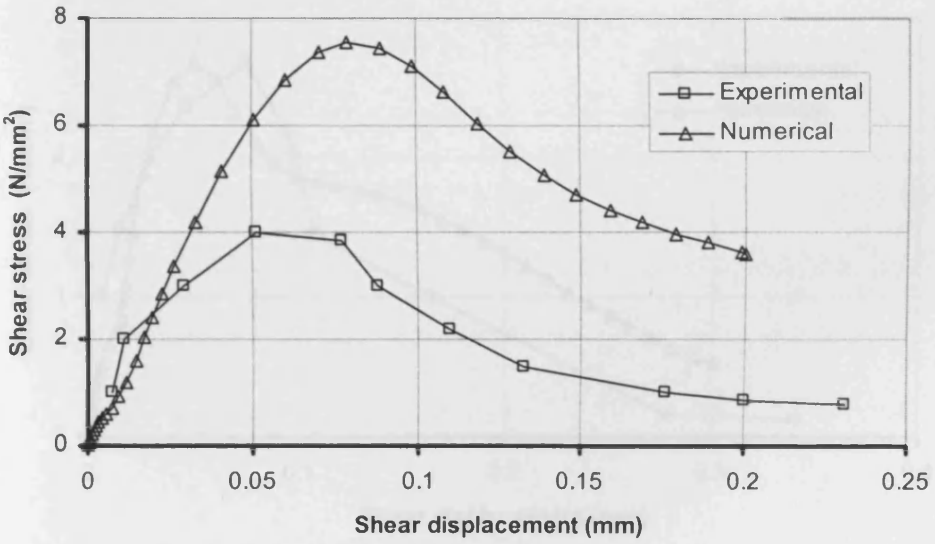

Figure 4.13. Shear stress-displacement relationship ($\alpha = 45°$)

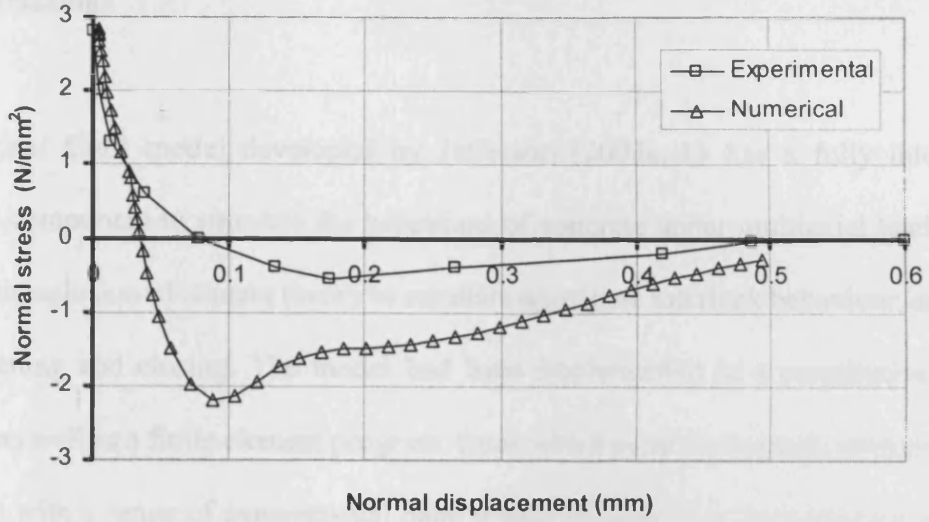

Figure 4.14. Normal stress-displacement relationship ($\alpha = 60°$)

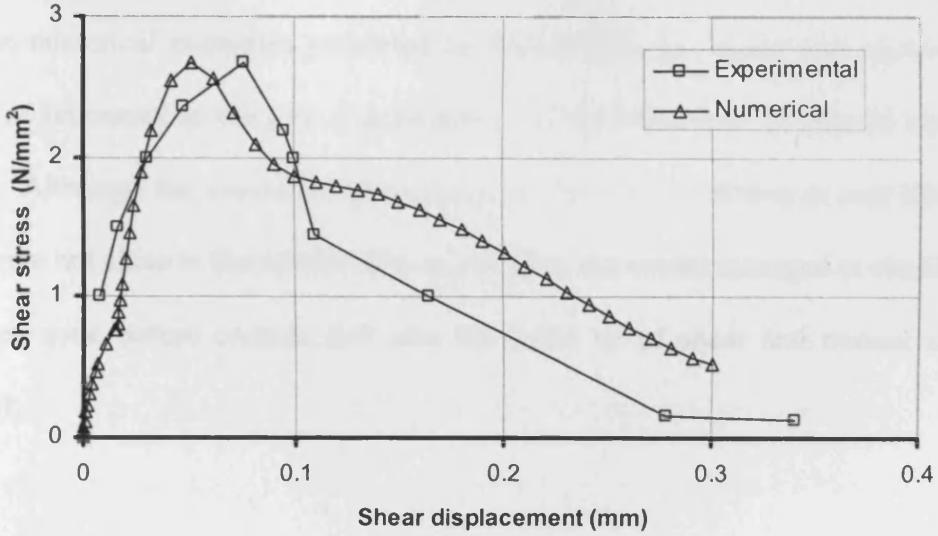

Figure 4.15. Shear stress-displacement relationship ($\alpha = 60°$)

4.10 Conclusions

The original Craft model developed by Jefferson (2003a, b) has a fully integrated plasticity component to simulate the behaviour of concrete under multiaxial loading, as well as the inclusion of contact theory to simulate aggregate interlock behaviour, and also crack opening and closing. The model had been implemented in a constitutive driver program as well as a finite element program, from which numerical results obtained were compared with a range of experimental data, which includes data from uniaxial tension tests, tests in which cracks are formed and then loaded in shear, and multiaxial compression tests.

From the numerical examples presented in Section 4.9, the model has shown to be capable of representing the key characteristics of the behaviour of formed cracks in concrete. Although the numerical predictions for the test of Walraven and Reinhardt (1981) were not close to that observed in experiment, the model managed to simulate the stress free zone before contact, and also the build up of shear and normal stresses reasonably.

As for the comparisons made with the data of Hassanzadeh (1991), the model seemed to overestimate the build up of post crack shear and normal stresses at small openings. This was due to the fact that the H_f function, as discussed in Section 4.3, was derived based on the data of Walraven and Reinhardt (1981). A modified function of H_f should be employed in order to simulate normal-shear tests on concrete specimens made from

relatively small coarse aggregate.

The Craft model is used as a basis of the crack plane models developed in the following chapters. Developments were carried out from the existing local damage-contact component of the model. This model has been chosen for several reasons:

1. The model has a proven triaxial failure envelope
2. Both plasticity and damage theory have already been implemented
3. The incorporation of contact mechanics has proven to simulate well the behaviour of crack opening and closing, as well as aggregate interlock
4. The constitutive relationships and stress update algorithm are well documented

The embedded planes model is suitable for the simulation of cracks in concrete. The model is however not applicable to massive concrete structures in which slip planes can develop as observed in construction joints. A new contact model, suitable for the simulation of smooth construction joints, is therefore proposed in Chapter 6. In addition, the original Craft model only predicts good concrete response under monotonic loading condition. In cyclic loading problems, the numerical predictions given by the model differ from those observed experimentally. This is mainly due to the assumption of a secant stiffness reduction, with no inelastic strains developed. Therefore, in order to simulate more realistically the behaviour of cracks in concrete, a new embedded planes model with local plasticity is proposed in Chapter 7.

Chapter Five

Dual-Surface Contact Model

5.1 Introduction

Experimental evidence has shown that the overall shear strength of a material is affected by the type, shape and size of aggregate particles. In normal strength concretes, both fine and coarse aggregate particles are evenly distributed within the mortar matrix. Large mismatches between the elastic moduli and strengths of aggregate and mortar matrix prevents cracks from penetrating into the aggregate particles. Crack paths tend to move towards the interface between aggregate and mortar, a region which is normally regarded as the weakest link in concrete (Karihaloo 1995). Figure 5.1 illustrates the path of a typical crack within a normal strength concrete matrix that comprises both coarse and fine aggregate particles. Paulay and Loeber (1974) undertook experiments to investigate the behaviour of such cracks in shear and, as may be seen from Figure 5.2, their results show that with increasing shear movement, for an open crack, the stiffness increases significantly at a certain shear displacement. Similar behaviour can also be seen in other such data (Walraven and Reinhardt 1981). Jefferson (2002a) interpreted this stiffness increase point as the first contact point and used it to define the interlock contact surface.

However, this ignores the fact that there are significant shear stresses before this point is reached. In order to better simulate the observed behaviour, a two-phase contact model is explored in which, tentatively, the two components are associated with the coarse particles and mortar (fine particles), as illustrated in Figure 5.1 (Hee *et al.* 2004).

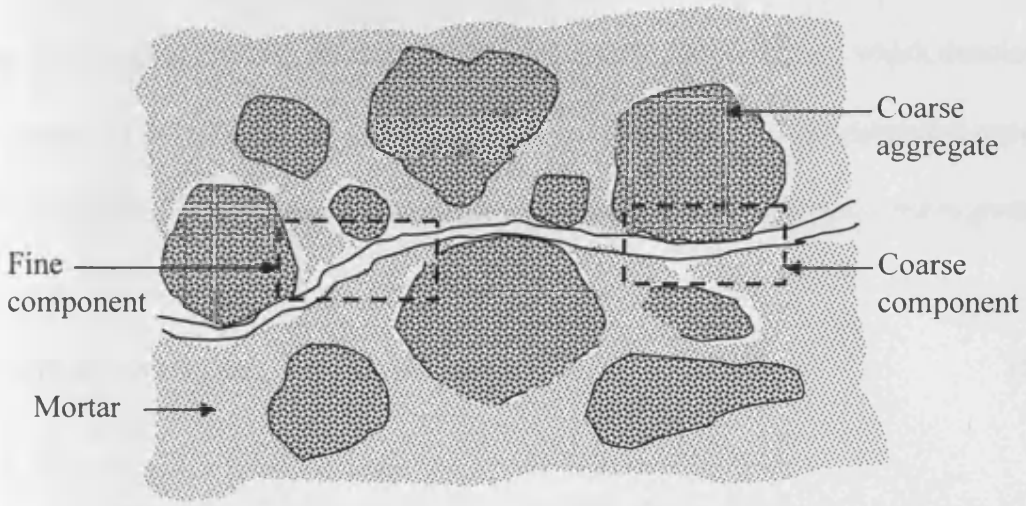

Figure 5.1. Crack path within concrete mix

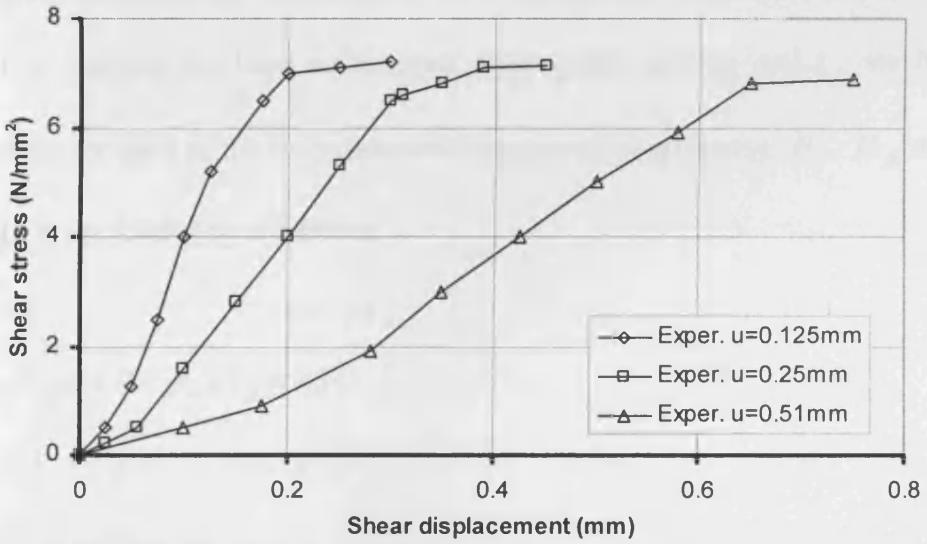

Figure 5.2. Shear deformations (Paulay and Loeber 1974)

5.2 Local damage-contact relationship

A two-phase contact model is proposed in which two contact surfaces are introduced, each of which captures the contact states of the damaged component on a crack plane. The proposed model employs a local stress-effective strain relationship similar to that used by Jefferson (2003a), with the addition of a new parameter α_c, which denotes the proportion of coarse particles in a representative volume of the fully debonded material. The local stress $\boldsymbol{s}_f$ is the sum of the stresses on each of the components, and is given by

$$\boldsymbol{s}_f = H_c \boldsymbol{s}_u + \alpha_c H_{fc} \omega \boldsymbol{s}_{fc} + (1-\alpha_c) H_{ff} \omega \boldsymbol{s}_{ff} \tag{5.1}$$

where H_c is a function of a scalar damage variable ζ, and both H_{fc} and H_{ff} govern the fully debonded component, with the subscripts *fc* and *ff* relating to the fraction of coarse and fine particles, respectively, in a representative volume of the damaged material. $\boldsymbol{s}_u$ denotes the local undamaged stress vector, and $\boldsymbol{s}_{fc}$ and $\boldsymbol{s}_{ff}$ are the local stress vector for each of the fully debonded component respectively. H_c, H_{fc} and H_{ff} must satisfy the following conditions

$$H_c + \alpha_c H_{fc} \omega + (1-\alpha_c) H_{ff} \omega = 1 \tag{5.2}$$

$$0 \le H_c \le 1 \tag{5.3}$$

$$0 \le \alpha_c H_{fc} \omega + (1-\alpha_c) H_{ff} \omega \le 1 \tag{5.4}$$

H_c denotes the proportion of undamaged material and can be expressed as

$$H_c = 1 - \omega \tag{5.5}$$

in which ω is a damage variable that lies in the range 0 to 1, and depends upon a local strain parameter ζ.

In the following derivations, it is noted that any terms with the subscript *f/c* should be treated as two separate variables i.e. *f* and *c* relating to the fine and coarse component respectively.

$H_{f/c}$ is a function that varies from 1 to 0 with the increasing crack opening parameter $e_{g_{f/c}}$. It represents the proportion of the fully debonded material on a crack plane that is in contact. The function is derived to simulate the observed phenomena in which the transfer of shear across a crack reduces with crack opening.

In the present model, the H_f function employed in the original Craft model was replaced by a modified function (Jefferson *et al.* 2004). The original H_f function, which was derived based on the data of Walraven and Reinhardt, was found to overestimate the build up of post crack shear and normal stresses at small openings. To remedy this, Jefferson *et al.* (2004) modified the function, in which a new parameter $m_{hi_{f/c}}$ that relates to the early stages of opening was introduced. The modified function is given as follows

$$H_{ff/c} = H_m \qquad \text{if} \qquad e_g < e_{bg} \tag{5.6}$$

$$H_{ff/c} = H_m H_{gf/c}\left[\frac{1}{1-f_h}\left(r_f\, e^{-\rho_{f1}\eta_0^2} + (1-r_f)e^{-\rho_{f2}\eta_1} - f_h e^{-\rho_{f1}\eta_0}\right)\right] \tag{5.7}$$

where

$$H_{gf/c} = 1 - e^{-c_g \frac{g_{f/c}}{e_{gf/c}+2\varepsilon_t}} \quad , \quad f_h = (1-r_f)\frac{\rho_{f2} m_{hif/c}}{\rho_{f1} m_{fulf/c}}$$

$$\eta_0 = \frac{e_{gf/c} - e_{bg}}{m_{hif/c}\varepsilon_0} \quad , \quad \eta_1 = \frac{e_{gf/c} - e_{bg}}{m_{fulf/c}\varepsilon_0}$$

and $r_f = 0.7$, $\rho_{f1} = 10$, $\rho_{f2} = 5$, $c_g = 3$, $H_m = 0.995$ and $e_{bg} = 1.1\varepsilon_t$. The $H_{gf/c}$ function provides a smooth but rapid transition to closed and interlock states. The last term in equation (5.7) provides a correction to give a zero initial slope and also makes the $H_{ff/c}$ function continuous at the start of contact reduction.

The $H_{ff/c}$ function also depends upon the condition of damage and the state of contact of the crack plane, as shown in Figure 5.3, which are termed open, interlock and closed.

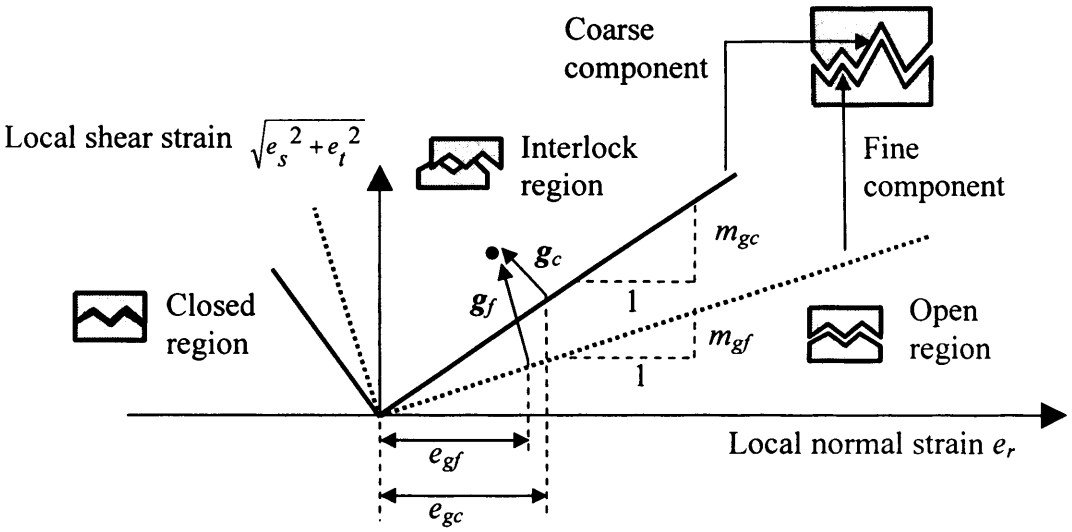

Figure 5.3. Dual-surface contact model

Both interlock and closed functions for each of the components are derived to identify the current state of contact,

$$\phi_{\text{int}f/c}(\boldsymbol{e}) = m_{gf/c}e_r - \sqrt{e_s^2 + e_t^2} \tag{5.8}$$

$$\phi_{clf\ c}(\boldsymbol{e}) = e_r + m_{gf/c}\sqrt{e_s^2 + e_t^2} \tag{5.9}$$

If $\phi_{clf/c}(\boldsymbol{e}) \le 0$ State = Closed (5.10)

If $\phi_{clf/c}(\boldsymbol{e}) > 0$ and $\phi_{\text{int}f/c}(\boldsymbol{e}) < 0$ and $e_r < e_{fulf/c}$ State = Interlock (5.11)

If $\phi_{intf/c}(\boldsymbol{e}) \ge 0$ or $e_r \ge e_{fulf/c}$ State = Open (5.12)

The gradient of the two interlock contact surfaces, m_{gc} and m_{gf} can be obtained from experimental data from tests in which an open crack is subjected to shear loading. $e_{ful_{f/c}}$ denotes the crack opening strain beyond which no further contact can be gained in shear for each component.

The crack opening parameter $e_{g_{f/c}}$ is related to the components of the effective local strain as follows

$$e_{g_{f/c}} = \frac{1}{1+m_{g_{f/c}}^{\ 2}}\left[e_r + m_{g_{f/c}}\sqrt{e_s^{\ 2}+e_t^{\ 2}}\right] \tag{5.13}$$

The embedments $\boldsymbol{g}_f$ and $\boldsymbol{g}_c$ denote the strain relative to each of the contact surfaces and is associated to the local effective strain by the relation

$$\boldsymbol{g}_{f/c} = \boldsymbol{\Phi}_{d_{f/c}}\boldsymbol{e} \tag{5.14}$$

The transformation matrix $\boldsymbol{\Phi}_{d_{f/c}}$ depends upon the state of contact as follows

$$\boldsymbol{\Phi}_{d_{f/c}} = \boldsymbol{0} \qquad \text{if State = Open} \tag{5.15}$$

$$\boldsymbol{\Phi}_{d_{f/c}} = \boldsymbol{\Phi}_{g_{f/c}} \qquad \text{if State = Interlock} \tag{5.16}$$

$$\boldsymbol{\Phi}_{d_{f/c}} = \boldsymbol{I} \qquad \text{if State = Closed} \tag{5.17}$$

where

$$\boldsymbol{\Phi}_{g_{f/c}} = \frac{1}{1+m_{g_{f/c}}{}^2}\left[\left(\frac{\partial \phi_{\text{int}f/c}}{\partial \boldsymbol{e}}\right)\cdot\left(\frac{\partial \phi_{\text{int}f/c}}{\partial \boldsymbol{e}}\right)^T + \phi_{\text{int}f/c}\frac{\partial^2 \phi_{\text{int}f/c}}{\partial \boldsymbol{e}^2}\right]$$

The constitutive relationship for the effective crack plane can now be written as

$$\begin{aligned} \boldsymbol{s}_f &= \boldsymbol{D}_L\left(H_c\boldsymbol{e} + \alpha_c H_{fc}\omega\boldsymbol{g}_c + (1-\alpha_c)H_{ff}\omega\boldsymbol{g}_f\right) \\ &= \boldsymbol{D}_L\left(H_c\boldsymbol{I} + \alpha_c H_{fc}\omega\boldsymbol{\Phi}_{dc} + (1-\alpha_c)H_{ff}\omega\boldsymbol{\Phi}_{df}\right)\boldsymbol{e} = \boldsymbol{D}_L\boldsymbol{M}_x\boldsymbol{e} = \boldsymbol{D}_{ls}\boldsymbol{e} \end{aligned} \tag{5.18}$$

In the present model, a smooth continuous softening function developed by Jefferson *et al.* (2004) was employed. The function, as illustrated in Figure 5.4, was derived in terms of the fracture stress f_s and the strain parameter ζ. The function utilises the uniaxial tensile strength f_t, the stress at first damage f_{ti} and the associated strain ε_{ti}, the strain at peak stress ε_k, and the strain at the effective end of the softening curve ε_0, as control parameters. The damage evolution function is given as follows

$$f_s = r_c f_{ti} + (1-r_c)f_{ti}e^{-c_1\eta}\left(a_m - b_m e^{-c_1 m\eta} - c_m e^{-c_1 mp\eta}\right) \tag{5.19}$$

in which

$$\eta = \frac{\zeta - \varepsilon_{ti}}{\varepsilon_0 - \varepsilon_{ti}}$$

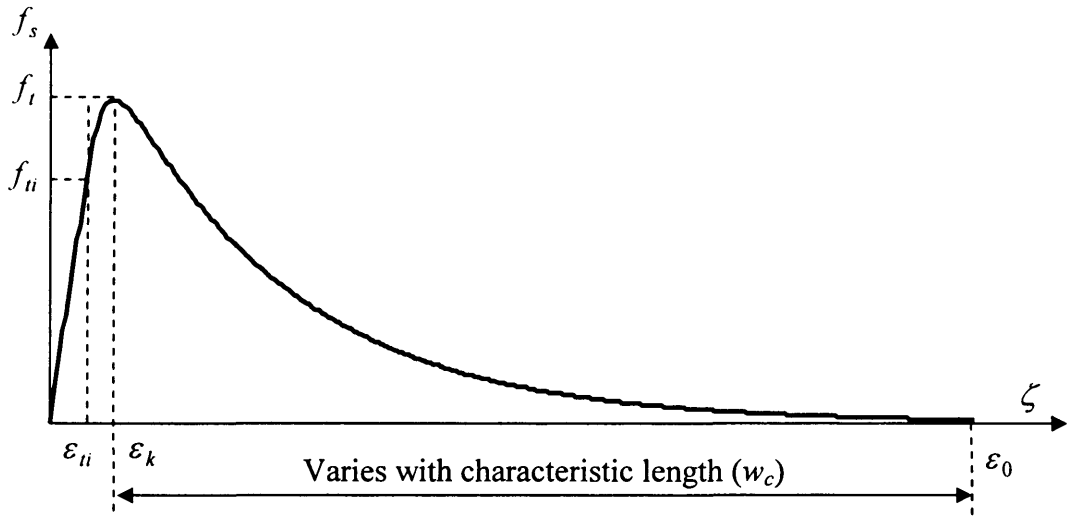

Figure 5.4. Damage evolution function

The term r_c provides residual damage strength at the end of the softening curve which, in turn, helps to stabilise numerical calculations. The constants c_1 and p in (5.19) were set to a fixed value of 5. The rest of the constants i.e. a_m, b_m, c_m and m were evaluated from the following conditions

$$f_s = f_{ti} \text{ at } \eta = 0 \tag{5.20}$$

$$\frac{\partial f_s}{\partial \zeta} = E \text{ at } \eta = 0 \tag{5.21}$$

$$f_s = f_t \text{ at } \eta = \eta_k \tag{5.22}$$

$$\frac{\partial f_s}{\partial \zeta} = 0 \text{ at } \eta = \eta_k \tag{5.23}$$

where the term η_k is η at $\zeta = \zeta_k$.

Making use of (5.20), a_m may be derived as follows

$$a_m = 1 + b_m + c_m \tag{5.24}$$

Utilising (5.21) and (5.24) yields

$$q = b_m m + c_m mp \tag{5.25}$$

in which $q = \dfrac{\varepsilon_0 - \varepsilon_{ti}}{c_1 \varepsilon_{ti}} + 1$

Using equations (5.24) and (5.25) to eliminate a_m and b_m, the following expressions for c_m may be derived using conditions (5.22) and (5.23) respectively

$$c_m = \frac{\dfrac{1}{a_t x_k} - 1 - \dfrac{q}{m}\left(1 - x_k{}^m\right)}{1 - x_k{}^{mp} + p x_k{}^m - p} \tag{5.26}$$

$$c_m = \frac{1+\frac{q}{m}\left(1-(1+m)x_k{}^m\right)}{p-1-(1+m)px_k{}^m+(1+mp)x_k{}^{mp}} \tag{5.27}$$

Finally, equating (5.26) to (5.27) and rearranging gives the following nonlinear equation, which may be solved for the unknown m.

$$\left(\frac{1}{a_t x_k}-1-\frac{q}{m}\left(1-x_k{}^m\right)\right)\left(p-1-p(1+m)x_k{}^m+(1+pm)x_k{}^{pm}\right)-\ \ldots$$

$$\ldots\left(1+\frac{q}{m}(1-(1+m)x_k{}^m)\right)\left(1-x_k{}^{mp}-p+px_k{}^m\right)=0 \tag{5.28}$$

in which

$$x_k = e^{-c_1\eta_k} \quad \text{and} \quad a_t = \frac{f_{ti}}{f_t}$$

Given that the value of m varies with x_k and q, which in turn are functions of a strain parameter ratio r_ε, an approximate relationship between m and r_ε, which is closely fitted to the actual function, was derived as follows (Jefferson *et al.* 2004)

$$m = z_1 + z_2 r_\varepsilon + z_3 r_\varepsilon{}^{1.005} \tag{5.29}$$

where

$$r_{\varepsilon} = \frac{\varepsilon_0 - \varepsilon_{ti}}{\varepsilon_{ti}}$$

The constants z_1, z_2 and z_3 were evaluated to minimise the error between the approximate and actual root functions for m. In the present model, a_t was set at 0.75, while the rest of the constants were set as follows

$z_1 = 0.223098944982796$, $z_2 = -67.0625617052971$ and $z_3 = 66.4302094339053$

5.3 Evaluation of contact parameters

For large opening displacements, the coarse component may dominate the overall stress due to the aggregate interlock behaviour, whereas at small opening displacements the fine component is also significant. Using the experimental data of Walraven and Reinhardt (1981), as shown in Figure 5.5, the m_g values for both fine m_{gf} and coarse m_{gc} components are determined by assuming the first half of the non-linear curve as being dominated more by the fine component, and the second half by the coarse component. In the proposed model, m_{gf} and m_{gc} are taken as 0.2 and 0.4 respectively.

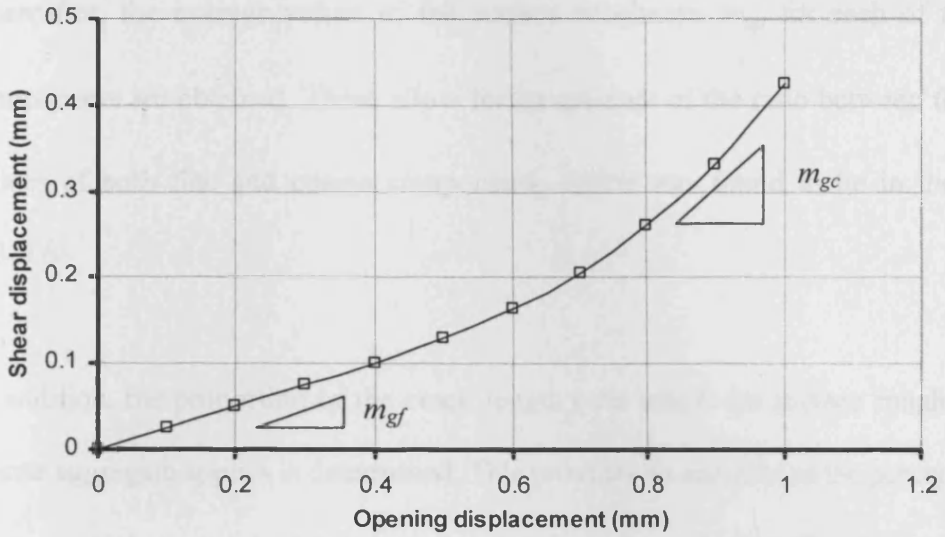

Figure 5.5. Normal-shear contact relationship (Walraven and Reinhardt 1981)

From the literature, a series of images captured using a Scanning Electron Microscope (SEM) at meso-level, as shown in Figures 5.6 and 5.7, were used to obtain average measurement of the crack surface roughness (Ollivier 1985; van Mier 1997). The procedure for deriving the contact parameters for the dual contact model, with reference to Figure 5.8, is as follows

1. A mean reference crack line is drawn parallel to the direction of crack propagation, which intersects aggregate particles whose perimeters form part of the crack faces.

2. By taking several sampling points along the crack, the distances between the free surface and reference line are measured, i.e. c_i and f_i for the coarse and fine components respectively, where i and j denote the number of sampling point for the coarse and fine particles respectively along the crack reference line.

3. Thereafter, the average values of the surface roughness m_{ful} for each of the two components are obtained. These allow for an estimate of the ratio between the m_{ful} values of both fine and coarse components, which was found to lie in the range 0.3-0.6.

4. In addition, the proportion of the crack length over which the surface roughness of coarse aggregate applies is determined. This provides an estimate of the percentage of coarse particles present within the concrete matrix ($\alpha_c = l_c / L$). Having examined a number of SEM images, it was found that α_c falls in the range 0.3-0.4.

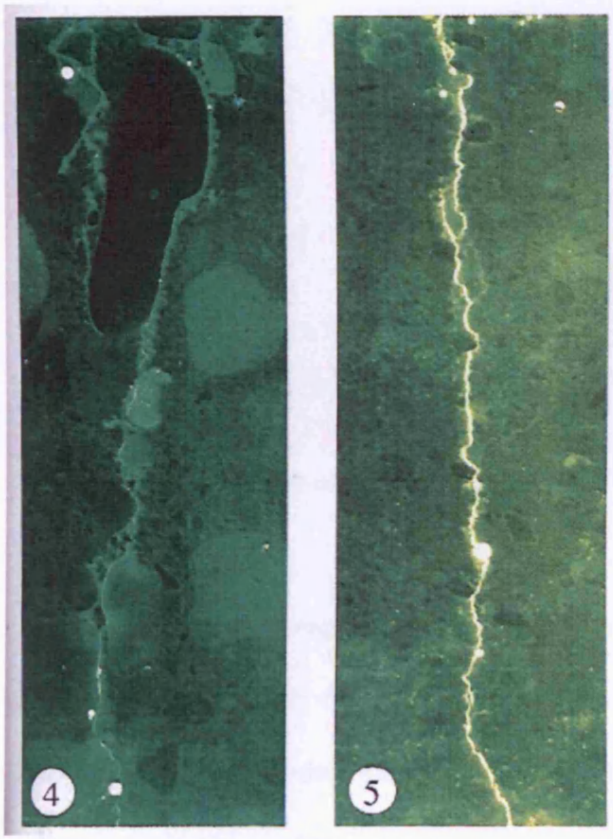

Figure 5.6. Formation of cracks in concrete (van Mier 1997)

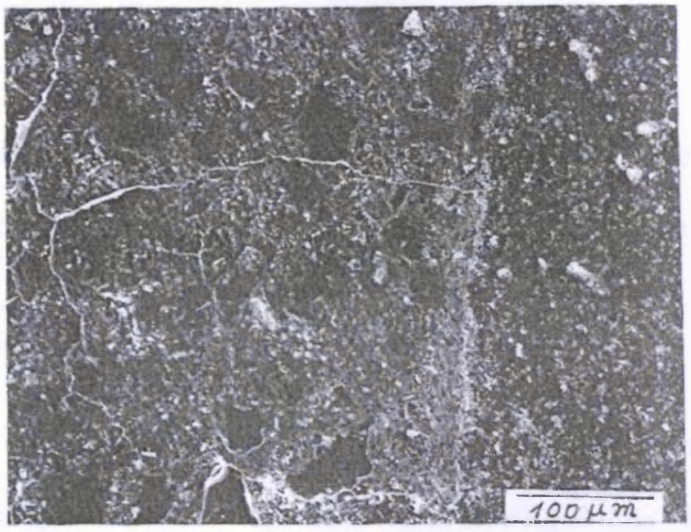

Figure 5.7. Crack paths in concrete (Ollivier 1985)

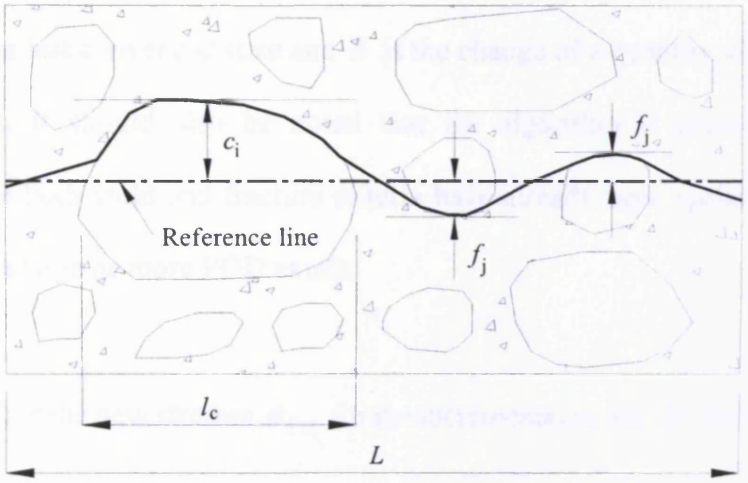

Figure 5.8. Derivation of contact parameters

Having determined all the necessary parameters for both contact surfaces, the dual-surface contact model can then be easily combined with the plasticity component, as discussed in Chapter 4, to form a fully integrated plastic-damage-contact model. The next section describes the return mapping algorithm.

5.4 Stress recovery algorithm

The algorithms described in this section are essentially the same as those given in Chapter 4, but with some differences in the local matrices. Nevertheless, they are included here for completeness.

In the context of a finite element incremental-iterative solution for a time independent problem, the stress update is made from the previous converged state. In this section, it is noted that the subscripts k and $k+1$ represents the values of quantities on entry to and exit from the return mapping algorithm respectively. Δ denotes the overall change of any quantity from the last converged state and δ is the change of a quantity within the stress update iteration. It should also be noted that the algorithm is presented with the assumptions that both yield and fracture criteria have already been violated, i.e. plastic yield is active and one or more POD exists.

In order to evaluate the new stresses $\boldsymbol{\sigma}_{k+1}$ for the incremental strain $\Delta\boldsymbol{\varepsilon}$ from the previous stresses $\boldsymbol{\sigma}_k$, the following relationships must be satisfied.

- total constitutive relationship

$$\boldsymbol{\sigma}_{k+1} = \boldsymbol{D}_e\left(\boldsymbol{\varepsilon}_{k+1} - \boldsymbol{\varepsilon}_{p_{k+1}} - \sum_{j=1}^{n_p} \boldsymbol{N}_j{}^T \boldsymbol{e}_{a_{j_{k+1}}}\right) \tag{5.30}$$

- stress transformation

$$\boldsymbol{s}_{f\,i\,k+1} = \boldsymbol{N}_{i\,k+1}\boldsymbol{\sigma}_{k+1} \tag{5.31}$$

- local stress-strain relationships for all PODs i

$$\boldsymbol{s}_{f\,i_{k+1}} = \boldsymbol{D}_{ls\,i\,k+1}\boldsymbol{e}_{i_{k+1}} \tag{5.32}$$

$$\boldsymbol{e}_{a\,i\,k+1} = \boldsymbol{C}_{lsf\,i\,k+1}\boldsymbol{s}_{f\,i\,k+1} \tag{5.33}$$

where $\boldsymbol{C}_{lsf}$ is the local compliance matrix.

- flow rule and plastic parameter

$$\Delta\boldsymbol{\varepsilon}_p = \frac{\partial G}{\partial \boldsymbol{\sigma}}_{k+1} \Delta\lambda \tag{5.34}$$

$$\Delta\kappa = X_{k+1}\Delta\lambda\boldsymbol{\sigma}_{k+1}{}^{T}\frac{\partial G}{\partial \boldsymbol{\sigma}}_{k+1} \tag{5.35}$$

- yield function

$$F(\boldsymbol{\sigma}_{k+1}, \kappa_{k+1}) = 0 \tag{5.36}$$

- total-local function

$$\boldsymbol{F}_{e\,i_{k+1}} = \boldsymbol{N}_{i_{k+1}}\boldsymbol{\sigma}_{k+1} - \boldsymbol{D}_{ls_{i_{k+1}}}\boldsymbol{e}_{i_{k+1}} = \boldsymbol{0} \tag{5.37}$$

The total-local function is used to ensure that equations (5.30) to (5.33) are simultaneously satisfied (Jefferson 2003b). The model adopts an algorithm similar to that of the Closest Point Projection (Simo and Hughes, 1998). The numerical solution method is chosen for its stability and enhanced rate of convergence. Error measures are introduced for the plastic strain and plastic parameter, which, along with the error in the yield function and total-local function, are used in a coupled Newton iterative solution procedure.

For clarity the overall iteration subscripts will now be dropped, it being assumed that all quantities on the right of an equation are those from the previous update iteration (or the values from the previous overall finite element increment for the 1st iteration).

The error measures for both plastic strain and hardening parameter are defined as follows

$$\boldsymbol{R}_{\varepsilon} = -\Delta\boldsymbol{\varepsilon}_{p} + \frac{\partial G}{\partial \boldsymbol{\sigma}}\Delta\lambda \tag{5.38}$$

$$R_{\kappa} = -\Delta\kappa + X\Delta\lambda\boldsymbol{\sigma}^{T}\frac{\partial G}{\partial \boldsymbol{\sigma}} \tag{5.39}$$

From which the iterative corrections are obtained as follows

$$\delta\boldsymbol{\varepsilon}_{p} = \boldsymbol{R}_{\varepsilon} + \delta\lambda\frac{\partial G}{\partial \boldsymbol{\sigma}} + \Delta\lambda\frac{\partial^{2} G}{\partial \boldsymbol{\sigma}^{2}}\delta\boldsymbol{\sigma} + \Delta\lambda\frac{\partial^{2} G}{\partial\boldsymbol{\sigma}\partial\kappa}\delta\kappa \tag{5.40}$$

$$\delta\kappa = a_{\kappa}\left(R_{\kappa} + \Delta\lambda\boldsymbol{k}_{\sigma}{}^{T}\delta\boldsymbol{\sigma} + c_{\kappa}\delta\lambda\right) \tag{5.41}$$

where

$$a_\kappa = \left(1 - \Delta\lambda X \boldsymbol{\sigma}^T \frac{\partial^2 G}{\partial \boldsymbol{\sigma} \partial \kappa}\right)^{-1} \quad , \qquad c_\kappa = X \boldsymbol{\sigma}^T \frac{\partial G}{\partial \boldsymbol{\sigma}} \qquad \text{and}$$

$$\boldsymbol{k}_\sigma = \frac{\partial X}{\partial \boldsymbol{\sigma}} \boldsymbol{\sigma}^T \frac{\partial G}{\partial \boldsymbol{\sigma}} + X \frac{\partial^2 G}{\partial \boldsymbol{\sigma}^2} \boldsymbol{\sigma} + X \frac{\partial G}{\partial \boldsymbol{\sigma}}$$

The yield function consistency condition is given by

$$F + \frac{\partial F}{\partial \boldsymbol{\sigma}}^T \delta\boldsymbol{\sigma} + \frac{\partial F}{\partial \kappa} \delta\kappa = 0 \tag{5.42}$$

Substituting (5.41) in (5.42) and rearranging gives

$$F + \boldsymbol{f}_\kappa{}^T \delta\boldsymbol{\sigma} + \frac{\partial F}{\partial \kappa} a_\kappa R_\kappa + h_\kappa \delta\lambda = 0 \tag{5.43}$$

where

$$\boldsymbol{f}_\kappa = \frac{\partial F}{\partial \boldsymbol{\sigma}} + \frac{\partial F}{\partial \kappa} a_\kappa \Delta\lambda \boldsymbol{k}_\sigma \qquad \text{and} \qquad h_\kappa = \frac{\partial F}{\partial \kappa} a_\kappa c_\kappa$$

Using (5.37), the total-local consistency condition can be written as follows

$$\boldsymbol{F}_{ei} + \boldsymbol{N}_i \delta\boldsymbol{\sigma} + \frac{\partial \boldsymbol{N}_i}{\partial \boldsymbol{\sigma}} \circ \boldsymbol{\sigma} \delta\boldsymbol{\sigma} - \frac{\partial \boldsymbol{D}_{lsi}}{\partial \boldsymbol{e}_i} \circ \boldsymbol{e}_i \delta\boldsymbol{e}_i - \frac{\partial \boldsymbol{D}_{lsi}}{\partial \kappa} \boldsymbol{e}_i \delta\kappa - \boldsymbol{D}_{lsi} \delta\boldsymbol{e}_i = \boldsymbol{0} \tag{5.44}$$

in which $\circ$ denotes a contraction with respect to the 'in-plane' components of a third order matrix. The third term in the above equation is null here as the orientation of the POD remains fixed during the stress update iterations. Then, substituting (5.41) in (5.44) yields

$$\boldsymbol{F}_{ei} + \boldsymbol{N}_{\Delta i} \delta\boldsymbol{\sigma} - \boldsymbol{D}_{l\kappa i} a_\kappa \left(R_\kappa + c_\kappa \delta\lambda\right) - \boldsymbol{D}_{lli} \delta\boldsymbol{e}_i = \boldsymbol{0} \tag{5.45}$$

where

$$\boldsymbol{D}_{lli} = \frac{\partial \boldsymbol{D}_{lsi}}{\partial \boldsymbol{e}_i} \circ \boldsymbol{e}_i + \boldsymbol{D}_{lsi} \quad , \quad \boldsymbol{D}_{l\kappa i} = \frac{\partial \boldsymbol{D}_{lsi}}{\partial \kappa} \boldsymbol{e}_i \quad \text{and}$$

$$\boldsymbol{N}_{\Delta i} = \boldsymbol{N}_i - \boldsymbol{D}_{l\kappa i} a_\kappa \boldsymbol{k}_\sigma{}^T \Delta\lambda$$

The initial trial stress is given by

$$\boldsymbol{\sigma} = \boldsymbol{D}_e \left(\boldsymbol{\varepsilon} + \Delta\boldsymbol{\varepsilon} - \boldsymbol{\varepsilon}_p - \sum_{j=1}^{n_p} \boldsymbol{N}_j{}^T \boldsymbol{e}_{aj} \right) \tag{5.46}$$

after which iterations are performed to satisfy equations (5.30) to (5.36). Since the total strain tensor does not change during the iterations, the iterative change in the stress may be written as

$$\delta\boldsymbol{\sigma} = -\boldsymbol{D}_e\left(\delta\boldsymbol{\varepsilon}_p + \sum_{j=1}^{n_p}\boldsymbol{N}_j{}^T\delta\boldsymbol{e}_{aj}\right) \tag{5.47}$$

The iterative change in the added strain $\boldsymbol{e}_a$ is given by

$$\delta\boldsymbol{e}_{ai} = \left(\boldsymbol{I} - \boldsymbol{m}'_{xi}\right)\delta\boldsymbol{e}_i + \boldsymbol{m}'_{\kappa i}\delta\kappa \tag{5.48}$$

where

$$\boldsymbol{m}'_{xi} = \boldsymbol{M}_{xi} + \frac{\partial \boldsymbol{M}_{xi}}{\partial \boldsymbol{e}_i}\circ\boldsymbol{e}_i \qquad \text{and} \qquad \boldsymbol{m}'_{\kappa i} = \frac{\partial \boldsymbol{M}_{xi}}{\partial\kappa}\boldsymbol{e}_i$$

Utilising (5.40), (5.41) and (5.48) in (5.47) and rearranging yields

$$\delta\boldsymbol{\sigma} = -\boldsymbol{A}\left[\boldsymbol{R}_{\varepsilon m} + \boldsymbol{g}_{\varepsilon m}\delta\lambda + \sum_{j=1}^{n_p}\boldsymbol{N}_j{}^T\left[\left(\boldsymbol{I} - \boldsymbol{m}'_{xj}\right)\delta\boldsymbol{e}_j + \boldsymbol{m}'_{\kappa j}a_\kappa\left(R_\kappa + c_\kappa\delta\lambda\right)\right]\right] \tag{5.49}$$

in which

$$\boldsymbol{g}_{\varepsilon m} = \frac{\partial G}{\partial \boldsymbol{\sigma}} + \frac{\partial^2 G}{\partial \boldsymbol{\sigma} \partial \kappa} \Delta\lambda a_\kappa c_\kappa$$

$$\boldsymbol{R}_{\varepsilon m} = \boldsymbol{R}_\varepsilon + \frac{\partial^2 G}{\partial \boldsymbol{\sigma} \partial \kappa} \Delta\lambda a_\kappa R_\kappa$$

$$\boldsymbol{A} = \left[\boldsymbol{I} + \boldsymbol{D}_e \left(\Delta\lambda \frac{\partial^2 G}{\partial \boldsymbol{\sigma}^2} + \Delta\lambda \frac{\partial^2 G}{\partial \boldsymbol{\sigma} \partial \kappa} \Delta\lambda a_\kappa c_\kappa - \sum_{j=1}^{n_p} \boldsymbol{N}_j{}^T \boldsymbol{m}'_{\kappa j} a_\kappa \boldsymbol{k}_\sigma{}^T \Delta\lambda \right) \right]^{-1} \boldsymbol{D}_e$$

Substituting for $\delta\boldsymbol{\sigma}$ from (5.49) in (5.43) and (5.44) gives a set of coupled equations with $\delta\lambda$ and $\delta\boldsymbol{e}_i$ as the unknowns. These are written in the following compact form, in which i and j are indices from 1 to n_p and in which the summation of repeated indices is implied. Note that $i.j$ does not here imply differentiation with respect to j components as it would in indicial notation.

$$F_\lambda = M_\lambda \delta\lambda + \boldsymbol{B}_{\lambda j} \delta\boldsymbol{e}_j \tag{5.50}$$

$$\boldsymbol{F}_{Ei} = \boldsymbol{M}_{Ei} \delta\lambda + \boldsymbol{B}_{Ei,j} \delta\boldsymbol{e}_j \tag{5.51}$$

in which

$$F_\lambda = F - \boldsymbol{f}_\kappa{}^T \boldsymbol{A}\left(\boldsymbol{R}_{\varepsilon m} - \sum_{k=1}^{n_p} \boldsymbol{N}_k{}^T \boldsymbol{m}'_{\kappa k} a_\kappa R_\kappa \right) + \frac{\partial F}{\partial \kappa} a_\kappa R_\kappa$$

$$\boldsymbol{F}_{Ei} = \boldsymbol{F}_{ei} - \boldsymbol{N}_{\Delta i}\boldsymbol{A}\left(\boldsymbol{R}_{\varepsilon m} - \sum_{k=1}^{n_p} \boldsymbol{N}_k{}^T \boldsymbol{m}'_{\kappa k} a_\kappa R_\kappa \right) - \boldsymbol{D}_{l\kappa i} a_\kappa R_\kappa$$

$$M_\lambda = \boldsymbol{f}_\kappa{}^T \boldsymbol{A}\left(\boldsymbol{g}_{\varepsilon m} - \sum_{k=1}^{n_p} \boldsymbol{N}_k{}^T \boldsymbol{m}'_{\kappa k} a_\kappa c_\kappa \right) - h_\kappa$$

$$\boldsymbol{M}_{Ei} = \boldsymbol{N}_{\Delta i}\boldsymbol{A}\left(\boldsymbol{g}_{\varepsilon m} - \sum_{k=1}^{n_p} \boldsymbol{N}_k{}^T \boldsymbol{m}'_{\kappa k} a_\kappa c_\kappa \right) + \boldsymbol{D}_{l\kappa i} a_\kappa c_\kappa$$

$$\boldsymbol{B}_{\lambda_j} = \boldsymbol{f}_\kappa{}^T \boldsymbol{A}\boldsymbol{N}_j{}^T \left(\boldsymbol{I} - \boldsymbol{m}'_{x_j} \right)$$

$$\boldsymbol{B}_{E_{i,j}} = \boldsymbol{N}_{\Delta i}\boldsymbol{A}\boldsymbol{N}_j{}^T \left(\boldsymbol{I} - \boldsymbol{m}'_{x_j} \right) + \boldsymbol{D}_{lti,j}\partial_{i,j}$$

where $\partial_{i,j}$ in the expression for $\boldsymbol{B}_E$ is the Kronecker delta.

The overall steps of the return mapping algorithm may now be summarised for the case when plastic yield is active and one or more POD exists.

Box 5.1. Return mapping algorithm

Step	Description
1	Initialise $\Delta\lambda = 0$ and $\Delta\kappa = 0$
2	Compute trial stress from (5.46)
3	Evaluate $F_\lambda, M_\lambda, \boldsymbol{B}_\lambda, \boldsymbol{F}_E, \boldsymbol{M}_E, \boldsymbol{B}_E$ from (5.50) and (5.51) and solve for $\delta\lambda$ and $\delta\boldsymbol{e}_i$
4	Compute $\delta\boldsymbol{\sigma}$ from (5.49)
5	Update $\boldsymbol{e}_i$ using $\boldsymbol{e}_i = \boldsymbol{e}_i + \delta\boldsymbol{e}_i$ and update ζ_i
6	Compute $\delta\boldsymbol{\varepsilon}_p$, $\delta\kappa$ from (5.40) and (5.41) respectively
7	Update plastic terms $\boldsymbol{\varepsilon}_p = \boldsymbol{\varepsilon}_p + \delta\boldsymbol{\varepsilon}_p$, $\Delta\boldsymbol{\varepsilon}_p = \Delta\boldsymbol{\varepsilon}_p + \delta\boldsymbol{\varepsilon}_p$, $\Delta\lambda = \Delta\lambda + \delta\lambda$, $\kappa = \kappa + \delta\kappa$ and $\Delta\kappa = \Delta\kappa + \delta\kappa$
8	Compute a new trial stress from $\boldsymbol{\sigma} = \boldsymbol{D}_e\left[\boldsymbol{\varepsilon} - \boldsymbol{\varepsilon}_p - \sum_{j=1}^{n_p} \boldsymbol{N}_j{}^T\left(\boldsymbol{I} - \boldsymbol{M}_{xj}\right)\boldsymbol{e}_j\right]$
9	Compute F, $\boldsymbol{F}_{ei}$, $\boldsymbol{R}_\varepsilon$ and R_κ (5.36), (5.37), (5.38) and (5.39) respectively

10	Check for convergence
	If $\lvert F\rvert \le \sigma_{tol}$, $\lvert\boldsymbol{F}_e\rvert \le \sigma_{tol}$, $\lvert\boldsymbol{R}_\varepsilon\rvert \le \varepsilon_{tol}$ and $\lvert R_\kappa\rvert \le \varepsilon_{tol}$
	Exit iteration
	Else
	Return to Step 2(1)
	End If

Note:

1. Tolerance levels are $\sigma_{tol} = f_t * 10^{-6}$ and $\varepsilon_{tol} = \varepsilon_t * 10^{-6}$

5.5 Consistent tangent constitutive relationship

The incorporation of consistent tangent operators with return mapping algorithms in computational mechanics have been recognised to provide fast convergence, accurate and stable solutions. In the solution of an incremental problem, it has been proved essential to use a tangent stiffness matrix that is consistent with the integration algorithm employed in order to preserve the quadratic rate of asymptotic convergence characteristic of Newton's iterative solution method (Simo and Taylor 1985). An algorithmic tangent constitutive matrix is now derived which is consistent with the above stress update algorithm. The differential form of equation (5.30) may be written as

$$\delta\boldsymbol{\sigma} = \boldsymbol{D}_e\left[\delta\boldsymbol{\varepsilon} - \delta\boldsymbol{\varepsilon}_p - \sum_{j=1}^{n_p}\left(\boldsymbol{N}_j{}^T\delta\boldsymbol{e}_{a_j} + \delta\boldsymbol{N}_j{}^T\boldsymbol{e}_{a_j}\right)\right] \tag{5.52}$$

The term $\delta\boldsymbol{N}_j$ is the differential of the transformation matrix with respect to the trial stress components used for the new POD detection. The choice of this trial stress $\boldsymbol{\sigma}_I$ is considered in greater detail later in this chapter. Thus equation (5.52) may now be written as

$$\delta\boldsymbol{\sigma} = \boldsymbol{D}_e\left(\delta\boldsymbol{\varepsilon} - \delta\boldsymbol{\varepsilon}_p - \sum_{j=1}^{n_p}\left(\boldsymbol{N}_j{}^T\delta\boldsymbol{e}_{a_j} + \frac{\partial\boldsymbol{N}_j{}^T}{\partial\boldsymbol{\sigma}_I}\circ\boldsymbol{e}_{a_j}\boldsymbol{D}_I\delta\boldsymbol{\varepsilon}\right)\right) \tag{5.53}$$

Differentiating equation (5.33) yields

$$\delta \boldsymbol{e}_{a_i} = \boldsymbol{C}_{ltf_i} \delta \boldsymbol{s}_{f_i} - \boldsymbol{M}_{\kappa i} \delta \kappa \tag{5.54}$$

in which

$$\boldsymbol{C}_{ltf_i} = \left(\boldsymbol{m}'^{-1}_{xi} - \boldsymbol{I}\right)\boldsymbol{C}_L \qquad \text{and} \qquad \boldsymbol{M}_{\kappa i} = \boldsymbol{m}'^{-1}_{xi}\boldsymbol{m}'_{\kappa i}$$

The differential quantities of the plastic strain, plastic parameter and the local stress vector may be written as follows

$$\delta \boldsymbol{\varepsilon}_p = \delta\lambda \frac{\partial G}{\partial \boldsymbol{\sigma}} + \Delta\lambda \frac{\partial^2 G}{\partial \boldsymbol{\sigma}^2}\delta\boldsymbol{\sigma} + \Delta\lambda \frac{\partial^2 G}{\partial \boldsymbol{\sigma}\partial\kappa}\delta\kappa \tag{5.55}$$

$$\delta\kappa = a_\kappa\left(\Delta\lambda \boldsymbol{k}_\sigma{}^T \delta\boldsymbol{\sigma} + c_\kappa \delta\lambda\right) \tag{5.56}$$

$$\delta \boldsymbol{s}_{f_i} = \boldsymbol{N}_i \delta\boldsymbol{\sigma} + \frac{\partial \boldsymbol{N}_i}{\partial \boldsymbol{\sigma}_I} \circ \boldsymbol{\sigma}_I \boldsymbol{D}_I \delta\boldsymbol{\varepsilon} \tag{5.57}$$

Making use of (5.54) to (5.57) in (5.53) and rearranging gives

$$\delta\boldsymbol{\sigma} = \boldsymbol{A}_{c\Delta}\left[\left(\boldsymbol{I} - \sum_{j=1}^{n_p}\left(\boldsymbol{N}_j{}^T \boldsymbol{C}_{ltf_j}\frac{\partial \boldsymbol{N}_j}{\partial \boldsymbol{\sigma}_I} \circ \boldsymbol{\sigma}_I \boldsymbol{D}_I + \frac{\partial \boldsymbol{N}_j{}^T}{\partial \boldsymbol{\sigma}_I} \circ \boldsymbol{e}_{a_j}\boldsymbol{D}_I\right)\right)\delta\boldsymbol{\varepsilon} - \ \ldots \right.$$

$$\left. \ldots \left(\boldsymbol{g}_{\varepsilon m} - \sum_{j=1}^{n_p}\left(\boldsymbol{N}_j{}^T \boldsymbol{M}_{\kappa j} a_\kappa c_\kappa\right)\right)\delta\lambda\right] \tag{5.58}$$

where

$$\boldsymbol{A}_{c\Delta} = \left[\boldsymbol{I} + \boldsymbol{D}_e \left[\sum_{j=1}^{n_p} \boldsymbol{N}_j{}^T (\boldsymbol{C}_{ltf\,j} \boldsymbol{N}_j - \boldsymbol{M}_{\kappa j} a_\kappa \Delta\lambda \boldsymbol{k}_\sigma{}^T) + \Delta\lambda \left(\frac{\partial^2 G}{\partial \boldsymbol{\sigma}^2} + \frac{\partial^2 G}{\partial \boldsymbol{\sigma} \partial \kappa} a_\kappa \Delta\lambda \boldsymbol{k}_\sigma{}^T \right) \right] \right]^{-1} \boldsymbol{D}_e$$

The consistency condition for the yield surface may be written as

$$\delta F = \boldsymbol{f}_\kappa{}^T \delta\boldsymbol{\sigma} + h_\kappa \delta\lambda = 0 \tag{5.59}$$

Substituting for $\delta\boldsymbol{\sigma}$ in (5.59) using (5.58) and rearranging gives

$$\delta\lambda = \frac{\boldsymbol{f}_\kappa{}^T \boldsymbol{A}_{c\Delta} \boldsymbol{I}_N}{\boldsymbol{f}_\kappa{}^T \boldsymbol{A}_{c\Delta} \boldsymbol{g}_m - h_\kappa} \delta\boldsymbol{\varepsilon} \tag{5.60}$$

in which

$$\boldsymbol{I}_N = \boldsymbol{I} - \sum_{j=1}^{n_p} \left(\boldsymbol{N}_j{}^T \boldsymbol{C}_{ltf\,j} \frac{\partial \boldsymbol{N}_j}{\partial \boldsymbol{\sigma}_I} \circ \boldsymbol{\sigma}_I \boldsymbol{D}_I + \frac{\partial \boldsymbol{N}_j{}^T}{\partial \boldsymbol{\sigma}_I} \circ \boldsymbol{e}_{a_j} \boldsymbol{D}_I \right)$$

$$\boldsymbol{g}_m = \frac{\partial G}{\partial \boldsymbol{\sigma}} - \sum_{j=1}^{n_p} \left(\boldsymbol{N}_j{}^T \boldsymbol{M}_{\kappa j} a_\kappa c_\kappa \right)$$

Substituting for $\delta\lambda$ in (5.58), and using (5.60), gives the consistent tangent relationship as follows

$$\delta\sigma = \left[A_{c\Delta} I_N - \frac{A_{c\Delta} g_m f_\kappa^{\ T} A_{c\Delta} I_N}{f_\kappa^{\ T} A_{c\Delta} g_m - h_\kappa} \right] \delta\varepsilon = D_{ep} \delta\varepsilon \tag{5.61}$$

where D_{ep} is the consistent tangent operator.

5.6 Numerical examples

This section presents the results from numerical simulations undertaken on examples of previously tested concrete structural elements. The results were obtained from the proposed model, which had been implemented into the constitutive driver as well as the finite element program LUSAS. Experimental tests conducted by Walraven and Reinhardt (1981) and Hassanzadeh (1991), which involved the application of normal and shear loadings on concrete specimens, were chosen for comparisons and to validate the proposed model. Table 5.1 gives the material parameters used in the analyses.

Table 5.1. Material properties used for analyses

Material parameters	Example 1	Example 2
E (N/mm^2)	30000	50000
υ	0.15	0.15
f_c (N/mm^2)	29.5	40
f_t (N/mm^2)	2.5	3
ε_c	0.0022	0.0023
ε_0	0.0026	-
G_f (N/mm)	-	0.1
m_g (coarse / fine)	0.4/0.2	0.4/0.2
m_{hi} (coarse / fine)	3.0/1.5	0.4/0.2
m_{ful} (coarse / fine)	13.5/9.0	2.0/1.0
α_c	0.3	0.3

5.6.1 Walraven and Reinhardt's tension-shear tests

This example involves a numerical simulation based on the normal-shear tests undertaken by Walraven and Reinhardt (1981). The tests were carried out on specimens with a shear plane of 300×120 mm^2, as illustrated in Figure 5.9. These specimens were tested in a stiff testing frame with external restraint bars to control the crack opening displacement. All specimens were initially loaded in tension to a set initial crack opening displacement before being loaded in shear. The tests were denoted by the code *a*/*b*/*c* where '*a*' is the concrete mix number, '*b*' the nominal opening and '*c*' the normal stress at an arbitrary crack width of 0.6 mm. The tests involved three different nominal values of opening displacement, i.e. 0.0, 0.2 and 0.4 mm, and for each of the three nominal values, two tests were carried out.

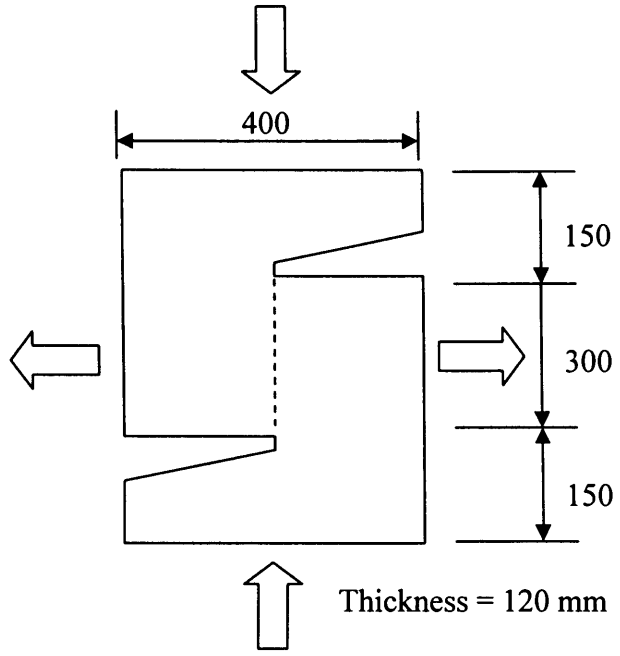

Figure 5.9. Walraven and Reinhardt's test specimen

The results of two experimental tests with initial opening displacements of 0.2 mm are shown in Figures 5.10 and 5.11, along with the numerical results from the constitutive driver. Figures 5.10 and 5.11 show the variation of normal and shear stress with the corresponding displacement respectively. At the initial stage of loading, the model predicts results that are within the bounds of the two experimental curves, after which it over-predicts the stress-displacement response. However, at the final stage of loading, the response gradually decreases and moves back to within the boundaries.

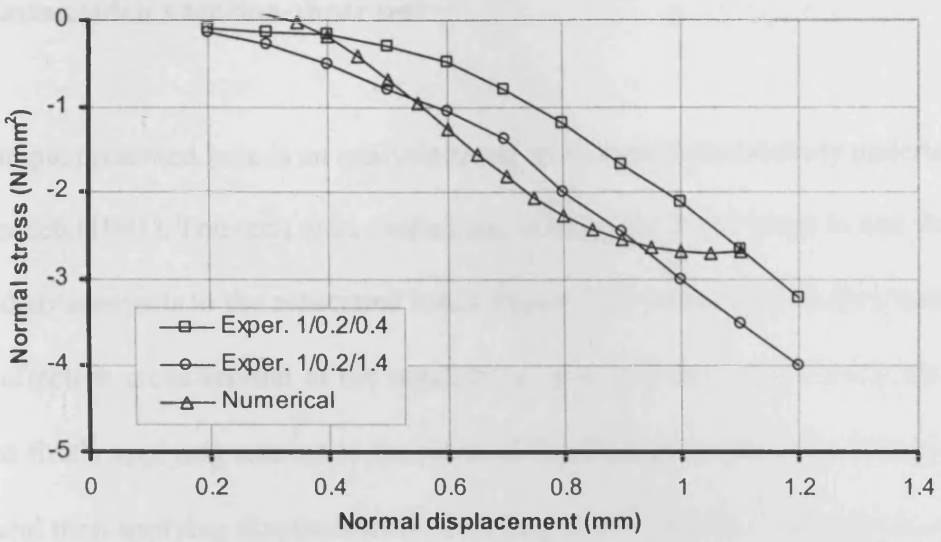

Figure 5.10. Normal stress-displacement relationship

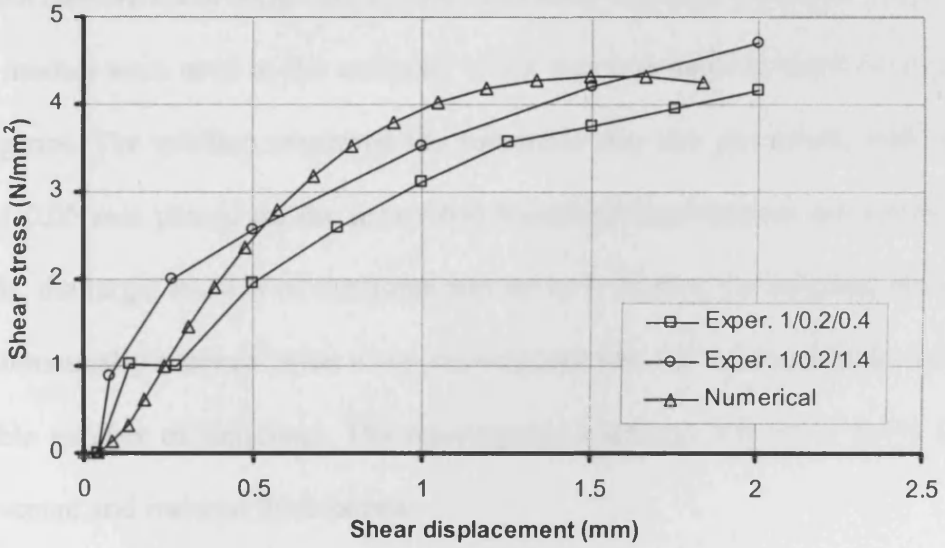

Figure 5.11. Shear stress-displacement relationship

5.6.2 Hassanzadeh's tension-shear test

The example presented here is an analysis based on an experimental study undertaken by Hassanzadeh (1991). The tests were carried out, utilising feedback loops to link shear and normal displacements to the associated loads. Figure 5.12 shows the test specimen which has an effective cross-section at the notch level of 40×40 mm^2. The testing procedure involved firstly applying tension to the point of first fracture (at the top of the softening curve) and then applying displacements according to $u = (\tan\alpha)*v$. The tests considered here are those with $\alpha = 45°$ and 60°.

The finite element mesh comprises 8-noded quadratic elements. It is noted that relatively coarse meshes were used in the analyses, which was inevitable in order to achieve full convergence. The solution employed the automatic step size procedure, with an upper limit of 0.05 mm placed on the prescribed boundary displacement increment. In this example, the target number of iterations was set to 8. During the solution, the step size was automatically reduced twice when convergence was not achieved in the maximum allowable number of iterations. The convergence tolerance was set to 0.1% for both displacement and residual force norms.

The deformed mesh and numerical crack plots at the final step of the analysis are presented in Figures 5.13 and 5.14, respectively. Figures 5.15 to 5.18 show the distribution of major principal stress and strain. Figures 5.19 to 5.22 give the stress-displacement responses and provide comparisons of the numerical predictions with

that of experimental results. As can be seen in these figures, the trends in the numerical results are similar to those of the experimental. However, the model over-predicts the initial stiffness of the material.

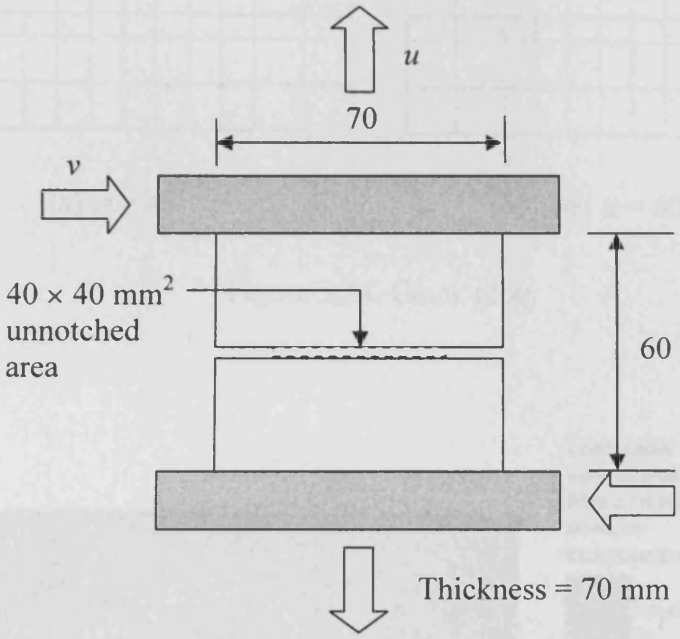

Figure 5.12. Hassanzadeh's test specimen.

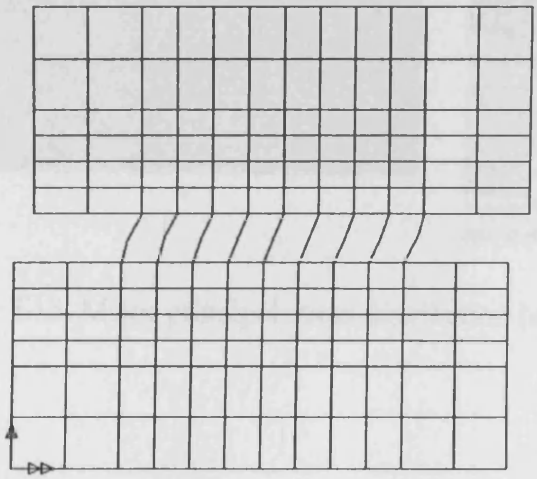

Figure 5.13. Deformed mesh plot

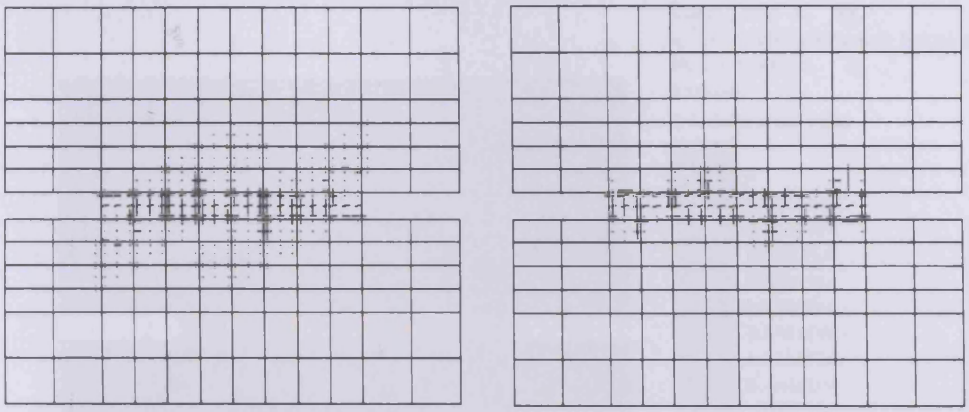

(a) $\alpha = 45^{\circ}$ (b) $\alpha = 60^{\circ}$

Figure 5.14. Crack plots

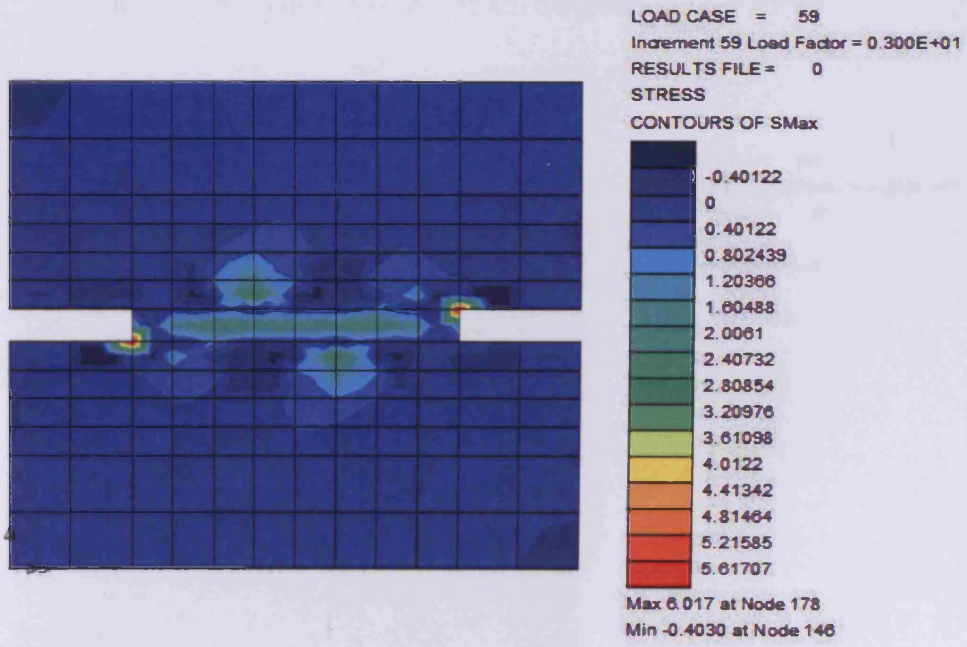

Figure 5.15. Major principal stress distribution ($\alpha = 45°$)

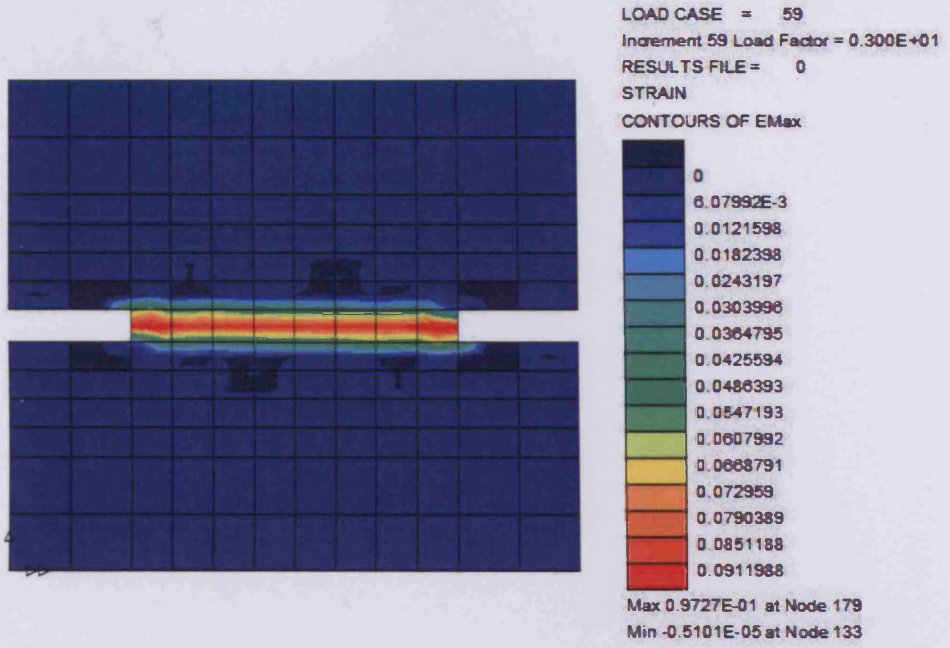

Figure 5.16. Major principal strain distribution ($\alpha = 45°$)

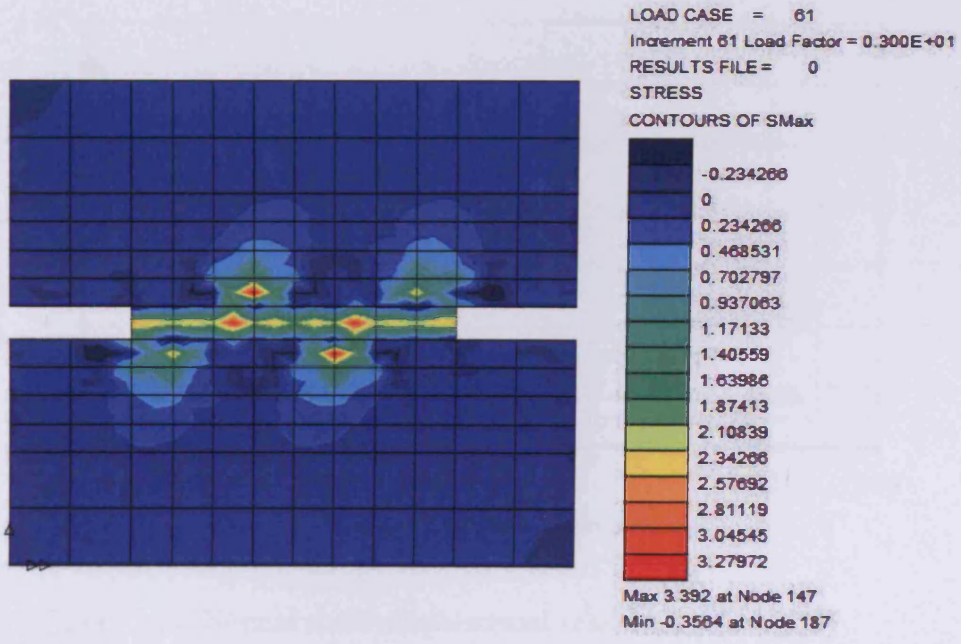

Figure 5.17. Major principal stress distribution ($\alpha = 60°$)

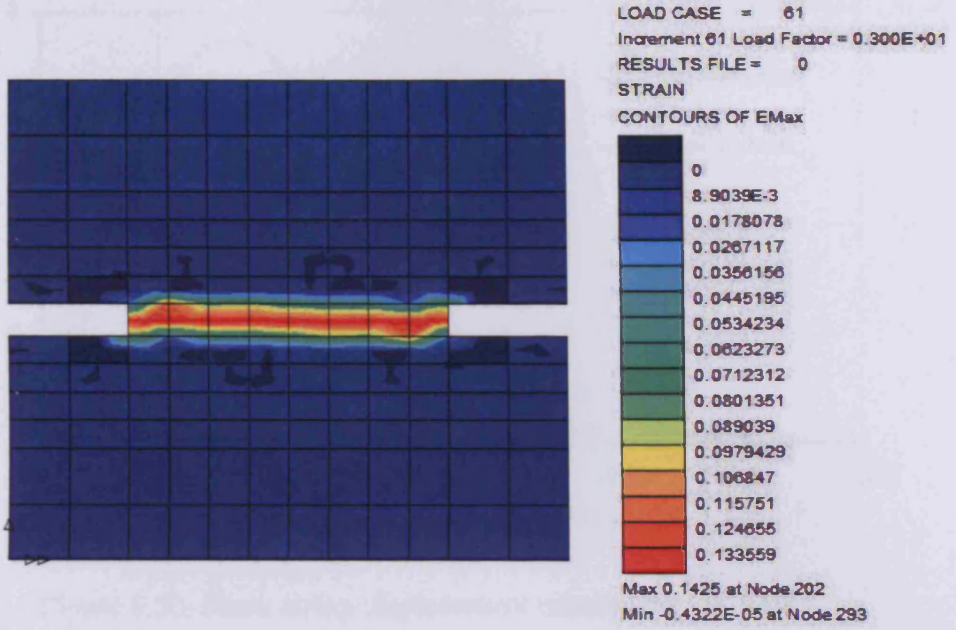

Figure 5.18. Major principal strain distribution ($\alpha = 60°$)

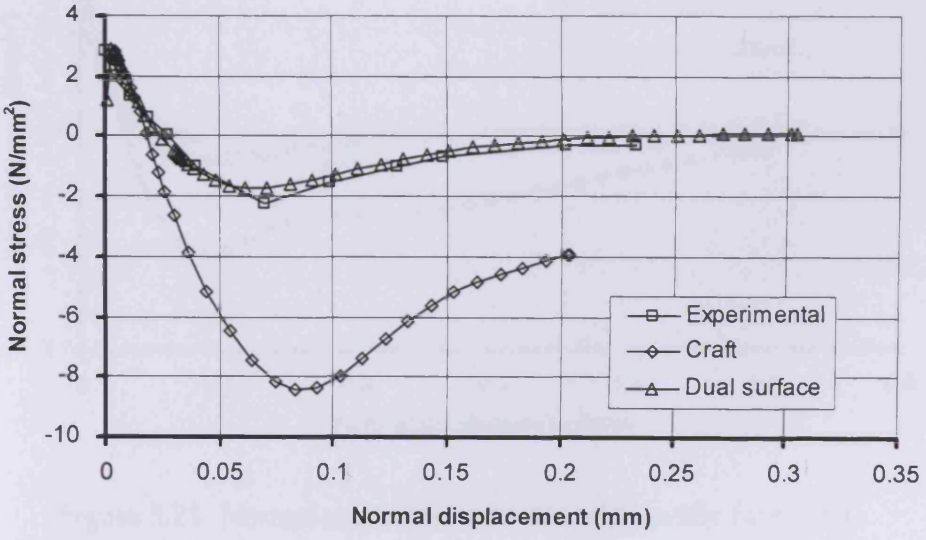

Figure 5.19. Normal stress-displacement relationship ($\alpha = 45°$)

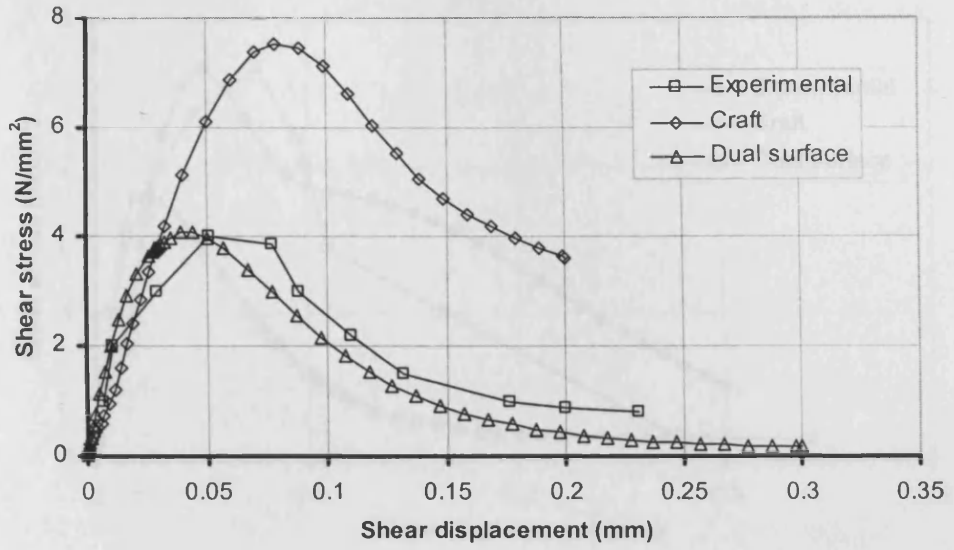

Figure 5.20. Shear stress-displacement relationship ($\alpha = 45°$)

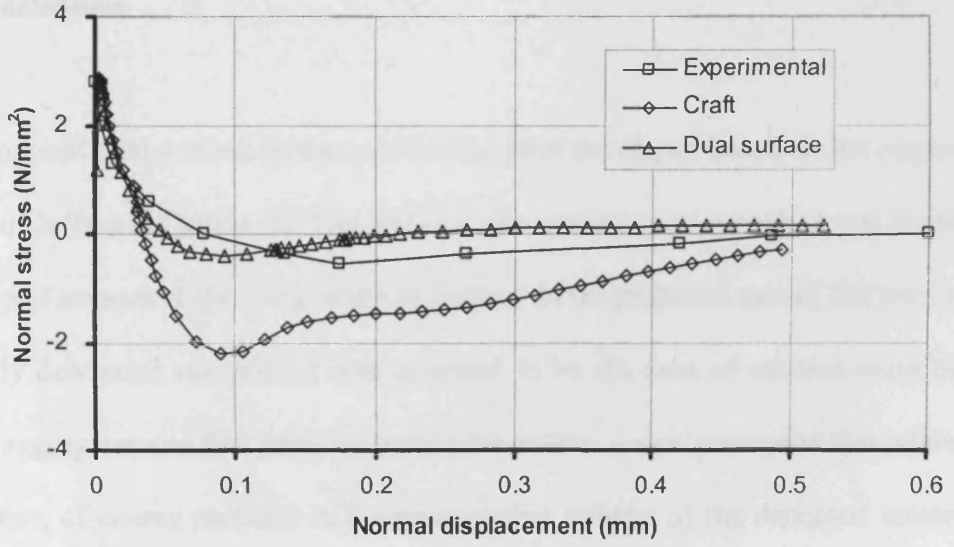

Figure 5.21. Normal stress-displacement relationship ($\alpha = 60°$)

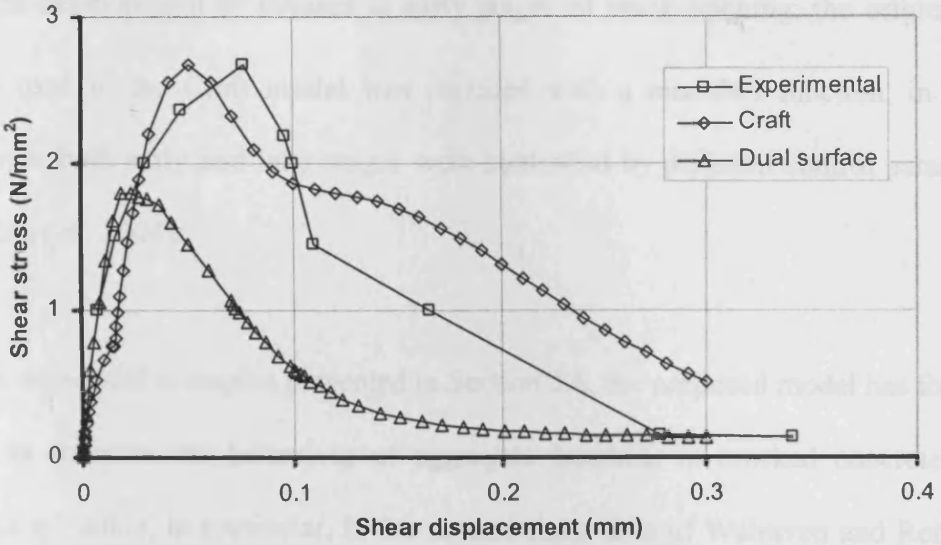

Figure 5.22. Shear stress-displacement relationship ($\alpha = 60°$)

5.7 Conclusions

The proposed dual-surface contact model has been developed based on the original Craft model of Jefferson (2003a, b). The addition of a second contact surface was to model the build up of stresses at the initial stage of contact. In the proposed model, the local stress in the fully debonded component was assumed to be the sum of stresses contributed by coarse aggregates and fine particles within the matrix. A new parameter that relates to the proportion of coarse particles in a representative volume of the damaged material was introduced in the local stress-effective strain relationship. Contact parameters associated with each of the damaged components were determined from a series of SEM images.

In the present approach, a modified damage evolution function was employed which gives a smooth continuous tensile softening curve (Jefferson *et al.* 2004). In order to

model the development of stresses at early stages of crack opening, the original H_f function used in the Craft model was replaced with a modified function, in which reduction at both early and later stages were controlled by different control parameters (Jefferson *et al.* 2004).

From the numerical examples presented in Section 5.6, the proposed model has found to be able to simulate the behaviour of aggregate interlock in cracked concrete. This behaviour is visible, in particular, in the normal-shear tests of Walraven and Reinhardt (1981). Although prefect agreement with experimental results was not achieved, the model was capable of simulating the build up of shear and normal stresses reasonably. Also visible is the capability of model to simulate the observed behaviour that the wider the crack the less the shear stress that can be developed with increasing shear displacement.

As for the comparisons made with the data of Hassanzadeh (1991), the model was found to be more effective than the original Craft model. However, it is noted that the numerical analyses had been carried out using relatively coarse finite element meshes as the model experienced difficulties when finer meshes were used. Nevertheless, the numerical predictions produced by the proposed model were closer to the results observed in the experiment.

Chapter Six

Smooth Frictional Contact Model

6.1 Introduction

This chapter describes the development of an embedded smooth frictional contact model for smooth construction joints within concrete structures. The presence of joints in most concrete structures, especially dams and retaining walls, results in embedded planes of weakness, which can jeopardise both the strength and response of these structures. (Jefferson 1998).

As with the previous model, the smooth frictional contact model was based on the original Craft model of Jefferson (2003a, b). What distinguishes the present approach from the original is the applicability of the model to simulate local plastic yield due to slip between joint surfaces.

6.2 Local damage-contact relationship

Unlike other interface models, the present model has been formulated in terms of stresses and strains rather than the more common terms of stresses and relative displacements. It is assumed that the joint has a finite dimension, given by its characteristic length. This characteristic length is used to relate strains to the relative displacements.

Recalling equation (4.11) in Section 4.3, the total local stress $\boldsymbol{s}_f$ is the sum of both undamaged and fully debonded stress components. In the present model, an additional variable is introduced in the fully debonded component to describe plastic frictional sliding on the crack plane. The local stress $\boldsymbol{s}_f$ is expressed as

$$\boldsymbol{s}_f = H_c \boldsymbol{s}_u + H_f \omega \boldsymbol{s}_d = H_c \boldsymbol{D}_L \boldsymbol{e} + H_f \omega \boldsymbol{D}_L \boldsymbol{\Phi}_d (\boldsymbol{e} - \boldsymbol{e}_s) \tag{6.1}$$

in which the first component represents the undamaged part of the material, which is assumed elastic, and the second component represents the fully debonded part of the material, which is frictional. As the current model deals with smooth surfaces, H_f is no longer a function of the crack opening strain e_g and embedment $\boldsymbol{g}$, as in previous crack models. Whilst H_f is set at 0.995, $\boldsymbol{\Phi}_d$ equals to 1 when the crack is closed, and 0 for opened crack. $\boldsymbol{e}_s$ denotes the local plastic slip strain vector. The added strain $\boldsymbol{e}_a$ is now expressed as

$$\boldsymbol{e}_a = \boldsymbol{e} - \boldsymbol{C}_L \boldsymbol{s}_f \tag{6.2}$$

Substituting for the local stress, $\boldsymbol{s}_f$ in (6.2) using (6.1) gives

$$\boldsymbol{e}_a = (1 - H_c)\boldsymbol{e} - H_f \omega \boldsymbol{\Phi}_d (\boldsymbol{e} - \boldsymbol{e}_s) = (1 - H_c)\boldsymbol{e} - h_\omega (\boldsymbol{e} - \boldsymbol{e}_s) \tag{6.3}$$

6.2.1 Slip function

The model adopts a simplified slip Mohr-Coulomb yield function, which is based on the assumption that a limiting condition is reached when the shear stress on a critical plane reaches a limiting value, which depends on the normal stress on the plane. The yield function is derived in local stress space and has the form

$$f_{es}(\boldsymbol{s}_d) = \sqrt{{s_{d_s}}^2 + {s_{d_t}}^2} + \mu_{es} s_{d_r} \tag{6.4}$$

where μ_{es} is the friction coefficient.

The local model also uses a non-associated flow rule

$$\delta \boldsymbol{e}_s = \frac{\partial \phi_s}{\partial \boldsymbol{s}_d} \delta\gamma \tag{6.5}$$

where γ is the positive slip multiplier, and ϕ_s is the plastic potential function expressed as follows

$$\phi_s(s_d) = \sqrt{{s_{ds}}^2 + {s_{dt}}^2} \tag{6.6}$$

The use of this plastic potential implies that there is no dilatancy, as indicated by the title of the model.

6.2.2 Local trial stress computation

In order to compute the initial trial value for the local stress s_d, it is necessary to first evaluate the plastic strain generated from the incremental strain. Consider a local strain increment, which starts from open and goes to the closed state, as illustrated in Figure 6.1.

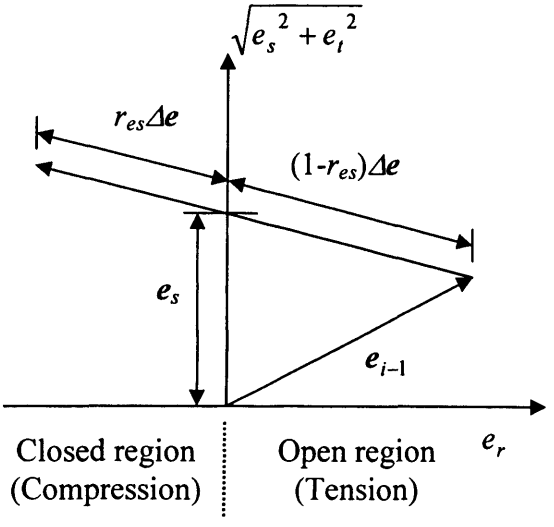

Figure 6.1. Computation of local trial stress

With reference to the above figure, the local plastic strain may be computed as

$$\boldsymbol{e}_s = \boldsymbol{e}_{i-1} + (1 - r_{es})\Delta\boldsymbol{e} \tag{6.7}$$

where

$$r_{es} = 1 + \frac{e_{r\,i-1}}{\Delta e_r}$$

In the case where the local strain increment is already in the closed state, r_{es} equals 1. Using the form of $\boldsymbol{e}_s$ given in equation (6.7), the initial trial local stress for the damaged component $\boldsymbol{s}_d$ may be given as

$$\boldsymbol{s}_d = \boldsymbol{D}_L(\boldsymbol{e} - \boldsymbol{e}_s) \tag{6.8}$$

6.3 Stress recovery algorithm

In this section the stress update is made from the previous converged state. The subscripts k and $k+1$ represent the values of quantities on entry to and exit from the return mapping algorithm respectively. Δ denotes the overall change of any quantity from the last converged state and δ is the change of a quantity within the stress update iteration. It is noted that the algorithm is presented with the assumptions that both fracture and local sliding criteria have already been violated.

In order to evaluate the new stresses $\boldsymbol{\sigma}_{k+1}$ for the incremental strain $\Delta\boldsymbol{\varepsilon}$ from the previous stresses $\boldsymbol{\sigma}_k$, the following relationships must be satisfied.

- total constitutive relationship

$$\boldsymbol{\sigma}_{k+1} = \boldsymbol{D}_e\left(\boldsymbol{\varepsilon}_{k+1} - \sum_{j=1}^{n_p} \boldsymbol{N}_j{}^T \boldsymbol{e}_{a\,j\,k+1}\right) \tag{6.9}$$

- stress transformation

$$\boldsymbol{s}_{i\,k+1} = \boldsymbol{N}_{i\,k+1}\boldsymbol{\sigma}_{k+1} \tag{6.10}$$

- local stress-strain relationships for all PODs *i*

$$\boldsymbol{s}_{i\,k+1} = H_{c\,i\,k+1}\boldsymbol{D}_L\boldsymbol{e}_{i\,k+1} + h_{\omega\,i\,k+1}\boldsymbol{D}_L(\boldsymbol{e}_{i\,k+1} - \boldsymbol{e}_{s\,i\,k+1}) \tag{6.11}$$

$$\boldsymbol{e}_{a\,i\,k+1} = (1 - H_{c\,i\,k+1})\boldsymbol{e}_{i\,k+1} - h_{\omega\,i\,k+1}(\boldsymbol{e}_{i\,k+1} - \boldsymbol{e}_{s\,i\,k+1}) \tag{6.12}$$

- flow rule and plastic parameters for local slip

$$\Delta\boldsymbol{e}_{s\,i} = \frac{\partial\phi_{s\,i}}{\partial\boldsymbol{s}_{d\,i\,k+1}}\Delta\gamma_i \tag{6.13}$$

- local slip or yield function

$$f_{es}(\boldsymbol{s}_{d\,i\,k+1}) = 0 \tag{6.14}$$

- total-local function

$$\boldsymbol{F}_{eik+1} = \boldsymbol{N}_{ik+1}\boldsymbol{\sigma}_{k+1} - \boldsymbol{D}_L\left(H_c\boldsymbol{e}_{ik+1} + h_{\omega ik+1}(\boldsymbol{e}_{ik+1} - \boldsymbol{e}_{sik+1})\right) = \boldsymbol{0} \tag{6.15}$$

The error measure for the local plastic strains, along with the errors in the slip function and total-local function, are used in a coupled Newton iterative solution procedure.

The error in the plastic strain $\boldsymbol{e}_s$ is defined as follows

$$\boldsymbol{R}_{esi} = -\Delta\boldsymbol{e}_{si} + \Delta\gamma_i \frac{\partial\phi_{si}}{\partial\boldsymbol{s}_{di}} \tag{6.16}$$

From which the iterative corrections are obtained as follows

$$\delta\boldsymbol{e}_{si} = \boldsymbol{A}_{ci}\left(\boldsymbol{R}_{esi} + \delta\gamma_i \frac{\partial\phi_{si}}{\partial\boldsymbol{s}_{di}} + \boldsymbol{B}_{ci}\delta\boldsymbol{e}_i\right) \tag{6.17}$$

where

$$\boldsymbol{A}_{ci} = \left(\boldsymbol{I} + \frac{\partial^2\phi_{si}}{\partial\boldsymbol{s}_{di}^{\,2}}\Delta\gamma_i\boldsymbol{D}_L\right)^{-1} \quad \text{and} \quad \boldsymbol{B}_{ci} = \frac{\partial^2\phi_{si}}{\partial\boldsymbol{s}_{di}^{\,2}}\Delta\gamma_i\boldsymbol{D}_L$$

The sliding yield function consistency condition is written as

$$f_{esi} + \frac{\partial f_{esi}}{\partial s_{di}}^{T} \delta s_{di} = 0 \tag{6.18}$$

Utilising (6.8) and (6.17) in (6.18) gives

$$f_{esi} + \frac{\partial f_{esi}}{\partial s_{di}}^{T} D_L \left[\delta e_i - A_{ci} \left(R_{esi} + \delta\gamma_i \frac{\partial \phi_{si}}{\partial s_{di}} + B_{ci} \delta e_i \right) \right] = 0 \tag{6.19}$$

The initial trial stress is computed by

$$\sigma = D_e \left(\varepsilon + \Delta\varepsilon - \sum_{j=1}^{n_p} N_j{}^T e_{aj} \right) \tag{6.20}$$

Thereafter, iterations are performed to satisfy equations (6.9) to (6.14). The total strain tensor does not change throughout the iterations. This then gives the iterative change in the stress as

$$\delta\sigma = -D_e \sum_{j=1}^{n_p} N_j{}^T \delta e_{aj} \tag{6.21}$$

The iterative change in the added strain $\boldsymbol{e}_a$ is given by

$$\delta \boldsymbol{e}_{ai} = \left(\boldsymbol{I} - \boldsymbol{m}'_{ci}\right)\delta \boldsymbol{e}_i + h_{\omega i}\delta \boldsymbol{e}_{si} \tag{6.22}$$

where

$$\boldsymbol{m}'_{ci} = H_{ci}\boldsymbol{I} + H_f \omega_i \boldsymbol{\Phi}_{di} + \frac{\partial H_{ci}}{\partial \zeta_i}\boldsymbol{e}_i \frac{\partial \zeta_i}{\partial \boldsymbol{e}_i}^T + \frac{\partial \omega_i}{\partial \zeta_i} H_f \boldsymbol{\Phi}_{di}\left(\boldsymbol{e}_i - \boldsymbol{e}_{si}\right)\frac{\partial \zeta_i}{\partial \boldsymbol{e}_i}^T$$

Making use of equations (6.17) and (6.22) in (6.21) yields

$$\delta \boldsymbol{\sigma} = -\boldsymbol{D}_e \sum_{j=1}^{n_p} \boldsymbol{N}_j^T \left[\left(\boldsymbol{I} - \boldsymbol{m}'_{cj}\right)\delta \boldsymbol{e}_j + h_{\omega j}\boldsymbol{A}_{cj}\left(\boldsymbol{R}_{esj} + \delta \gamma_j \frac{\partial \phi_{sj}}{\partial \boldsymbol{s}_{dj}} + \boldsymbol{B}_{cj}\delta \boldsymbol{e}_j \right)\right] \tag{6.23}$$

Expanding the total-local function in (6.15) as a Taylors' expansion yields

$$\boldsymbol{F}_{ei} + \boldsymbol{N}_i \delta \boldsymbol{\sigma} - \boldsymbol{D}_L\left(\boldsymbol{m}'_{ci}\delta \boldsymbol{e}_i - h_{\omega i}\delta \boldsymbol{e}_{si}\right) = \boldsymbol{0} \tag{6.24}$$

Utilising (6.17) and (6.23) in (6.24) gives

$$\boldsymbol{F}_{ei} - \boldsymbol{N}_i \boldsymbol{D}_e \sum_{j=1}^{n_p} \boldsymbol{N}_j{}^T \left[\left(\boldsymbol{I} - \boldsymbol{m}'_{cj} \right) \delta \boldsymbol{e}_j + h_f \boldsymbol{A}_{cj} \left(\boldsymbol{R}_{esj} + \delta \gamma_j \frac{\partial \phi_{sj}}{\partial \boldsymbol{s}_{dj}} + \boldsymbol{B}_{cj} \delta \boldsymbol{e}_j \right) \right] - \ldots$$

$$\ldots \boldsymbol{D}_L \left[\boldsymbol{m}'_{ci} \delta \boldsymbol{e}_i - h_{\omega i} \boldsymbol{A}_{ci} \left(\boldsymbol{R}_{esi} + \delta \gamma_i \frac{\partial \phi_{si}}{\partial \boldsymbol{s}_{di}} + \boldsymbol{B}_{ci} \delta \boldsymbol{e}_i \right) \right] = \boldsymbol{0} \tag{6.25}$$

The overall procedure results in a set of coupled equations with $\delta\gamma$ and $\delta\boldsymbol{e}$ as the unknowns. These could be written in the following compact form, in which i and j are indices from 1 to n_p and in which the summation of repeated indices is implied. Note that i, j does not imply differentiation with respect to j components as it would in indicial notation.

$$\boldsymbol{F}_{Ei} = \boldsymbol{B}_{Ei,j} \delta \boldsymbol{e}_j + \boldsymbol{P}_{Ei,j} \delta \gamma_j \tag{6.26}$$

$$F_{\gamma i} = \boldsymbol{B}_{\gamma i} \delta \boldsymbol{e}_i + P_{\gamma i} \delta \gamma_i \tag{6.27}$$

where

$$\boldsymbol{F}_{Ei} = \boldsymbol{F}_{ei} - \boldsymbol{N}_i \boldsymbol{D}_e \sum_{k=1}^{n_p} \boldsymbol{N}_k{}^T h_{\omega k} \boldsymbol{A}_{ck} \boldsymbol{R}_{esk} + \boldsymbol{D}_L h_{\omega i} \boldsymbol{A}_{ci} \boldsymbol{R}_{esi}$$

$$\boldsymbol{B}_{Ei,j} = \boldsymbol{N}_i \boldsymbol{D}_e \boldsymbol{N}_j{}^T \left[\left(\boldsymbol{I} - \boldsymbol{m}'_{cj} \right) + h_{\omega j} \boldsymbol{A}_{cj} \boldsymbol{B}_{cj} \right] + \boldsymbol{D}_L \left(\boldsymbol{m}'_{ci,j} - h_{\omega i,j} \boldsymbol{A}_{ci,j} \boldsymbol{B}_{ci,j} \right) \partial_{i,j}$$

$$\boldsymbol{P}_{Ei,j} = \boldsymbol{N}_i \boldsymbol{D}_e \boldsymbol{N}_j{}^T h_{\omega j} \boldsymbol{A}_{cj} \frac{\partial \boldsymbol{\phi}_{sj}}{\partial \boldsymbol{s}_{dj}} - \boldsymbol{D}_L h_{\omega i,j} \boldsymbol{A}_{ci,j} \frac{\partial \boldsymbol{\phi}_{si,j}}{\partial \boldsymbol{s}_{di,j}} \partial_{i,j}$$

$$F_{\gamma i} = f_{esi} - \frac{\partial f_{esi}}{\partial \boldsymbol{s}_{di}}^T \boldsymbol{D}_L \boldsymbol{A}_{ci} \boldsymbol{R}_{esi}$$

$$\boldsymbol{B}_{\gamma i} = -\frac{\partial f_{esi}}{\partial \boldsymbol{s}_{di}}^T \boldsymbol{D}_L \left(\boldsymbol{I} - \boldsymbol{A}_{ci} \boldsymbol{B}_{ci} \right)$$

$$P_{\gamma i} = \frac{\partial f_{esi}}{\partial \boldsymbol{s}_{di}}^T \boldsymbol{D}_L \boldsymbol{A}_{ci} \frac{\partial \boldsymbol{\phi}_{si}}{\partial \boldsymbol{s}_{di}}$$

where $\partial_{i,j}$ in the expression for $\boldsymbol{B}_E$ and $\boldsymbol{P}_E$ is the Kronecker delta.

Box 6.1. Return mapping algorithm

Step	Description
1	Initialise $\Delta\gamma = 0$
2	Compute trial stress from (6.20)
3	Evaluate F_γ, $\boldsymbol{B}_\gamma$, P_γ, $\boldsymbol{F}_E$, $\boldsymbol{B}_E$ and $\boldsymbol{P}_E$, from (6.26) and (6.27), and solve for $\delta\gamma_i$ and $\delta\boldsymbol{e}_i$
4	Compute $\delta\boldsymbol{\sigma}$ from (6.23)
5	Update $\boldsymbol{e}_i$ using $\boldsymbol{e}_i = \boldsymbol{e}_i + \delta\boldsymbol{e}_i$ and update ζ_i
6	Compute $\delta\boldsymbol{e}_{si}$ from (6.17)
7	Update plastic sliding terms $\boldsymbol{e}_{si} = \boldsymbol{e}_{si} + \delta\boldsymbol{e}_{si}$, $\Delta\boldsymbol{e}_{si} = \Delta\boldsymbol{e}_{si} + \delta\boldsymbol{e}_{si}$, $\Delta\gamma_i = \Delta\gamma_i + \delta\gamma_i$
8	Compute a new trial stress from $\boldsymbol{\sigma} = \boldsymbol{D}_e\left[\boldsymbol{\varepsilon} - \sum_{j=1}^{n_p} \boldsymbol{N}_j{}^T\left[(1-H_{cj})\boldsymbol{e}_j - h_{\omega j}(\boldsymbol{e}_j - \boldsymbol{e}_{sj})\right]\right]$
9	Compute f_{esi}, $\boldsymbol{F}_{ei}$, and $\boldsymbol{R}_{esi}$ from (6.14), (6.15) and (6.16) respectively

10	Check for convergence
	If $\lvert\boldsymbol{F}_e\rvert \le \sigma_{tol}$, $\lvert f_{es}\rvert \le \sigma_{tol}$ and $\lvert\boldsymbol{R}_{es}\rvert \le \varepsilon_{tol}$
	Exit iteration
	Else
	Return to Step 2[1]
	End If

Note:

1. Tolerance levels are $\sigma_{tol} = f_t * 10^{-6}$ and $\varepsilon_{tol} = \varepsilon_t * 10^{-6}$.

6.4 Consistent tangent constitutive relationship

This section describes the derivation of an algorithmic tangent constitutive matrix that is consistent with the stress update algorithm formulated in Section 6.3. The use of a tangent stiffness matrix that is consistent with the integration algorithm has been proved to provide fast and stable solutions by preserving the quadratic rate of asymptotic convergence characteristic of Newton's iterative solution method (Simo and Taylor 1985).

6.4.1 Method 1

Recalling the total constitutive relationship in equation (6.9), the differential form of the equation may be written as

$$\delta\boldsymbol{\sigma} = \boldsymbol{D}_e\left(\delta\boldsymbol{\varepsilon} - \sum_{j=1}^{n_p}\left(\boldsymbol{N}_j{}^T\delta\boldsymbol{e}_{a_j} + \delta\boldsymbol{N}_j{}^T\boldsymbol{e}_{a_j}\right)\right) \tag{6.28}$$

Given that the term $\delta\boldsymbol{N}_j$ is the differential of the transformation matrix with respect to the trial stress $\boldsymbol{\sigma}_I$, equation (6.28) may now be written as

$$\delta\boldsymbol{\sigma} = \boldsymbol{D}_e\left(\delta\boldsymbol{\varepsilon} - \sum_{j=1}^{n_p}\left(\boldsymbol{N}_j{}^T\delta\boldsymbol{e}_{a_j} + \frac{\partial\boldsymbol{N}_j{}^T}{\partial\boldsymbol{\sigma}_I}\circ\boldsymbol{e}_{a_j}\boldsymbol{D}_I\delta\boldsymbol{\varepsilon}\right)\right) \tag{6.29}$$

Differentiating equation (6.12) yields

$$\delta \boldsymbol{e}_{ai} = \left(\boldsymbol{I} - \boldsymbol{m}'_{ci}\right)\delta \boldsymbol{e}_i + h_{\omega i}\delta \boldsymbol{e}_{si} \tag{6.30}$$

The differential quantities of the plastic slip strain may be written as

$$\delta \boldsymbol{e}_{si} = \frac{\partial \phi_{si}}{\partial \boldsymbol{s}_{di}}\delta\gamma_i + \frac{\partial^2 \phi_{si}}{\partial \boldsymbol{s}_{di}^{\,2}}\Delta\gamma_i \delta \boldsymbol{s}_{di} \tag{6.31}$$

Differentiating the damaged stress component in (6.8) yields

$$\delta \boldsymbol{s}_{di} = \boldsymbol{D}_L\left(\delta \boldsymbol{e}_i - \delta \boldsymbol{e}_{si}\right) \tag{6.32}$$

Substituting for $\delta \boldsymbol{s}_d$ in (6.31) and rearranging gives

$$\delta \boldsymbol{e}_{si} = \boldsymbol{A}_{ci}\left(\frac{\partial \phi_{si}}{\partial \boldsymbol{s}_{di}}\delta\gamma_i + \boldsymbol{B}_{ci}\delta \boldsymbol{e}_i\right) \tag{6.33}$$

The iterative change in the added strain $\boldsymbol{e}_a$ may be written as

$$\delta \boldsymbol{e}_{ai} = \delta \boldsymbol{e}_i - \boldsymbol{C}_L \delta \boldsymbol{s}_{fi} \tag{6.34}$$

Substituting for $\delta \boldsymbol{e}$ in (6.33) using (6.34) gives

$$\delta \boldsymbol{e}_{si} = \boldsymbol{A}_{ci}\left[\frac{\partial \boldsymbol{\phi}_{si}}{\partial \boldsymbol{s}_{di}}\delta\gamma_i + \boldsymbol{B}_{ci}\left(\delta \boldsymbol{e}_{ai} + \boldsymbol{C}_L \delta \boldsymbol{s}_{fi}\right)\right] \tag{6.35}$$

Utilising equations (6.30) and (6.35) and rearranging yields an expression of $\delta \boldsymbol{e}_a$ in terms of $\delta \boldsymbol{s}_f$ and $\delta\gamma$

$$\delta \boldsymbol{e}_{ai} = \boldsymbol{C}_{csi}\delta \boldsymbol{s}_{fi} + \boldsymbol{C}_{c\gamma i}\frac{\partial \boldsymbol{\phi}_{si}}{\partial \boldsymbol{s}_{di}}\delta\gamma_i \tag{6.36}$$

where

$$\boldsymbol{C}_{csi} = \left(\boldsymbol{m}'_{ci} - h_{\omega i}\boldsymbol{A}_{ci}\boldsymbol{B}_{ci}\right)^{-1}\left(\boldsymbol{I} + h_{\omega i}\boldsymbol{A}_{ci}\boldsymbol{B}_{ci} - \boldsymbol{m}'_{ci}\right)\boldsymbol{C}_L$$

$$\boldsymbol{C}_{c\gamma i} = \left(\boldsymbol{m}'_{ci} - h_{\omega i}\boldsymbol{A}_{ci}\boldsymbol{B}_{ci}\right)^{-1} h_{\omega i}\boldsymbol{A}_{ci}$$

Substituting for $\delta \boldsymbol{e}_a$ in (6.29) using (6.36) and given that

$$\delta \boldsymbol{s}_{fi} = \boldsymbol{N}_i \delta\boldsymbol{\sigma} + \frac{\partial \boldsymbol{N}_i}{\partial \boldsymbol{\sigma}_I} \circ \boldsymbol{\sigma}_I \boldsymbol{D}_I \delta\boldsymbol{\varepsilon} \tag{6.37}$$

Equation (6.29) may be rewritten as

$$\delta\boldsymbol{\sigma} = \boldsymbol{A}_{c\Delta}\left(\boldsymbol{I}_{c\Delta}\delta\boldsymbol{\varepsilon} - \sum_{j=1}^{n_p} \boldsymbol{N}_j{}^T \boldsymbol{C}_{c\gamma j} \frac{\partial \phi_{sj}}{\partial \boldsymbol{s}_{dj}} \delta\gamma_j \right) \tag{6.38}$$

where

$$\boldsymbol{A}_{c\Delta} = \left(\boldsymbol{I} + \sum_{j=1}^{n_p} \boldsymbol{N}_j{}^T \boldsymbol{C}_{csj} \boldsymbol{N}_j \right)^{-1} \boldsymbol{D}_e$$

$$\boldsymbol{I}_{c\Delta} = \left(\boldsymbol{I} - \sum_{j=1}^{n_p} \boldsymbol{N}_j{}^T \boldsymbol{C}_{csj} \frac{\partial \boldsymbol{N}_j}{\partial \boldsymbol{\sigma}_I} \circ \boldsymbol{\sigma}_I \boldsymbol{D}_I - \sum_{j=1}^{n_p} \frac{\partial \boldsymbol{N}_j{}^T}{\partial \boldsymbol{\sigma}_I} \circ \boldsymbol{e}_{aj} \boldsymbol{D}_I \right)$$

The iterative change in the local stress $\boldsymbol{s}_f$ may be written as

$$\delta \boldsymbol{s}_{fi} = \boldsymbol{D}_L \left(\boldsymbol{m}'_{ci} \delta \boldsymbol{e}_i - h_{\omega i} \delta \boldsymbol{e}_{si} \right) \tag{6.39}$$

Utilising equations (6.33) and (6.41) allows both $\delta\boldsymbol{e}$ and $\delta\boldsymbol{e}_s$ be expressed in terms of $\delta\boldsymbol{s}_f$ and $\delta\gamma$ as follows

$$\delta \boldsymbol{e}_i = \boldsymbol{C}_{c\gamma i} \frac{\partial \phi_{si}}{\partial \boldsymbol{s}_{di}} \delta\gamma_i + \boldsymbol{C}_{cai} \delta \boldsymbol{s}_{fi} \tag{6.40}$$

$$\delta \boldsymbol{e}_{si} = \boldsymbol{C}_{cgi} \frac{\partial \phi_{si}}{\partial \boldsymbol{s}_{di}} \delta\gamma_i + \boldsymbol{C}_{cci} \delta \boldsymbol{s}_{fi} \tag{6.41}$$

where

$$\boldsymbol{C}_{ca_i} = \left(\boldsymbol{m}'_{c_i} - h_{\omega i}\boldsymbol{A}_{c_i}\boldsymbol{B}_{c_i}\right)^{-1}\boldsymbol{C}_L$$

$$\boldsymbol{C}_{cc_i} = \left(\boldsymbol{I} - \boldsymbol{A}_{c_i}\boldsymbol{B}_{c_i}\boldsymbol{m}'^{-1}_{c_i}h_{\omega i}\right)^{-1}\boldsymbol{A}_{c_i}\boldsymbol{B}_{c_i}\boldsymbol{m}'^{-1}_{c_i}\boldsymbol{C}_L$$

$$\boldsymbol{C}_{cg_i} = \left(\boldsymbol{I} - \boldsymbol{A}_{c_i}\boldsymbol{B}_{c_i}\boldsymbol{m}'^{-1}_{c_i}h_{\omega i}\right)^{-1}\boldsymbol{A}_{c_i}$$

Now considering the consistency of the slip function f_{es}

$$\frac{\partial f_{es_i}}{\partial \boldsymbol{s}_{d_i}}^T \delta\boldsymbol{s}_{d_i} = 0 \tag{6.42}$$

which can also be expressed as

$$\frac{\partial f_{es_i}}{\partial \boldsymbol{s}_{d_i}}^T \boldsymbol{D}_L\left(\delta\boldsymbol{e}_i - \delta\boldsymbol{e}_{s_i}\right) = 0 \tag{6.43}$$

Making use of equations (6.37), (6.40) and (6.41) in (6.43) and collecting terms gives

$$\delta\gamma_j = \boldsymbol{\Omega}^{-1}{}_{i,j}\boldsymbol{\Gamma}_i\delta\boldsymbol{\varepsilon} \tag{6.44}$$

where

$$\boldsymbol{\Omega}_{i,j} = \frac{\partial \boldsymbol{f}_{esi}}{\partial \boldsymbol{s}_{di}}^{T} \boldsymbol{D}_L \left(\boldsymbol{C}_{cui} \boldsymbol{N}_i \boldsymbol{A}_{c\Delta} \boldsymbol{N}_j \boldsymbol{C}_{c\gamma j} \frac{\partial \boldsymbol{\phi}_{sj}}{\partial \boldsymbol{s}_{dj}} \right) - \frac{\partial \boldsymbol{f}_{esi,j}}{\partial \boldsymbol{s}_{di,j}}^{T} \boldsymbol{D}_L \boldsymbol{C}_{c\phi i,j} \frac{\partial \boldsymbol{\phi}_{si,j}}{\partial \boldsymbol{s}_{di,j}} \partial_{i,j}$$

$$\boldsymbol{\Gamma}_i = \frac{\partial \boldsymbol{f}_{esi}}{\partial \boldsymbol{s}_{di}}^{T} \boldsymbol{D}_L \boldsymbol{C}_{cui} \left(\boldsymbol{N}_i \boldsymbol{A}_{c\Delta} \boldsymbol{I}_{c\Delta} + \frac{\partial \boldsymbol{N}_i}{\partial \boldsymbol{\sigma}_I} \circ \boldsymbol{\sigma}_I \boldsymbol{D}_I \right)$$

$$\boldsymbol{C}_{c\phi_i} = \boldsymbol{C}_{c\gamma_i} - \boldsymbol{C}_{cg_i}$$

$$\boldsymbol{C}_{cui} = \boldsymbol{C}_{cai} - \boldsymbol{C}_{cci}$$

Hence, by substituting (6.44) in (6.38), the consistent tangent constitutive relationship may be obtained as

$$\delta\boldsymbol{\sigma} = \boldsymbol{A}_{c\Delta} \left(\boldsymbol{I}_{c\Delta} - \boldsymbol{\Xi}\boldsymbol{\Omega}^{-1}\boldsymbol{\Gamma} \right) \delta\boldsymbol{\varepsilon} = \boldsymbol{D}_{ep} \delta\boldsymbol{\varepsilon} \tag{6.45}$$

where

$$\boldsymbol{\Xi} = \sum_{j=1}^{n_p} \boldsymbol{N}_j^{T} \boldsymbol{C}_{c\gamma j} \frac{\partial \boldsymbol{\phi}_{sj}}{\partial \boldsymbol{s}_{dj}}$$

and $\boldsymbol{D}_{ep}$ is the consistent tangent operator.

6.4.2 Method 2

The following describes an alternative approach to deriving the consistent tangent constitutive relationship.

Using (6.30) and (6.33) in (6.29) and rearranging gives

$$\delta\boldsymbol{\sigma} = \boldsymbol{D}_e\left[\boldsymbol{I}_e\delta\boldsymbol{\varepsilon} - \sum_{j=1}^{n_p}\boldsymbol{N}_j{}^T\left(\boldsymbol{I}_{dcj}\delta\boldsymbol{e} + h_{\omega j}\boldsymbol{A}_{cj}\frac{\partial\phi_{sj}}{\partial\boldsymbol{s}_{dj}}\delta\gamma_j\right)\right] \tag{6.46}$$

where

$$\boldsymbol{I}_e = \boldsymbol{I} - \sum_{j=1}^{n_p}\frac{\partial\boldsymbol{N}_j}{\partial\boldsymbol{\sigma}_I}^T \circ \boldsymbol{e}_{aj}\boldsymbol{D}_I$$

$$\boldsymbol{I}_{dcj} = \left(\boldsymbol{I} - \boldsymbol{m}'_{cj}\right) + h_{\omega j}\boldsymbol{A}_{cj}\boldsymbol{B}_{cj}$$

Substituting for $\delta\boldsymbol{e}_s$ in (6.43) using (6.33) and rearranging yields

$$\delta\gamma_i = \frac{\frac{\partial f_{esi}}{\partial\boldsymbol{s}_{di}}^T\boldsymbol{D}_L(\boldsymbol{I} - \boldsymbol{A}_{ci}\boldsymbol{B}_{ci})}{\frac{\partial f_{esi}}{\partial\boldsymbol{s}_{di}}^T\boldsymbol{D}_L\boldsymbol{A}_{ci}\frac{\partial\phi_{si}}{\partial\boldsymbol{s}_{di}}}\delta\boldsymbol{e}_i \tag{6.47}$$

The total-local consistency condition can be expressed as

$$\boldsymbol{N}_i \delta\boldsymbol{\sigma} + \frac{\partial \boldsymbol{N}_i}{\partial \boldsymbol{\sigma}_I} \circ \boldsymbol{\sigma}_I \boldsymbol{D}_I \delta\boldsymbol{\varepsilon} - \boldsymbol{D}_L \left(\boldsymbol{m}'_{ci} \delta\boldsymbol{e}_i - h_{\omega i} \delta\boldsymbol{e}_{si} \right) = \boldsymbol{0} \tag{6.48}$$

Utilising (6.33), (6.46) and (6.47) in (6.48) and rearranging gives

$$\delta\boldsymbol{e}_j = \boldsymbol{\Omega}_{ei,j}^{-1} \boldsymbol{\Gamma}_{ei} \delta\boldsymbol{\varepsilon} \tag{6.49}$$

where

$$\boldsymbol{\Omega}_{ei,j} = \boldsymbol{N}_i \boldsymbol{D}_e \boldsymbol{N}_j^T \left[\boldsymbol{I}_{dcj} + \frac{h_{\omega j} \boldsymbol{A}_{cj} \dfrac{\partial \phi_{sj}}{\partial \boldsymbol{s}_{dj}} \dfrac{\partial f_{esj}}{\partial \boldsymbol{s}_{dj}}^T \boldsymbol{D}_L \left(\boldsymbol{I} - \boldsymbol{A}_{cj} \boldsymbol{B}_{cj} \right)}{\dfrac{\partial f_{esj}}{\partial \boldsymbol{s}_{dj}}^T \boldsymbol{D}_L \boldsymbol{A}_{cj} \dfrac{\partial \phi_{sj}}{\partial \boldsymbol{s}_{dj}}} \right] + \ldots$$

$$\ldots \boldsymbol{D}_L \left[\boldsymbol{m}'_{ci,j} - h_{\omega i,j} \boldsymbol{A}_{ci,j} \boldsymbol{B}_{ci,j} - \frac{h_{\omega i,j} \boldsymbol{A}_{ci,j} \dfrac{\partial \phi_{si,j}}{\partial \boldsymbol{s}_{di,j}} \dfrac{\partial f_{esi,j}}{\partial \boldsymbol{s}_{di,j}}^T \boldsymbol{D}_L \left(\boldsymbol{I} - \boldsymbol{A}_{ci,j} \boldsymbol{B}_{ci,j} \right)}{\dfrac{\partial f_{esi,j}}{\partial \boldsymbol{s}_{di,j}}^T \boldsymbol{D}_L \boldsymbol{A}_{ci,j} \dfrac{\partial \phi_{si,j}}{\partial \boldsymbol{s}_{di,j}}} \right] \partial_{i,j}$$

$$\boldsymbol{\Gamma}_{ei} = \boldsymbol{N}_i \boldsymbol{D}_e \left(\boldsymbol{I}_e - \sum_{j=1}^{n_p} \boldsymbol{N}_j^T \boldsymbol{C}_{csj} \frac{\partial \boldsymbol{N}_j}{\partial \boldsymbol{\sigma}_I} \circ \boldsymbol{\sigma}_I \boldsymbol{D}_I \right)$$

Hence, substituting (6.47) and (6.49) in (6.46) yields the consistent tangent relationship

$$\delta\boldsymbol{\sigma} = \boldsymbol{D}_e\left(\boldsymbol{I}_e - \boldsymbol{\Psi}\boldsymbol{\Omega}_e^{-1}\boldsymbol{\Gamma}_e\right)\delta\boldsymbol{\varepsilon} = \boldsymbol{D}_{ep}\delta\boldsymbol{\varepsilon} \tag{6.50}$$

where

$$\boldsymbol{\Psi} = \sum_{j=1}^{n_p} \boldsymbol{N}_j^T \left[\boldsymbol{I}_{dcj} + \frac{h_{\omega j}\boldsymbol{A}_{cj}\dfrac{\partial \phi_{sj}}{\partial \boldsymbol{s}_{dj}}\dfrac{\partial f_{esj}}{\partial \boldsymbol{s}_{dj}}^T \boldsymbol{D}_L\left(\boldsymbol{I} - \boldsymbol{A}_{cj}\boldsymbol{B}_{cj}\right)}{\dfrac{\partial f_{esj}}{\partial \boldsymbol{s}_{dj}}^T \boldsymbol{D}_L\boldsymbol{A}_{cj}\dfrac{\partial \phi_{sj}}{\partial \boldsymbol{s}_{dj}}} \right]$$

6.5 Numerical implementation

The implementation of the proposed constitutive model has been carried out using Mathcad. The overall procedure is detailed as follows.

- Initialise the total stress $\boldsymbol{\sigma}_t$ and strain $\boldsymbol{\varepsilon}$ vectors
- Update total stresses

  $\boldsymbol{\sigma}_t = \boldsymbol{\sigma}_t + \Delta\boldsymbol{\sigma}_a$

  where $\boldsymbol{\sigma}_a$ is the applied stress increment
- Set the initial value of the out of balance stresses for this increment

  $\Delta\boldsymbol{\sigma} = \boldsymbol{\sigma}_t - \Delta\boldsymbol{\sigma}_a$
- Enter the iteration loop

- Form consistent tangent matrix $\boldsymbol{D}_{ep}$. For situations where no crack plane has formed, $\boldsymbol{D}_{ep}$ is essentially the elastic matrix $\boldsymbol{D}_e$ (6.50).
- Compute strain increment from the out of balance stresses and tangent operator using the Gaussian reduction method, and extract 'reaction' stress $\Delta\boldsymbol{\sigma}_{rc}$, if required

  $\Delta\boldsymbol{\varepsilon} = \boldsymbol{D}_{ep}^{-1}\Delta\boldsymbol{\sigma}$
- Update total stress and strain

  $\boldsymbol{\sigma}_t = \boldsymbol{\sigma}_t + \Delta\boldsymbol{\sigma}_{rc}, \qquad \boldsymbol{\varepsilon} = \boldsymbol{\varepsilon} + \Delta\boldsymbol{\varepsilon}$
- Enter stress recovery loop
  - Calculate the trial stress $\boldsymbol{\sigma}_{tr}$.

    $\boldsymbol{\sigma}_{tr} = \boldsymbol{\sigma}_{old} + \boldsymbol{D}_e\Delta\boldsymbol{\varepsilon}$

    where $\boldsymbol{\sigma}_{old}$ is the current stress, either from the first increment or converged stress from previous increment
  - Check the POD formation criteria. If a new crack has formed, compute the transformation matrix using the trial stress (see Chapter 4)
  - Evaluate the incremental local strain $\delta\boldsymbol{e}_i$ using (6.26). If there is a change in contact (i.e. from open to closed state), evaluate the local trial stress for the damaged component $\boldsymbol{s}_{d\,i}$ from (6.8)
  - Evaluate the local yield function $f_{es\,i}$. If the yield function is less than zero then the material has not slipped for the current applied load increment. If the material has slipped, i.e. $f_{es\,i} > 0$

- Evaluate the incremental local strain δe_i and the plastic multiplier $\delta\gamma_i$ using (6.26) and (6.27)
- Update the local strain e_i and the damage strain ζ_i
- Update the local plastic strain e_{s_i} from (6.17) and the total incremental plastic multiplier $\Delta\gamma_i$
- Compute the new trial stress and local stress from

$$\sigma_{new} = D_e\left[\varepsilon - \sum_{j=1}^{n_p} N_j{}^T\left[(1-H_{cj})e_j - h_{\omega j}(e_j - e_{sj})\right]\right]$$

$$s_{di} = D_L(e_i - e_{si})$$

- Evaluate the local yield function (6.14), the total-local function (6.15) and the error measure for local plastic strain R_{esi} (6.16)
- If converged to within the specified tolerance, exit the stress recovery loop

- Compute the out of balance stress

$$\Delta\sigma = \sigma_t - \sigma_{new}$$

- Compute the relative error

$$\varpi = \frac{|\Delta\sigma|}{|\sigma_t|}$$

If converged to within the specified tolerance, exit the iteration loop

Else return to the start of the iteration loop

- End of increment loop

6.6 Numerical examples

This section serves to assess the response of the proposed model to various strain paths. Validation of the constitutive model by means of comparisons with experimental data has not been carried out as the model is only available in a Mathcad implementation. Nevertheless, the consistency between the return mapping algorithm and the tangent stiffness operator was verified. The material properties used are listed in Table 6.1 and Figure 6.2 illustrates the strain paths used for the test. The results predicted were compared to those given by the original Craft model.

Table 6.1. Material properties

E (N/mm^2)	ν	f_t (N/mm^2)	ε_0	μ_{es}
40000	0.15	2.86	0.002	0.7

The first example was a uniaxial tensile strain path, which is illustrated in Figure 6.3. The second example involved a pure shear strain path, which was applied after a crack plane has been formed. The result for the shear stress-strain relationship is shown in Figure 6.4. Figure 6.5 depicts the numerical results for a combined tensile normal-shear strain path. In the fourth example, a uniaxial tensile strain was first applied, followed by a compressive strain path. The normal stress-strain response is shown in Figure 6.6. The last example was a combined compressive normal-shear strain path. Figure 6.7 shows the numerical results for the stress-strain relationships.

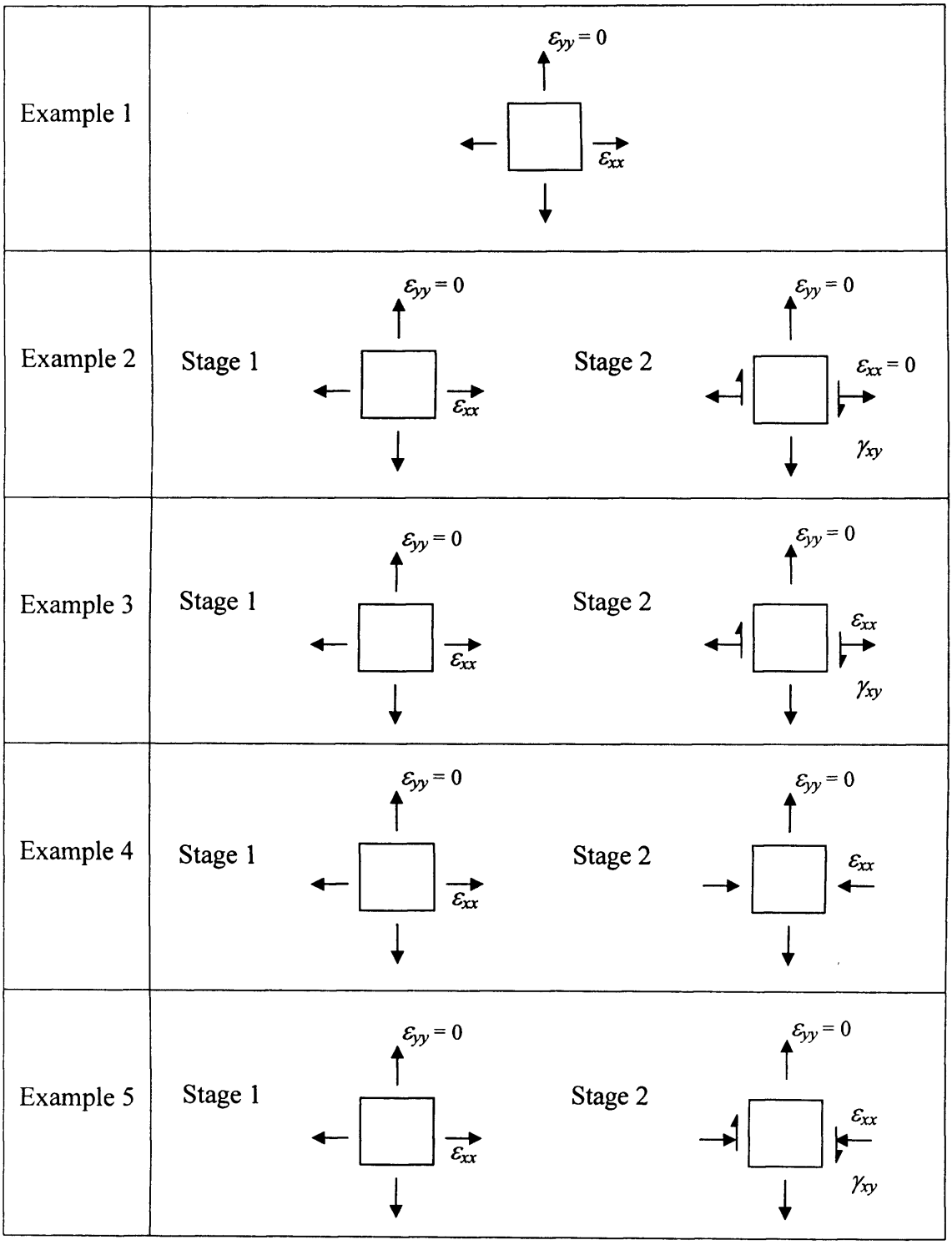

Figure 6.2. Strain paths

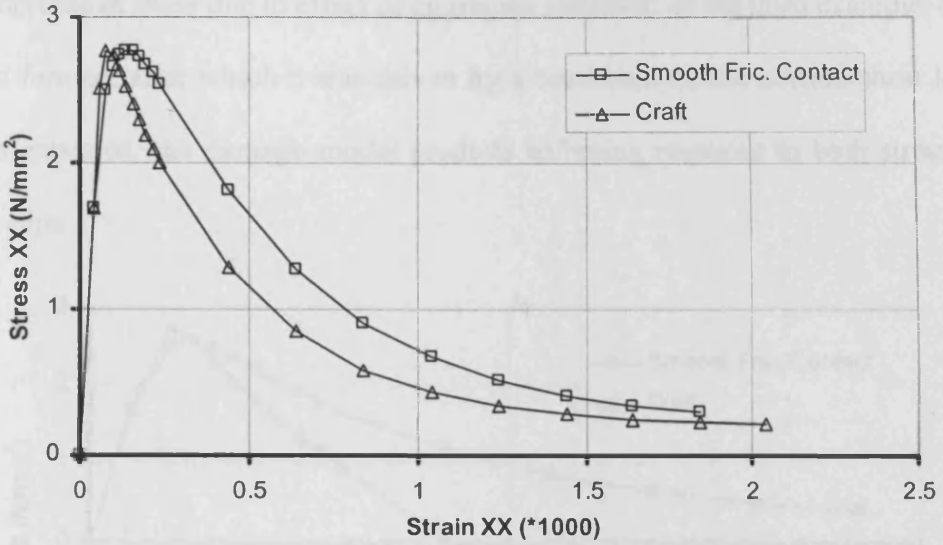

Figure 6.3. Example 1 – Uniaxial tensile response

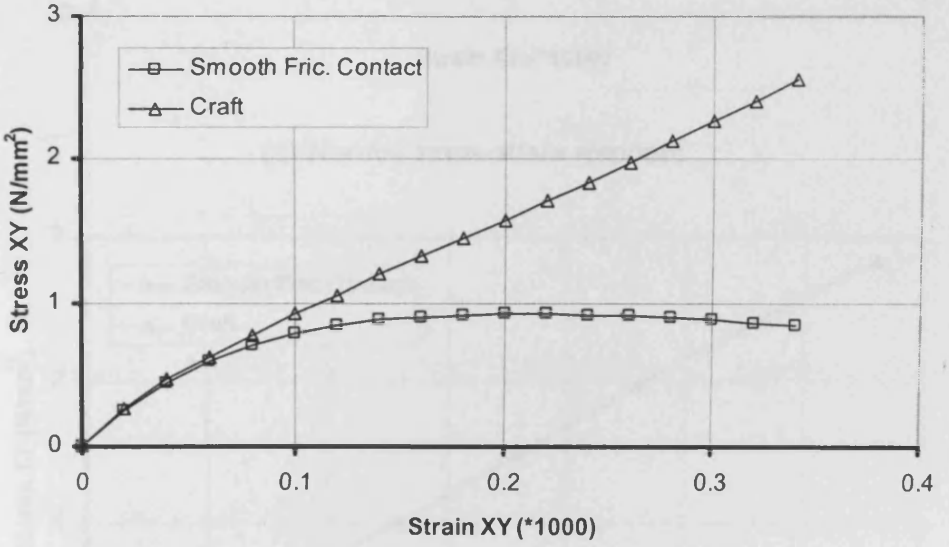

Figure 6.4. Example 2 – Pure shear response

The uniaxial tensile response agrees with those generally observed in experiments. Under pure shear loading condition, the model is able to simulate the initial build up of shear up to the peak strength, after which it starts to decrease. The Craft model predicts a much

higher increase in shear due to effect of aggregate interlock. In the third example, a crack was first formed, after which it was driven by a combined tensile normal-shear loading path. As expected, the damage model predicts softening response in both stress-strain relationships.

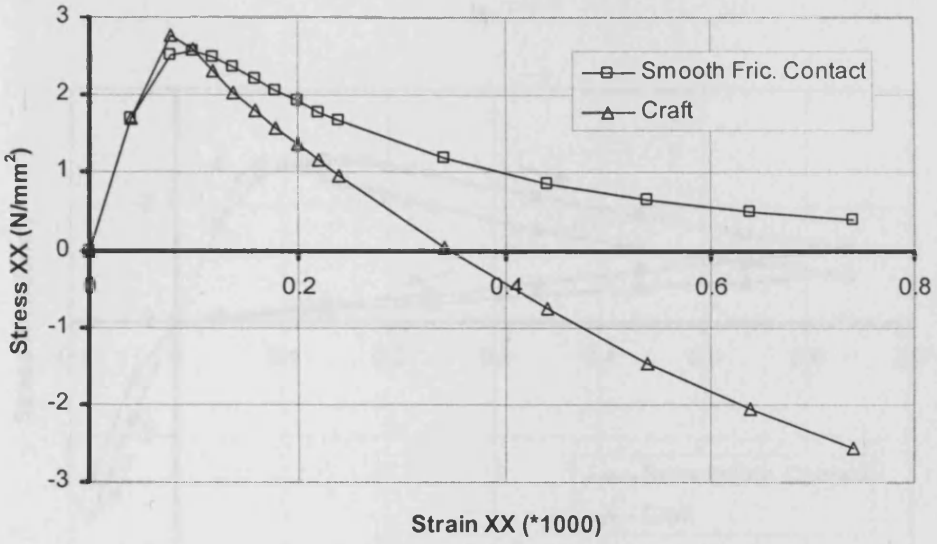

(a) Normal stress-strain response

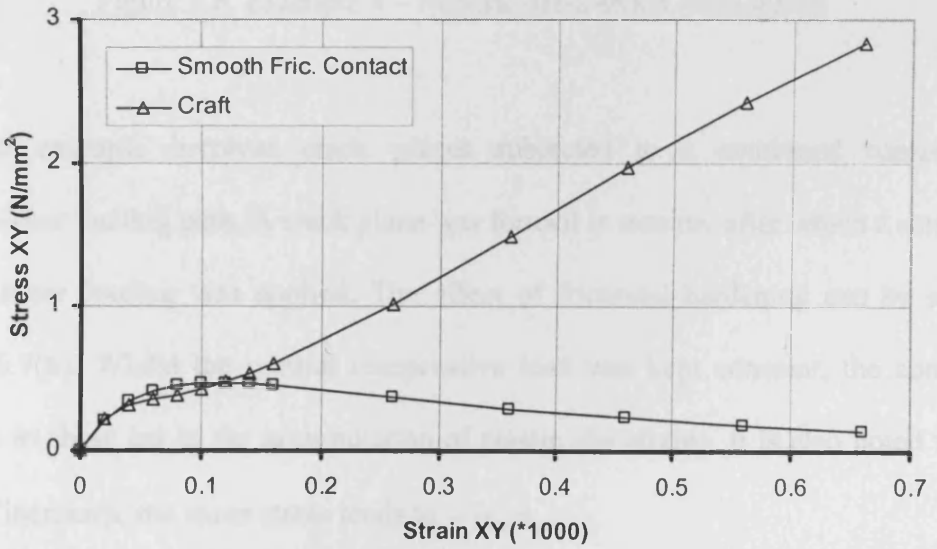

(b) Shear stress-strain response

Figure 6.5. Example 3 – Stress-strain relationships

In this example, a crack was first opened in tension and then closed by a compressive normal strain path. Upon unloading, the model simulates stiffness degradation due to damage. The proposed model, as with the Craft model, captures stiffness recovery upon full crack closure.

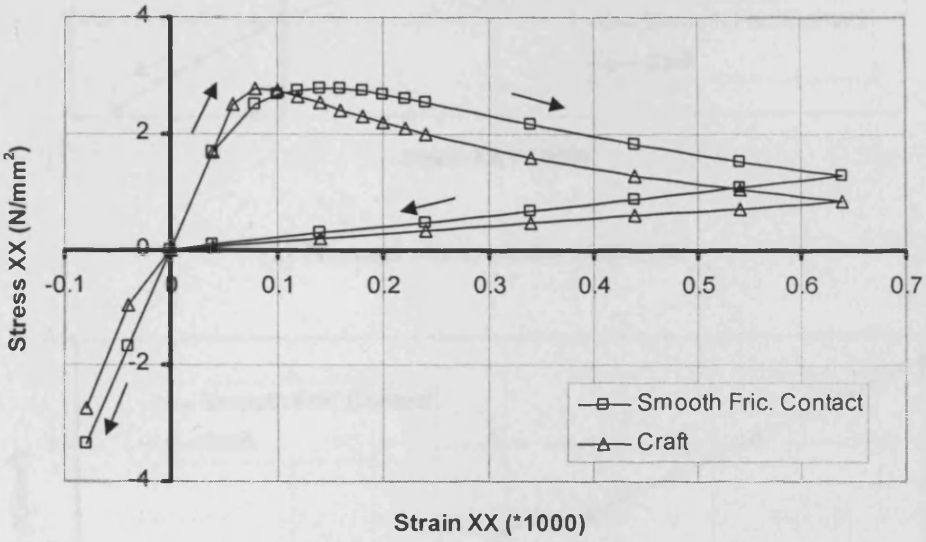

Figure 6.6. Example 4 – Normal stress-strain relationship

The last example involves crack planes subjected to a combined compressive normal-shear loading path. A crack plane was formed in tension, after which a combined normal-shear loading was applied. The effect of frictional hardening can be seen in Figure 6.7(b). Whilst the normal compressive load was kept constant, the continued increase in shear led to the accumulation of plastic slip strains. It is also noted that as damage increases, the shear stress tends to $-\mu_{es}\sigma_{xx}$.

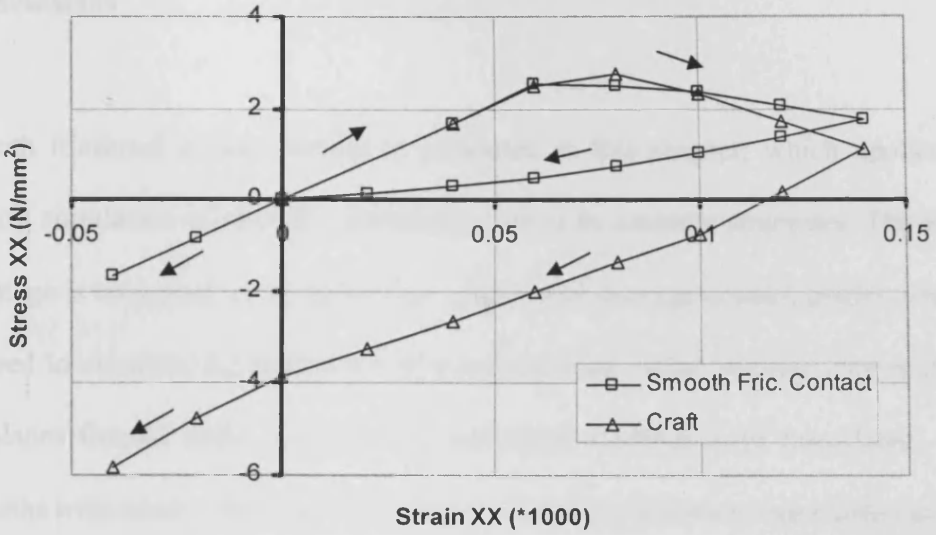

(a) Normal stress-strain response

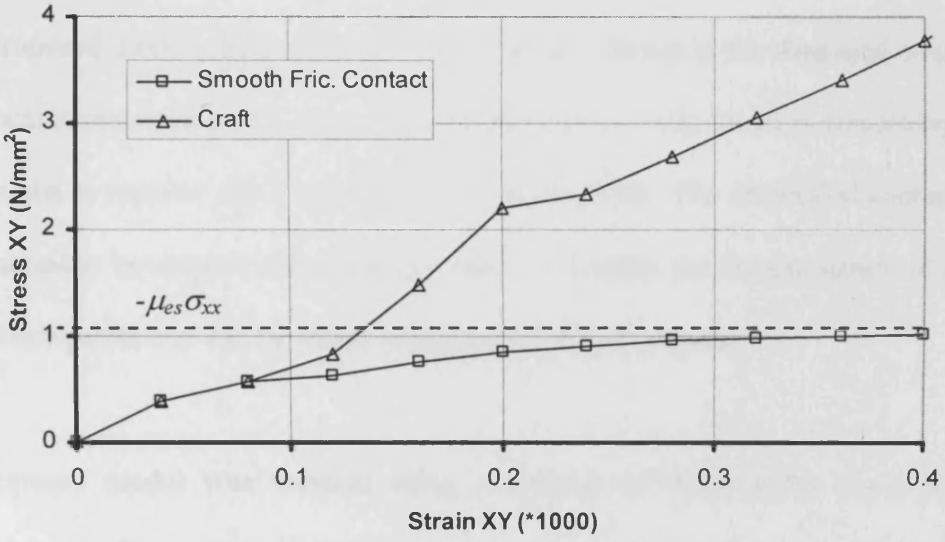

(b) Shear stress-strain response

Figure 6.7. Example 5 – Stress-strain relationships

6.7 Conclusions

A smooth frictional contact model is presented in this chapter, which applies to the numerical simulation of smooth construction joints in concrete structures. The attention at this stage is only paid to the behaviour of the local damage-contact model, which was developed to simulate the behaviour of cracks formed under loading. The response of crack planes formed under uniaxial and multiaxial loadings were considered. Various strain paths were used to distinguish the behaviour of crack planes under different loading conditions.

In the proposed model, the local plastic term was introduced in the damaged component of the local stress-strain constitutive relationship. A plastic slip function was incorporated in the model to monitor any local plastic slip on the joints. The embedded contact plane was assumed to be smooth and frictional, which is suitable for the simulation of smooth construction joints that can be found in large concrete structures.

The proposed model was verified using a number of strain paths via a Mathcad implementation. From these numerical examples, it can be concluded that the model has shown the potential to predict the typical characteristics of joints at different contact states, as well as under different loading conditions.

Chapter Seven

Embedded Planes with Local Plasticity Contact Model

7.1 Introduction

This chapter is dedicated to the formulation of a local damage-contact model, with the inclusion of local plasticity on embedded crack planes. Experimental evidence has proved that permanent strains develop in cracked concrete specimens subjected to cyclic loading. Experimental stress-strain curves clearly show the gradual development of residual strains throughout the unloading-reloading process. The development of these permanent strains is mainly due to the distortion of the particle structure within the specimen when it is subjected to applied load.

The same applies to cracks formed when the fracture strength of the material has been reached. Cracks that are open during the loading process are unable to close completely when the load is fully removed. Hence, it is the aim of this chapter to enhance the local damage-contact model of Jefferson (2003a, b) by taking into consideration local plastic yielding on crack planes.

7.2 Local damage-contact relationships

7.2.1 Overall local stress-strain relationships

As oppose to the simplified local stress-strain relationship described in Chapter 4, the total local stress $\boldsymbol{s}_f$ in the present model is expressed as follows

$$\boldsymbol{s}_f = \boldsymbol{D}_L(H_c\boldsymbol{I} + H_f\omega\boldsymbol{\Phi}_d)\boldsymbol{e}_{rec} = \boldsymbol{D}_L\boldsymbol{M}_x\boldsymbol{e}_{rec} = \boldsymbol{D}_L\boldsymbol{M}_x(\boldsymbol{e}-\boldsymbol{e}_p) = \boldsymbol{D}_{ls}(\boldsymbol{e}-\boldsymbol{e}_p) \tag{7.1}$$

in which the recoverable strain vector $\boldsymbol{e}_{rec}$ is now derived as $\boldsymbol{e}_{rec} = \boldsymbol{e}-\boldsymbol{e}_p$ where $\boldsymbol{e}_p$ is the local plastic strain vector. In addition, the new added strain $\boldsymbol{e}_a$ is written as

$$\boldsymbol{e}_a = \boldsymbol{e}-\boldsymbol{e}_e = \boldsymbol{e}-\boldsymbol{C}_L\boldsymbol{s}_f \tag{7.2}$$

where $\boldsymbol{e}_e$ is the local elastic strain vector. Substituting for the local stress $\boldsymbol{s}_f$ in (7.2) using (7.1) yields

$$\boldsymbol{e}_a = \boldsymbol{e}-\boldsymbol{M}_x(\boldsymbol{e}-\boldsymbol{e}_p) \tag{7.3}$$

Noting that $\boldsymbol{C}_L\boldsymbol{D}_L = \boldsymbol{I}$, i.e. the identity matrix. Figure 7.1 describes schematically the definition of the local strain vectors used in the present damage-contact model.

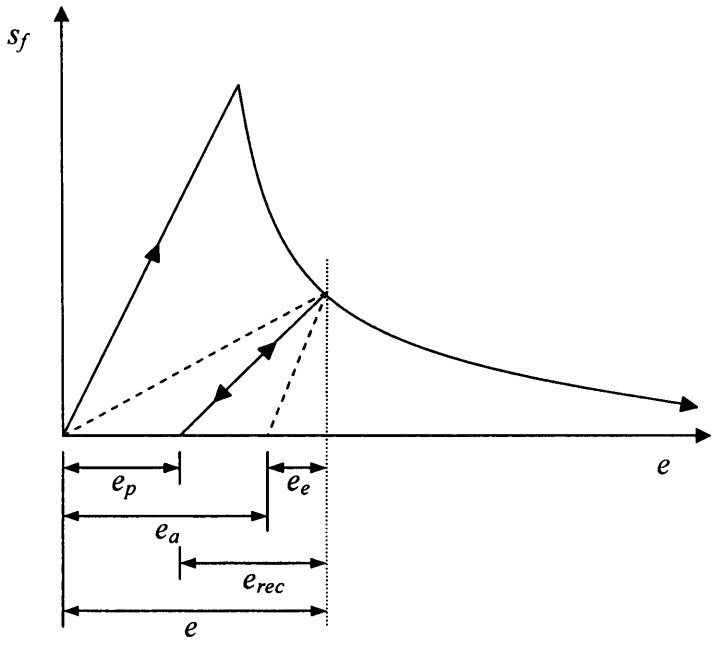

Figure 7.1. Definition of local strain vectors

7.2.2 Modified softening function

Recalling the softening function employed in the original version of the local damage-contact model, as described in Chapter 4, the function is expressed as follows

$$f_s = (1-\omega(\zeta))E\zeta \tag{7.4}$$

in which

$$\omega = 1 - r_c\frac{\varepsilon_t}{\zeta} - \left[(1-r_c)\frac{\varepsilon_t}{\zeta}e^{-c_1\frac{\zeta-\varepsilon_t}{\varepsilon_0-\varepsilon_t}}\right]e^{-2\frac{\kappa}{\kappa_p}}$$

In the present model, the ω function is modified by incorporating an additional parameter a_p which, in one-dimensional problems, is the ratio between the local plastic strain e_p and $\zeta - \varepsilon_t$, such that

$$e_p = a_p(\zeta - \varepsilon_t) \tag{7.5}$$

This parameter is included to control the amount of damage at a given level of local strain. The modified softening function is now expressed as follows

$$f_s = \left(r_c \frac{\varepsilon_t}{\zeta(1-a_p)+\varepsilon_t a_p} + \left[(1-r_c) \frac{\varepsilon_t}{\zeta(1-a_p)+\varepsilon_t a_p} e^{-c_1 \frac{\zeta-\varepsilon_t}{\varepsilon_0-\varepsilon_t}} \right] e^{-2\frac{\kappa}{\kappa_p}} \right) E\zeta \tag{7.6}$$

in which the parameter a_p takes any value ranging from 0 to 1. It is noted that the modified function recovers its original form when a_p = 0, i.e. local damage-contact formulation with no plasticity.

7.2.3 Local yield criterion and flow rule

A local yield function f_e is employed within the crack model to simulate plasticity on crack planes. The yield function takes the same general form as the original damage function but is now expressed in stress rather than strain space.

$$f_e(s_f, f_s) = \frac{(\mu_\sigma^2 - r_\sigma^2) f_t + 2\mu_\sigma^2 s_{f_r} + \sqrt{r_\mu + 4\mu_\sigma^2 (s_{f_s}^2 + s_{f_t}^2)}}{2\mu_\sigma^2} - f_s \qquad (7.7)$$

where $r_\mu = r_\sigma^4 f_t^2 - 2(r_\sigma f_t \mu_\sigma)^2 + \mu_\sigma^4 f_t^2$

f_t is the uniaxial tensile strength and r_σ and μ_σ are the relative shear stress intercept and the asymptotic friction factor respectively. The convexity of the yield surface is preserved with $r_\sigma \geq \mu_\sigma$. The equivalent fracture stress parameter f_s is derived as

$$f_s(\zeta, \kappa) = \left[r_c \varepsilon_t + (1 - r_c)\varepsilon_t e^{-c_1 \frac{\zeta - \varepsilon_t}{\varepsilon_0 - \varepsilon_t}} e^{-2\frac{\kappa}{\kappa_p}} \right] E \qquad (7.8)$$

in which r_c denotes the residual fracture of tensile strength. The damage function ϕ, which is the same as that employed in the original model, is expressed as

$$\phi(e, \zeta) = \frac{e_r}{2}\left[1 + \left(\frac{\mu_\varepsilon}{r_\zeta} \right)^2 \right] + \frac{1}{2r_\zeta^2}\sqrt{(r_\zeta^2 - \mu_\varepsilon^2)^2 e_r^2 + 4r_\zeta^2 (e_s^2 + e_t^2)} - \zeta \qquad (7.9)$$

The material constants r_ζ and μ_ε are the strain equivalents of r_σ and μ_σ respectively. It is noted that the shape of the local yield surface is similar to that of the damage surface, as illustrated in Figure 7.2.

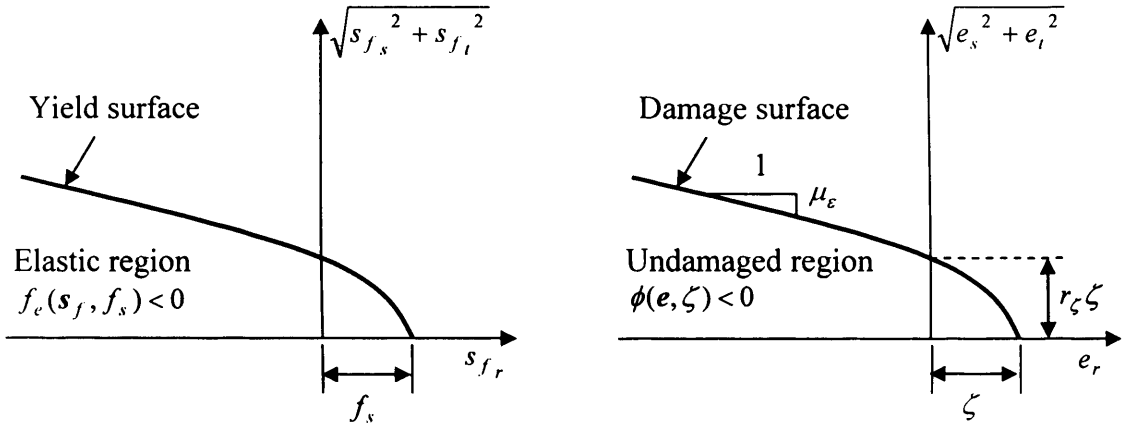

(a) Local yield surface (b) Damage surface

Figure 7.2. Local yield surface and damage surface

Considering equations (7.7) to (7.9), the dependence of the fracture stress f_s on the damage parameter ζ implies that both the size of the local plastic yield surface in stress space and damage surface in strain space depend upon a single local evolution variable.

A non-associative flow rule is adopted for the local model, which has the form

$$\delta \boldsymbol{e}_p = \delta\mu \frac{\partial g_e}{\partial \boldsymbol{s}_f} \tag{7.10}$$

where μ denotes the local plastic multiplier. The plastic potential function g_e is simply derived as follows

$$g_e(\boldsymbol{s}_f) = \sqrt{s_{f_r}^2 + s_{f_s}^2 + s_{f_t}^2} \tag{7.11}$$

This spherical form of plastic potential is different from that normally used in dilatant interface models. However, here, the model is not a standard interface model, but a contact model between rough surfaces. The plastic strains or deformations need to reflect the plastic embedment of one surface into another. This, as may be implied from the work of Walraven and Reinhardt (1981), tended to be in the direction of the principal stress. The concept is illustrated in Figure 7.3.

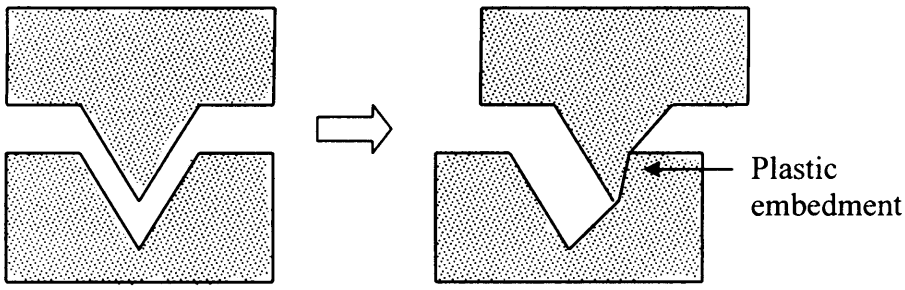

Figure 7.3. Concept of plastic embedment on aggregate interlock

7.3 Stress recovery algorithm

In this section the stress update is made from the previous converged state. The subscripts k and $k+1$ represent the values of quantities on entry to and exit from the return mapping algorithm respectively. Δ denotes the overall change of any quantity from the last converged state and δ is the change of a quantity within the stress update iteration. It is noteworthy that the algorithm is presented with the assumptions that global yield and fracture criteria, as well as the local yield criterion have already been violated, i.e. global plastic yield is active and one or more POD exists with local plastic yield.

In order to evaluate the new stresses σ_{k+1} for the incremental strain $\Delta\varepsilon$ from the previous stresses σ_k, the following relationships must be satisfied.

- total constitutive relationship

$$\sigma_{k+1} = D_e\left(\varepsilon_{k+1} - \varepsilon_{pk+1} - \sum_{j=1}^{n_p} N_j{}^T e_{a_{j_{k+1}}}\right) \tag{7.12}$$

- stress transformation

$$s_{f_{ik+1}} = N_{ik+1}\sigma_{k+1} \tag{7.13}$$

- local stress-strain relationships for all PODs *i*

$$s_{f_{i_{k+1}}} = D_{ls_{ik+1}}(e_{ik+1} - e_{p_{ik+1}}) \tag{7.14}$$

$$e_{a_{ik+1}} = C_{lsf_{ik+1}} s_{f_{ik+1}} \tag{7.15}$$

where C_{lsf} is the local compliance matrix.

- flow rule and plastic parameters for both global and local plastic yield

$$\Delta\varepsilon_p = \frac{\partial G}{\partial\sigma}_{k+1} \Delta\lambda \tag{7.16}$$

$$\Delta\kappa = X_{k+1}\Delta\lambda\sigma_{k+1}{}^T \frac{\partial G}{\partial\sigma}_{k+1} \tag{7.17}$$

$$\Delta e_{p_i} = \Delta\mu_i \frac{\partial g_{ei}}{\partial s_{f_i\,k+1}} \tag{7.18}$$

- global and local yield functions

$$F(\boldsymbol{\sigma}_{k+1}, \kappa_{k+1}) = 0 \tag{7.19}$$

$$f_e(\boldsymbol{s}_{f\,ik+1}, \kappa_{k+1}, \zeta_{ik+1}) = 0 \tag{7.20}$$

- total-local function

$$\boldsymbol{F}_{e\,ik+1} = \boldsymbol{N}_{ik+1}\boldsymbol{\sigma}_{k+1} - \boldsymbol{D}_{ls\,ik+1}(\boldsymbol{e}_{ik+1} - \boldsymbol{e}_{p\,ik+1}) = \boldsymbol{0} \tag{7.21}$$

Error measures are computed for both global and local plastic strains and plastic parameters, which along with the errors in the yield functions and total-local function are used in a coupled Newton iterative solution procedure.

For clarity the overall iteration subscripts will now be dropped, it being assumed that all quantities on the right of an equation are those from the previous update iteration (or the values from the previous overall finite element increment for the 1st iteration).

The plastic strain and hardening parameter errors are defined as follows

$$\boldsymbol{R}_{\varepsilon} = -\Delta\boldsymbol{\varepsilon}_p + \frac{\partial G}{\partial \boldsymbol{\sigma}}\Delta\lambda \tag{7.22}$$

$$R_{\kappa} = -\Delta\kappa + X\Delta\lambda\boldsymbol{\sigma}^T\frac{\partial G}{\partial \boldsymbol{\sigma}} \tag{7.23}$$

$$\boldsymbol{R}_{ep_i} = -\Delta\boldsymbol{e}_{p_i} + \Delta\mu_i\frac{\partial g_{ei}}{\partial \boldsymbol{s}_{f_i}} \tag{7.24}$$

From which the iterative corrections are obtained as follows

$$\delta\varepsilon_p = \boldsymbol{R}_\varepsilon + \delta\lambda \frac{\partial G}{\partial \boldsymbol{\sigma}} + \Delta\lambda \frac{\partial^2 G}{\partial \boldsymbol{\sigma}^2}\delta\boldsymbol{\sigma} + \Delta\lambda \frac{\partial^2 G}{\partial \boldsymbol{\sigma}\partial\kappa}\delta\kappa \tag{7.25}$$

$$\delta\kappa = a_\kappa (R_\kappa + \Delta\lambda \boldsymbol{k}_\sigma{}^T \delta\boldsymbol{\sigma} + c_\kappa \delta\lambda) \tag{7.26}$$

$$\delta\boldsymbol{e}_{p_i} = \boldsymbol{R}_{ep_i} + \delta\mu_i \frac{\partial g_{ei}}{\partial \boldsymbol{s}_{f_i}} + \Delta\mu_i \frac{\partial^2 g_{ei}}{\partial \boldsymbol{s}_{f_i}{}^2}\delta\boldsymbol{s}_{f_i} \tag{7.27}$$

where

$$a_\kappa = \left(1 - \Delta\lambda X \boldsymbol{\sigma}^T \frac{\partial^2 G}{\partial\boldsymbol{\sigma}\partial\kappa}\right)^{-1} \quad , \qquad c_\kappa = X\boldsymbol{\sigma}^T \frac{\partial G}{\partial\boldsymbol{\sigma}} \qquad \text{and}$$

$$\boldsymbol{k}_\sigma = \frac{\partial X}{\partial\boldsymbol{\sigma}}\boldsymbol{\sigma}^T \frac{\partial G}{\partial\boldsymbol{\sigma}} + X\frac{\partial^2 G}{\partial\boldsymbol{\sigma}^2}\boldsymbol{\sigma} + X\frac{\partial G}{\partial\boldsymbol{\sigma}}$$

The global yield function consistency condition is written as

$$F + \frac{\partial F}{\partial\boldsymbol{\sigma}}^T \delta\boldsymbol{\sigma} + \frac{\partial F}{\partial\kappa}\delta\kappa = 0 \tag{7.28}$$

Substituting (7.26) in (7.28) and rearranging gives

$$F + \boldsymbol{f}_\kappa{}^T \delta\boldsymbol{\sigma} + h_\kappa \delta\lambda + \frac{\partial F}{\partial\kappa} a_\kappa R_\kappa = 0 \tag{7.29}$$

where

$$\boldsymbol{f}_\kappa = \frac{\partial F}{\partial \boldsymbol{\sigma}} + \frac{\partial F}{\partial \kappa} a_\kappa \Delta\lambda \boldsymbol{k}_\sigma \qquad \text{and} \qquad h_\kappa = \frac{\partial F}{\partial \kappa} a_\kappa c_\kappa$$

The local yield function consistency condition is written as

$$f_{ei} + \frac{\partial f_{ei}}{\partial \boldsymbol{s}_{f_i}}^T \delta \boldsymbol{s}_{f_i} + \frac{\partial f_{ei}}{\partial \kappa} \delta\kappa + \frac{\partial f_{ei}}{\partial \zeta_i} \frac{\partial \zeta_i}{\partial \boldsymbol{e}_i}^T \delta \boldsymbol{e}_i = 0 \tag{7.30}$$

Substituting for $\delta \boldsymbol{s}_f$ using $\delta \boldsymbol{s}_f = \boldsymbol{N} \delta \boldsymbol{\sigma}$, utilising (7.26) in (7.30) and rearranging gives

$$f_{ei} + \boldsymbol{f}_{e\kappa i}^T \delta \boldsymbol{\sigma} + \frac{\partial f_{ei}}{\partial \kappa} a_\kappa R_\kappa + \frac{\partial f_{ei}}{\partial \kappa} a_\kappa c_\kappa \delta\lambda + \frac{\partial f_{ei}}{\partial \zeta_i} \frac{\partial \zeta_i}{\partial \boldsymbol{e}_i}^T \delta \boldsymbol{e}_i = 0 \tag{7.31}$$

where

$$\boldsymbol{f}_{e\kappa i} = \boldsymbol{N}_i \frac{\partial f_{ei}}{\partial \boldsymbol{s}_{f_i}} + \frac{\partial f_{ei}}{\partial \kappa} a_\kappa \Delta\lambda \boldsymbol{k}_\sigma$$

Using (7.21), the total-local consistency condition can be written as follows

$$\boldsymbol{F}_{ei} + \boldsymbol{N}_i \delta\boldsymbol{\sigma} + \frac{\partial \boldsymbol{N}_i}{\partial \boldsymbol{\sigma}} \circ \boldsymbol{\sigma}\delta\boldsymbol{\sigma} - \frac{\partial \boldsymbol{D}_{lsi}}{\partial \boldsymbol{e}_i} \circ (\boldsymbol{e}_i - \boldsymbol{e}_{p_i})\,\delta\boldsymbol{e}_i \ \ldots$$

$$\ldots + \frac{\partial \boldsymbol{D}_{lsi}}{\partial(\boldsymbol{e}_i - \boldsymbol{e}_{p_i})} \circ (\boldsymbol{e}_i - \boldsymbol{e}_{p_i})(\delta\boldsymbol{e}_i - \delta\boldsymbol{e}_{p_i}) - \frac{\partial \boldsymbol{D}_{lsi}}{\partial \kappa}(\boldsymbol{e}_i - \boldsymbol{e}_{p_i})\delta\kappa = \boldsymbol{0} \tag{7.32}$$

in which $\circ$ denotes a contraction with respect to the 'in-plane' components of a third order matrix. The third term in the above equation is null here as the orientation of the POD remains fixed during the stress update iterations. Then, utilising (7.26) and (7.27) in (7.32) and rearranging yields

$$\boldsymbol{F}_{ei} + \boldsymbol{D}_{lp_i}\boldsymbol{R}_{ep_i} - \boldsymbol{D}_{l\kappa i}a_\kappa R_\kappa + \boldsymbol{N}_{ei}\,\delta\boldsymbol{\sigma} - \boldsymbol{D}_{lti}\delta\boldsymbol{e}_i + \boldsymbol{D}_{lp_i}\frac{\partial g_{ei}}{\partial \boldsymbol{s}_{f_i}}\delta\mu_i - \boldsymbol{D}_{l\kappa i}a_\kappa c_\kappa \delta\lambda = \boldsymbol{0} \tag{7.33}$$

where

$$\boldsymbol{N}_{ei} = \boldsymbol{N}_i + \boldsymbol{D}_{lp_i}\Delta\mu_i \frac{\partial^2 g_{ei}}{\partial \boldsymbol{s}_{f_i}^{\,2}}\boldsymbol{N}_i - \boldsymbol{D}_{l\kappa i}a_\kappa \Delta\lambda \boldsymbol{k}_\sigma{}^T$$

$$\boldsymbol{D}_{lti} = \frac{\partial \boldsymbol{D}_{lsi}}{\partial \boldsymbol{e}_i} \circ (\boldsymbol{e}_i - \boldsymbol{e}_{p_i}) + \frac{\partial \boldsymbol{D}_{lsi}}{\partial(\boldsymbol{e}_i - \boldsymbol{e}_{p_i})} \circ (\boldsymbol{e}_i - \boldsymbol{e}_{p_i}) + \boldsymbol{D}_{lsi}$$

$$\boldsymbol{D}_{l\kappa i} = \frac{\partial \boldsymbol{D}_{lsi}}{\partial \kappa}(\boldsymbol{e}_i - \boldsymbol{e}_{p_i})$$

$$\boldsymbol{D}_{lp_i} = \frac{\partial \boldsymbol{D}_{lsi}}{\partial(\boldsymbol{e}_i - \boldsymbol{e}_{p_i})} \circ (\boldsymbol{e}_i - \boldsymbol{e}_{p_i}) + \boldsymbol{D}_{lsi}$$

The first trial stress is given by

$$\boldsymbol{\sigma} = \boldsymbol{D}_e\left(\boldsymbol{\varepsilon} + \Delta\boldsymbol{\varepsilon} - \boldsymbol{\varepsilon}_p - \sum_{j=1}^{n_p} \boldsymbol{N}_j{}^T \boldsymbol{e}_{a_j} \right) \tag{7.34}$$

and thereafter iterations are performed to satisfy equations (7.12) to (7.20), throughout which the total strain tensor does not change and thus the iterative change in the stress may be written as

$$\delta\boldsymbol{\sigma} = -\boldsymbol{D}_e\left(\delta\boldsymbol{\varepsilon}_p + \sum_{j=1}^{n_p} \boldsymbol{N}_j{}^T \delta\boldsymbol{e}_{a_j} \right) \tag{7.35}$$

The iterative change in the added strain $\boldsymbol{e}_a$ is given by

$$\delta\boldsymbol{e}_{a_i} = (\boldsymbol{I} - \boldsymbol{m}'_{x_i})\,\delta\boldsymbol{e}_i + \boldsymbol{m}'_{p_i}\,\delta\boldsymbol{e}_{p_i} - \boldsymbol{m}'_{\kappa_i}\delta\kappa \tag{7.36}$$

where

$$\boldsymbol{m}'_{x_i} = \boldsymbol{M}_{x_i} + \frac{\partial H_{ci}}{\partial \zeta_i}(\boldsymbol{e}_i - \boldsymbol{e}_{p_i})\frac{\partial \zeta_i}{\partial \boldsymbol{e}_i}^T + \ldots$$

$$\ldots\left(\frac{\partial \omega_i}{\partial \zeta_i} H_{f_i}(\boldsymbol{e}_i - \boldsymbol{e}_{p_i})\frac{\partial \zeta_i}{\partial \boldsymbol{e}_i}^T + \frac{\partial H_{f_i}}{\partial e_{g_i}}\omega_i(\boldsymbol{e}_i - \boldsymbol{e}_{p_i})\frac{\partial e_{g_i}}{\partial \boldsymbol{e}_i}^T \right)\boldsymbol{\Phi}_{di}$$

$$\boldsymbol{m}'_{p_i} = \boldsymbol{M}_{x_i} + \left(\frac{\partial H_{f_i}}{\partial g_i} \omega_i (\boldsymbol{e}_i - \boldsymbol{e}_{p_i}) \frac{\partial g_i}{\partial (\boldsymbol{e}_i - \boldsymbol{e}_{p_i})} \right)^T \boldsymbol{\Phi}_{d_i}$$

$$\boldsymbol{m}'_{\kappa i} = \frac{\partial H_{c_i}}{\partial \kappa} (\boldsymbol{e}_i - \boldsymbol{e}_{p_i}) + \frac{\partial \omega_i}{\partial \kappa} H_{f_i} \boldsymbol{\Phi}_{d_i} (\boldsymbol{e}_i - \boldsymbol{e}_{p_i})$$

Making use of (7.25), (7.26), (7.27) and (7.36), (7.35) may be rearranged to be

$$\delta\boldsymbol{\sigma} = -\boldsymbol{A}_e \left[\boldsymbol{R}_{\varepsilon\kappa p} + \left\{ \frac{\partial G}{\partial \boldsymbol{\sigma}} + \Delta\lambda \frac{\partial^2 G}{\partial \boldsymbol{\sigma} \partial \kappa} a_\kappa c_\kappa - \sum_{j=1}^{n_p} \boldsymbol{N}_j{}^T \boldsymbol{m}'_{\kappa_j} a_\kappa c_\kappa \right\} \delta\lambda + \ \ldots \right.$$

$$\left. \ldots \sum_{j=1}^{n_p} \boldsymbol{N}_j{}^T \left(I - \boldsymbol{m}'_{x_j} \right) \delta \boldsymbol{e}_j + \sum_{j=1}^{n_p} \boldsymbol{N}_j{}^T \boldsymbol{m}'_{p_j} \frac{\partial g_{e_j}}{\partial \boldsymbol{s}_{f_j}} \delta\mu_j \right] \qquad (7.37)$$

in which

$$\boldsymbol{A}_e = \left[\boldsymbol{I} + \boldsymbol{D}_e \left\{ \left(\frac{\partial^2 G}{\partial \boldsymbol{\sigma}^2} + \frac{\partial^2 G}{\partial \boldsymbol{\sigma} \partial \kappa} a_\kappa \Delta\lambda \boldsymbol{k}_\sigma{}^T \right) \Delta\lambda + \ \ldots \right. \right.$$

$$\left. \left. \ldots \sum_{j=1}^{n_p} \boldsymbol{N}_j{}^T \left(\boldsymbol{m}'_{p_j} \Delta\mu_j \frac{\partial^2 g_{e_j}}{\partial \boldsymbol{s}_{f_j}{}^2} \boldsymbol{N}_j - \boldsymbol{m}'_{\kappa_j} a_\kappa \Delta\lambda \boldsymbol{k}_\sigma{}^T \right) \right\} \right]^{-1} \boldsymbol{D}_e$$

$$\boldsymbol{R}_{\varepsilon\kappa p} = \boldsymbol{R}_\varepsilon + \frac{\partial^2 G}{\partial \boldsymbol{\sigma} \partial \kappa} a_\kappa R_\kappa + \sum_{j=1}^{n_p} \boldsymbol{N}_j{}^T (\boldsymbol{m}'_{p_j} \boldsymbol{R}_{ep_j} - \boldsymbol{m}'_{\kappa_j} a_\kappa R_\kappa)$$

Substituting for $\delta\boldsymbol{\sigma}$ using (7.37) in equations (7.29), (7.31) and (7.32) gives a set of coupled equations with $\delta\lambda$, $\delta\mu_i$ and $\delta\boldsymbol{e}_i$ as the unknowns. These are written in the following compact form, in which i and j are indices from 1 to n_p and in which the summation of repeated indices is implied. Note that i, j does not imply differentiation with respect to j components as it would in indicial notation.

$$F_\lambda = M_\lambda \delta\lambda + \boldsymbol{B}_{\lambda j}\delta\boldsymbol{e}_j + P_{\lambda j}\delta\mu_j \tag{7.38}$$

$$F_{\mu_i} = M_{\mu_i}\delta\lambda + \boldsymbol{B}_{\mu_{i,j}}\delta\boldsymbol{e}_j + P_{\mu_{i,j}}\delta\mu_j \tag{7.39}$$

$$\boldsymbol{F}_{E_i} = \boldsymbol{M}_{E_i}\delta\lambda + \boldsymbol{B}_{E_{i,j}}\delta\boldsymbol{e}_j + \boldsymbol{P}_{E_{i,j}}\delta\mu_j \tag{7.40}$$

in which

$$F_\lambda = F - \boldsymbol{f}_\kappa{}^T \boldsymbol{A}_e \boldsymbol{R}_{\varepsilon\kappa p} + \frac{\partial F}{\partial \kappa} a_\kappa R_\kappa$$

$$F_{\mu_i} = f_{e_i} - \boldsymbol{f}_{e\kappa i}{}^T \boldsymbol{A}_e \boldsymbol{R}_{\varepsilon\kappa p} + \frac{\partial f_{e_i}}{\partial \kappa} a_\kappa R_\kappa$$

$$\boldsymbol{F}_{E_i} = \boldsymbol{F}_{e_i} - \boldsymbol{N}_{e_i}\boldsymbol{A}_e\boldsymbol{R}_{\varepsilon\kappa p} + \boldsymbol{D}_{lp_i}\boldsymbol{R}_{ep_i} - \boldsymbol{D}_{lk_i}a_\kappa R_\kappa$$

$$M_\lambda = \boldsymbol{f}_\kappa{}^T \boldsymbol{A}_e \left(\frac{\partial G}{\partial \boldsymbol{\sigma}} + \Delta\lambda \frac{\partial^2 G}{\partial \boldsymbol{\sigma}\partial\kappa} a_\kappa c_\kappa - \sum_{j=1}^{n_p} \boldsymbol{N}_k{}^T \boldsymbol{m}'_{\kappa k} a_\kappa c_\kappa \right) - h_\kappa$$

$$M_{\mu_i} = \boldsymbol{f}_{e\kappa i}{}^T \boldsymbol{A}_e \left(\frac{\partial G}{\partial \boldsymbol{\sigma}} + \Delta\lambda \frac{\partial^2 G}{\partial \boldsymbol{\sigma}\partial\kappa} a_\kappa c_\kappa - \sum_{k=1}^{n_p} \boldsymbol{N}_k{}^T \boldsymbol{m}'_{\kappa k} a_\kappa c_\kappa \right) - \frac{\partial f_{e_i}}{\partial \kappa} a_\kappa c_\kappa$$

$$\boldsymbol{M}_{Ei} = \boldsymbol{N}_{ei}\boldsymbol{A}_e\left(\frac{\partial G}{\partial \boldsymbol{\sigma}} + \Delta\lambda\frac{\partial^2 G}{\partial \boldsymbol{\sigma}\partial\kappa}a_\kappa c_\kappa - \sum_{j=1}^{n_p}\boldsymbol{N}_k{}^T\boldsymbol{m}'_{\kappa k}a_\kappa c_\kappa\right) + \boldsymbol{D}_{l\kappa i}a_\kappa c_\kappa$$

$$\boldsymbol{B}_{\lambda_j} = \boldsymbol{f}_\kappa{}^T\boldsymbol{A}_e\boldsymbol{N}_j{}^T(\boldsymbol{I} - \boldsymbol{m}'_{x_j})$$

$$\boldsymbol{B}_{\mu_{i,j}} = \boldsymbol{f}_{e\kappa i}{}^T\boldsymbol{A}_e\boldsymbol{N}_j{}^T(\boldsymbol{I} - \boldsymbol{m}'_{x_j}) - \frac{\partial f_{ei,j}}{\partial\zeta_{i,j}}\frac{\partial\zeta_{i,j}}{\partial \boldsymbol{e}_{i,j}}\partial_{i,j}$$

$$\boldsymbol{B}_{E_{i,j}} = \boldsymbol{N}_{ei}\boldsymbol{A}_e\boldsymbol{N}_j{}^T(\boldsymbol{I} - \boldsymbol{m}'_{x_j}) + \boldsymbol{D}_{lt_{i,j}}\partial_{i,j}$$

$$P_{\lambda j} = \boldsymbol{f}_\kappa{}^T\boldsymbol{A}_e\boldsymbol{N}_j{}^T\boldsymbol{m}'_{pj}\frac{\partial g_{ej}}{\partial \boldsymbol{s}_{fj}}$$

$$P_{\mu_{i,j}} = \boldsymbol{f}_{e\kappa i}{}^T\boldsymbol{A}_e\boldsymbol{N}_j{}^T\boldsymbol{m}'_{pj}\frac{\partial g_{ej}}{\partial \boldsymbol{s}_{fj}}$$

$$\boldsymbol{P}_{Ei,j} = \boldsymbol{N}_{ei}\boldsymbol{A}_e\boldsymbol{N}_j{}^T\boldsymbol{m}'_{pj}\frac{\partial g_{ej}}{\partial \boldsymbol{s}_{fj}} - \boldsymbol{D}_{lp_{i,j}}\frac{\partial g_{ei,j}}{\partial \boldsymbol{s}_{f_{i,j}}}\partial_{i,j}$$

where $\partial_{i,j}$ in the expression for $\boldsymbol{B}_\mu$, $\boldsymbol{B}_E$, and $\boldsymbol{P}_E$ is the Kronecker delta.

The overall steps of the return mapping algorithm may now be summarised for the case when global plastic yield is active and one or more POD exists with local plastic yield.

Box 7.1. Return mapping algorithm

Step	Description
1	Initialise $\Delta\lambda = 0$, $\Delta\kappa = 0$ and $\Delta\mu_i = 0$
2	Compute trial stress using (7.34)
3	Evaluate F_λ, M_λ, $\boldsymbol{B}_\lambda$, P_λ, $\boldsymbol{F}_E$, $\boldsymbol{M}_E$, $\boldsymbol{B}_E$, $\boldsymbol{P}_E$, F_μ, M_μ, $\boldsymbol{B}_\mu$ and P_μ from (7.38) to (7.40) and solve for $\delta\lambda$, $\delta\mu_i$ and $\delta\boldsymbol{e}_i$
4	Compute $\delta\sigma$ using (7.37)
5	Update $\boldsymbol{e}_i$ using $\boldsymbol{e}_i = \boldsymbol{e}_i + \delta\boldsymbol{e}_i$ and update ζ_i
6	Compute $\delta\boldsymbol{\varepsilon}_p$, $\delta\kappa$ and $\delta\boldsymbol{e}_{p_i}$ from (7.25), (7.26) and (7.27) respectively
7	Update plastic terms $\boldsymbol{\varepsilon}_p = \boldsymbol{\varepsilon}_p + \delta\boldsymbol{\varepsilon}_p$, $\Delta\boldsymbol{\varepsilon}_p = \Delta\boldsymbol{\varepsilon}_p + \delta\boldsymbol{\varepsilon}_p$, $\Delta\lambda = \Delta\lambda + \delta\lambda$, $\kappa = \kappa + \delta\kappa$, $\Delta\kappa = \Delta\kappa + \delta\kappa$, $\boldsymbol{e}_{p_i} = \boldsymbol{e}_{p_i} + \delta\boldsymbol{e}_{p_i}$, $\Delta\boldsymbol{e}_{p_i} = \Delta\boldsymbol{e}_{p_i} + \delta\boldsymbol{e}_{p_i}$, $\Delta\mu_i = \Delta\mu_i + \delta\mu_i$
8	Compute a new trial stress using $\boldsymbol{\sigma} = \boldsymbol{D}_e\left[\boldsymbol{\varepsilon} - \boldsymbol{\varepsilon}_p - \sum_{j=1}^{n_p} \boldsymbol{N}_j{}^T\left(\boldsymbol{e}_j - \boldsymbol{M}_{xj}(\boldsymbol{e}_j - \boldsymbol{e}_{p_j})\right)\right]$
9	Compute F, f_{ei}, $\boldsymbol{F}_{ei}$, $\boldsymbol{R}_\varepsilon$, R_κ and $\boldsymbol{R}_{ep_i}$ from (7.19), (7.20), (7.21), (7.22), (7.23) and (7.24) respectively

10	Check for convergence
	If $\lvert F\rvert \le \sigma_{tol}$, $\lvert\boldsymbol{F}_e\rvert \le \sigma_{tol}$, $\lvert\boldsymbol{f}_e\rvert \le \sigma_{tol}$, $\lvert\boldsymbol{R}_\varepsilon\rvert \le \varepsilon_{tol}$, $\lvert R_\kappa\rvert \le \varepsilon_{tol}$ and $\lvert\boldsymbol{R}_{ep}\rvert \le \varepsilon_{tol}$,
	Exit iteration
	Else
	Return to Step 2[1]
	End If

Note:

1. Tolerance levels are $\sigma_{tol} = f_t * 10^{-6}$ and $\varepsilon_{tol} = \varepsilon_t * 10^{-6}$.

7.4 Consistent tangent constitutive relationship

This section describes the derivation of an algorithmic tangent constitutive matrix that is consistent with the stress update algorithm derived in Section 7.3. Recalling the total constitutive relationship in equation (7.12), the differential form of the equation may be written as

$$\delta\boldsymbol{\sigma} = \boldsymbol{D}_e\left[\delta\boldsymbol{\varepsilon} - \delta\boldsymbol{\varepsilon}_p - \sum_{j=1}^{n_p}\left(\boldsymbol{N}_j{}^T\delta\boldsymbol{e}_{a_j} + \delta\boldsymbol{N}_j{}^T\boldsymbol{e}_{a_j}\right)\right] \tag{7.41}$$

The term $\delta\boldsymbol{N}_j$ is only non-zero for PODs that have formed since the last converged state. This term is computed from the differential of the transformation matrix with respect to the trial stress components used for new POD detection. Equation (7.41) may be rewritten as

$$\delta\boldsymbol{\sigma} = \boldsymbol{D}_e\left[\delta\boldsymbol{\varepsilon} - \delta\boldsymbol{\varepsilon}_p - \sum_{j=1}^{n_p}\left(\boldsymbol{N}_j{}^T\delta\boldsymbol{e}_{a_j} + \frac{\partial\boldsymbol{N}_j{}^T}{\partial\boldsymbol{\sigma}_I}\circ\boldsymbol{e}_{a_j}\boldsymbol{D}_I\delta\boldsymbol{\varepsilon}\right)\right] \tag{7.42}$$

in which $\boldsymbol{\sigma}_I$ is the trial stress. Differentiating equation (7.15) yields

$$\delta\boldsymbol{e}_{a_i} = \boldsymbol{C}_{ltf_i}\delta\boldsymbol{s}_{f_i} + \boldsymbol{M}_{p_i}\delta\boldsymbol{e}_{p_i} - \boldsymbol{M}_{\kappa_i}\delta\kappa \tag{7.43}$$

where

$$\boldsymbol{C}_{ltf} = (\boldsymbol{m}_x'^{-1} - \boldsymbol{I})\boldsymbol{C}_L \ , \qquad \boldsymbol{M}_\kappa = \boldsymbol{m}_x'^{-1}\boldsymbol{m}_\kappa' \qquad \text{and} \qquad \boldsymbol{M}_p = \boldsymbol{m}_x'^{-1}\boldsymbol{m}_p'$$

The differential quantities of both global and local plastic strains, plastic parameter and the local stress vector may be written as follows

$$\delta\varepsilon_p = \delta\lambda \frac{\partial G}{\partial \sigma} + \Delta\lambda \frac{\partial^2 G}{\partial \sigma^2}\delta\sigma + \Delta\lambda \frac{\partial^2 G}{\partial \sigma \partial \kappa}\delta\kappa \tag{7.44}$$

$$\delta\kappa = a_\kappa(\Delta\lambda \boldsymbol{k}_\sigma{}^T \delta\sigma + c_\kappa \delta\lambda) \tag{7.45}$$

$$\delta e_{p_i} = \delta\mu_i \frac{\partial g_{ei}}{\partial s_{f_i}} + \Delta\mu_i \frac{\partial^2 g_{ei}}{\partial s_{f_i}^2}\delta s_{f_i} \tag{7.46}$$

$$\delta s_{f_i} = \boldsymbol{N}_i \delta\sigma + \frac{\partial \boldsymbol{N}_i}{\partial \sigma_I} \circ \sigma_I \boldsymbol{D}_I \delta\varepsilon \tag{7.47}$$

Using equations (7.43) to (7.47) in (7.42) and rearranging gives

$$\delta\sigma = \boldsymbol{A}_{c\Delta}\left[\boldsymbol{I}_{\Delta N}\delta\varepsilon - \boldsymbol{g}_m\delta\lambda - \sum_{j=1}^{n_p}\left(\boldsymbol{N}_j{}^T \boldsymbol{M}_{pj} \frac{\partial g_{ej}}{\partial s_{f_j}}\delta\mu_j\right)\right] \tag{7.48}$$

where

$$\boldsymbol{A}_{c\Delta} = \left[\boldsymbol{I} + \boldsymbol{D}_e \left(\sum_{j=1}^{n_p} \boldsymbol{N}_j{}^T \left(\boldsymbol{C}_{ltf_j} \boldsymbol{N}_j - \boldsymbol{M}_{\kappa j} a_\kappa \Delta\lambda \boldsymbol{k}_\sigma{}^T + \boldsymbol{M}_{p_j} \Delta\mu_j \frac{\partial^2 g_{e_j}}{\partial \boldsymbol{s}_{f_j}{}^2} \boldsymbol{N}_j \right) + \ldots \right. \right.$$

$$\left. \left. \ldots \Delta\lambda \frac{\partial^2 G}{\partial \boldsymbol{\sigma}^2} + \Delta\lambda \frac{\partial^2 G}{\partial \boldsymbol{\sigma} \partial \kappa} a_\kappa \Delta\lambda \boldsymbol{k}_\sigma{}^T \right) \right]^{-1} \boldsymbol{D}_e$$

$$\boldsymbol{I}_{\Delta N} = \boldsymbol{I} - \sum_{j=1}^{n_p} \left(\boldsymbol{N}_j{}^T \left\{ \boldsymbol{C}_{ltf_j} \frac{\partial \boldsymbol{N}_j}{\partial \boldsymbol{\sigma}_I} \circ \boldsymbol{\sigma}_I \boldsymbol{D}_I + \boldsymbol{M}_{p_j} \Delta\mu_j \frac{\partial^2 g_{e_j}}{\partial \boldsymbol{s}_{f_j}{}^2} \frac{\partial \boldsymbol{N}_j}{\partial \boldsymbol{\sigma}_I} \circ \boldsymbol{\sigma}_I \boldsymbol{D}_I \right\} + \frac{\partial \boldsymbol{N}_j{}^T}{\partial \boldsymbol{\sigma}_I} \circ \boldsymbol{e}_a \boldsymbol{D}_I \right)$$

$$\boldsymbol{g}_m = \frac{\partial G}{\partial \boldsymbol{\sigma}} + \Delta\lambda \frac{\partial^2 G}{\partial \boldsymbol{\sigma} \partial \kappa} a_\kappa c_\kappa - \sum_{j=1}^{n_p} \left(\boldsymbol{N}_j{}^T \boldsymbol{M}_{\kappa j} a_\kappa c_\kappa \right)$$

The consistency condition for the global yield surface may be written as

$$\frac{\partial F}{\partial \boldsymbol{\sigma}}^T \delta\boldsymbol{\sigma} + \frac{\partial F}{\partial \kappa} \delta\kappa = 0 \tag{7.49}$$

Substituting for $\delta\boldsymbol{\sigma}$ and $\delta\kappa$ in (7.49) using (7.48) and (7.45), and rearranging gives

$$\delta\lambda = \left[\boldsymbol{f}_\kappa{}^T \boldsymbol{A}_{c\Delta} \boldsymbol{g}_m - h_\kappa \right]^{-1} \left(\boldsymbol{f}_\kappa{}^T \boldsymbol{A}_{c\Delta} \boldsymbol{I}_{\Delta N} \delta\boldsymbol{\varepsilon} - \boldsymbol{f}_\kappa{}^T \boldsymbol{A}_{c\Delta} \sum_{j=1}^{n_p} \boldsymbol{N}_j{}^T \boldsymbol{M}_{p_j} \frac{\partial g_{e_j}}{\partial \boldsymbol{s}_{f_j}} \delta\mu_j \right) \tag{7.50}$$

The consistency condition for the local yield surface gives

$$\frac{\partial f_{ei}}{\partial \boldsymbol{s}_{f_i}}^T \delta \boldsymbol{s}_{f_i} + \frac{\partial f_{ei}}{\partial \kappa}\delta\kappa + \frac{\partial f_{ei}}{\partial \zeta_i}\frac{\partial \zeta_i}{\partial \boldsymbol{e}_i}^T \delta \boldsymbol{e}_i = 0 \tag{7.51}$$

The term $\delta \boldsymbol{e}$ can be eliminated from the above equation by differentiating equation (7.14), which yields

$$\delta \boldsymbol{s}_{f_i} = \boldsymbol{D}_L(\boldsymbol{m}'_{x_i}\delta \boldsymbol{e}_i - \boldsymbol{m}'_{p_i}\delta \boldsymbol{e}_{p_i} + \boldsymbol{m}'_{\kappa i}\delta\kappa) \tag{7.52}$$

Rearranging (7.52) for $\delta \boldsymbol{e}$ gives

$$\delta \boldsymbol{e}_i = \boldsymbol{m}'^{-1}_{x_i}\boldsymbol{C}_L\delta \boldsymbol{s}_{f_i} + \boldsymbol{M}_{p_i}\delta \boldsymbol{e}_{p_i} - \boldsymbol{M}_{\kappa i}\delta\kappa \tag{7.53}$$

Utilising equations (7.45), (7.47), (7.48), (7.50) and (7.53) in (7.51), and collecting terms gives an expression of the local plastic multiplier $\delta\mu$ in terms of the global strain $\delta\boldsymbol{\varepsilon}$

$$\delta\mu_j = \boldsymbol{\Omega}^{-1}_{i,j}\boldsymbol{\Gamma}_i\delta\boldsymbol{\varepsilon} \tag{7.54}$$

where

$$\boldsymbol{\Gamma}_i = \boldsymbol{N}_{\Phi i}\boldsymbol{A}_{c\Delta}\boldsymbol{I}_{\Delta N} + f_{ni}\frac{\partial \boldsymbol{N}_i}{\partial \boldsymbol{\sigma}_I}\circ\boldsymbol{\sigma}_I\boldsymbol{D}_I + f_{\kappa ei}\left[f_\kappa{}^T\boldsymbol{A}_{c\Delta}\boldsymbol{g}_m - h_\kappa\right]^{-1}f_\kappa{}^T\boldsymbol{A}_{c\Delta}\boldsymbol{I}_{\Delta N}$$

$$\boldsymbol{\Omega}_{i,j} = \left(f_{\kappa e i} \left[\boldsymbol{f}_{\kappa}^{\,T} \boldsymbol{A}_{c\Delta} \boldsymbol{g}_m - h_{\kappa} \right]^{-1} \boldsymbol{f}_{\kappa}^{\,T} + \boldsymbol{N}_{\Phi i} \right) \boldsymbol{A}_{c\Delta} \boldsymbol{N}_j^{\,T} \boldsymbol{M}_{p_j} \frac{\partial g_{ej}}{\partial \boldsymbol{s}_{f_j}} - \ \ldots$$

$$\ldots \frac{\partial f_{ei,j}}{\partial \zeta_{i,j}} \frac{\partial \zeta_{i,j}}{\partial \boldsymbol{e}_{i,j}}^{T} \boldsymbol{M}_{p\,i,j} \frac{\partial f_{ei,j}}{\partial \boldsymbol{s}_{f\,i,j}} \partial_{i,j}$$

$$\boldsymbol{N}_{\Phi i} = \boldsymbol{f}_{ni} \boldsymbol{N}_i + \frac{\partial f_{ei}}{\partial \kappa} a_{\kappa} \Delta\lambda \boldsymbol{k}_{\sigma}^{\,T} - \frac{\partial f_{ei}}{\partial \zeta_i} \frac{\partial \zeta_i}{\partial \boldsymbol{e}_i}^{T} \boldsymbol{M}_{\kappa i} a_{\kappa} \Delta\lambda \boldsymbol{k}_{\sigma}^{\,T}$$

$$\boldsymbol{f}_{ni} = \frac{\partial f_{ei}}{\partial \boldsymbol{s}_{f_i}} + \frac{\partial f_{ei}}{\partial \zeta_i} \frac{\partial \zeta_i}{\partial \boldsymbol{e}_i}^{T} \left(\boldsymbol{m}'^{\,-1}_{xi} \boldsymbol{C}_L + \boldsymbol{M}_{p_i} \Delta\mu_i \frac{\partial^2 g_{ei}}{\partial \boldsymbol{s}_{f_i}^{\,2}} \right)$$

$$f_{\kappa e i} = \frac{\partial f_{ei}}{\partial \kappa} a_{\kappa} c_{\kappa} - \frac{\partial f_{ei}}{\partial \zeta_i} \frac{\partial \zeta_i}{\partial \boldsymbol{e}_i}^{T} \boldsymbol{M}_{\kappa i} a_{\kappa} c_{\kappa} - \boldsymbol{N}_{\Phi i} \boldsymbol{A}_{c\Delta} \boldsymbol{g}_m$$

Substituting for $\delta\mu$ in (7.50) using (7.54) gives

$$\delta\lambda = \boldsymbol{\Psi} \delta\boldsymbol{\varepsilon} \tag{7.55}$$

in which

$$\boldsymbol{\Psi} = \left[\boldsymbol{f}_{\kappa}^{\,T} \boldsymbol{A}_{c\Delta} \boldsymbol{g}_m - h_{\kappa} \right]^{-1} \left\{ \boldsymbol{f}_{\kappa}^{\,T} \boldsymbol{A}_{c\Delta} \boldsymbol{I}_{\Delta N} - \boldsymbol{f}_{\kappa}^{\,T} \boldsymbol{A}_{c\Delta} \sum_{j=1}^{n_p} \boldsymbol{N}_j^{\,T} \left(\boldsymbol{M}_{p_j} \frac{\partial g_{ej}}{\partial \boldsymbol{s}_{f_j}} \boldsymbol{\Omega}_{i,j}^{\,-1} \boldsymbol{\Gamma}_j \right) \right\}$$

Using equations (7.54) and (7.55) in (7.48) gives the consistent tangent relationship

$$\delta\boldsymbol{\sigma} = \boldsymbol{A}_{c\Delta} \left(\boldsymbol{I}_{\Delta N} - \boldsymbol{g}_m \boldsymbol{\Psi} - \boldsymbol{\Xi} \boldsymbol{\Omega}^{-1} \boldsymbol{\Gamma} \right) \delta\boldsymbol{\varepsilon} = \boldsymbol{D}_{ep} \delta\boldsymbol{\varepsilon} \tag{7.56}$$

where $\boldsymbol{D}_{ep}$ is the consistent tangent operator and

$$\boldsymbol{\Xi} = \sum_{j=1}^{n_p} \boldsymbol{N}_j^T \boldsymbol{M}_{p_j} \frac{\partial g_{e_j}}{\partial s_{f_j}}$$

7.5 Stress computation procedure

The inclusion of local plastic yield on crack planes has greatly increased the complexity of the overall formulation. The proposed model, like previously described contact models in this thesis, allows for the formation of multiple crack planes upon violation of the fracture criteria. This approach has made solution convergence difficult to achieve for some of the finite element examples presented later in this chapter. It was, therefore, proposed to use a single crack plane instead. This very much simplifies the overall solution procedure. However, it has later been found that the approach of using a single crack plane has made the model susceptible to stress locking problems. This hinders the ability of the model to solve certain numerical problems, especially under multiaxial loading condition.

In order to remedy the shortcomings of the crack plane model, instead of retaining the crack plane orientation throughout the loading process, as adopted in previously mentioned crack models, the present approach allows for the newly formed crack to 'float' throughout the loading process. In other words, the crack plane is free to rotate until later stages along the damage softening region, where its direction is fixed. The

condition for which the crack plane is fixed is given by $\varphi * \varepsilon_0$, where φ takes the value ranging from 0 to 1. This approach is similar to that used in the rotating crack model by Rots (1988).

Recalling the stress computation procedure described in Chapter 4, the trial stress, upon which yield and new POD formation decisions are made, is given by

$$\boldsymbol{\sigma}_I = \left(\boldsymbol{I} + \boldsymbol{D}_e \sum_{j=1}^{n_p} \boldsymbol{N}_j{}^T \boldsymbol{C}_{lsf_j} \boldsymbol{N}_j \right)^{-1} \boldsymbol{D}_e (\boldsymbol{\varepsilon}_k + \Delta\boldsymbol{\varepsilon} - \boldsymbol{\varepsilon}_{p_k}) = \boldsymbol{D}_I (\boldsymbol{\varepsilon}_k + \Delta\boldsymbol{\varepsilon} - \boldsymbol{\varepsilon}_{p_k}) \tag{7.57}$$

Upon the completion of the stress recovery procedure for a particular increment, a check is performed to see whether the newly formed crack plane is fixed or 'floating'. If a 'floating' crack is active, the crack is removed from the next trial stress computation. Hence, the secant elastic-damage constitutive matrix $\boldsymbol{D}_I$ in (7.57) reduces to the elastic constitutive matrix $\boldsymbol{D}_e$. The return mapping procedure is again carried out, after which check is performed on any newly formed crack. Crack in the 'floating' stage is however included in the consistent tangent matrix.

Box 7.2. Overall stress calculation procedure

Step	Description
1	Record all state variables on entry

2	Compute $\boldsymbol{\sigma}_I$ from (7.57)
	If $\zeta < \varphi^* \varepsilon_0$ ('floating' POD) Then
	Remove POD formed from previous increment
	$\boldsymbol{D}_I = \boldsymbol{D}_e$
	Else (fixed POD)
	$\boldsymbol{D}_I = \left(\boldsymbol{I} + \boldsymbol{D}_e \sum_{j=1}^{n_p} \boldsymbol{N}_j{}^T \boldsymbol{C}_{lsf} \boldsymbol{N}_j \right)^{-1} \boldsymbol{D}_e$
	End If

3	If $F(\boldsymbol{\sigma}_I, \kappa) > 0$ and $I_1(\boldsymbol{\sigma}_I) < 0$ Then
	Carry out return mapping with plasticity and existing POD to obtain new stress $\boldsymbol{\sigma}$
	If $\Delta\lambda < 0$ Then
	Reset state variables and carry out mapping without plasticity
	End If
	Else If ($n_p > 0$)
	If $f_e(\boldsymbol{s}_f, f_s) > 0$ Then
	Carry out return mapping with local plasticity and existing POD to obtain new stress $\boldsymbol{\sigma}$
	If $\Delta\mu < 0$ Then
	Reset state variables and carry out mapping without local plasticity
	End If
	End If
	Else
	$\boldsymbol{\sigma} = \boldsymbol{\sigma}_I$
	End If

4	For $i = 1, n_{max}$ [1]
	If $\sigma_1(\boldsymbol{\sigma}) > f_t$ Then
	Form new POD using principal direction of $\boldsymbol{\sigma}_I$
	Reset all state variables
	Carry out return mapping to obtain new stress $\boldsymbol{\sigma}$
	Else
	No new POD, record final stress
	End If
	End For

Notes:

1. n_{max} = maximum number of PODs permitted to form

7.6 Verification of consistent algorithm

A consistent tangent operator with return mapping algorithm has been derived to provide efficient integration for constitutive modelling. Verification of the consistent algorithm had been carried out using a Mathcad implementation (see Appendix I). The following describes the overall procedure undertaken. For simplicity, the case of an applied strain increment is considered here.

- Initialise all stresses, strains and state variables
- Apply the strain increment $\Delta\boldsymbol{\varepsilon}$
- Compute and record the final converged stress $\boldsymbol{\sigma}_{rec}$
- Form the consistent tangent operator $\boldsymbol{D}_{ep}$ using the converged stress and state variables
- Apply a small strain increment $\delta\boldsymbol{\varepsilon}$ and compute the corresponding stress increment using $\boldsymbol{D}_{ep}$, i.e. $\delta\boldsymbol{\sigma} = \boldsymbol{D}_{ep}\delta\boldsymbol{\varepsilon}$
- Reset all stresses, strains and state variables to their initial values
- Re-compute the final converged stress $\boldsymbol{\sigma}_{new}$ from the updated applied strain increment of $\Delta\boldsymbol{\varepsilon} + \delta\boldsymbol{\varepsilon}$
- Evaluate the error measure for the converged stresses using

$$\varpi = \left| \frac{(\boldsymbol{\sigma}_{new} - \boldsymbol{\sigma}_{rec}) - \delta\boldsymbol{\sigma}}{\boldsymbol{\sigma}_{new} - \boldsymbol{\sigma}_{rec}} \right|$$

The acceptable tolerance for ϖ is about 10^{-6}, which was achieved in the consistency verification, as shown in Appendix I.

7.7 Numerical examples

7.7.1 Single point stress-strain path benchmark

The key element of the proposed model being the local damage-contact component, which is used to capture the behaviour of crack opening and closing, as well as shear contact from the behaviour of aggregate interlock. In this section, a series of strain paths were chosen, which forms the basis of a benchmark, highlighting the characteristics of cracked concrete under combined shear and normal loading. The simulations were undertaken using a constitutive driver program in which the proposed model has been implemented. Table 7.1 shows the data used for the benchmark study.

Table 7.1. Material properties for benchmark study

E (N/mm^2)	ν	f_t (N/mm^2)	ε_0	m_g	m_{hi}	m_{ful}
30000	0.2	3.0	0.002	0.3	1.0	3.0

In the following simulations, a compressive yy-stress of -3 N/mm^2 is first applied and then a crack is opened in the xx-direction to five different opening strains of 0.0002 (BM1), 0.001 (BM2), 0.002 (BM3), 0.003 (BM4) and 0.007 (BM5). xy-shear strains are then applied, whilst the xx-strain and yy-stress are kept constant. Figure 7.4 shows the tensile softening response for the same set of properties and indicates the normal opening strains for the five cases considered. Figures 7.5 and 7.6 show the overall results obtained from the simulations.

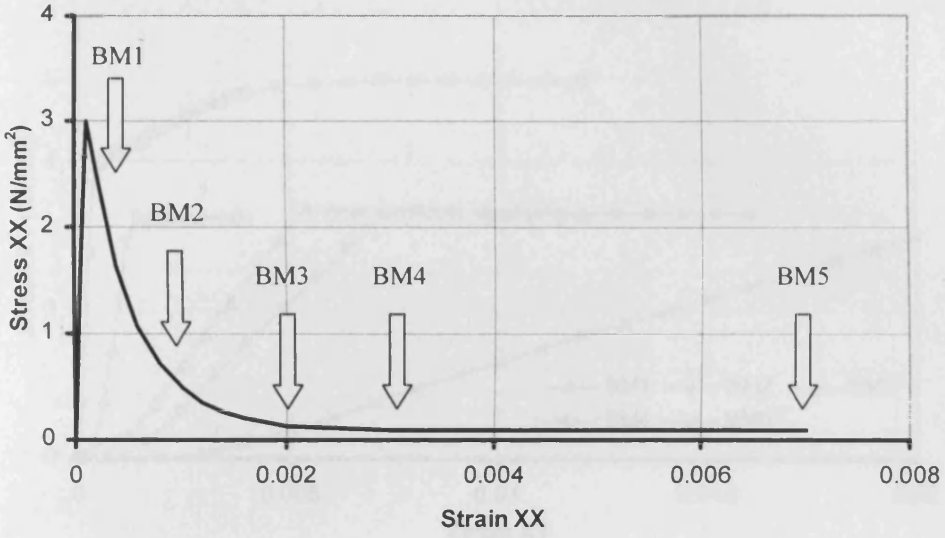

Figure 7.4. Tensile softening curve, showing opening points

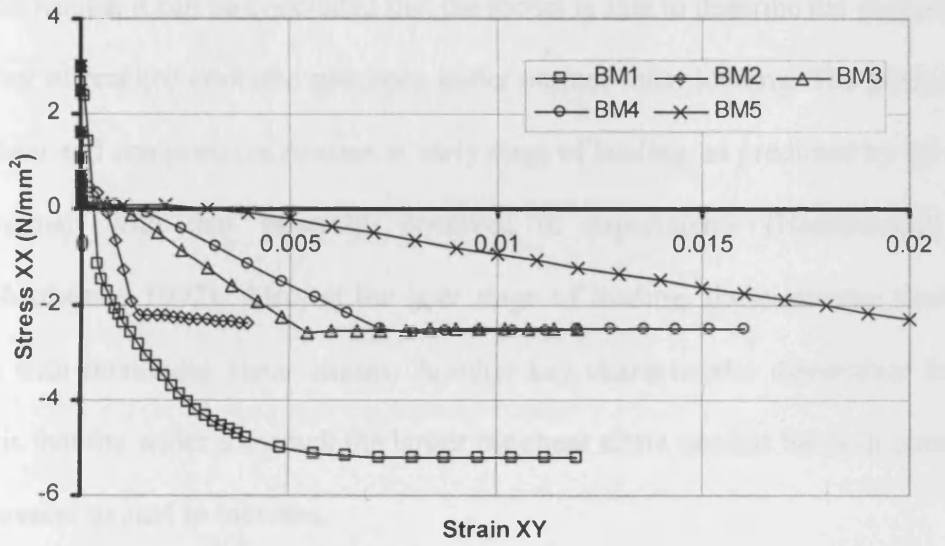

Figure 7.5. Variation of normal stress with shear strain

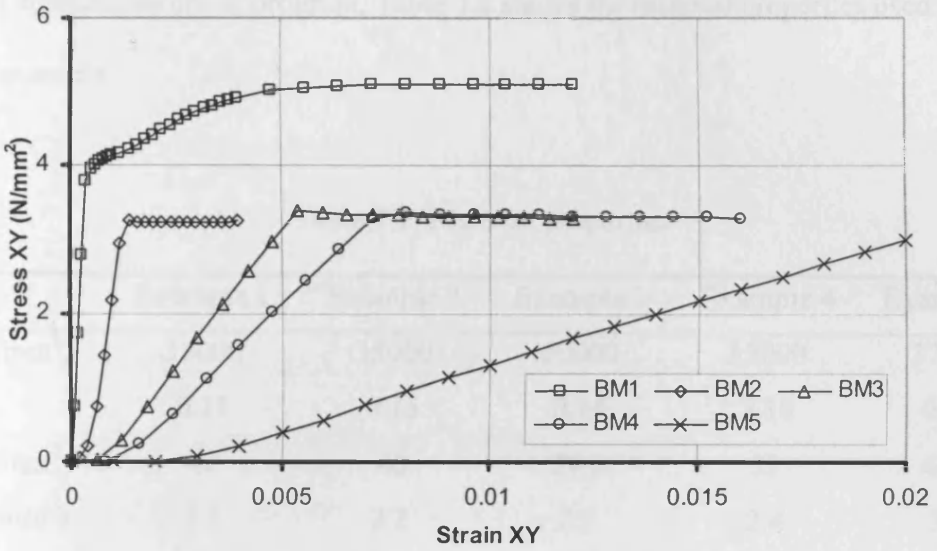

Figure 7.6. Variation of shear stress with shear strain

From the results, it can be concluded that the model is able to describe the characteristics behaviour of cracked concrete specimen under normal-shear loading. The gradual build up of shear and compressive stresses at early stage of loading, as predicted by the model, is consistent with that generally observed in experiments (Hassanzadeh 1991; Nooru-Mohamed 1992). Also, at the later stage of loading, these stresses tend to the plateau with increasing shear strains. Another key characteristic discernible from the results is that the wider the crack the larger the shear strain needed for both normal and shear stresses to start to increase.

7.7.2 Single point stress-strain examples

In this section, a number of single point stress-strain path examples are given, which provide comparisons with test data. As before, the numerical analyses were undertaken

using a constitutive driver program. Table 7.2 shows the material properties used for each of the example.

Table 7.2. Material properties

	Example 1	Example 2	Example 3	Example 4	Example 5
E (N/mm^2)	35000	35000	30000	35000	37000
ν	0.15	0.15	0.15	0.18	0.15
f_c (N/mm^2)	40	40	29.5	32	46.9
f_t (N/mm^2)	3.2	3.2	2.5	2.4	3.0
ε_c	0.02	0.0022	0.0022	0.0021	0.0023
ε_0	0.0027	0.06	0.002	0.002	0.003
b_r	1.15	1.15	1.15	1.15	1.1
Z_0	0.5	0.5	0.5	0.5	0.25
ψ	-0.1	-0.1	-0.1	-0.2	-0.3
m_g	0.4	0.4	0.425	0.4	0.4
m_{hi}	2	2	2	2	2
m_{ful}	10	10	10	10	10

It is noted that the model has been developed with relatively few non-fixed material parameters. Each of these chosen parameters relates to a particular physical characteristic that could be measured directly from experiment tests. Among these parameters, those which are non-standard are as follows; b_r, Z_0, ψ, m_g, m_{hi}, and m_{ful}. The decisions to use only a few parameters and to choose only those that could be directly related to a physical characteristic were made in order to provide better understanding on the parameters used and their respective influence on the overall model behaviour. The recommended method of determination of these parameters, as well as their typical values, are given in

Appendix II.

7.7.2.1 Example 1 - Uniaxial tensile test

The first of these tests employed Hordijk's (1991) uniaxial tensile softening curve. Hordijk's function is recognised to match well a wide range of data, and here the numerical results obtained are compared to the data reported by van Mier (1997). In the simulation, the fracture process zone is assumed to be of 60 mm and the opening displacements are evaluated by removing the elastic deformations from the overall displacements. Figure 7.7 shows the results obtained for the uniaxial tensile softening path.

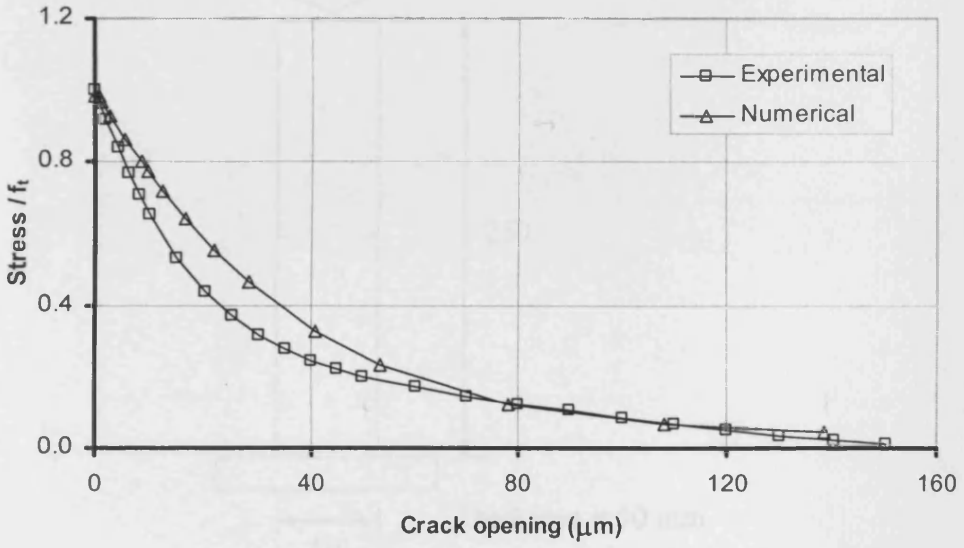

Figure 7.7. Uniaxial tension curve

7.7.2.2 Example 2 – Uniaxial cyclic test

The second test considered was to replicate a series of test on notched fracture specimens carried out by Reinhardt (1984). The specimens had an effective area at the notch of 50×50 mm^2, as depicted in Figure 7.8. It was the data from the LCLS (Large Compressive Lower Stress) tests, which were carried out on narrow specimens, that was used for comparisons in this example. The characteristic crack dimension was assumed to be equal to the gauge length (35 mm), which was then used to obtain the limiting strain parameter ε_0, i.e. by dividing the opening displacement at the end of the softening curve (0.21 mm) by the gauge length.

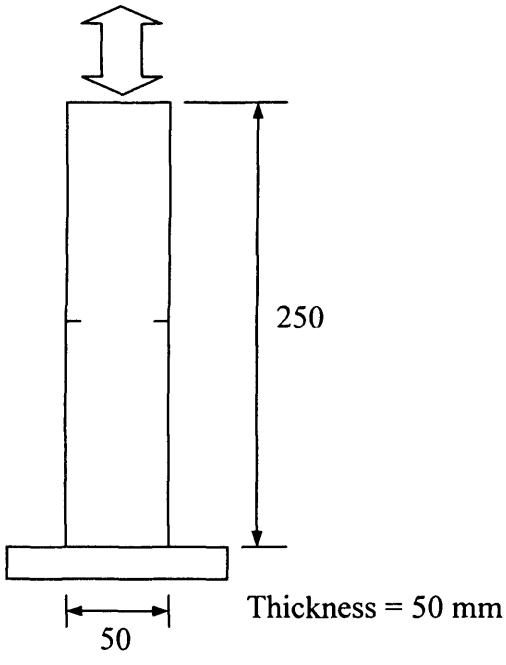

Figure 7.8. Reinhardt's cyclic testing arrangement

The results from the experimental test, as well as those from the numerical analysis, are shown in Figure 7.9. In contrast to the original crack plane model by Jefferson (2003a), which simulates secant unloading-reloading and full crack closure at zero axial strain, the present model is capable of capturing local plastic yielding on the embedded crack plane. Hence, upon unloading, permanent strains developed. As previously discussed in Section 7.2.2, the model parameter a_p introduced in the modified softening function governs the level of plasticity captured on the damage plane. Figure 7.10 shows the influence of the parameter a_p on the unloading-reloading process. It is noted that the model predicts full crack closure at zero axial strain when $a_p = 0$. Also apparent in Figure 7.10 is the smooth transition from open to closed state.

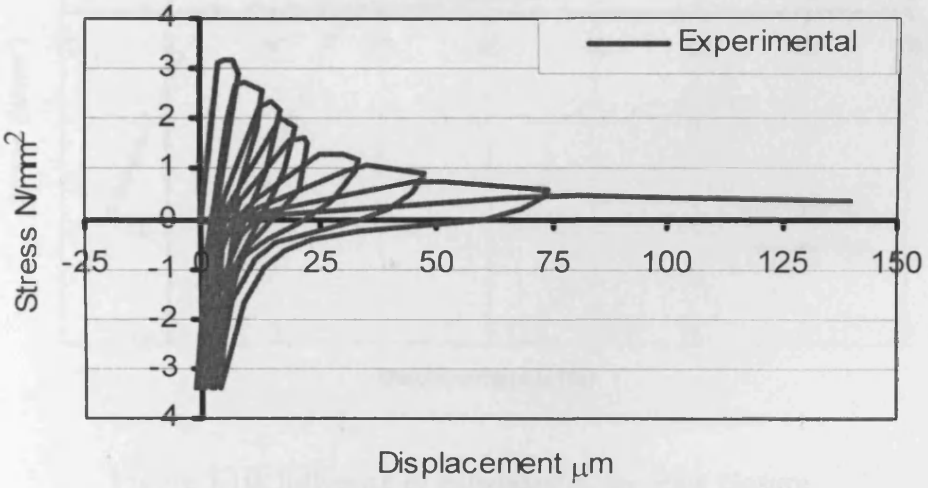

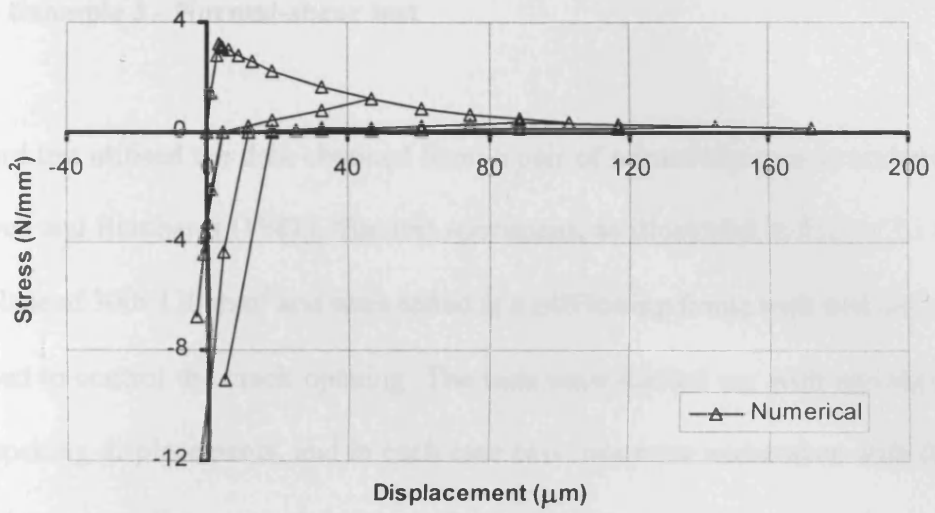

Figure 7.9. Uniaxial tension with crack opening and closing

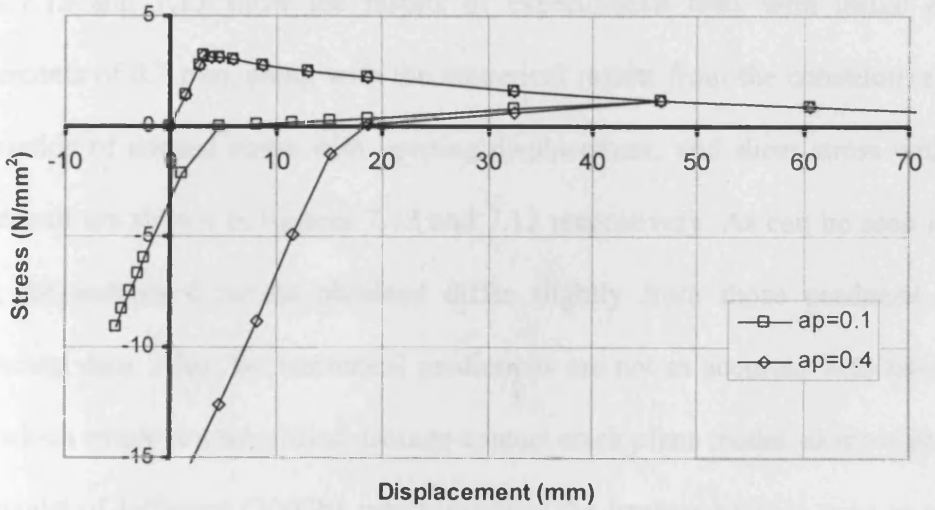

Figure 7.10. Influence of parameter a_p on crack closure

7.7.2.3 Example 3 - Normal-shear test

The third test utilised the data obtained from a pair of normal-shear tests undertaken by Walraven and Reinhardt (1981). The test specimens, as illustrated in Figure 7.11, had a shear plane of 300×120 mm^2 and were tested in a stiff testing frame with external restraint bars used to control the crack opening. The tests were carried out with specified initial crack opening displacements, and in each case two tests were undertaken with the same nominal openings. Once a crack had been formed to the required opening, the specimens were then sheared whilst the normal and shear displacements were monitored.

Figures 7.12 and 7.13 show the results of experimental tests with initial opening displacements of 0.2 mm, along with the numerical results from the constitutive driver. The variation of normal stress with opening displacement, and shear stress with shear displacement are shown in Figures 7.12 and 7.13 respectively. As can be seen in these figures, the numerical results obtained differ slightly from those produced by the experimental data. Also, the numerical predictions are not as accurate with the present model, which employs a simplified damage-contact crack plane model, as those predicted by the model of Jefferson (2002b), which assumes the fracture process zone as a region consisting of four components; material that is undamaged and continuous (i.e. undamaged), material that has debonded but still in contact (i.e. bridging), and material adjacent to surfaces that has fully debonded and lost all contact (i.e. fully debonded). Nevertheless, the present model does simulate the stress free zone before contact, as well as the build up of shear and normal stresses reasonably.

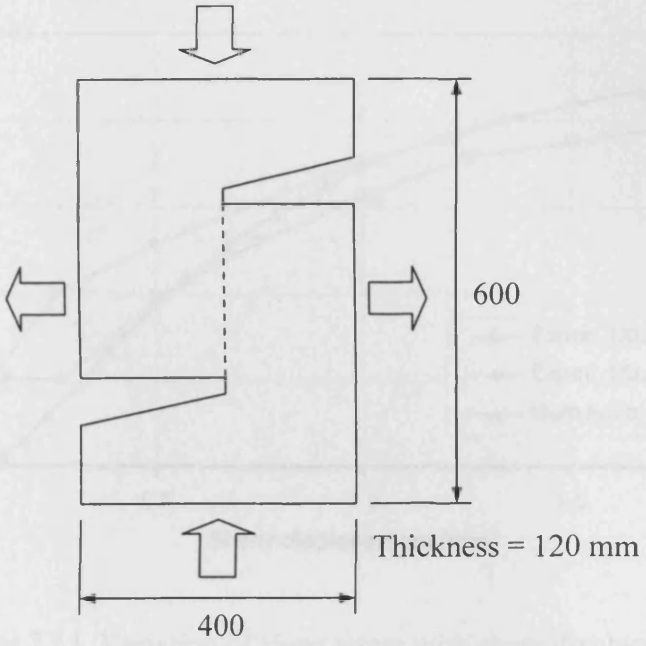

Figure 7.11. Walraven and Reinhardt's test specimen

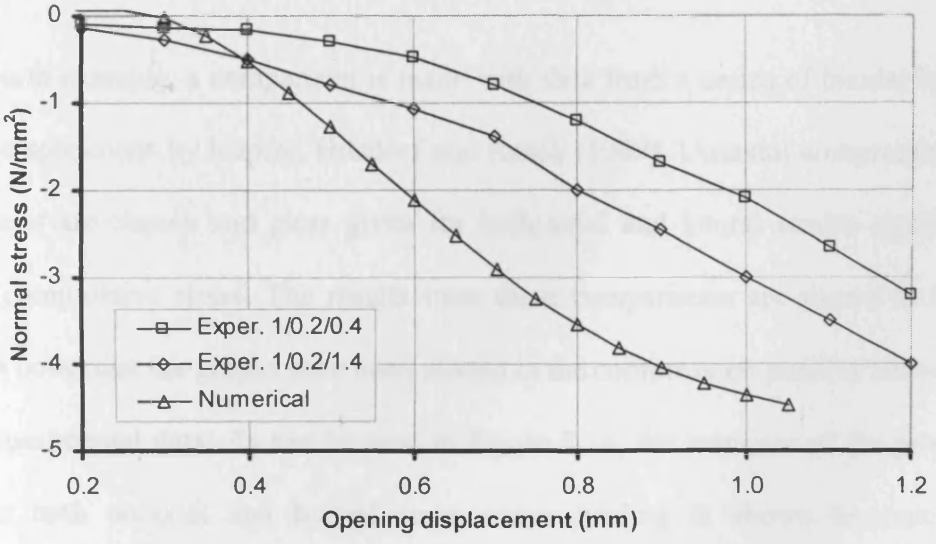

Figure 7.12. Variation of normal stress with opening displacement

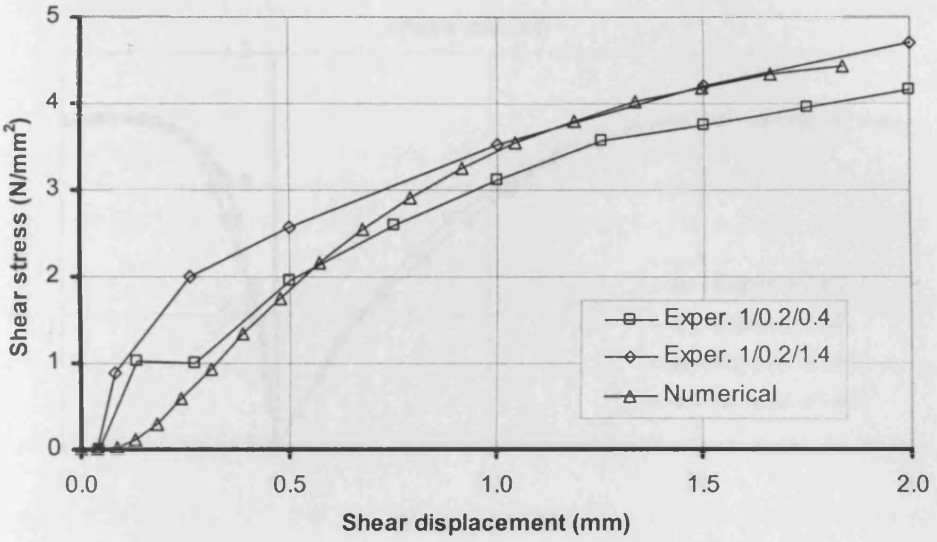

Figure 7.13. Variation of shear stress with shear displacement

7.7.2.4 Example 4 - Uniaxial and biaxial tests

In the fourth example, a comparison is made with data from a series of biaxial tests on plate type specimens by Kupfer, Hilsdorf and Rusch (1969). Uniaxial compressive and biaxial tests are chosen and plots given for both axial and lateral strains against the uniaxial compressive stress. The results from these comparisons are shown in Figure 7.14. It is noted that the graphs have been plotted in the compression positive convention of the experimental data. As can be seen in Figure 7.14, the response of the proposed model to both uniaxial and biaxial compressive loading is shown to match the experimental curves closely. These are not significantly different from those of the original Craft model but are included to demonstrate that the new constitutive model does produce the same response.

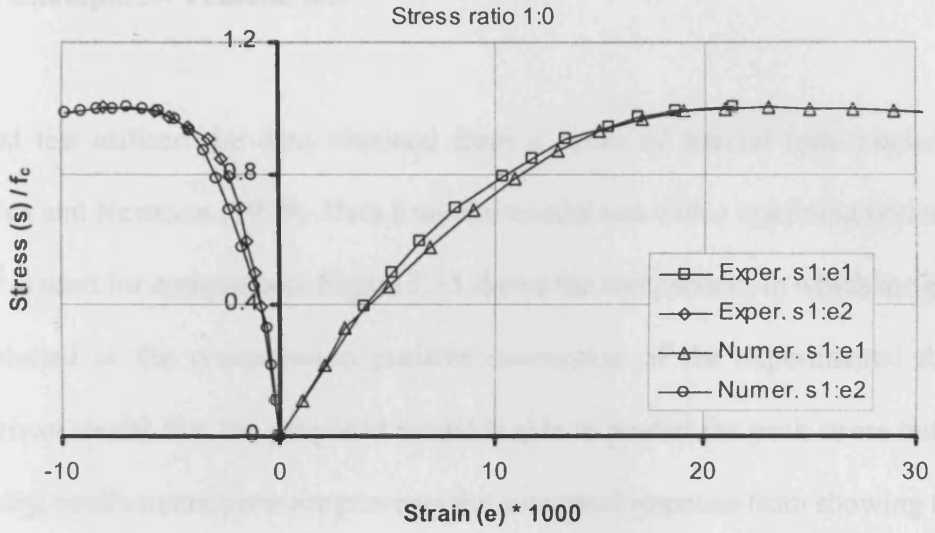

(a) Uniaxial compression response

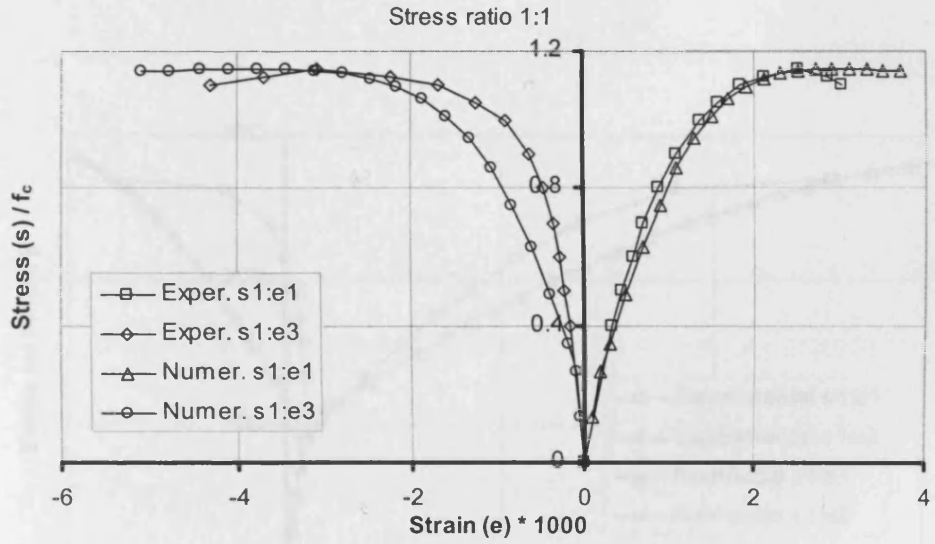

(b) Biaxial compression response

Figure 7.14. Comparison with test data from Kupfer, Hilsdorf and Rusch

7.7.2.5 Example 5 - Triaxial test

The last test utilised the data obtained from a series of triaxial tests carried out by Kotsovos and Newman (1979). Data from the triaxial test with a confining pressure of 70 N/mm^2 is used for comparison. Figure 7.15 shows the comparison, in which the graph has been plotted in the compression positive convention of the experimental data. The comparison shows that the proposed model is able to predict the peak stress but that the increasing confinement pressure prevents the numerical response from showing the same ductility as the experimental data. Again, the results are not significantly different from those of the original Craft model but are included here to demonstrate that the proposed model does produce the same response.

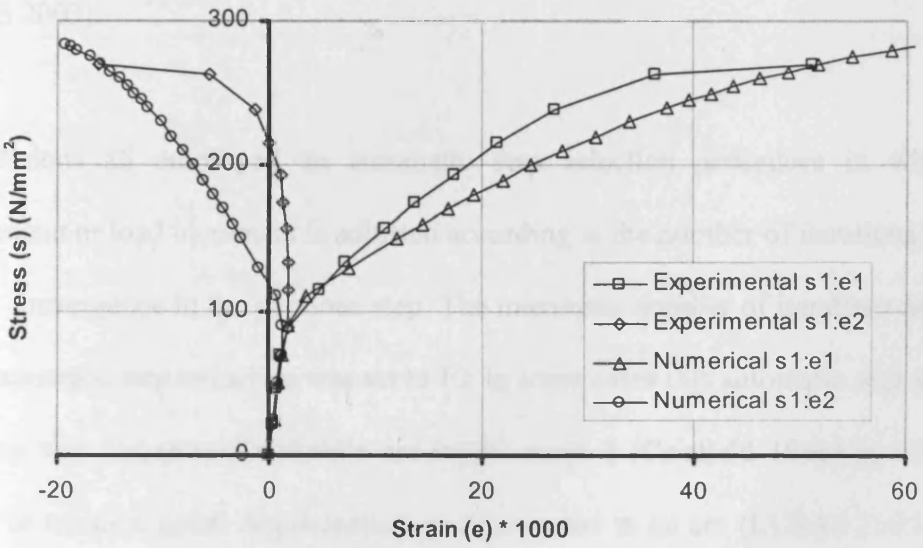

Figure 7.15. Comparison with triaxial test data from Kotsovos and Newman

7.7.3 Finite element analysis examples

This section presents results from various numerical simulations undertaken on examples of previously tested concrete structural elements. The results were obtained from the proposed model, which had been implemented in the finite element program LUSAS via the material model interface.

In the following examples, quadratic elements were used, which includes 6-noded triangular and 8-noded quadrilateral elements for two-dimensional examples and 20-noded hexahedral elements for three-dimensional example. Full numerical integration was performed for all 2D elements, i.e. 3×3 Gaussian for quadrilateral elements and 6 point Radau for triangular elements, and Iron's 14 point rule was used for 3D elements (LUSAS 2003).

The solutions all employed an automatic step selection procedure in which the displacement or load increment is adjusted according to the number of iterations taken to achieve convergence in the previous step. The maximum number of iterations permitted before automatic step reduction was set to 10. In some cases this automatic step selection procedure was linked to Crisfield's arc-length method (Crisfield 1981) in which the product of iterative nodal displacements is constrained to an arc (LUSAS 2003). Table 7.3 shows the material properties used for each of the following finite element example.

Table 7.3. Material properties

	Example 1	Example 2	Example 3	Example 4	Example 5
E (kN/mm^2)	35	30.6	30	25	50
ν	0.2	0.15	0.18	0.2	0.15
f_c (N/mm^2)	40	50	35	53	50
f_t (N/mm^2)	3.35	2.6	3.2	2.5	3.0
ε_c	0.0022	0.0035	0.0022	0.003	0.003
ε_0	-	-	-	0.005	-
G_f (N/mm)	0.1	0.15	0.1	-	0.15
b_r	1.15	1.15	1.1	1.1	1.1
Z_0	0.6	0.6	0.6	0.6	0.6
ψ	-0.1	-0.1	-0.1	-0.1	-0.1
m_g	0.5	0.5	0.5	0.5	0.5
m_{hi}	0.5	0.5	0.4	0.5	0.5
m_{ful}	5	5	3	5	1.2
φ	0.005	0.5	0.7	0.5	0.005

7.7.3.1 Example 1 - Direct fracture test

The first example involves comparisons of results obtained from a plane stress analysis of a fracture test specimen. The test was carried out by Petersson (1980) on an unreinforced fracture specimen. The specimen was loaded in direct tension under displacement control. Figure 7.16 illustrates the dimensions of the specimen used and the corresponding finite element mesh generated for the numerical analysis is shown in Figure 7.17.

The solution employed the automatic step size procedure, with an upper limit of 0.01 mm placed on the prescribed boundary displacement increment. In this example, the target number of iterations was set to 10 and the convergence tolerance to 0.1% and 10% for displacement and residual force norms respectively. The latter convergence tolerance was relatively large but was inevitable in order to obtain full convergence. Nevertheless, most of the increments converged to a much tighter tolerance.

The experimental and numerical load displacement responses are shown in Figure 7.18. Figure 7.19 shows a crack plot for the mesh at the opening displacement marked. Figures 7.20 and 7.21 show the distribution of major principal stress and strain, respectively.

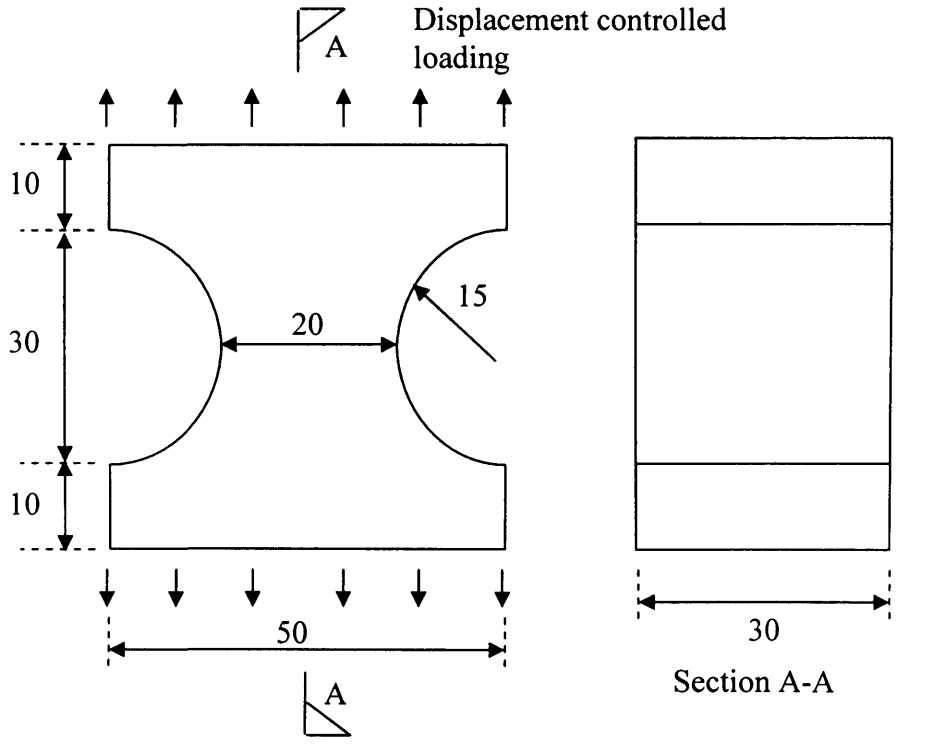

Figure 7.16. Test specimen

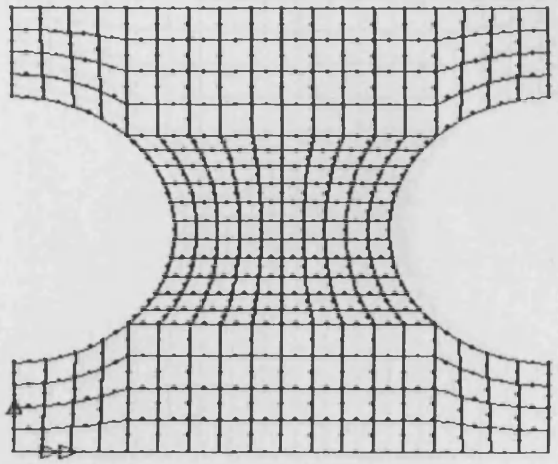

2D mesh

Figure 7.17. 2D finite element mesh

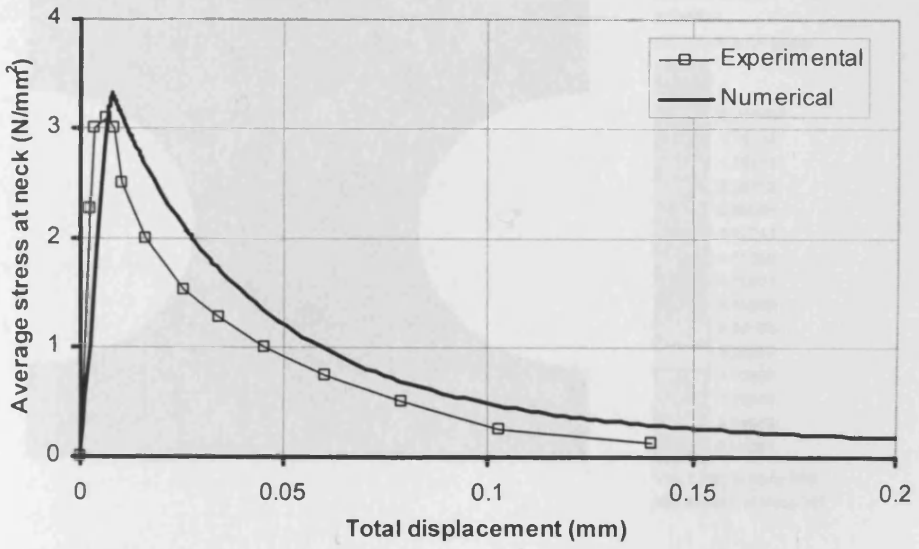

Figure 7.18. Load-displacement response

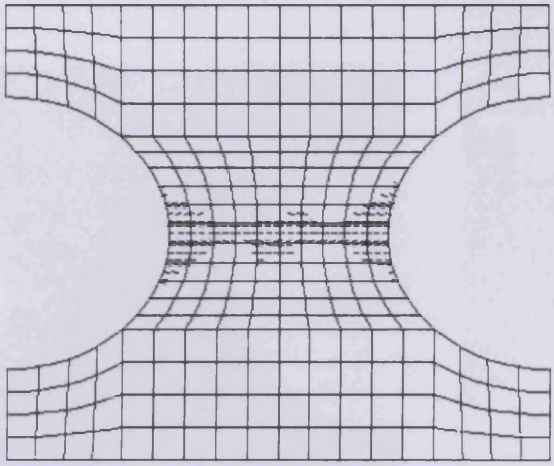

Figure 7.19. Crack plot

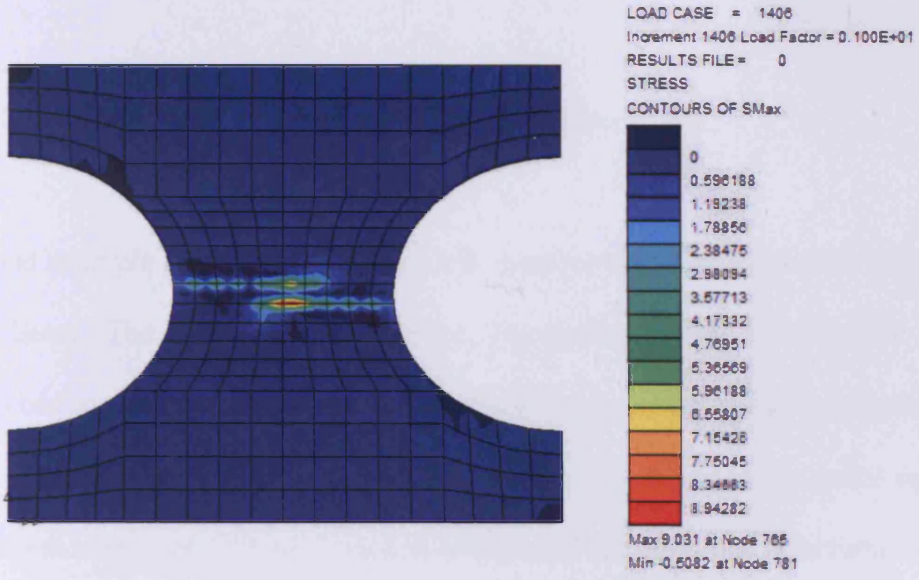

Figure 7.20. Major principal stress distribution

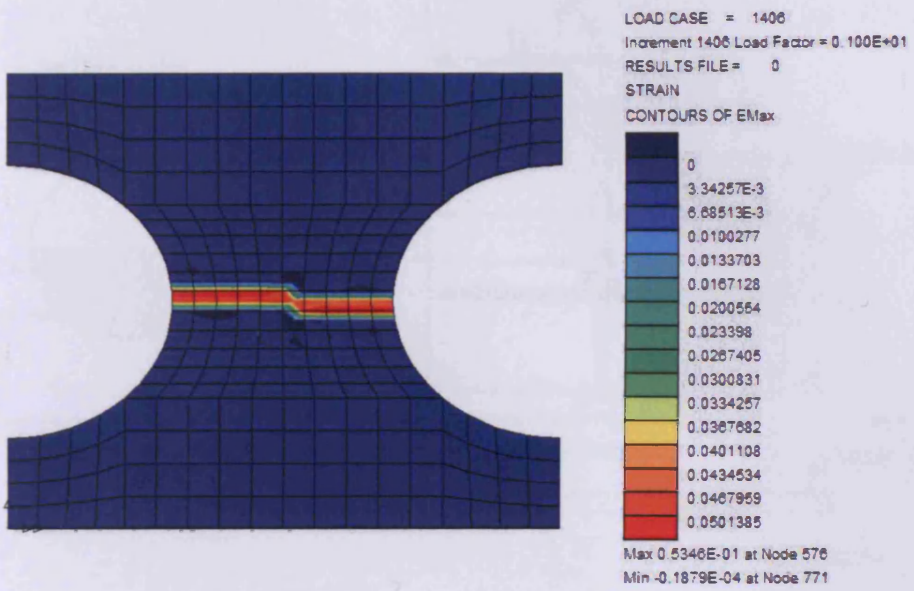

Figure 7.21. Major principal strain distribution

7.7.3.2 Example 2 - Cylindrical notched fracture beam

The second example presents results from a three-dimensional analysis of a cylindrical notched beam. The tests were carried out by Jefferson and Barr (1995) on an un-reinforced concrete beam. In the test, the specimen was loaded via a shaped yoke with the load level being controlled by feedback from a clip gauge at the notch tip. The specimen was supported on curved cradles, as depicted in Figure 7.22. The finite element mesh generated for the analysis, which makes use of double symmetry, is shown in Figure 7.23.

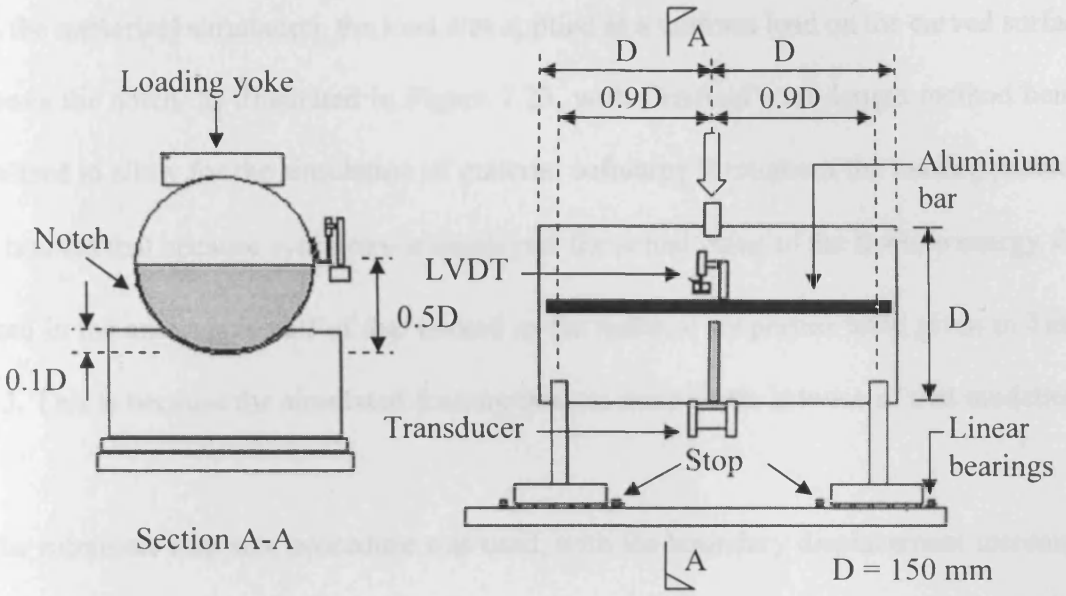

Figure 7.22. Experimental arrangement of cylindrical notched beam

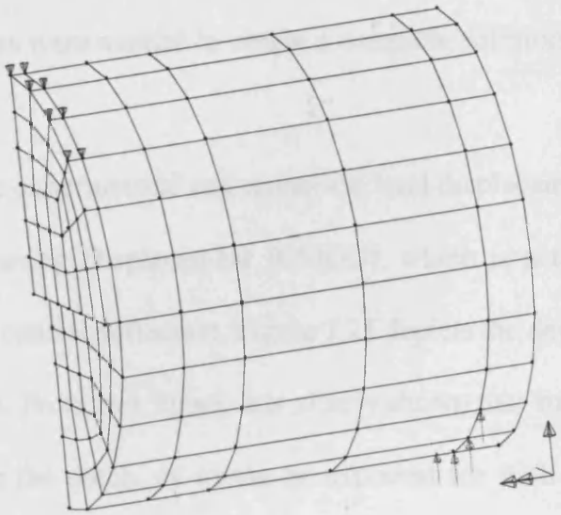

Figure 7.23. Finite element mesh for notched cylinder

In the numerical simulation, the load was applied as a uniform load on the curved surface above the notch, as illustrated in Figure 7.23, with Crisfield's arc-length method being utilised to allow for the simulation of material softening throughout the loading process. It is noted that because symmetry is employed, the actual value of the fracture energy G_f used in the analysis is half of that quoted in the material properties table given in Table 7.3. This is because the simulated fracture process zone width is twice of that modelled.

The automatic step size procedure was used, with the boundary displacement increment prescribed at an upper limit of 0.1 mm. In this example, the maximum number of iterations permitted per increment was set to 10, and the convergence tolerance to 0.1% and 5% for displacement and residual force norms respectively. Again, relatively large convergence tolerances were needed to obtain a complete solution.

Figure 7.24 shows the experimental and numerical load displacement responses for both the Crack Mouth Opening Displacement (CMOD), which is actually the notch mouth opening here, and the central deflection. Figure 7.25 depicts the deformed mesh at the end of the loading process. From this figure, it is clearly shown that strain localisation occurs in the material above the notch, as would be expected for such a test. The agreement between the numerical and experimental responses is generally good.

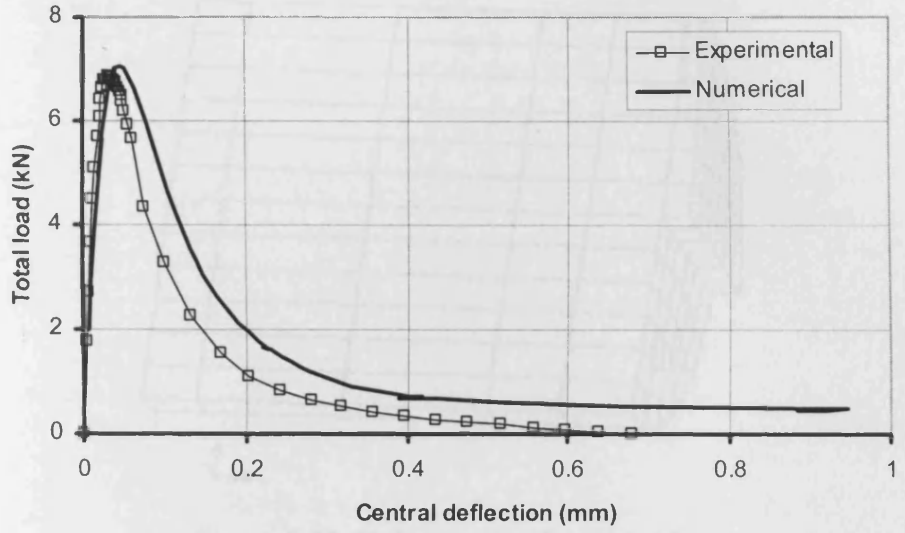

(a) Variation of load with central deflection

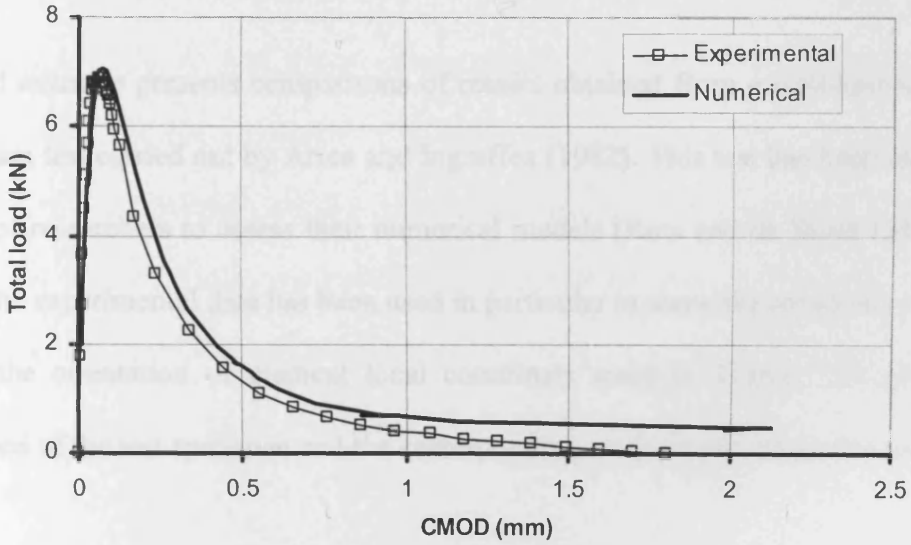

(b) Variation of load with Crack Mouth Opening Displacement (CMOD)

Figure 7.24. Load-displacement responses

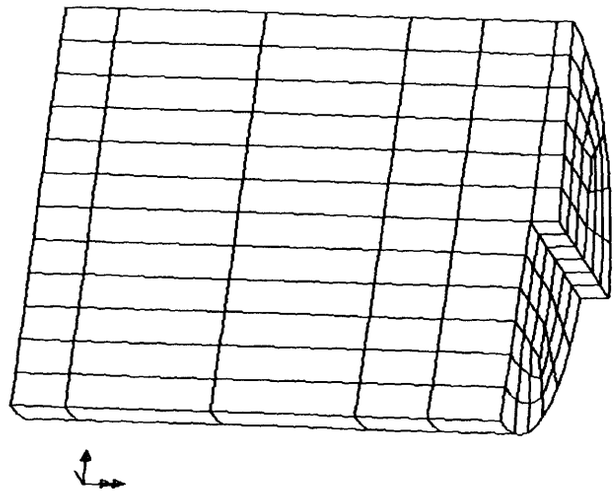

Figure 7.25. Deformed mesh plot (×10)

7.7.3.3 Example 3 - Single edged notch beam

The third example presents comparisons of results obtained from a well-known single notch beam test carried out by Arrea and Ingraffea (1982). This test has been used by a number of researchers to assess their numerical models (Rots and de Borst 1987; Rots 1988). The experimental data has been used in particular to show the sensitivity of crack path to the orientation of element local coordinate systems. Figure 7.26 gives the dimensions of the test specimen and the corresponding mesh employed for the analysis.

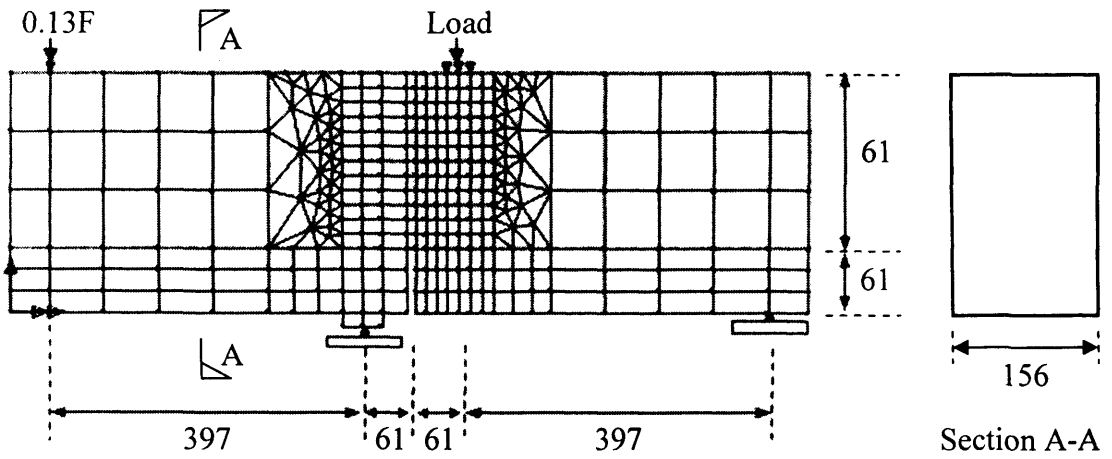

Figure 7.26. Test arrangement and finite element mesh

In the numerical analysis, the main load was applied in a patch on the upper edge, as shown in Figure 7.26. As with the previous example, Crisfield's arc-length method was utilised to allow for the simulation of material softening. 50 steps were used in the solution, with the maximum number of iterations per increment set to 10. During the solution, the step size was automatically reduced twice when convergence was not achieved in the maximum allowable number of iterations. In this example, the convergence tolerance was set to 1% and 5% for displacement and residual force norm, respectively.

It is noted that the aim of this example is to validate that the constitutive model is capable of predicting a curved crack with softening down to a relatively small proportion of the peak load. It is also noted that in order to simulate the curved crack path, the constitutive model allowed the POD formed to 'float' until the fracture strain reached a value of

$0.5*\varepsilon_0$ (i.e. $a_p = 0.5$).

Figure 7.27 shows the variation of load with the crack mouth sliding displacement (CMSD). As can be seen in this figure, the initial response is a little less stiff than that observed in the experiment, which was also found by Rots (1988) and Jefferson (2003b). Figure 7.28 and Figure 7.29 show the deformed mesh and crack plot at the final step of loading respectively. The distribution of major principal stress and strain are illustrated in Figure 7.30 and 7.31 respectively.

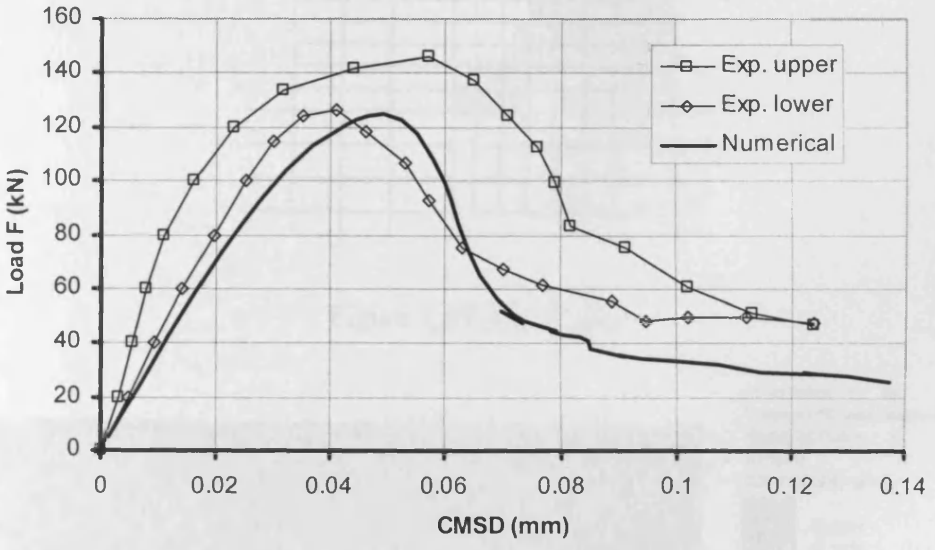

Figure 7.27. Load-displacement responses

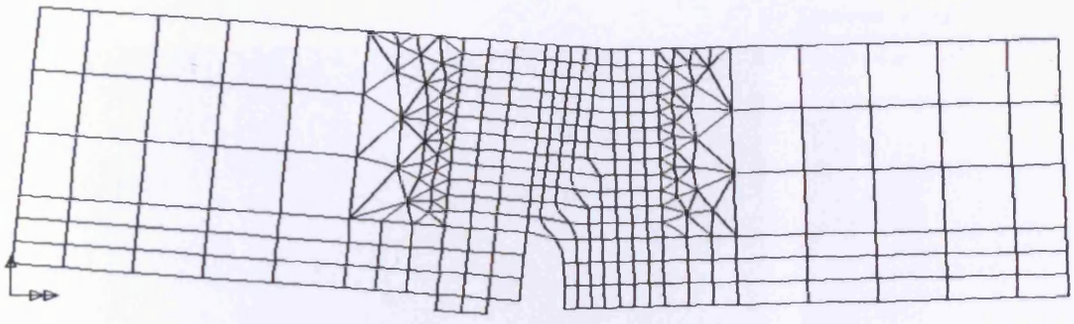

Figure 7.28. Deformed mesh plot (×10)

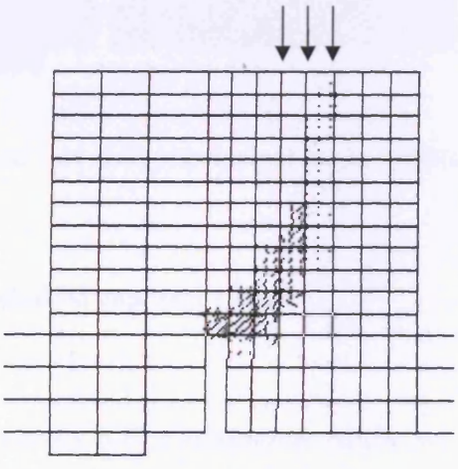

Figure 7.29. Crack plot

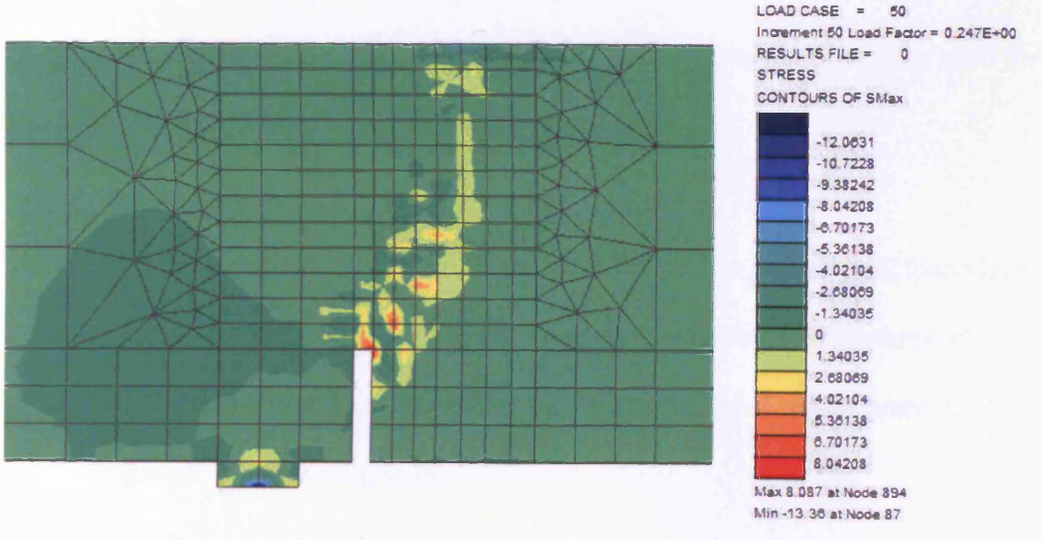

Figure 7.30. Major principal stress distribution

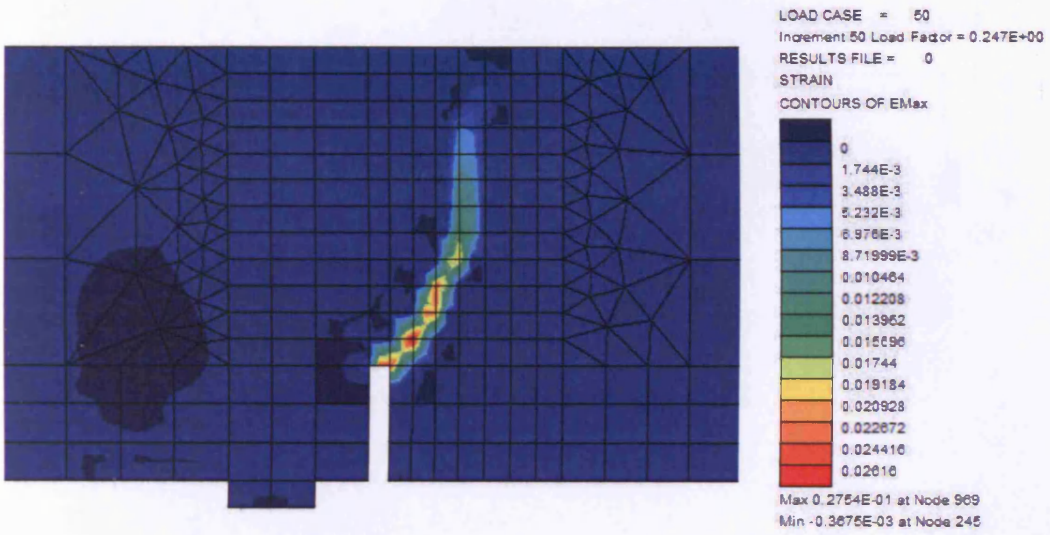

Figure 7.31. Major principal strain distribution

7.7.3.4 Example 4 - Reinforced concrete beam

This example involves the analysis of a rectangular reinforced concrete beam, which has been used over many years as a test for numerical models for concrete (ASCE 1982). The reinforced concrete beam test was carried out by Bresler and Scordelis (1963). Figure 7.32 shows the geometry of the concrete beam, and also the finite element mesh used for the analysis.

The reasons for having chosen this example amongst the studies are twofold; to evaluate the response of the constitutive model to problems in which concrete crushing plays a significant role, and to assess the capability of the model to simulate cracking in a full-scale reinforced concrete specimen.

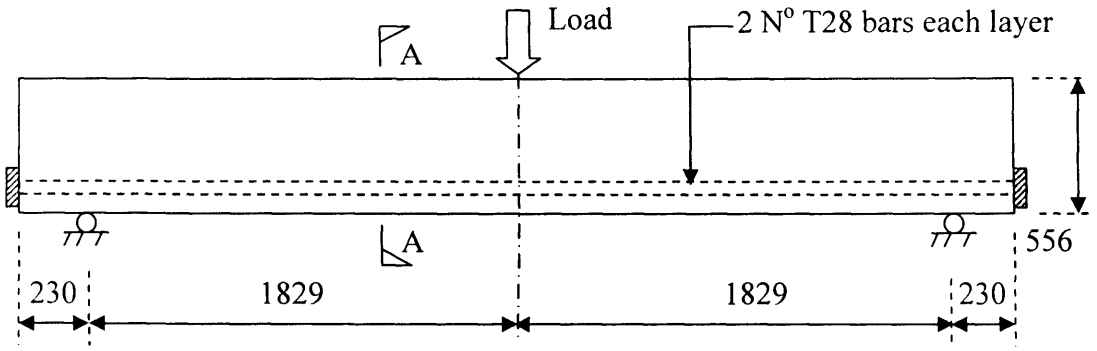

Elevation of beam showing reinforcement

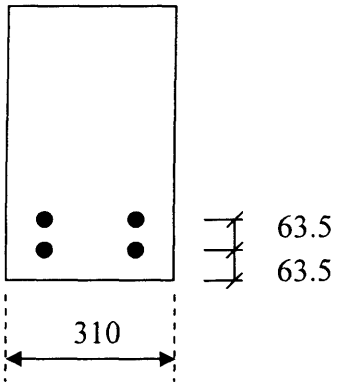

Section A-A (all dimensions in mm)

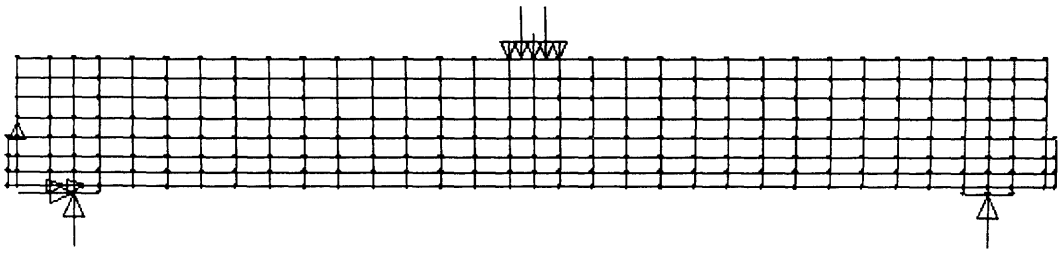

Finite element mesh

Figure 7.32. Geometry and FE mesh of test specimen

In this example, the boundary displacement increment was prescribed at an upper limit of 0.02 mm. 100 steps were used in the solution, with the maximum number of iterations per increment set to 10. The step size was automatically reduced twice when convergence was not achieved in the maximum allowable number of iterations. In this example, only the displacement norm was used here to control solution convergence, which was set to 1%. It is also noted that the compressive strength was set to 53 N/mm^2, as oppose to the much lower f_c i.e. about half the value, reported in the experimental data. This, again, was inevitable in order to get reasonable simulation. Hence, the effect of concrete crushing has not been completely modelled in this particular analysis.

Figure 7.33 shows a comparison of the load displacement response. The eventual deformed mesh is illustrated in Figure 7.34. Figure 7.35 shows crack plots at the final step of loading.

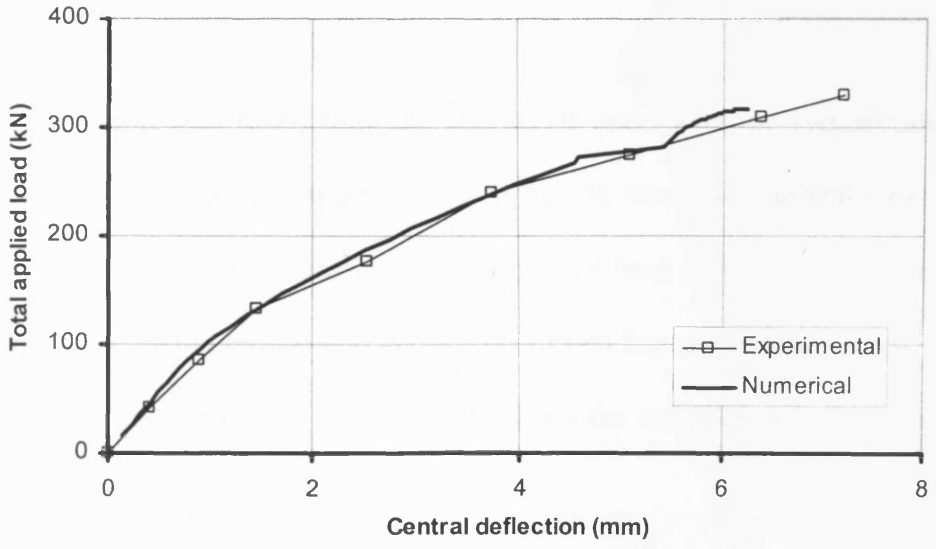

Figure 7.33. Load-displacement response

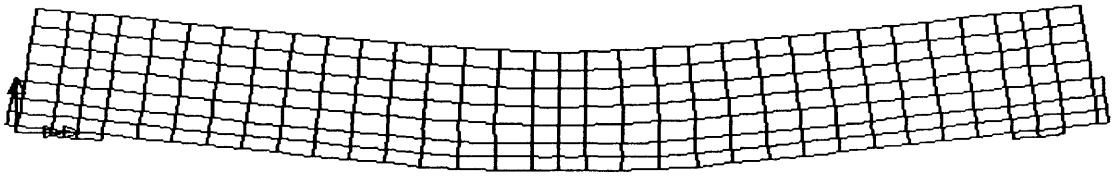

Figure 7.34. Deformed mesh plot (×10)

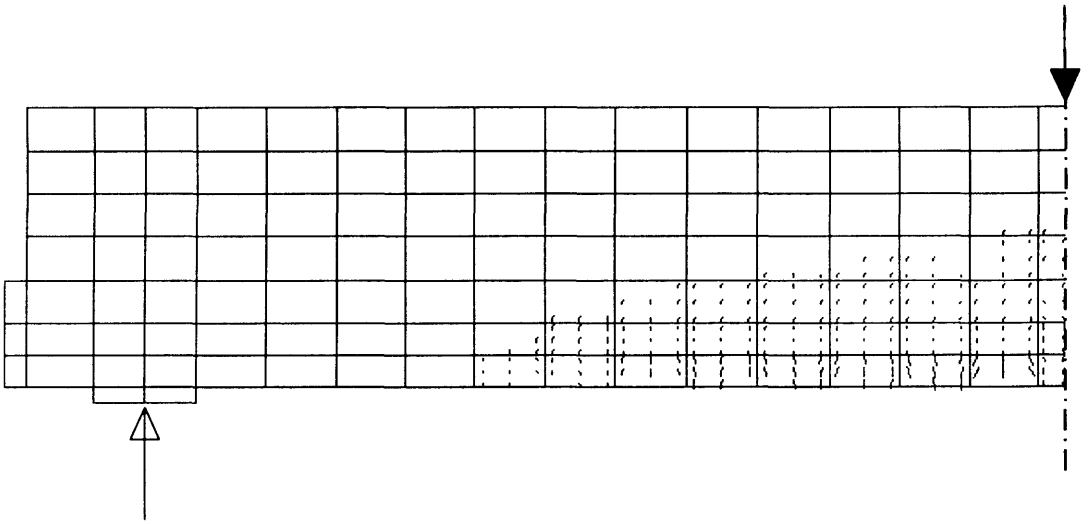

Figure 7.35. Crack plot

7.7.3.4 Example 5 – Normal-shear test

The last example was taken from the test series undertaken by Hassanzadeh (1991). Figure 7.36 shows the test specimens used for the combined normal-shear test. The specimen had an effective cross-section at the notch level of 40×40 mm^2. The specimen was first subjected to a tensile load to the point of first fracture and then shear was applied according to the relationship, $u = (\tan\alpha)*v$. Only the test with $\alpha = 45°$ are considered here.

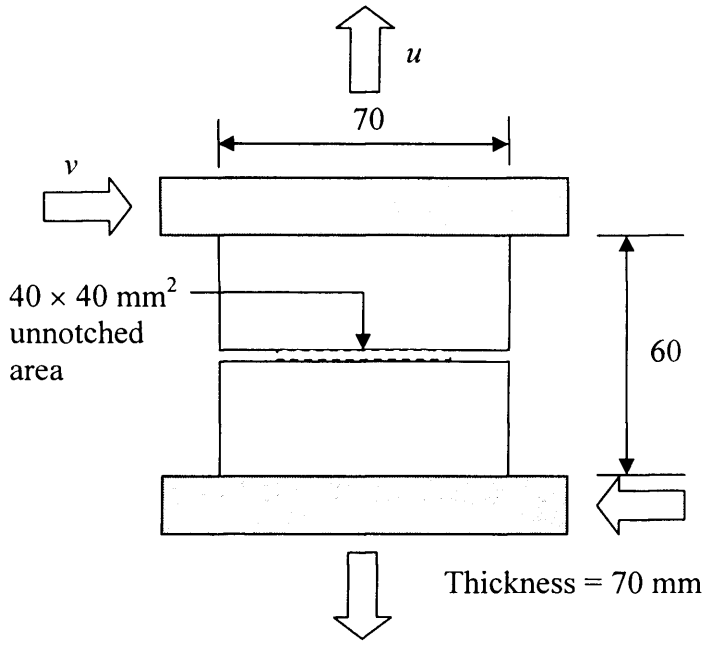

Figure 7.36. Hassanzadeh's test specimen

In this example, the boundary displacement increment was prescribed at an upper limit of 0.1 mm, whilst the maximum number of iterations per increment was set to 10. During the solution, the step size was automatically reduced twice when convergence was not achieved in the maximum allowable number of iterations. The overall solution convergence was controlled by the displacement norm which was set to 1%.

Figures 7.37 and 7.38 give the stress-displacement responses and provide comparisons of the numerical predictions with that of experimental results. This example has, in particular, proven difficult to simulate by the proposed model. Various attempts were made in order to get the best match to the experimental data, which include using relatively lenient convergence tolerances, reducing the size of load step increment, and modifying model parameters. Over the course of the analyses, it has been found that the

model tends to predict spurious stress-strain response when the contact changes from open to interlock state.

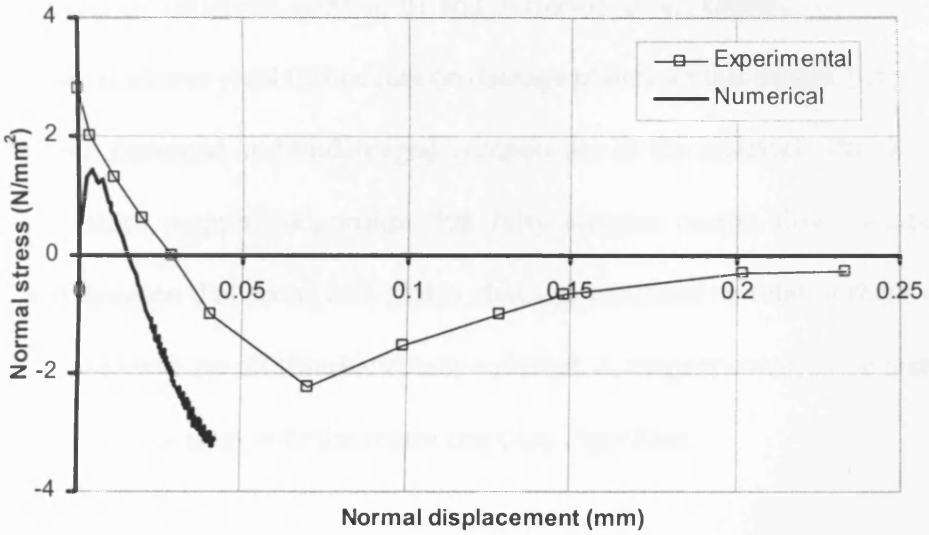

Figure 7.37. Normal stress-displacement response

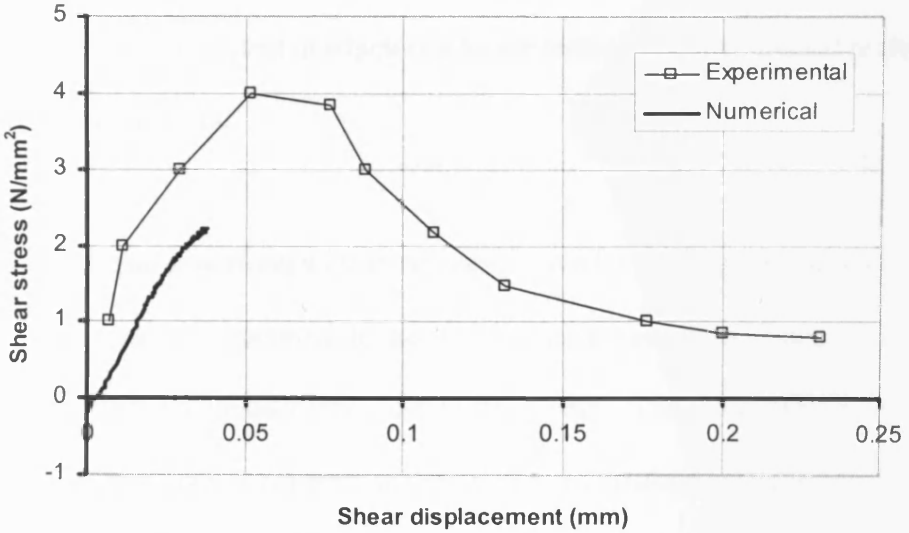

Figure 7.38. Shear stress-displacement response

7.8 Conclusions

The proposed contact model with embedded local plasticity has been developed based on the Craft model of Jefferson (2003a, b) and Jefferson *et al.* (2004). The idea was to capture any local plastic yield that occurs on damage planes. In this model, plasticity was applied to both damaged and undamaged components of the material. The model also employed a return mapping algorithm that fully couples plastic flow to directional damage, and ensures that local and global damage constitutive relationships and the plastic yield condition are all simultaneously satisfied. A tangent constitutive matrix was derived which is consistent with the return mapping algorithm.

The model had been implemented in a constitutive driver program as well as a finite element program, from which numerical results obtained were compared with a range of experimental data, which includes data from uniaxial tension tests with or without unloading-reloading cycles, test in which cracks are formed and then loaded in shear, and multiaxial compression test.

The model was found to perform well at the constitutive level, compared to finite element analysis on structural test specimen. In the single point stress-strain examples, the model simulated reasonably well most of the loading stress paths. The effect of using embedded planes with local plasticity is apparent in the analysis of uniaxial cyclic test by Reinhardt (1984), in which permanent strains were predicted upon unloading and gradually increased as the unloading-reloading process continued.

The proposed model was also found to be able to simulate well the behaviour of aggregate interlock and crack closure. In the analysis of normal-shear test by Walraven and Reinhardt (1981), the interaction between both normal and shear component is apparent. The sudden build up of shear stiffness was simulated at the early stage of loading. The shear strength continued to increase with displacement, up until a point, after which it remained unchanged with further displacement. At this later stage of loading, the crack was wide opened such that no further contact is possible with increasing shear displacement. In the compression test analyses, the frictional hardening plasticity component of the model was found to give adequate prediction on the compressive behaviour of concrete.

In the finite element analyses, the model experienced difficulties in achieving overall convergence. Relatively high convergence tolerances were needed in order to obtain complete simulations. Nevertheless, the model was able to represent the 2D direct fracture test and 3D cylindrical notched fracture beam reasonably well throughout the response range.

The fact that only one crack plane is allowed to form at each integration point is thought to have hindered the ability of the model to solve problems in which multiaxial loadings are applied, for example in the single notch beam example. In order to overcome this problem, an approach was proposed in which the direction of any new crack plane formed is not fixed, but is free to rotate until later stages when the damage strain has reached a certain limit. This approach was inspired by the rotating crack model of Rots (1988).

The proposed model was found to be less robust than the other contact models. Complete simulation of finite element example is difficult to achieve without the use of relatively lenient convergence tolerances, although much of the increments converged to a much tighter tolerance. Convergence problems have made it difficult to properly assess the performance of the proposed model in some complex finite element examples. Further work would involve the implementation of the model in a non-local format, which hopefully would allow the full benefits of the model to be realised.

References

Addessi, D., Marfia, S. and Sacco, E. (2002). "A plastic nonlocal damage model". *Computer Methods in Applied Mechanics and Engineering*, **191**(13-14), pp. 1291-1310.

Ali, M. A. and White, R. N. (1999). "Enhanced contact model for shear friction of normal and high-strength concrete". *ACI Structural Journal*, **96**(3), pp. 348-360.

Arrea, M. and Ingraffea, A. R. (1982). Mixed-mode crack propagation in mortar and concrete. Report No. 81-13, Department of Structural Engineering, Cornell University.

ASCE (1982). Task Committee on Finite Element Analysis of Reinforced Concrete Structures. Finite element analysis of reinforced concrete structures, ASCE.

Askes, H. and Metrikine, A. V. (2005). "Higher-order continua derived from discrete media: continualisation aspects and boundary conditions". *International Journal of Solids and Structures*, **42**(1), pp. 187-202.

Babuška, I. and Melenk, J. M. (1997). "The Partition of unity method". *International Journal for Numerical Methods in Engineering*, **40**(4), pp. 727-758.

Batdorf, B. and Budianski, D. (1949). A Mathematical Theory of Plasticity Based on the Concept of Slip. NACA Tech, Note TN1871.

Bažant, Z. P. (1984). "Microplane Model for Strain Controlled Inelastic Behaviour". In Mechanics of Engineering Materials, Eds C. S. Desai and R.H. Gallagher, John Wiley, London, pp. 45-59.

Bažant, Z. P. and Caner, F. C. (2005a). "Microplane Model M5 with Kinematic and Static Constraints for Concrete Fracture and Anelasticity. I: Theory". *Journal of Engineering Mechanics*, **131**, pp. 31-40.

Bažant, Z. P. and Caner, F. C. (2005b). "Microplane Model M5 with Kinematic and Static Constraints for Concrete Fracture and Anelasticity. II: Computation". *Journal of Engineering Mechanics*, **131**, pp. 41-47.

Bažant, Z. P. and Gambarova, R.G. (1984). "Crack Shear in Concrete: Crack Band Micro-plane Model". *Journal of Engineering Mechanics*, ASCE, **110**, pp. 2015-2035.

Bažant, Z. P. and Lin, F. B. (1988). "Non-local Yield Limit Degradation". *International Journal for Numerical Methods in Engineering*, **26**, pp. 1805-1823.

Bažant, Z. P. and Oh, B. H. (1983). "Crack band theory for fracture of concrete". *Materials and Structures*, **16**, pp. 155-177.

Bažant, Z. P. and Oh, B. H. (1985) "Microplane Model for Progressive Fracture of Concrete and Rock". *Journal of Engineering Mechanics*, ASCE, **111**, pp. 559-582.

Bažant, Z. P. and Ožbolt, J. (1990). "Nonlocal microplane model for fracture, damage, and size effect in structures". *Journal of Engineering Mechanics*, **116**(11), pp. 2485-2505.

Bažant, Z. P. and Pijaudier-Cabot, G. (1988). "Nonlocal Continuum Damage, Localization Instabilities and Convergence". *Journal of Applied Mechanics*, ASME, **55**, pp. 287-293.

Bažant, Z. P. and Prat, P. C. (1988a). "Microplane Model for Brittle Plastic Material: I. Theory". *Journal of Engineering Mechanics*, ASCE, **114**(10), pp. 1672-1688.

Bažant, Z. P. and Prat, P. C. (1988b). "Microplane Model for Brittle Plastic Material: II. Verification". *Journal of Engineering Mechanics*, ASCE, **114**(10), pp. 1689-1702.

Bažant, Z. P., Adley, M. D., Carol, I., Jirásek, M., Akers, S. A., Rohani, B., Cargile, J. D. and Caner, F. C. (2000b). "Large-Strain Generalization of Microplane Model for Concrete and Application". *Journal of Engineering Mechanics*, **126**(9), pp. 971-980.

Bažant, Z. P., Belytschko, T. and Chang, T. P. (1984). "Continuum model for strain softening". *Journal of Structural Engineering*, ASCE, **110**, pp. 1666-1692.

Bažant, Z. P., Caner, F. C., Carol, I., Adley, M. D. and Akers, S. A. (2000a). "Microplane Model M4 for Concrete. I: Formulation with Work-Conjugate Deviatoric Stress". *Journal of Engineering Mechanics*, **126**(9), pp. 944-953.

Bažant, Z. P., Xiang, Y. Y. and Prat, P. C. (1996a). "Microplane model for concrete. I. Stress-strain boundaries and finite strain". *Journal of Engineering Mechanics*, ASCE, **122**(3), pp. 245-254.

Bažant, Z. P., Xiang, Y., Adley, M. D., Prat, P. C. and Akers, S. A. (1996b). "Microplane model for concrete. II. Data delocalization and verification". *Journal of Engineering Mechanics*, **122**(3), pp. 255–262.

Belytschko, T. and Black, T. (1999). "Elastic crack growth in finite elements with minimal remeshing". *International Journal for Numerical Methods in Engineering*, **45**(5), pp. 601-620.

Brencich, A. and Gambarotta, L. (2001). "Isotropic damage model with different tensile-compressive response for brittle materials". *International Journal of Solids and Structures*, **38**(34-35), pp. 5865-5892.

Bresler, B. and Scordelis, A. C. (1963). "Shear strength of reinforced concrete beams". *ACI Journal*, pp. 51-72.

Burlion, N., Gatuingt, F., Pijaudier-Cabot, G. and Daudeville, L. (2000). "Compaction and tensile damage in concrete: constitutive modelling and application to dynamics". *Computer Methods in Applied Mechanics and Engineering*, **183**(3-4), pp. 291-308.

Buyukozturk, O. (1977). "Non-linear Analysis of Reinforced Concrete Structures". *Computers and Structures*, **7**, pp. 149-156.

Carol, I., Jirásek, M. and Bažant, Z. P. (2001). "A thermodynamically consistent approach to microplane theory Part I. Free energy and consistent microplane stresses". *International Journal of Solids and Structures*, **38**(17), pp. 2921-2931.

Carol, I., Rizzi, E. and Willam, K. (1994). "A unified theory of elastic degradation and damage based on a loading surface". *International Journal of Solids and Structures*, **31**(20), pp. 2835.

Chen, A. C. T. and Chen, W. F. (1975). "Constitutive Relations for Concrete". *Journal of Engineering Mechanics*, ASCE, **101**, pp. 465-481.

Comi, C. and Perego, U. (2001). "Fracture energy based bi-dissipative damage model for concrete". *International Journal of Solids and Structures*, **38**(36-37), pp. 6427-6454.

Cope, D., Yazdani, S. and Ju, J. W. (2005). "A Method to Generate Damage Functions for Quasi-Brittle Solids". *Journal of Applied Mechanics*, ASME, **72**, pp. 553-557.

Crisfield, M. A. (1981). "A fast incremental/iterative solution procedure that handles snap-through". *Computers and Structures*, **13**, pp. 55-62.

Daux, C., Moes, N., Dolbow, J., Sukumar, N. and Belytschko, T. (2000). "Arbitrary branched and intersecting cracks with the extended finite element method". *International Journal for Numerical Methods in Engineering*, **48**, pp. 1741-1760.

de Borst, R. (1987). "Integration of Plasticity Equations for Singular Yield Functions". *Computers and Structures*, **26**(5), pp. 823-829.

de Borst, R. (2001). "Some recent issues in computational failure mechanics". *International Journal for Numerical Methods in Engineering*, **52**(1/2), pp. 63-96.

de Borst, R., Gutierrez, M. A., Wells, G. N., Remmers, J. J. C. and Askes, H. (2004). "Cohesive-zone models, higher-order continuum theories and reliability methods for computational failure analysis". *International Journal for Numerical Methods in Engineering*, **60**(1), pp. 289-316.

Divakar, M. P., Fafitis, A. and Shah, S. P. (1987). "Constitutive Model for Shear Transfer in Cracked Concrete". *Journal of Structural Engineering*, **113**(5), pp. 1046-1062.

Dolbow, J., Möes, N. and Belytschko, T. (2001). "An extended finite element method for modeling crack growth with frictional contact". *Computer Methods in Applied Mechanics and Engineering*, **190**(51-52), pp. 6825-6846.

Dragon, A., Halm, D. and Desoyer, T. (2000). "Anisotropic damage in quasi-brittle solids: modelling, computational issues and applications". *Computer Methods in Applied Mechanics and Engineering*, **183**(3-4), pp. 331-352.

Ekh, M., Menzel, A., Runesson, K. and Steinmann, P. (2003). "Anisotropic damage with the MCR effect coupled to plasticity". *International Journal of Engineering Science*, **41**(13-14), pp. 1535-1551.

Eringen, A. C. and Edelen, D. G. D. (1972). "On Nonlocal Elasticity". *International Journal of Engineering Science*, **10**, pp. 233-248.

Este, G. and Willam, K. (1994). "Fracture energy formulation for inelastic behavior of plain concrete". *Journal of Engineering Mechanics*, **120**(9), pp. 1983-2011.

Feenstra, P. H. and de Borst, R. (1996). "A composite plasticity model for concrete". *International Journal of Solids and Structures*, **33**(5), pp. 707-730.

Fenwick, R. C. and Paulay, T. (1968). "Mechanisms of Shear Resistance of Concrete Beams". *Journal of the Structural Division*, ASCE, **94**(10), pp. 2325-2350.

Fichant, S., La Borderie, C. and Pijaudier-Cabot, G. (1999). "Isotropic and Anisotropic Descriptions of Damage in Concrete Structures". *Mechanics of Cohesive Frictional Materials*, **4**(4), pp. 339-360.

Grassl, P., Lundgren, K. and Gylltoft, K. (2002). "Concrete in compression: a plasticity theory with a novel hardening law". *International Journal of Solids and Structures*, **39**(20), pp. 5205-5223.

Hansen, N. R. and Schreyer, H. L. (1995). "Damage Deactivation". *Journal of Applied Mechanics*, ASME, **62**(2), pp. 450-458.

Hansen, E., Willam, K. and Carol, I. (2001). A two-surface anisotropic damage/plasticity model for plain concrete. Fracture mechanics of Concrete Structures, Cachan, France, Balkema.

Hasegawa, T. (1995). "Enhanced micro-plane concrete model". In Proceedings of 2nd International Conference on Fracture of Concrete and Concrete Structures (FraMCoS-II), ed Wittmann, F. H., July, Zurich, pp. 857-870.

Hassanzadeh, M. (1991). "Behaviour of fracture process zones in concrete influenced by simultaneously applied normal and shear displacements". PhD Thesis, Lund Institute of Technology, Sweden.

Hee, S. C., Jefferson, A. D. and Bennett, T. (2004). "Embedded rough surfaces in a 3D constitutive model for concrete". In Proceedings of 5th International Conference on Fracture of Concrete and Concrete Structures (FraMCoS-V), Eds Li, V. C., Leung, C. K. Y., Willam, K. J. and Billington, S. L., Vail, Colorado, April 12-16, Evanston, Illinois, pp. 139-146.

Hoek, E. and Brown, E. T. (1980). "Empirical Strength Criterion for Rock Masses". *Journal of the Geotechnical Engineering Division*, ASCE, **106**(9), pp. 1013-1035.

Hordijk, D. A. (1991). Local Approach to Failure of Concrete. PhD Thesis, Delft University of Technology, The Netherlands.

Hsieh, S. S., Ting, E. C. and Chen, W. F. (1982). "A Plastic Fracture Model for Concrete". *International Journal of Solids and Structures*, **18**(3), pp. 181-197.

Imran, I. and Pantazopoulou, S. J. (2001). "Plasticity Model for Concrete under Triaxial Compression". *Journal of Engineering Mechanics*, **127**(3), pp. 281-290.

Jefferson, A. D. (1989). Finite Element Analysis of Composite Structures. PhD Thesis, Cardiff University, United Kingdom.

Jefferson, A. D. (1998). "Plastic-damage model for interfaces in cementitious materials". *Journal of Engineering Mechanics*, **124**(7), pp. 775-781.

Jefferson, A. D. (2002a). "Constitutive modelling of aggregate interlock in concrete. *International Journal for Numerical and Analytical Methods in Geomechanics*, **26**(5), pp. 515-535.

Jefferson, A. D. (2002b). "Tripartite cohesive crack model". *Journal of Engineering Mechanics*, ASCE, **128**(6), pp. 644-653.

Jefferson, A. D. (2003a). "Craft, a plastic-damage-contact model for concrete. I. Model theory and thermodynamic considerations". *International Journal of Solids and Structures,* **40**(22), pp. 5973-5999.

Jefferson, A. D. (2003b). "Craft, a plastic-damage-contact model for concrete. II. Model implementation with implicit return mapping algorithm and consistent tangent matrix". *International Journal of Solids and Structures,* **40**(22), pp. 6001-6002.

Jefferson, A. D. and Barr, B. I. G. (1995). Unified test procedure for evaluation the fracture characteristics of concrete. In Proceedings of 2nd International Conference on Fracture Mechanics of Concrete Structures (FraMCoS-II), ed Wittmann, F. H., Zurich.

Jefferson, A. D., Barr, B. I. G., Bennett, T. and Hee, S. C. (2004). "Three dimensional finite element simulations of fracture tests using the Craft concrete model". *Computers and Concrete*, **1**(3), pp. 261-284.

Jirásek, M. (1993). Modeling of Fracture and Damage in Quasi-brittle Materials. PhD Thesis, Northwestern University, Evanston, Illinois.

Jirásek, M. (2000). "Comparative study on finite elements with embedded discontinuities". *Computer Methods in Applied Mechanics and Engineering*, **188**(1-3), pp. 307-330.

Jirásek, M. and Belytschko, T. (2002). "Computational Resolution of Strong Discontinuities". In Proceedings of 5th World Congress on Computational Mechanics, Eds Mang, H. A., Rammerstorfer, F. G. and Eberhardsteiner, J., July 7-12, Vienna, Austria.

Jirásek, M. and Zimmerman, T. (2001a). "Embedded crack model. Part I. Basic formulation". *International Journal for Numerical Methods in Engineering*, **50**(6), pp. 1269-1290.

Jirásek, M. and Zimmerman, T. (2001b). "Embedded crack model. Part II. Combination with smeared cracks". *International Journal for Numerical Methods in Engineering*, **50**(6), pp. 1291-1305.

Johnson, W. and Mellor, P. B. (1978). Engineering Plasticity, Van Nostrand Reinhold.

Ju, J. W. (1989). "On energy-based coupled elastoplastic damage theories: constitutive modeling and computational aspects". *International Journal of Solids and Structures*, **25**(7), pp. 803-833.

Kachanov, M. (1980). "Continuum Model of Medium with Cracks". *Journal of Engineering Mechanics*, ASCE, **106**, pp. 1039-1051.

Kang, H. D. and Willam, K. J. (1999). "Localization Characteristics of Triaxial Concrete Model". *Journal of Engineering Mechanics*, 125(8), pp. 941-950.

Karihaloo, B. L. (1995). Fracture mechanics and structural concrete. Longman, New York.

Karnawat, S. and Yazdani, S. (2001). "Effects of Preloading on Brittle Solids". *Journal of Engineering Mechanics*, **127**(1), pp. 11-17.

Kotsovos, M. D. and Newman, J. B. (1979). "A mathematical description of the deformable behaviour of concrete under complex loading". *Magazine of Concrete Research*, **31**, pp. 77-90.

Krajcinovic, D. and Fonseka, G. U. (1981). "The Continuous Damage Theory of Brittle Metals". *Journal of Applied Mechanics*, ASME, **48**, pp. 809-824.

Kroplin, B. and Weihe, S. (1997). "Aspects of fracture induced anisotropy". In Proceedings of 5th International Conference on Computational Plasticity (COMPLAS5), Barcelona, pp. 255-279.

Kuhl, E., Steinmann, P. and Carol, I. (2001). "A thermodynamically consistent approach to microplane theory. Part II. Dissipation and inelastic constitutive modeling". *International Journal of Solids and Structures*, **38**(17), pp. 2933-2952.

Kupfer, H. B. and Gerstle, K. H. (1973). "Behaviour of Concrete under Biaxial Stresses". *Journal of Engineering Mechanics*, ASCE, **99**(4), pp. 852-866.

Kupfer, H. B., Hilsdorf, H. K. and Rusch, H. (1969) "Behaviour of Concrete under Biaxial Stresses". *ACI Journal*, **66**(8), pp. 656-666.

Labadi, Y. and Hannachi, N. E. (2005). "Numerical Simulation of Brittle Damage in Concrete Specimens". *Strength of Materials*, **37**(3), pp. 268-281.

Larsson, R. and Runesson, K. (1996). "Element-embedded localization band based on regularized displacement discontinuity". *Journal of Engineering Mechanics*, ASCE, **122**(5), pp. 402-411.

Lee, J. and Fenves, G. L. (1998). "Plastic-Damage Model for Cyclic Loading of Concrete Structures". *Journal of Engineering Mechanics*, **124**(8), pp. 892-900.

Lemaitre, J. (1992). A Course on Damage Mechanics. Springer Verlag.

Li, Q. and Ansari, F. (1999). "Mechanics of Damage and Constitutive Relationships for High-Strength Concrete in Triaxial Compression". *Journal of Engineering Mechanics*, **125**(1), pp. 1-10.

Lubliner, J., Oliver, J., Oller, S. and Onate, E. (1989). "A plastic-damage model for concrete". *International Journal of Solids and Structures*, **25**(3), pp. 299-326.

Luccioni, B. M. and Rougier, V. C. (2005). "A plastic damage approach for confined concrete". *Computers and Structures*, **83**(27), pp. 2238-2256.

Luccioni, B., Oller, S. and Danesi, R. (1996). "Coupled plastic-damaged model". *Computer Methods in Applied Mechanics and Engineering*, **129**(1-2), pp. 81-89.

LUSAS (2003). User reference manual, FEA Ltd.

Mazars, J. and Pijaudier-Cabot, G. (1989). "Continuum damage theory - application to concrete". *Journal of Engineering Mechanics*, **115**(2), pp. 345-365.

Menétrey, P. and Willam, K. J. (1995). "Triaxial Failure Criterion for Concrete and Its Generalization". *ACI Structural Journal*, **92**(3), pp. 311.

Meschke, G., Lackner, R. and Mang, H. A. (1998). "An anisotropic elastoplastic-damage model for plain concrete". *International Journal for Numerical Methods in Engineering*, **42**(4), pp. 703-727.

Möes, N., Dolbow, J. and Belytschko, T. (1999). "A Finite Element Method for Crack Growth without Remeshing". *International Journal for Numerical Methods in Engineering*, **46**(1), pp. 131-150.

Mosler, J. and Meschke, G. (2003). "3D modelling of strong discontinuities in elastoplastic solids: Fixed and rotating localization formulations". *International Journal for Numerical Methods in Engineering*, **57**(11), pp. 553-1576.

Ngo, D. and Scordelis, A. C. (1967). "Finite Element Analysis of Reinforced Beams". *ACI Journal*, **64**(3), pp. 152-163.

Nooru-Mohamed, M. B. (1992). Mixed-mode fracture of concrete: An experimental approach. PhD Thesis, Delft University. of Technology, Delft, The Netherlands.

Oliver, J., Cervera, M., Oller, S. and Lubliner, J. (1990). "Isotropic damage models and smeared crack analysis of concrete". Computer Aided Analysis and Design of Concrete Structures. Pinebridge Press. Swansea, England: pp. 945-957.

Oliver, J., Huespe, A. E., Samaniego, E. and Chaves, E. W. V. (2004). "Continuum approach to the numerical simulation of material failure in concrete". *International Journal for Numerical and Analytical Methods in Geomechanics*, **28**(7/8), pp. 609-632.

Ollivier, J. P. (1985). "A non destructive procedure to observe the microcracks of concrete by scanning electron-microscopy". *Cement and Concrete Research*, **15**(6), pp. 1055-1060.

Ortiz, M. (1985). "Constitutive Theory for The Inelastic Behavior of Concrete". *Mechanics of Materials*, **4**(1), pp. 67-93.

Ortiz, M. and Simo, J. C. (1986). "An Analysis of a New Class of Integration Algorithms for Elasto Plastic Constitutive Relations". *International Journal for Numerical Methods in Engineering*, **23**, pp. 353-366.

Ottosen, N. S. (1979). "Constitutive Model for Short Time Loading of Concrete". *Journal of Engineering Mechanics*, ASCE, **105**(1), pp. 127-141.

Owen, D. R. J. and Hinton, E. (1980). Finite Elements in Plasticity: Theory and Practice. Pineridge Press, Swansea.

Ožbolt, J. and Bažant, Z. P. (1992). "Microplane Model for Cyclic Triaxial Behaviour of Concrete". *Journal of Engineering Mechanics*, ASCE, **118**(7), pp. 1365-1386.

Ožbolt, J., Li, Y. and Kozar, I. (2001). "Microplane model for concrete with relaxed kinematic constraint". *International Journal of Solids and Structures*, **38**(16), pp. 2683-2711.

Park, H. and Kim, J. Y. (2005). "Plasticity model using multiple failure criteria for concrete in compression". *International Journal of Solids and Structures*, **42**(8), pp. 2303-2322.

Paulay, T. and Loeber P. J. (1974). "Shear transfer by aggregate interlock". In Shear in reinforced concrete, ACI Publication, SP-42, pp. 1-15.

Peerlings, R. H. J., de Borst, R., Brekelmans, W. A. M. and De Vree, J. H. P. (1996). "Gradient Enhanced Damage for Quasi-brittle Materials". *International Journal for Numerical Methods in Engineering*, **39**(19), pp. 3391-3403.

Petrangeli, M. and Ožbolt, J. (1996). "Smeared crack approaches - Material modeling". *Journal of Engineering Mechanics*, ASCE, **122**(6), pp. 545-554.

Petersson, P. (1981). Crack growth and development of failure zones in plain concrete and similar materials. Lund Institute of Technology, Sweden.

Pijaudier-Cabot, G. and Bažant, Z. P. (1987). "Nonlocal Damage Theory". *Journal of Engineering Mechanics*, ASCE, **113**, pp. 1512-1533.

Pivonka, P., Ožbolt, J., Lackner, R. and Mang, H. A. (2004). "Comparative studies of 3D-constitutive models for concrete: application to mixed-mode fracture". *International Journal for Numerical Methods in Engineering*, **60**(2), pp. 549-570.

Rashid, Y. R. (1968). Analysis of Prestressed Concrete Pressure Vessels. Nuclear Engineering and Design, **7**(4).

Reinhardt, H. W. (1984). "Fracture mechanics of an elastic softening material like concrete". Heron, **29**(2), Delft, The Netherlands, pp. 1-42.

Rots, J. G. (1988). Computational modelling of concrete fracture. PhD Thesis, Delft University, The Netherlands.

Rots, J. G. and de Borst, R. (1987). "Analysis of mixed-mode fracture in concrete". *Journal of Engineering Mechanics*, ASCE, **113**(11), pp. 1739-1758.

Saenz, L. P. (1964). Discussion of "Equation for the stress-strain curve for concrete" by Desai and Krishnan, *ACI Journal*, **61**(9), pp. 1229-1235.

Salari, M. R., Saeb, S., Willam, K. J., Patchet, S. J. and Carrasco, R. C. (2004). "A coupled elastoplastic damage model for geomaterials". *Computer Methods in Applied Mechanics and Engineering*, **193**(27-29), pp. 2625-2643.

Schreyer, H. L. and Neilsen, M. K. (1996). "Analytical and Numerical Tests for Loss of Material Stability". *International Journal for Numerical Methods in Engineering*, **39**(10), pp. 1721-1736.

Sfer, D., Carol, I., Gettu, R. and Etse, G. (2002). "Study of the Behavior of Concrete under Triaxial Compression". *Journal of Engineering Mechanics*, **128**(2), pp. 156-163.

Shen, X., Yang, L. and Zhu, F. (2004). "A Plasticity-based Damage Model for Concrete". *Advances in Structural Engineering*, **7**(5), pp. 461-467.

Simo, J. C. and Hughes, T. J. R. (1998). Computational Inelasticity. Springer-Velag, New York.

Simo, J. C. and Ju, J. W. (1987). "Relative displacement and stress based continuum damage models—I Formulation". *International Journal of Solids and Structures*, **23**(7), pp. 821–840.

Simo, J. C. and Taylor R. L. (1986). "A return mapping algorithm for plane stress elastoplasticity". *International Journal for Numerical Methods in Engineering*, **22**, pp. 649-670.

Simo, J. C., Oliver, J. and Armero, F. (1993). "An analysis of strong discontinuities induced by strain-softening in rate-independent inelastic solids". *Computational Mechanics*, **12**, pp. 277-296.

Simone, A., Askes, H. and Sluys, L. J. (2004). "Incorrect initiation and propagation of failure in non-local and gradient-enhanced media". *International Journal of Solids and Structures*, **41**(2), pp. 351-363.

Sluys, L. J. and Berends, A. H. (1998). "Discontinuous failure analysis for mode-I and mode-II localization problems". *International Journal of Solids and Structures*, **35**(31/32), pp. 4257-4274.

Stevens, D. J. and Liu, D. J. (1992). "Strain-based Constitutive Model with Mixed Evolution Rules for Concrete". *Journal of Engineering Mechanics*, ASCE, **118**(6), pp. 1184-1200.

Sukumar, N., Möes, N., Moran, B. and Belytschko, T. (2000). "Extended finite element method for three-dimensional crack modelling". *International Journal for Numerical Methods in Engineering*, **48**(11), pp. 1549-1570.

Tao, X. and Phillips, D. V. (2005). "A simplified isotropic damage model for concrete under bi-axial stress states". *Cement and Concrete Composites*, **27**(6), pp. 716-726.

Taylor, G. I. (1938). "The Mechanisms of Plastic Deformation of Crystals". In Proceedings of the Royal Society, **145**, pp. 362-404.

Thionnet, A. and Renard, J. (1999). "Modelling unilateral damage effect in strongly anisotropic materials by the introduction of the loading mode in damage mechanics". *International Journal of Solids and Structures*, **36**(28), pp. 4269-4288.

van Mier, J. G. M. (1997). Fracture Process of Concrete. CRC Press, Florida.

Vermeer, P. A. and de Borst, R. (1984). Non-Associated Plasticity for Soils, Concrete and Rock. Heron, **29**(3), Delft, The Netherlands.

Walraven, J. C. and Reinhardt, H. W. (1981). Theory and experiments on the mechanical behaviour of cracks in plain and reinforced concrete subjected to shear loading. Heron, **26**(1A), Delft, The Netherlands.

Wells, G. N. and Sluys, L. J. (2001). "A new method for modelling cohesive cracks using finite elements". *International Journal for Numerical Methods in Engineering*, **50**(12), pp. 2667-2682.

Willam, K. J., Pramono, E. and Sture, S. (1987). "Fundamental issues of smeared crack models". In Proceedings of International Conference on Fracture of Concrete and Rock, SEM/RILEM, Eds Shah, S. P. and Swartz, S. E., pp. 142-153.

William, K. J. and Warnke, E. P. (1974). Constitutive Model for Triaxial Behaviour of Concrete. In Proceedings of International Association for Bridges and Structural Engineering, Colloquium on Concrete Structures Subjected to Triaxial Stresses, 19, Bergamo, Italy.

Yazdani, S. and Schreyer, H. L. (1990). "Combined plasticity and damage mechanics model for plain concrete". *Journal of Engineering Mechanics*, **116**(7), pp. 1435-1450.

Yazdani, S., Cope, D. and Very, K. (2002). "Requirements on Damage Functions". *Journal of Engineering Mechanics*, **128**(1), pp. 126-129.

APPENDICES

Appendix I Verification of consistent algorithm (EPLPC model)

Appendix II Derivation of material parameters

Embedded Planes with Local Plasticity Contact Model (EPLPC)

Material parameters

ORIGIN := 1

$E := 40000$	N/mm²	Young's modulus	
$\upsilon := 0.15$		Poisson's ratio	
$f_c := 40$	N/mm²	Compressive strength	
$f_t := 2.9$	N/mm²	Tensile strength	
$\varepsilon_c := 0.0022$		Strain at peak uniaxial compressive strength > fc/E	
$\varepsilon_0 := 0.0027$		Strain at end of softening curve	
$m_{hi} := 0.5$		Factor for end of first section of shear contact function	
$m_{ful} := 10$		Factor for shear contact limiting strain	
$Z_0 := 0.6$		Initial position of yield function (0Z<=1)	
$\Psi := -0.1$		Dilatancy factor	
$tol := \frac{f_t}{1000}$		Yield function convergence tolerance	
$\alpha_p := \frac{\pi}{2.9}$	$\alpha_p = 1.083308$	POD formation angle tolerance	$\alpha_p \frac{180}{\pi} = 62.068966$ degrees

Computed material parameters

$$E_{ef} := E\frac{1-\upsilon}{(1+\upsilon)\cdot(1-2\cdot\upsilon)}$$

$G := \frac{E}{2\cdot(1+\upsilon)}$ $G = 1.73913 \times 10^{4}$ Shear modulus

Smooth tensile softening curve parameters

$a_t := 1$		Proportion of peak tensile strength at which damage starts
$\varepsilon_{ti} := \frac{a_t \cdot f_t}{E_{ef}}$	$\varepsilon_{ti} = 6.866176 \times 10^{-5}$	Strain at first damage
$f_{ti} := a_t \cdot f_t$	$f_{ti} = 2.9$	First damage stress
$\varepsilon_t := \frac{f_t}{E}$	$\varepsilon_t = 7.25 \times 10^{-5}$	Elastic strain at peak uniaxial stress
$e_{beg} := \varepsilon_{ti} \cdot 1.1$	$e_{beg} = 7.552794 \times 10^{-5}$	Relative normal displacement at start of contact loss in interlock state
$\varepsilon_0 := if(\varepsilon_0 < 26\cdot\varepsilon_{ti}, 26\cdot\varepsilon_{ti}, \varepsilon_0)$	$\varepsilon_0 = 2.7 \times 10^{-3}$	Put lower limit on ε0

$e_{ful} := m_{ful} \cdot \varepsilon_0$ $e_{ful} = 0.027$ Strain beyond which contact is minimum

$e_{hi} := m_{hi} \cdot \varepsilon_0$ $e_{hi} = 1.35 \times 10^{-3}$ Strain at end of 1st section of shear contact function

$rat_\varepsilon := \frac{\varepsilon_0 - \varepsilon_{ti}}{\varepsilon_{ti}}$ $rat_\varepsilon = 38.323196$ Limiting strain ratios

$a_k := \frac{1.3}{a_t}$ $a_k = 1.3$ Factor governing where peak strain occurs relative to ε_{tii}

$c_1 := 5$ Primary softening curve factor

$\eta_k := \frac{(a_k - 1)}{rat_\varepsilon}$ $\eta_k = 7.828157 \times 10^{-3}$ Relative strain at peak of tensile curve

$q_c := \frac{rat_\varepsilon}{c_1} + 1$ $q_c = 8.664639$

$x_k := e^{-c_1 \cdot \eta_k}$ $x_k = 0.961615$

Approximate function for the factor m. Note this must change if a_k is changed

$d_m := 1.005$ $z := \begin{pmatrix} 0.223098944982796 \\ -67.0625617052971 \\ 66.4302094339053 \end{pmatrix}$ $m := z_1 + z_2 \cdot rat_\varepsilon + z_3 \cdot rat_\varepsilon^{d_m}$

$p := 5$

Final constants for continuous softening curve

$c_m := \frac{\frac{1}{a_t \cdot x_k} - 1 - \frac{q_c}{m} \cdot \left(1 - x_k^{\,m}\right)}{1 - x_k^{\,p \cdot m} - p + p \cdot x_k^{\,m}}$ $c_m = 0.093796$

$b_m := \frac{q_c}{m} - p \cdot c_m$ $b_m = -0.089381$ $a_m := 1 + b_m + c_m$ $a_m = 1.004414$

$c_{t1} := c_1$ $c_{t2} := m \cdot c_{t1}$ $c_{t2} = 114.129645$ $c_{t3} := m \cdot p \cdot c_{t1}$ $c_{t3} = 570.648223$

Smooth hardening curve parameters

$c_{c2} := 5$ Constant governing initial platic slope

$c_{c1} := \frac{c_{c2} \cdot e^{-c_{c2}}}{1 - e^{-c_{c2}}}$ $c_{c1} = 0.033918274531521$ Compute other constant to ensure correct peak

$a_c := e^{-c_{c1} \cdot \left(1 - e^{-c_{c2}}\right)}$ $a_c = 0.960137261529619$ Further hardening curve parameter

$\kappa_p := f_c \cdot \left(0.72 \cdot \varepsilon_c - \frac{f_c}{2 \cdot E}\right)$ $\kappa_p = 0.04336$ Plastic parameter limit, from integrating Saenz's equation

Yield and damage function shape parameters

$r_\sigma := 1.25$ — cohesion to tensile strength ratio

$r_\zeta := \frac{E}{G} \cdot r_\sigma$ $\quad r_\zeta = 2.875$ — γ to εt ratio

$\mu_\sigma := 0.8$ — Residual friction factor

$\mu_\varepsilon := \mu_\sigma \frac{E}{G}$ $\quad \mu_\varepsilon = 1.84$ — Equivalent friction factor in strain terms

$b_c := 1.15$ — Biaxial strength/uniaxial ratio

$\rho := \frac{1}{\sqrt{2}}$ — eccentricity parameter

$\alpha := \frac{b_c - 1}{2 \cdot b_c - 1}$ $\quad \alpha = 0.115385$ — α constant from Lubliner

$\gamma := 3\frac{(1-\rho)}{2 \cdot \rho - 1}$ $\quad \gamma = 2.12132$ — γ constant from Lubliner

Global and local Elastic D-matrices and Identity and null matrices

$\alpha 1 := \frac{\upsilon}{1-\upsilon}$ $\qquad \alpha 2 := \frac{1-2\cdot\upsilon}{2\cdot(1-\upsilon)}$

$$D_{el} := \left[E\frac{1-\upsilon}{(1+\upsilon)\cdot(1-2\cdot\upsilon)}\right]\cdot\begin{pmatrix} 1 & \alpha 1 & \alpha 1 & 0 & 0 & 0 \\ \alpha 1 & 1 & \alpha 1 & 0 & 0 & 0 \\ \alpha 1 & \alpha 1 & 1 & 0 & 0 & 0 \\ 0 & 0 & 0 & \alpha 2 & 0 & 0 \\ 0 & 0 & 0 & 0 & \alpha 2 & 0 \\ 0 & 0 & 0 & 0 & 0 & \alpha 2 \end{pmatrix}$$

$$D_{e3x3} := E\frac{1-\upsilon}{(1+\upsilon)\cdot(1-2\cdot\upsilon)}\cdot\begin{pmatrix} 1 & \alpha 1 & \alpha 1 \\ \alpha 1 & 1 & \alpha 1 \\ \alpha 1 & \alpha 1 & 1 \end{pmatrix}$$

$$D_L := \begin{pmatrix} E_{ef} & 0 & 0 \\ 0 & G & 0 \\ 0 & 0 & G \end{pmatrix}$$

$$C_L := \begin{pmatrix} \frac{1}{E_{ef}} & 0 & 0 \\ 0 & \frac{1}{G} & 0 \\ 0 & 0 & \frac{1}{G} \end{pmatrix}$$

$$I_6 := \begin{pmatrix} 1 & 0 & 0 & 0 & 0 & 0 \\ 0 & 1 & 0 & 0 & 0 & 0 \\ 0 & 0 & 1 & 0 & 0 & 0 \\ 0 & 0 & 0 & 1 & 0 & 0 \\ 0 & 0 & 0 & 0 & 1 & 0 \\ 0 & 0 & 0 & 0 & 0 & 1 \end{pmatrix}$$

$$I_3 := \begin{pmatrix} 1 & 0 & 0 \\ 0 & 1 & 0 \\ 0 & 0 & 1 \end{pmatrix}$$

$$I_{nul} := \begin{pmatrix} 0 & 0 & 0 \\ 0 & 0 & 0 \\ 0 & 0 & 0 \end{pmatrix}$$

$$Nul6x6 := \begin{pmatrix} 0 & 0 & 0 & 0 & 0 & 0 \\ 0 & 0 & 0 & 0 & 0 & 0 \\ 0 & 0 & 0 & 0 & 0 & 0 \\ 0 & 0 & 0 & 0 & 0 & 0 \\ 0 & 0 & 0 & 0 & 0 & 0 \\ 0 & 0 & 0 & 0 & 0 & 0 \end{pmatrix}$$

$\zeta := \varepsilon_{ti} \cdot 0.9999999999999$ — Initialise the damage parameter

Closure and interlock functions

$m_g := 0.45$

$\phi_{cl}(e) := e_1 + m_g\left[\sqrt{(e_2)^2 + (e_3)^2}\right]$

Closure function ϕ>0 open, ϕ<0 closed

$$\phi grad_{cl}(e) := \begin{bmatrix} 1 \\ \left[m_g \cdot e_2\left[(e_2)^2 + (e_3)^2\right]^{-0.5}\right] \\ \left[m_g \cdot e_3\left[(e_2)^2 + (e_3)^2\right]^{-0.5}\right] \end{bmatrix}$$

Gradient of closure function

$\phi_{inter}(e) := m_g e_1 - \sqrt{(e_2)^2 + (e_3)^2}$

Interlock function ϕ>0 open, ϕ<0 interlock

$$\phi grad(e) := \begin{bmatrix} m_g \\ -\left[\dfrac{e_2}{\left[(e_2)^2 + (e_3)^2\right]^{0.5} + 10^{-25}}\right] \\ -\left[\dfrac{e_3}{\left[(e_2)^2 + (e_3)^2\right]^{0.5} + 10^{-25}}\right] \end{bmatrix}$$

Gradient of interlock function

$$n(e) := \frac{\phi grad(e)}{|\phi grad(e)|}$$

Unit gradient

$$g(e) := \frac{\phi_{inter}(e)}{1 + m_g^2} \cdot \phi grad(e)$$

$$d2\phi de(e) := \begin{bmatrix} 0 & 0 & 0 \\ 0 & \dfrac{-(e_3)^2}{\left[(e_2)^2 + (e_3)^2\right]^{1.5} + 10^{-25}} & \dfrac{e_2 \cdot e_3}{\left[(e_2)^2 + (e_3)^2\right]^{1.5} + 10^{-25}} \\ 0 & \dfrac{e_2 \cdot e_3}{\left[(e_2)^2 + (e_3)^2\right]^{1.5} + 10^{-25}} & \dfrac{-(e_2)^2}{\left[(e_2)^2 + (e_3)^2\right]^{1.5} + 10^{-25}} \end{bmatrix}$$

$$\Phi g(e) := \frac{1}{1 + m_g^2} \cdot \left(\phi grad(e) \cdot \phi grad(e)^T + \phi_{inter}(e) \cdot d2\phi de(e)\right)$$

Softening and contact functions

$$\zeta f(e) := \frac{e_1}{2}\left[1 + \left(\frac{\mu_\varepsilon}{r_\zeta}\right)^2\right] + \frac{1}{2 \cdot r_\zeta^2}\cdot\sqrt{\left(r_\zeta^2 - \mu_\varepsilon^2\right)^2 \cdot (e_1)^2 + 4 \cdot r_\zeta^2\left[(e_2)^2 + (e_3)^2\right]}$$

Equivalent damage strain

$$\phi(e,\zeta) := \frac{e_1}{2}\left[1 + \left(\frac{\mu_\varepsilon}{r_\zeta}\right)^2\right] + \frac{1}{2 \cdot r_\zeta^2}\cdot\sqrt{\left(r_\zeta^2 - \mu_\varepsilon^2\right)^2 \cdot (e_1)^2 + 4 \cdot r_\zeta^2\left[(e_2)^2 + (e_3)^2\right]} - \zeta$$

Damage surface

$$\phi_\sigma(s, f_s) := \frac{s_1}{2}\left[1 + \left(\frac{\mu_\sigma}{r_\sigma}\right)^2\right] + \frac{1}{2 \cdot r_\sigma^2}\cdot\sqrt{\left(r_\sigma^2 - \mu_\sigma^2\right)^2 \cdot (s_1)^2 + 4 \cdot r_\sigma^2\left[(s_2)^2 + (s_3)^2\right]} - f_s$$

Damage surface in stress space

$$d\phi de(e) := \begin{bmatrix} \frac{1}{2}\left[1 + \left(\frac{\mu_\varepsilon}{r_\zeta}\right)^2\right] + \frac{\left(r_\zeta^2 - \mu_\varepsilon^2\right)^2 \cdot (e_1)}{2 \cdot r_\zeta^2 \cdot \sqrt{\left(r_\zeta^2 - \mu_\varepsilon^2\right)^2 \cdot (e_1)^2 + 4 \cdot r_\zeta^2\left[(e_2)^2 + (e_3)^2\right]}} \\ \frac{2 \cdot (e_2)}{\sqrt{\left(r_\zeta^2 - \mu_\varepsilon^2\right)^2 \cdot (e_1)^2 + 4 \cdot r_\zeta^2\left[(e_2)^2 + (e_3)^2\right]}} \\ \frac{2 \cdot (e_3)}{\sqrt{\left(r_\zeta^2 - \mu_\varepsilon^2\right)^2 \cdot (e_1)^2 + 4 \cdot r_\zeta^2\left[(e_2)^2 + (e_3)^2\right]}} \end{bmatrix}$$

Damage gradient function

$$\gamma eqv(e,\zeta) := \sqrt{r_\zeta^2 \cdot \zeta^2 - \left(r_\zeta^2 + \mu_\varepsilon^2\right) \cdot \zeta \cdot e_1 + \mu_\varepsilon^2 \cdot (e_1)^2}$$

Shear strain check on surface

Emdedment damage and intersection functions

$$\begin{aligned} &e_{gn}(e, ee) := \\ &\quad e_{bg} \leftarrow e_{beg} \cdot 0.9999999999999 \\ &\quad e_g \leftarrow 0 \\ &\quad e_g \leftarrow e_1 \text{ if } (\phi_{inter}(ee) < 0) \cdot (\phi_{cl}(ee) > 0) \\ &\quad e_g \leftarrow e_{bg} \text{ if } (\phi_{cl}(ee) \le 0) \\ &\quad e_g \leftarrow e_{bg} \text{ if } e_g < e_{beg} \\ &\quad e_g \end{aligned}$$

Normal local strain intersection with interlock surface

$$de_{gn}(e) := \begin{pmatrix} 1 \\ 0 \\ 0 \end{pmatrix}$$

Gradient of normal embedment intersection

$$gbar(ee) := \begin{cases} gbar \leftarrow 0 \\ gbar \leftarrow \dfrac{-\phi_{inter}(ee)}{\sqrt{1 + m_g^{\,2}}} \text{ if } (\phi_{inter}(ee) < 0) \cdot (\phi_{cl}(ee) > 0) \\ gbar \leftarrow \sqrt{(ee_1)^2 + (ee_2)^2 + (ee_3)^2} \text{ if } (\phi_{cl}(ee) \le 0) \\ gbar \end{cases}$$

Contact function

$res\_ft := 0.03$ **Residual fracture of tensile strength i.e. don't let it quite decay to zero**

$a_p := 0.1$ **Control amount of damage**

$$h_c(\zeta, \kappa) := \begin{cases} r \leftarrow res\_ft \\ \eta \leftarrow \dfrac{(\zeta - \varepsilon_{ti})}{(\varepsilon_0 - \varepsilon_{ti})} \\ 1 \text{ if } \zeta < \varepsilon_{ti} \\ r\dfrac{\varepsilon_{ti}}{\zeta \cdot (1 - a_p) + \varepsilon_{ti} \cdot a_p} + (1 - r) \cdot \left[\dfrac{\varepsilon_{ti}}{\zeta \cdot (1 - a_p) + \varepsilon_{ti} \cdot a_p} \cdot e^{-c_{t1} \cdot \eta} \right] \cdot e^{-2\frac{\kappa}{\kappa_p}} \text{ otherwise} \end{cases}$$

$$dhd\zeta_c(\zeta, \kappa) := \begin{cases} r \leftarrow res\_ft \\ \eta \leftarrow \dfrac{(\zeta - \varepsilon_{ti})}{(\varepsilon_0 - \varepsilon_{ti})} \\ 0 \text{ if } \zeta < \varepsilon_{ti} \\ \left[\left[\dfrac{-r \cdot \varepsilon_{ti} \cdot (1 - a_p)}{[\zeta \cdot (1 - a_p) + \varepsilon_{ti} \cdot a_p]^2} \right] + (1 - r) \dfrac{\varepsilon_{ti}}{\zeta \cdot (1 - a_p) + \varepsilon_{ti} \cdot a_p} \cdot e^{-c_{t1} \cdot \eta} \left[\dfrac{-c_{t1}}{\varepsilon_0 - \varepsilon_{ti}} - \dfrac{(1 - a_p)}{\zeta \cdot (1 - a_p) + \varepsilon_{ti} \cdot a_p} \right] \cdot e^{-2\frac{\kappa}{\kappa_p}} \right] \text{ otherwise} \end{cases}$$

$$dhd\kappa_c(\zeta, \kappa) := \begin{cases} r \leftarrow res\_ft \\ \eta \leftarrow \dfrac{(\zeta - \varepsilon_{ti})}{(\varepsilon_0 - \varepsilon_{ti})} \\ 0 \text{ if } \zeta < \varepsilon_{ti} \\ (1 - r) \cdot \left[\dfrac{\varepsilon_{ti}}{\zeta \cdot (1 - a_p) + \varepsilon_{ti} \cdot a_p} \cdot e^{-c_{t1} \cdot \eta} \right] \dfrac{-2}{\kappa_p} \cdot e^{-2\frac{\kappa}{\kappa_p}} \text{ otherwise} \end{cases}$$

Relative fully debonded area function and derivatives

Smooth closure function

$c_g := 3$

$$H(e_g, g_b) := \begin{cases} e_g \leftarrow e_{beg} \text{ if } e_g \le e_{beg} \\ 1 - e^{-c_g \frac{g_b}{e_g + 2\cdot\varepsilon_{ti}}} \end{cases}$$

$$dHdg(e_g, g_b) := \begin{cases} e_g \leftarrow e_{beg} \text{ if } e_g \le e_{beg} \\ \frac{c_g}{e_g + 2\cdot\varepsilon_{ti}} \cdot e^{-c_g \frac{g_b}{e_g + 2\cdot\varepsilon_{ti}}} \end{cases}$$

$$dHdeg(e_g, g_b) := \begin{cases} dh \leftarrow 0 \text{ if } e_g < e_{beg} \\ dh \leftarrow \frac{-c_g \cdot g_b}{(e_g + 2\cdot\varepsilon_{ti})^2} \cdot e^{-c_g \frac{g_b}{e_g + 2\cdot\varepsilon_{ti}}} \text{ if } e_g \ge e_{beg} \\ dh \end{cases}$$

$\eta_h := 0.9 \qquad f_0 := 10 \qquad f_1 := 2$

$$h_f(\zeta, \kappa, e_g, g_b) := \begin{cases} h \leftarrow (1 - h_c(\zeta, \kappa)) \cdot H(e_g, g_b) \\ h_f \leftarrow h \\ \text{if } e_g \ge e_{beg} \\ \quad \eta 0 \leftarrow \frac{(e_g - e_{beg})}{e_{hi}} \\ \quad \eta 1 \leftarrow \frac{(e_g - e_{beg})}{e_{ful}} \\ \quad fac \leftarrow \frac{(1 - \eta_h) \cdot f_1 \cdot m_{hi}}{m_{ful} \cdot f_0} \\ \quad h_f \leftarrow \left[\eta_h \cdot e^{-f_0 \cdot (\eta 0)^2} + (1 - \eta_h) \cdot e^{-f_1 \cdot \eta 1} - fac \cdot e^{-f_0 \cdot \eta 0}\right] \frac{h}{1 - fac} \\ h_f \end{cases}$$

$$dh_{f\zeta}(\zeta, \kappa, e_g, g_b) := \begin{cases} dh \leftarrow -dhd\zeta_c(\zeta, \kappa) \cdot H(e_g, g_b) \\ dh_f \leftarrow dh \text{ if } e_g < e_{beg} \\ \text{if } e_g \ge e_{beg} \\ \quad \eta 0 \leftarrow \frac{(e_g - e_{beg})}{e_{hi}} \\ \quad \eta 1 \leftarrow \frac{(e_g - e_{beg})}{e_{ful}} \\ \quad fac \leftarrow \frac{(1 - \eta_h) \cdot f_1 \cdot m_{hi}}{m_{ful} \cdot f_0} \\ \quad dh_f \leftarrow \left[\eta_h \cdot e^{-f_0 \cdot (\eta 0)^2} + (1 - \eta_h) \cdot e^{-f_1 \cdot \eta 1} - fac \cdot e^{-f_0 \cdot \eta 0}\right] \frac{dh}{1 - fac} \\ dh_f \end{cases}$$

$$dh_{f\kappa}(\zeta, \kappa, e_g, g_b) := \begin{cases} dh \leftarrow -dhd\kappa_c(\zeta, \kappa) \cdot H(e_g, g_b) \\ dh_f \leftarrow dh \text{ if } e_g < e_{beg} \\ \text{if } e_g \ge e_{beg} \\ \quad \eta 0 \leftarrow \frac{(e_g - e_{beg})}{e_{hi}} \\ \quad \eta 1 \leftarrow \frac{(e_g - e_{beg})}{e_{ful}} \\ \quad fac \leftarrow \frac{(1 - \eta_h) \cdot f_1 \cdot m_{hi}}{m_{ful} \cdot f_0} \\ \quad dh_f \leftarrow \left[\eta_h \cdot e^{-f_0 \cdot (\eta 0)^2} + (1 - \eta_h) \cdot e^{-f_1 \cdot \eta 1} - fac \cdot e^{-f_0 \cdot \eta 0}\right] \frac{dh}{1 - fac} \\ dh_f \end{cases}$$

$$dh_{fg}(\zeta, \kappa, e_g, g_b) := \begin{cases} h \leftarrow (1 - h_c(\zeta, \kappa)) \\ h_f \leftarrow h \\ \text{if } e_g \ge e_{beg} \\ \quad \eta 0 \leftarrow \frac{(e_g - e_{beg})}{e_{hi}} \\ \quad \eta 1 \leftarrow \frac{(e_g - e_{beg})}{e_{ful}} \\ \quad fac \leftarrow \frac{(1 - \eta_h) \cdot f_1 \cdot m_{hi}}{m_{ful} \cdot f_0} \\ \quad h_f \leftarrow \left[\eta_h \cdot e^{-f_0 \cdot (\eta 0)^2} + (1 - \eta_h) \cdot e^{-f_1 \cdot \eta 1} - fac \cdot e^{-f_0 \cdot \eta 0}\right] \frac{h}{1 - fac} \\ h_f \cdot dHdg(e_g, g_b) \end{cases}$$

$$dhfeg(\zeta, \kappa, e_g, g_b) := \left| \begin{array}{l} h \leftarrow (1 - h_c(\zeta, \kappa)) \\ dh_f \leftarrow 0 \\ \text{if } e_g \geq e_{beg} \\ \quad \left| \begin{array}{l} \eta 0 \leftarrow \dfrac{(e_g - e_{beg})}{e_{hi}} \\ \eta 1 \leftarrow \dfrac{(e_g - e_{beg})}{e_{ful}} \\ fac \leftarrow \dfrac{(1 - r_h) \cdot f_1 \cdot m_{hi}}{m_{ful} \cdot f_0} \\ h_f \leftarrow \left[r_h \cdot e^{-f_0 \cdot (\eta 0)^2} + (1 - r_h) \cdot e^{-f_1 \cdot \eta 1} - fac \cdot e^{-f_0 \cdot \eta 0} \right] \dfrac{h}{fac} \\ dh_f \leftarrow \left[\dfrac{-2 \cdot f_0 \cdot \eta 0}{e_{hi}} \cdot r_h \cdot e^{-f_0 \cdot (\eta 0)^2} + \dfrac{-f_1}{e_{ful}} \cdot (1 - r_h) \cdot e^{-f_1 \cdot \eta 1} + \dfrac{fac \cdot f_0}{e_{hi}} \cdot e^{-f_0 \cdot \eta 0} \right] \dfrac{h}{1 - fac} \cdot H(e_g, g_b) \ldots \\ \quad + \left[r_h \cdot e^{-f_0 \cdot (\eta 0)^2} + (1 - r_h) \cdot e^{-f_1 \cdot \eta 1} - fac \cdot e^{-f_0 \cdot \eta 0} \right] \dfrac{h}{1 - fac} \cdot dH deg(e_g, g_b) \end{array} \right. \\ dh_f \end{array} \right.$$

Shear direction function

$np := 9$ $\quad ip := 1 .. np$ $\quad il := 1 .. 3$ **Assuming no more than 4 Planes of Degradtion**

Generate consistent shear directions

Set global axes to which local s axes is to be made normal (local being r,s,t)

$$nseq := \begin{pmatrix} 3 \\ 1 \\ 2 \end{pmatrix} \qquad ns_{ip} := 0 \qquad i7 := 1 .. 7 \qquad ns_{(i7-1) \cdot 3 + il} := nseq_{il}$$

Set global axes to which local s axes is to be made normal (local being r,s,t)

$$idx := \begin{pmatrix} 2 & 3 \\ 1 & 3 \\ 1 & 2 \end{pmatrix}$$

Component indices for normal vector (r) from which is created for a given ns axis

Function to generate local s axis

$$\text{sloc}(id, rv) := \left| \begin{array}{l} \text{denom} \leftarrow \sqrt{\left[rv\left(idx_{id,1}\right)\right]^2 + \left[rv\left(idx_{id,2}\right)\right]^2} \\ out_{id} \leftarrow 0 \\ idr \leftarrow id \\ \text{if } \text{denom} < 10^{-12} \\ \quad \left| \begin{array}{l} idr \leftarrow id + 1 \\ idr \leftarrow 1 \text{ if } idr > 3 \\ \text{denom} \leftarrow \sqrt{\left[rv\left(idx_{idr,1}\right)\right]^2 + \left[rv\left(idx_{idr,2}\right)\right]^2} \end{array} \right. \\ out\left(idx_{idr,1}\right) \leftarrow (-1)^{idr} \frac{rv\left(idx_{idr,2}\right)}{\text{denom}} \\ out\left(idx_{idr,2}\right) \leftarrow (-1)^{idr+1} \frac{rv\left(idx_{idr,1}\right)}{\text{denom}} \\ \begin{pmatrix} out_1 \\ out_2 \\ out_3 \end{pmatrix} \end{array} \right.$$

Invariants and principal stresses

$$I_1(\sigma) := \left(\sigma_1 + \sigma_2 + \sigma_3\right)$$

$$J_2(\sigma) := \frac{1}{6}\left[\left(\sigma_1 - \sigma_2\right)^2 + \left(\sigma_2 - \sigma_3\right)^2 + \left(\sigma_3 - \sigma_1\right)^2\right] + \left(\sigma_4\right)^2 + \left(\sigma_5\right)^2 + \left(\sigma_6\right)^2$$

$$sd(\sigma) := \left(\sigma_1 - \frac{I_1(\sigma)}{3} \quad \sigma_2 - \frac{I_1(\sigma)}{3} \quad \sigma_3 - \frac{I_1(\sigma)}{3} \quad \sigma_4 \quad \sigma_5 \quad \sigma_6\right)^T$$

$$J_3(\sigma) := \left| \begin{array}{l} \sigma d \leftarrow sd(\sigma) \\ \left[\sigma d_1 \cdot \sigma d_2 \cdot \sigma d_3 + 2 \cdot \left(\sigma d_4 \cdot \sigma d_5 \cdot \sigma d_6\right)\right] - \left(\sigma d_1 \cdot \sigma d_5 \cdot \sigma d_5 + \sigma d_2 \cdot \sigma d_6 \cdot \sigma d_6 + \sigma d_3 \cdot \sigma d_4 \cdot \sigma d_4\right) \end{array} \right.$$

$$\theta(\sigma) := \left| \begin{array}{l} fac \leftarrow \frac{\frac{3\sqrt{3}}{2} \cdot J_3(\sigma)}{J_2(\sigma)^{1.5}} \\ fac \leftarrow 1 \text{ if } fac \geq 1 \\ fac \leftarrow -1 \text{ if } fac \leq -1 \\ \frac{\text{acos}(fac)}{3} \end{array} \right.$$

$$pr1(\sigma) := \begin{bmatrix} \frac{2}{\sqrt{3}} \cdot \left(\sqrt{J_2(\sigma)}\right) \cdot \cos(\theta(\sigma)) + \frac{I_1(\sigma)}{3} \\ \frac{2}{\sqrt{3}} \cdot \left(\sqrt{J_2(\sigma)}\right) \cdot \cos\left(\theta(\sigma) - 2\frac{\pi}{3}\right) + \frac{I_1(\sigma)}{3} \\ \frac{2}{\sqrt{3}} \cdot \left(\sqrt{J_2(\sigma)}\right) \cdot \cos\left(\theta(\sigma) + 2\frac{\pi}{3}\right) + \frac{I_1(\sigma)}{3} \end{bmatrix}$$

Invariant gradients

$$dJ3(\sigma) := \left| \begin{array}{l} \sigma d \leftarrow sd(\sigma) \\ \begin{bmatrix} \left(\sigma d_2 \cdot \sigma d_3 - \sigma d_5 \cdot \sigma d_5\right) + \frac{J2(\sigma)}{3} \\ \left(\sigma d_1 \cdot \sigma d_3 - \sigma d_6 \cdot \sigma d_6\right) + \frac{J2(\sigma)}{3} \\ \left(\sigma d_1 \cdot \sigma d_2 - \sigma d_4 \cdot \sigma d_4\right) + \frac{J2(\sigma)}{3} \\ 2 \cdot \left(\sigma d_5 \cdot \sigma d_6 - \sigma d_3 \cdot \sigma d_4\right) \\ 2 \cdot \left(\sigma d_4 \cdot \sigma d_6 - \sigma d_1 \cdot \sigma d_5\right) \\ 2 \cdot \left(\sigma d_4 \cdot \sigma d_5 - \sigma d_2 \cdot \sigma d_6\right) \end{bmatrix} \end{array} \right.$$

$$da2d\sigma := \frac{1}{3} \cdot \begin{pmatrix} 2 & -1 & -1 & 0 & 0 & 0 \\ -1 & 2 & -1 & 0 & 0 & 0 \\ -1 & -1 & 2 & 0 & 0 & 0 \\ 0 & 0 & 0 & 6 & 0 & 0 \\ 0 & 0 & 0 & 0 & 6 & 0 \\ 0 & 0 & 0 & 0 & 0 & 6 \end{pmatrix}$$

$$dI1 := (1 \ 1 \ 1 \ 0 \ 0 \ 0)^T$$

$$dJ2(\sigma) := \left| \begin{array}{l} \sigma d \leftarrow sd(\sigma) \\ \left(\sigma d_1 \ \sigma d_2 \ \sigma d_3 \ 2 \cdot \sigma d_4 \ 2 \cdot \sigma d_5 \ 2 \cdot \sigma d_6\right)^T \end{array} \right.$$

$$dcos3T(\sigma) := \left(1.5 \frac{\sqrt{3}}{J2(\sigma)^{\frac{3}{2}}} \right) \cdot \left[dJ3(\sigma) - \left(1.5 \frac{J3(\sigma)}{J2(\sigma)} \right) \cdot dJ2(\sigma) \right]$$

$$d\theta(\sigma) := \frac{1}{3 \cdot \sin(3 \cdot \theta(\sigma))} \cdot dcos3T(\sigma)$$

$$da3d\sigma(\sigma) := \left| \begin{array}{l} \sigma d \leftarrow sd(\sigma) \\ \frac{2}{3} \cdot \begin{pmatrix} \sigma d_1 & \sigma d_3 & \sigma d_2 & \sigma d_4 & -2 \cdot \sigma d_5 & \sigma d_6 \\ \sigma d_3 & \sigma d_2 & \sigma d_1 & \sigma d_4 & \sigma d_5 & -2 \cdot \sigma d_6 \\ \sigma d_2 & \sigma d_1 & \sigma d_3 & -2 \cdot \sigma d_4 & \sigma d_5 & \sigma d_6 \\ \sigma d_4 & \sigma d_4 & -2 \cdot \sigma d_4 & -3 \cdot \sigma d_3 & 3 \cdot \sigma d_6 & 3 \cdot \sigma d_5 \\ -2 \cdot \sigma d_5 & \sigma d_5 & \sigma d_5 & 3 \cdot \sigma d_6 & -3 \cdot \sigma d_1 & 3 \cdot \sigma d_4 \\ \sigma d_6 & -2 \cdot \sigma d_6 & \sigma d_6 & 3 \cdot \sigma d_5 & 3 \cdot \sigma d_4 & -3 \cdot \sigma d_2 \end{pmatrix} \end{array} \right.$$

Functions in Principal stress gradient functions which depend on Lode angle. Ip =1, 2 or 3 for principal stre

$$A\theta(\theta, Ip) := \left| \begin{array}{l} A \leftarrow \cos(\theta) \ \text{ if } Ip = 1 \\ A \leftarrow 0.5\left(-\cos(\theta) + \sqrt{3} \cdot \sin(\theta)\right) \ \text{ if } Ip = 2 \\ A \leftarrow -0.5\left(\cos(\theta) + \sqrt{3} \cdot \sin(\theta)\right) \ \text{ if } Ip = 3 \\ A \end{array} \right.$$

$$dA\theta(\theta, Ip) := \left| \begin{array}{l} dA \leftarrow -\sin(\theta) \ \text{ if } Ip = 1 \\ dA \leftarrow 0.5\left(\sin(\theta) + \sqrt{3} \cdot \cos(\theta)\right) \ \text{ if } Ip = 2 \\ dA \leftarrow 0.5\left(\sin(\theta) - \sqrt{3} \cdot \cos(\theta)\right) \ \text{ if } Ip = 3 \\ dA \end{array} \right.$$

$$d2As3(\theta, Ip) := \left| \begin{array}{l} dAs3 \leftarrow \frac{-\cos(\theta)}{\sin(3 \cdot \theta)} + \frac{3 \cdot \sin(\theta) \cdot \cos(3 \cdot \theta)}{\sin(3 \cdot \theta)^2} \ \text{ if } Ip = 1 \\ dAs3 \leftarrow 0.5 \cdot \left[\frac{\cos(\theta) - \sqrt{3} \cdot \sin(\theta)}{\sin(3 \cdot \theta)} - \frac{3 \cdot \left(\sin(\theta) + \sqrt{3} \cdot \cos(\theta)\right) \cdot \cos(3 \cdot \theta)}{\sin(3 \cdot \theta)^2} \right] \ \text{ if } Ip = 2 \\ dAs3 \leftarrow 0.5 \cdot \left[\frac{\cos(\theta) + \sqrt{3} \cdot \sin(\theta)}{\sin(3 \cdot \theta)} - \frac{3 \cdot \left(\sin(\theta) - \sqrt{3} \cdot \cos(\theta)\right) \cdot \cos(3 \cdot \theta)}{\sin(3 \cdot \theta)^2} \right] \ \text{ if } Ip = 3 \\ dAs3 \end{array} \right.$$

Combination of Willam-Warnke withLubliner compressive yield surface $x=\cos\theta$

$\rho t := \sqrt{3} + 2\frac{\gamma}{\sqrt{3}}$ $\rho c := \sqrt{3} + \frac{\gamma}{\sqrt{3}}$ $\rho t = 4.181541$ $\rho c = 2.956796$ $\eta := \rho$ $\eta = 0.707107$

$a := 1 - \eta^2$ $b := 2\cdot\eta - 1$ $d := 5\cdot\eta^2 - 4\cdot\eta$

$$rx(x) := \frac{4\cdot a\cdot x^2 + b^2}{2\cdot a\cdot x + b\sqrt{4\cdot a\cdot x^2 + d}}$$

$$drdx(x) := \frac{\left(8\cdot a^2\cdot x^2 - 2\cdot a\cdot b^2\right)\sqrt{4\cdot a\cdot x^2 + d} + 8\cdot a\cdot b\cdot x\cdot\left(4\cdot a\cdot x^2 + d\right) - 16\cdot a^2\cdot b\cdot x^3 - 4\cdot a\cdot b^3\cdot x}{\sqrt{4\cdot a\cdot x^2 + d}\cdot\left(2\cdot a\cdot x + b\sqrt{4\cdot a\cdot x^2 + d}\right)^2}$$

$$\pi 1(x) := \left(8\cdot a^2\cdot x^2 - 2\cdot a\cdot b^2\right)\cdot 0.5\cdot\left(4\cdot a\cdot x^2 + d\right)^{-0.5}\cdot 8\cdot a\cdot x + \left(4\cdot a\cdot x^2 + d\right)^{0.5}\cdot 16\cdot a^2\cdot x$$

$$\pi 2(x) := 8\cdot a\cdot b\cdot x\cdot 8\cdot a\cdot x + \left(4\cdot a\cdot x^2 + d\right)\cdot 8\cdot a\cdot b - 48\cdot a^2\cdot b\cdot x^2 - 4\cdot a\cdot b^3$$

$$\pi 3(x) := \left(4\cdot a\cdot x^2 + d\right)^{0.5}\cdot 2\left[2\cdot a\cdot x + b\cdot\left(4\cdot a\cdot x^2 + d\right)^{0.5}\right]\left[2\cdot a + b\cdot 0.5\cdot\left(4\cdot a\cdot x^2 + d\right)^{-0.5}\cdot 8\cdot a\cdot x\right]$$

$$\pi 4(x) := \left[2\cdot a\cdot x + b\cdot\left(4\cdot a\cdot x^2 + d\right)^{0.5}\right]^2\cdot 0.5\cdot\left(4\cdot a\cdot x^2 + d\right)^{-0.5}\cdot 8\cdot a\cdot x$$

$$d2rdx2(x) := \frac{\left(4\cdot a\cdot x^2 + d\right)^{0.5}\left[2\cdot a\cdot x + b\cdot\left(4\cdot a\cdot x^2 + d\right)^{0.5}\right]^2\cdot(\pi 1(x) + \pi 2(x)) - \left[\left(8\cdot a^2\cdot x^2 - 2\cdot a\cdot b^2\right)\cdot\left(4\cdot a\cdot x^2 + d\right)^{0.5} + 8\cdot a\cdot b\cdot x\cdot\left(4\cdot a\cdot x^2 + d\right) - 16\cdot a^2\cdot b\cdot x^3 - 4\cdot a\cdot b^3\cdot x\right]\cdot(\pi 3(x) + \pi 4(x))}{\left(4\cdot a\cdot x^2 + d\right)\left[2\cdot a\cdot x + b\cdot\left(4\cdot a\cdot x^2 + d\right)^{0.5}\right]^4}$$

Derivatives of Ar(θ)

$Ar(\theta) := \rho c\cdot rx(\cos(\theta))$ $dArd\theta(\theta) := -\sin(\theta)\cdot drdx(\cos(\theta))\cdot\rho c$ $d2Ard\theta(\theta) := \left(-\cos(\theta)\cdot drdx(\cos(\theta)) + \sin(\theta)^2\cdot d2rdx2(\cos(\theta))\right)\cdot\rho c$

Yield function and plastic potential

$$F(\sigma, Z) := \left[\sqrt{J_2(\sigma)}\cdot Ar(\theta(\sigma)) + \left(\alpha + \frac{\gamma}{3}\right)\cdot I_1(\sigma)\cdot Z\right] - f_c\cdot Z\cdot(1 - \alpha)$$

$$G(\sigma, Z) := \left[\sqrt{J_2(\sigma)}\cdot Ar(\theta(\sigma)) + \left(\alpha + \frac{\gamma}{3}\right)\cdot I_1(\sigma)\cdot Z\cdot\Psi\right] - f_c\cdot Z\cdot\Psi\cdot(1 - \alpha)$$

Function gradients

$J2tol := f_t^2 \cdot 10^{-10}$ $\quad \theta tol := 10^{-6}$

cterms(σ, Z) :=
- $c \leftarrow (0\ 0\ 0)^T$
- $J2 \leftarrow J_2(\sigma)$
- $J3 \leftarrow J_3(\sigma)$
- $t \leftarrow \theta(\sigma)$
- $t \leftarrow \theta tol$ if $t < \theta tol$
- $t \leftarrow \frac{\pi}{3} - \theta tol$ if $|t| \geq \frac{\pi}{3} - \theta tol$
- $\cos\theta \leftarrow \cos(t)$
- $\sin\theta \leftarrow \sin(t)$
- $\sin 3\theta \leftarrow \sin(3 \cdot t)$
- $A \leftarrow Ar(t)$
- $dA \leftarrow dArd\theta(t)$
- $c_1 \leftarrow \left(\alpha + \frac{\gamma}{3}\right) \cdot Z$
- if $J2 > J2tol$
  - $c_2 \leftarrow \frac{A}{2\sqrt{J2}} + \frac{3\sqrt{3} \cdot J3 \cdot dA}{\sin 3\theta \cdot 4 \cdot J2^2}$
  - $c_3 \leftarrow \frac{-dA\sqrt{3}}{2 \cdot \sin 3\theta \cdot J2}$
- c

Yield function gradient

dFdσ(σ, Z) :=
- $c \leftarrow cterms(\sigma, Z)$
- $dFd\sigma \leftarrow c_1 \cdot dI1 + c_2 \cdot dJ2(\sigma) + c_3 \cdot dJ3(\sigma)$

Plastic potential gradient

$dGd\sigma(\sigma, Z) := dFd\sigma(\sigma, Z \cdot \Psi)$

d2F(σ, Z) :=
- $c2 \leftarrow c2f(\sigma, Z)$
- $c \leftarrow cterms(\sigma, Z)$
- $a2 \leftarrow dJ2(\sigma)$
- $a3 \leftarrow dJ3(\sigma)$
- $Nul6x6 + c_2 \cdot da2d\sigma + c_3 \cdot da3d\sigma(\sigma) + c2_1 \cdot a2 \cdot a2^T + c2_2 \cdot a2 \cdot a3^T + c2_3 \cdot a3 \cdot a2^T + c2_4 \cdot a3 \cdot a3^T$

$d2G(\sigma, Z) := d2F(\sigma, Z \cdot \Psi)$

$d2Gd\sigma Z := \left(\alpha + \frac{\gamma}{3}\right) \cdot \Psi \cdot dI1$

Coefficients of 2nd derivative of yield function w.r.t stresses

c2f(σ, Z) :=
- "coeffs for 2nd derivs. c1=c22, c2=c23, c3=c32, c4=c33"
- $c2s \leftarrow (0\ 0\ 0\ 0)^T$
- $J2 \leftarrow J_2(\sigma)$
- $J3 \leftarrow J_3(\sigma)$
- $t \leftarrow \theta(\sigma)$
- $t \leftarrow \theta tol$ if $t < \theta tol$
- $t \leftarrow \frac{\pi}{3} - \theta tol$ if $|t| \geq \frac{\pi}{3} - \theta tol$
- $\cos\theta \leftarrow \cos(t)$
- $\sin\theta \leftarrow \sin(t)$
- $\sin 3\theta \leftarrow \sin(3 \cdot t)$
- $\cos 3\theta \leftarrow \cos(3 \cdot t)$
- $A \leftarrow Ar(t)$
- $dA \leftarrow dArd\theta(t)$
- $d2A \leftarrow d2Ard\theta(t)$
- $d2As3 \leftarrow \frac{d2A}{\sin 3\theta} - \frac{3 \cdot \cos 3\theta \cdot dA}{\sin 3\theta^2}$
- if $J2 > J2tol$
  - $dc2dj2 \leftarrow \frac{-A}{4 \cdot J2^{1.5}} - \frac{3\sqrt{3} \cdot J3 \cdot dA}{2 \cdot \sin 3\theta \cdot J2^3}$
  - $dc2dj3 \leftarrow \frac{\sqrt{3} \cdot 3 \cdot dA}{4 \cdot \sin 3\theta \cdot J2^2}$
  - $dc3dj2 \leftarrow \frac{dA\sqrt{3}}{2 \cdot J2^2 \cdot \sin 3\theta}$
  - $dc2d\theta \leftarrow \frac{dA}{2\sqrt{J2}} + \frac{3\sqrt{3} \cdot J3 \cdot d2As3}{4 \cdot J2^2}$
  - $dc3d\theta \leftarrow \frac{-\sqrt{3}}{2 \cdot J2} \cdot d2As3$
  - $d\theta dJ2 \leftarrow \frac{\sqrt{3} \cdot 3 \cdot J3}{4 \cdot \sin 3\theta \cdot J2^{2.5}}$
  - $d\theta dJ3 \leftarrow \frac{-\sqrt{3}}{2 \cdot \sin 3\theta \cdot J2^{1.5}}$
  - $c2s_1 \leftarrow dc2dj2 + dc2d\theta \cdot d\theta dJ2$
  - $c2s_2 \leftarrow dc2dj3 + dc2d\theta \cdot d\theta dJ3$
  - $c2s_3 \leftarrow dc3dj2 + dc3d\theta \cdot d\theta dJ2$
  - $c2s_4 \leftarrow dc3d\theta \cdot d\theta dJ3$
- c2s

First and second derivatives of principal stress components w.r.t cartesian stresses

Ip = Stress component required
v=variable stress or adjusted strain
vref = reference stress or strain

$a_1 := dI1 \qquad a_2(v) := dJ2(v) \qquad a_3(v) := dJ3(v)$

$$c(v, vref, Ip) := \begin{| J2tol \leftarrow vref^2 \cdot 10^{-10} \\ J2 \leftarrow J_2(v) \\ t \leftarrow \theta(v) \\ J3 \leftarrow J_3(v) \\ A \leftarrow A\theta(t, Ip) \\ c \leftarrow (0 \;\; 0 \;\; 0)^T \\ c_1 \leftarrow \frac{1}{3} \\ \text{if } J2 > J2tol \\ \quad \begin{| \text{if } (t > \theta tol) \cdot \left(t < \frac{\pi}{3} - \theta tol\right) \\ \quad\quad \begin{| dA \leftarrow dA\theta(t, Ip) \\ \quad\quad c_2 \leftarrow \frac{A}{\sqrt{3} \cdot J2} + \frac{3 \cdot dA}{2 \cdot \sin(3 \cdot t) \cdot J2^2} \cdot J3 \\ \quad\quad c_3 \leftarrow \frac{-dA}{J2 \cdot \sin(3 \cdot t)} \\ \quad \text{if } [(t \le \theta tol) \cdot (Ip = 1)] + \left(t \ge \frac{\pi}{3} - \theta tol\right) \cdot (Ip = 3) \\ \quad\quad \begin{| c_2 \leftarrow \frac{A}{\sqrt{3} \cdot J2} - \frac{J3}{2 \cdot J2^2} \\ \quad\quad c_3 \leftarrow \frac{1}{3 \cdot J2} \\ \quad c_2 \leftarrow \frac{A}{\sqrt{3} \cdot J2} \text{ if } \left[\left(t \ge \frac{\pi}{3} - \theta tol\right) \cdot [(Ip = 1) + (Ip = 2)]\right] + [(t \le \theta tol) \cdot [(Ip = 3) + (Ip = 2)]] \\ c \end{|$$

$$c2s(v, vref, Ip) := \begin{| \text{"coeffs for 2nd derivatives. c1=c22. c2=c23. c3=c32. c4=c33"} \\ J2tol \leftarrow vref^2 \cdot 10^{-10} \\ J2 \leftarrow J_2(v) \\ t \leftarrow \theta(v) \\ J3 \leftarrow J_3(v) \\ A \leftarrow A\theta(t, Ip) \\ dc2d\theta \leftarrow 0 \\ dc3d\theta \leftarrow 0 \\ c \leftarrow (0 \;\; 0 \;\; 0 \;\; 0)^T \\ \text{if } J2 > J2tol \\ \quad \begin{| \text{if } (t > \theta tol) \cdot \left[t < \left(\frac{\pi}{3} - \theta tol\right)\right] \\ \quad\quad \begin{| dA \leftarrow dA\theta(t, Ip) \\ \quad\quad d2As \leftarrow d2As3(t, Ip) \\ \quad\quad dc2d\theta \leftarrow \frac{dA}{\sqrt{3} \cdot J2} + \frac{3 \cdot J3}{2 \cdot J2^2} \cdot d2As \\ \quad\quad dc3d\theta \leftarrow \frac{-d2As}{J2} \\ \quad\quad c_1 \leftarrow \frac{-A}{2\sqrt{3} \cdot J2^{1.5}} - \frac{3 \cdot dA \cdot J3}{\sin(3 \cdot t) \cdot (J2)^3} + \frac{\sqrt{3} \cdot 3 \cdot J3}{4 \cdot \sin(3 \cdot t) \cdot J2^{2.5}} \cdot dc2d\theta \\ \quad\quad c_2 \leftarrow \frac{3 \cdot dA}{2 \cdot \sin(3 \cdot t) \cdot J2^2} - \frac{\sqrt{3}}{2 \cdot \sin(3t) \cdot J2^{1.5}} \cdot dc2d\theta \\ \quad\quad c_3 \leftarrow \frac{dA}{\sin(3 \cdot t) \cdot J2^2} + \frac{\sqrt{3} \cdot 3 \cdot J3}{4 \cdot \sin(3 \cdot t) \cdot J2^{2.5}} \cdot dc3d\theta \\ \quad\quad c_4 \leftarrow \frac{-\sqrt{3}}{2 \cdot \sin(3 \cdot t) \cdot J2^{1.5}} \cdot dc3d\theta \\ \quad \text{if } \left[[(t \le \theta tol) \cdot (Ip = 1)] + \left[\left(t \ge \frac{\pi}{3} - \theta tol\right) \cdot (Ip = 3)\right]\right] \\ \quad\quad \begin{| c_1 \leftarrow \frac{-A}{2\sqrt{3} \cdot J2^{1.5}} + \frac{J3}{J2^3} \\ \quad\quad c_2 \leftarrow \frac{-1}{2 \cdot J2^2} \\ \quad\quad c_3 \leftarrow \frac{-1}{3 \cdot J2^2} \\ \quad c_1 \leftarrow \frac{-A}{2\sqrt{3} \cdot J2^{1.5}} \text{ if } \left[\left[\left(t \ge \frac{\pi}{3} - \theta tol\right) \cdot [(Ip = 1) + (Ip = 2)]\right] + [(t \le \theta tol) \cdot [(Ip = 3) + (Ip = 2)]]\right] \\ c \end|$$

Generalised gradient

$$dPId\sigma(v, vref, Ip) := \begin{| ca \leftarrow c(v, vref, Ip) \\ ca_1 \cdot dI1 + ca_2 \cdot dJ2(v) + ca_3 \, dJ3(v) \end{|}$$

2nd differential

$$d2PI(v, vref, Ip) := \begin{| ca \leftarrow c(v, vref, Ip) \\ cb \leftarrow c2s(v, vref, Ip) \\ a2 \leftarrow a_2(v) \\ a3 \leftarrow a_3(v) \\ d2PI \leftarrow Nul6x6 + ca_2 \cdot da2d\sigma + ca_3 \cdot da3d\sigma(v) + cb_1 \cdot a2 \cdot a2^T + cb_2 \cdot a2 \cdot a3^T + cb_3 \cdot a3 \cdot a2^T + cb_4 \cdot a3 \cdot a3^T \\ d2PI \end{|}$$

Hardening function terms

$$\kappa_p := f_c \cdot \left(0.72 \cdot \varepsilon_c - \frac{f_c}{2 \cdot E} \right) \qquad \kappa_p = 0.04336 \qquad \rho f := 10$$

$$Zf(\kappa) := \begin{| \eta \leftarrow \frac{\kappa}{\kappa_p} \\ Z \leftarrow Z_0 + \frac{(1 - Z_0)}{a_c} \cdot e^{-c_{c1} \cdot \eta} \cdot \left(1 - e^{-c_{c2} \cdot \eta} \right) \end{|}$$

$$dZd\kappa(\kappa) := \begin{| \eta \leftarrow \frac{\kappa}{\kappa_p} \\ dZ \leftarrow \frac{(1 - Z_0)}{a_c \cdot \kappa_p} \cdot e^{-c_{c1} \cdot \eta} \left[-c_{c1} \cdot \left(1 - e^{-c_{c2} \cdot \eta} \right) + c_{c2} \cdot e^{-c_{c2} \cdot \eta} \right] \end{|}$$

$$dFdZ(\sigma) := \left[\left(\alpha + \frac{\gamma}{3} \right) \cdot I_1(\sigma) \right] - f_c \cdot (1 - \alpha)$$

$$X(\sigma) := \begin{| \chi \leftarrow \frac{I_1(\sigma)}{f_c \cdot 0.9} + 0.55 \\ e^{\chi} + e^{\chi - 1} + 0.0022 \end{|}$$

$$dXd\sigma(\sigma) := \begin{| \chi \leftarrow \frac{I_1(\sigma)}{f_c \cdot 0.9} + 0.55 \\ d\chi \leftarrow \frac{dI1}{f_c \cdot 0.9} \\ dX \leftarrow \left(e^{\chi} + e^{\chi - 1} \right) \cdot d\chi \end{|}$$

$$d2G\sigma\kappa(\kappa) := d2Gd\sigma Z \cdot dZd\kappa(\kappa)$$

$$c_\kappa(\sigma, \kappa) := X(\sigma) \cdot (\sigma \cdot dGd\sigma(\sigma, Zf(\kappa)))$$

$$K_\sigma(\sigma, Z) := (\sigma \cdot dGd\sigma(\sigma, Z)) \cdot dXd\sigma(\sigma) + X(\sigma) \cdot d2G(\sigma, Z) \cdot \sigma + X(\sigma) \cdot dGd\sigma(\sigma, Z)$$

$$a_\kappa(\sigma, \kappa, \Delta\lambda) := \frac{1}{[\, 1 - \Delta\lambda \cdot X(\sigma) \cdot (\sigma \cdot d2Gd\sigma Z) \cdot dZd\kappa(\kappa)\,]}$$

$$ac_\kappa(\sigma, \kappa, \Delta\lambda) := c_\kappa(\sigma, \kappa) \cdot a_\kappa(\sigma, \kappa, \Delta\lambda)$$

$$h_\sigma(\sigma, \kappa, \Delta\lambda) := dFdZ(\sigma) \cdot dZd\kappa(\kappa) \cdot K_\sigma(\sigma, Zf(\kappa)) \cdot a_\kappa(\sigma, \kappa, \Delta\lambda)$$

$$h_\kappa(\sigma, \kappa, \Delta\lambda) := (dFdZ(\sigma) \cdot dZd\kappa(\kappa)) \cdot c_\kappa(\sigma, \kappa) \cdot a_\kappa(\sigma, \kappa, \Delta\lambda)$$

Local yield function

$$r_\mu := r_\sigma^4 \cdot f_{ti}^2 - 2 \cdot r_\sigma^2 \cdot f_{ti}^2 \cdot \mu^2 + \mu^4 \cdot f_{ti}^2$$

$$fe(\zeta, \kappa, s) := \left| \begin{array}{l} \eta \leftarrow \dfrac{(\zeta - \varepsilon_{ti})}{(\varepsilon_0 - \varepsilon_{ti})} \\ fs \leftarrow \left[res\_ft \cdot \varepsilon_{ti} + (1 - res\_ft) \cdot \left(\varepsilon_{ti} \cdot e^{-c_{t1} \cdot \eta} \right) \cdot e^{-2 \frac{\kappa}{\kappa_p}} \right] \cdot E_{ef} \\ fe \leftarrow \dfrac{\left(\mu^2 - r_\sigma^2 \right) \cdot f_{ti} + 2 \cdot \mu^2 \cdot s_1 + \left[r_\mu + 4 \cdot \mu^2 \left[(s_2)^2 + (s_3)^2 \right] \right]^{\frac{1}{2}}}{2 \cdot \mu^2} - fs \end{array} \right.$$

Local plastic potential function

$$g(s) := \sqrt{(s_1)^2 + (s_2)^2 + (s_3)^2}$$

$$d\zeta de(e) := \begin{bmatrix} \dfrac{1}{2}\left[1 + \left(\dfrac{\mu_\varepsilon}{r_\zeta} \right)^2 \right] + \dfrac{\left(r_\zeta^2 - \mu_\varepsilon^2 \right)^2 \cdot (e_1)}{2 \cdot r_\zeta^2 \cdot \sqrt{\left(r_\zeta^2 - \mu_\varepsilon^2 \right)^2 \cdot (e_1)^2 + 4 \cdot r_\zeta^2 \left[(e_2)^2 + (e_3)^2 \right]}} \\ \dfrac{2 \cdot (e_2)}{\sqrt{\left(r_\zeta^2 - \mu_\varepsilon^2 \right)^2 \cdot (e_1)^2 + 4 \cdot r_\zeta^2 \left[(e_2)^2 + (e_3)^2 \right]}} \\ \dfrac{2 \cdot (e_3)}{\sqrt{\left(r_\zeta^2 - \mu_\varepsilon^2 \right)^2 \cdot (e_1)^2 + 4 \cdot r_\zeta^2 \left[(e_2)^2 + (e_3)^2 \right]}} \end{bmatrix}$$

First and second derivatives of functions

$$dfeds(\zeta, \kappa, s) := \begin{bmatrix} 1 \\ \dfrac{2 \cdot s_2}{\left[r_\mu + 4 \cdot \mu^2 \left[(s_2)^2 + (s_3)^2 \right] \right]^{0.5}} \\ \dfrac{2 \cdot s_3}{\left[r_\mu + 4 \cdot \mu^2 \left[(s_2)^2 + (s_3)^2 \right] \right]^{0.5}} \end{bmatrix}$$

$$d2feds(\zeta, \kappa, s) := \begin{bmatrix} 0 & 0 & 0 \\ 0 & \dfrac{-16 \cdot \mu^2 \cdot (s_2)^2 + 2\left[r_\mu + 4 \cdot \mu^2 \left[(s_2)^2 + (s_3)^2 \right] \right]}{\left[r_\mu + 4 \cdot \mu^2 \left[(s_2)^2 + (s_3)^2 \right] \right]^{1.5}} & \dfrac{-s_2 \cdot 8 \cdot \mu^2 s_3}{\left[r_\mu + 4 \cdot \mu^2 \left[(s_2)^2 + (s_3)^2 \right] \right]^{1.5}} \\ 0 & \dfrac{-s_3 \cdot 8 \cdot \mu^2 s_2}{\left[r_\mu + 4 \cdot \mu^2 \left[(s_2)^2 + (s_3)^2 \right] \right]^{1.5}} & \dfrac{-16 \cdot \mu^2 \cdot (s_3)^2 + 2\left[r_\mu + 4 \cdot \mu^2 \left[(s_2)^2 + (s_3)^2 \right] \right]}{\left[r_\mu + 4 \cdot \mu^2 \left[(s_2)^2 + (s_3)^2 \right] \right]^{1.5}} \end{bmatrix}$$

$$dgds(s) := \frac{1}{\sqrt{(s_1)^2 + (s_2)^2 + (s_3)^2}} \cdot \begin{pmatrix} s_1 \\ s_2 \\ s_3 \end{pmatrix}$$

$$d2gds(s) := \frac{1}{\left[(s_1)^2 + (s_2)^2 + (s_3)^2 \right]^{1.5}} \begin{bmatrix} (s_2)^2 + (s_3)^2 & -s_1 \cdot s_2 & -s_1 \cdot s_3 \\ -s_2 \cdot s_1 & (s_1)^2 + (s_3)^2 & -s_2 \cdot s_3 \\ -s_3 \cdot s_1 & -s_3 \cdot s_2 & (s_1)^2 + (s_2)^2 \end{bmatrix}$$

$$dfedζ(\zeta, \kappa, s) := \left| \begin{array}{l} r \leftarrow res\_ft \\ \eta \leftarrow \dfrac{(\zeta - \varepsilon_{ti})}{(\varepsilon_0 - \varepsilon_{ti})} \\ 0 \text{ if } \zeta < \varepsilon_{ti} \\ -\left[(1 - r) \cdot e^{-c_{t1} \cdot \eta} \cdot \varepsilon_{ti} \cdot \left(\dfrac{-c_{t1}}{\varepsilon_0 - \varepsilon_{ti}} \right) \cdot e^{-2 \frac{\kappa}{\kappa_p}} \right] \cdot E_{ef} \text{ otherwise} \end{array} \right.$$

$$dfedκ(\zeta, \kappa, s) := \left| \begin{array}{l} r \leftarrow res\_ft \\ \eta \leftarrow \dfrac{(\zeta - \varepsilon_{ti})}{(\varepsilon_0 - \varepsilon_{ti})} \\ 0 \text{ if } \zeta < \varepsilon_{ti} \\ -\left[(1 - r) \cdot \left(\varepsilon_{ti} \cdot e^{-c_{t1} \cdot \eta} \right) \dfrac{-2}{\kappa_p} \cdot e^{-2 \frac{\kappa}{\kappa_p}} \cdot E_{ef} \right] \text{ otherwise} \end{array} \right.$$

Normal vectors for all principal stress or strain directions

r_all(v, vref) :=
- $r \leftarrow (0\ \ 0\ \ 0)^T$
- for $Ip \in 1..3$
  - $N \leftarrow dPIdo(v, vref, Ip)$
  - for $i \in 1..3$
    - $r_i \leftarrow 0$
    - $r_i \leftarrow \sqrt{N_i}$ if $N_i > 0$
  - $r_2 \leftarrow -r_2$ if $N_4 < 0$
  - $r_3 \leftarrow -r_3$ if $N_6 < 0$
  - $r_3 \leftarrow -r_3$ if $(r_2 \cdot r_3 \cdot N_5) < 0$
  - $rd_{Ip} \leftarrow r$
- " Check for clashes"
- if $|rd_1 \cdot rd_2| > 0.01 \wedge |rd_2 \cdot rd_3| > 0.01 \wedge (|rd_1 \cdot rd_3| > 0.01)$
  - $rd_1 \leftarrow (1\ \ 0\ \ 0)^T$
  - $rd_2 \leftarrow (0\ \ 1\ \ 0)^T$
  - $rd_3 \leftarrow (0\ \ 0\ \ 1)^T$
- otherwise
  - if $|rd_1 \cdot rd_2| > 0.01$
    - $rd_1 \leftarrow sloc(1, rd_3)$
    - $rd_2 \leftarrow rd_3 \times rd_1$
  - if $|rd_2 \cdot rd_3| > 0.01$
    - $rd_2 \leftarrow sloc(3, rd_1)$
    - $rd_3 \leftarrow rd_1 \times rd_2$
  - if $|rd_1 \cdot rd_3| > 0.01$
    - $rd_1 \leftarrow sloc(2, rd_2)$
    - $rd_3 \leftarrow rd_1 \times rd_2$
- rd

$$isq := \begin{pmatrix} 1 & 2 & 3 \\ 2 & 1 & 3 \\ 3 & 2 & 1 \end{pmatrix} \qquad nsq := \begin{pmatrix} 1 & 4 & 6 \\ 2 & 4 & 5 \\ 3 & 5 & 6 \end{pmatrix}$$

$$Nul3x6 := \begin{pmatrix} 0 & 0 & 0 & 0 & 0 & 0 \\ 0 & 0 & 0 & 0 & 0 & 0 \\ 0 & 0 & 0 & 0 & 0 & 0 \end{pmatrix} \qquad Nul3x3 := \begin{pmatrix} 0 & 0 & 0 \\ 0 & 0 & 0 \\ 0 & 0 & 0 \end{pmatrix}$$

POD unit vector gradients

r_grad(v, vref, Ip) :=
- $rgrad \leftarrow I_{nul}$
- $r \leftarrow r\_all(v, vref)_{Ip}$
- $d2Pdv \leftarrow d2PI(v, vref, Ip)$
- $dPdvT \leftarrow Nul3x6^T$
- for $i \in 1..3$
  - $dPdvT^{\langle i \rangle} \leftarrow \frac{1}{2 \cdot r_i} \cdot d2Pdv^{\langle i \rangle}$ if $|r_i| > 10^{-4}$
  - otherwise
    - $dPdvT^{\langle i \rangle} \leftarrow \frac{1}{2 \cdot r_{(isq_{i,2})}} \cdot d2Pdv^{\langle (nsq_{i,2}) \rangle}$ if $|r_{isq_{i,2}}| > 10^{-4}$
    - $dPdvsT^{\langle i \rangle} \leftarrow \frac{1}{2 \cdot r_{(isq_{i,3})}} \cdot d2Pdv^{\langle (nsq_{i,3}) \rangle}$ otherwise
- $dPdvT^T$

$$
\text{s\_grad}(v, vref, Ip, id) := \left|
\begin{array}{l}
r \leftarrow r\_all(v, vref)_{Ip} \\
drdv \leftarrow r\_grad(v, vref, Ip) \\
denom \leftarrow \sqrt{\left[r\left(idx_{id,1}\right)\right]^2 + \left[r\left(idx_{id,2}\right)\right]^2} \\
dsdr \leftarrow Nul3x3 \\
idr \leftarrow id \\
\text{if } denom < 10^{-12} \\
\quad \left|
\begin{array}{l}
idr \leftarrow id + 1 \\
idr \leftarrow 1 \text{ if } idr > 3 \\
denom \leftarrow \sqrt{\left[r\left(idx_{idr,1}\right)\right]^2 + \left[r\left(idx_{idr,2}\right)\right]^2}
\end{array}
\right. \\
denom3 \leftarrow denom^3 \\
dsdr \leftarrow \frac{-1}{denom3} \cdot \begin{pmatrix} -r_2 \cdot r_1 & -(r_2)^2 & 0 \\ (r_1)^2 & r_2 \cdot r_1 & 0 \\ 0 & 0 & 0 \end{pmatrix} + \frac{1}{denom} \cdot \begin{pmatrix} 0 & -1 & 0 \\ 1 & 0 & 0 \\ 0 & 0 & 0 \end{pmatrix} \text{ if } idr = 3 \\
dsdr \leftarrow \frac{-1}{denom3} \cdot \begin{pmatrix} 0 & 0 & 0 \\ 0 & -r_2 \cdot r_3 & -(r_3)^2 \\ 0 & (r_2)^2 & r_2 \cdot r_3 \end{pmatrix} + \frac{1}{denom} \cdot \begin{pmatrix} 0 & 0 & 0 \\ 0 & 0 & -1 \\ 0 & 1 & 0 \end{pmatrix} \text{ if } idr = 1 \\
dsdr \leftarrow \frac{-1}{denom3} \cdot \begin{pmatrix} r_1 \cdot r_3 & 0 & (r_3)^2 \\ 0 & 0 & 0 \\ -(r_1)^2 & 0 & -r_1 \cdot r_3 \end{pmatrix} + \frac{1}{denom} \cdot \begin{pmatrix} 0 & 0 & 1 \\ 0 & 0 & 0 \\ -1 & 0 & 0 \end{pmatrix} \text{ if } idr = 2 \\
dsdr \cdot drdv
\end{array}
\right.
$$

$$
\text{t\_grad}(v, vref, Ip, id) := \left|
\begin{array}{l}
r \leftarrow r\_all(v, vref)_{Ip} \\
s \leftarrow sloc(id, r) \\
drdv \leftarrow r\_grad(v, vref, Ip) \\
dsdv \leftarrow s\_grad(v, vref, Ip, id) \\
dtdr \leftarrow \begin{pmatrix} 0 & s_3 & -s_2 \\ -s_3 & 0 & s_1 \\ s_2 & -s_1 & 0 \end{pmatrix} \\
dtds \leftarrow \begin{pmatrix} 0 & -r_3 & r_2 \\ r_3 & 0 & -r_1 \\ -r_2 & r_1 & 0 \end{pmatrix} \\
dtdr \cdot drdv + dtds \cdot dsdv
\end{array}
\right.
$$

Terms for orthogonally generated PODs. Direction switched when α proximity introduced

$$
\text{r\_ortho}(r1, r\sigma) := \begin{bmatrix} r\sigma_1 \left[(r1_2)^2 + (r1_3)^2\right] - r\sigma_2 \cdot r1_1 \cdot r1_2 - r\sigma_3 \cdot r1_1 \cdot r1_3 \\ -r\sigma_1 \cdot r1_1 \cdot r1_2 + r\sigma_2 \left[(r1_3)^2 + (r1_1)^2\right] - r\sigma_3 \cdot r1_2 \cdot r1_3 \\ -r\sigma_1 \cdot r1_1 \cdot r1_3 - r\sigma_2 \cdot r1_2 \cdot r1_3 + r\sigma_3 \left[(r1_1)^2 + (r1_2)^2\right] \end{bmatrix} \frac{1}{\sqrt{\left(r1_2 \cdot r\sigma_3 - r1_3 \cdot r\sigma_2\right)^2 + \left(r1_3 \cdot r\sigma_1 - r1_1 \cdot r\sigma_3\right)^2 + \left(r1_1 \cdot r\sigma_2 - r1_2 \cdot r\sigma_1\right)^2}}
$$

$$dor1(r1, r\sigma) := \begin{bmatrix} \left[(r1_2)^2 + (r1_3)^2\right] & -r1_1 \cdot r1_2 & -r1_1 \cdot r1_3 \\ -r1_1 \cdot r1_2 & \left[(r1_3)^2 + (r1_1)^2\right] & -r1_2 \cdot r1_3 \\ -r1_1 \cdot r1_3 & -r1_2 \cdot r1_3 & \left[(r1_1)^2 + (r1_2)^2\right] \end{bmatrix} \frac{1}{\sqrt{(r1_2 \cdot r\sigma_3 - r1_3 \cdot r\sigma_2)^2 + (r1_3 \cdot r\sigma_1 - r1_1 \cdot r\sigma_3)^2 + (r1_1 \cdot r\sigma_2 - r1_2 \cdot r\sigma_1)^2}}$$

$$dor2(r1, r\sigma) := \frac{-r\_ortho(r1, r\sigma)}{2\left[(r1_2 \cdot r\sigma_3 - r1_3 \cdot r\sigma_2)^2 + (r1_3 \cdot r\sigma_1 - r1_1 \cdot r\sigma_3)^2 + (r1_1 \cdot r\sigma_2 - r1_2 \cdot r\sigma_1)^2\right]} \cdot \begin{bmatrix} 2 \cdot (r1_3 \cdot r\sigma_1 - r1_1 \cdot r\sigma_3) \cdot r1_3 - 2 \cdot (r1_1 \cdot r\sigma_2 - r1_2 \cdot r\sigma_1) \cdot r1_2 \\ -\left[2 \cdot (r1_2 \cdot r\sigma_3 - r1_3 \cdot r\sigma_2)\right] \cdot r1_3 + 2 \cdot (r1_1 \cdot r\sigma_2 - r1_2 \cdot r\sigma_1) \cdot r1_1 \\ 2 \cdot (r1_2 \cdot r\sigma_3 - r1_3 \cdot r\sigma_2) \cdot r1_2 - 2 \cdot (r1_3 \cdot r\sigma_1 - r1_1 \cdot r\sigma_3) \cdot r1_1 \end{bmatrix}^T$$

$$drdor(r1, r\sigma) := dor1(r1, r\sigma) + dor2(r1, r\sigma)$$

Terms for PODs at α_p to existing

$$drdr_\alpha(r1, r\sigma) := \begin{bmatrix} mul \leftarrow 1 \\ mul \leftarrow -1 \text{ if } r1 \cdot r\sigma < 0 \\ (dor1(r1, r\sigma \cdot mul) + dor2(r1, r\sigma \cdot mul)) \cdot \sin(\alpha_p) \cdot mul \end{bmatrix}$$

$$t\_grado(v, vref, Ip, id, r1) := \begin{bmatrix} r\sigma \leftarrow r\_all(v, vref)_{Ip} \\ r \leftarrow r\_ortho(r1, r\sigma) \\ drdv \leftarrow drdor(r1, r\sigma) \cdot r\_grad(v, vref, Ip) \\ s \leftarrow sloc(id, r) \\ dsdv \leftarrow s\_grado(v, vref, Ip, id, r1) \\ dtdr \leftarrow \begin{pmatrix} 0 & s_3 & -s_2 \\ -s_3 & 0 & s_1 \\ s_2 & -s_1 & 0 \end{pmatrix} \\ dtds \leftarrow \begin{pmatrix} 0 & -r_3 & r_2 \\ r_3 & 0 & -r_1 \\ -r_2 & r_1 & 0 \end{pmatrix} \\ dtdr \cdot drdv + dtds \cdot dsdv \end{bmatrix}$$

$$s\_grado(v, vref, Ip, id, r1) := \begin{bmatrix} r\sigma \leftarrow r\_all(v, vref)_{Ip} \\ r \leftarrow r\_ortho(r1, r\sigma) \\ drdv \leftarrow drdor(r1, r\sigma) \cdot r\_grad(v, vref, Ip) \\ denom \leftarrow \sqrt{\left[r\left(idx_{id,1}\right)\right]^2 + \left[r\left(idx_{id,2}\right)\right]^2} \\ dsdr \leftarrow Nul3x3 \\ idr \leftarrow id \\ \text{if } denom < 10^{-12} \\ \quad \begin{bmatrix} idr \leftarrow id + 1 \\ idr \leftarrow 1 \text{ if } idr > 3 \\ denom \leftarrow \sqrt{\left[r\left(idx_{idr,1}\right)\right]^2 + \left[r\left(idx_{idr,2}\right)\right]^2} \end{bmatrix} \\ denom3 \leftarrow denom^3 \\ dsdr \leftarrow \frac{-1}{denom3} \begin{bmatrix} -r_2 \cdot r_1 & -(r_2)^2 & 0 \\ (r_1)^2 & r_2 \cdot r_1 & 0 \\ 0 & 0 & 0 \end{bmatrix} + \frac{1}{denom} \cdot \begin{pmatrix} 0 & -1 & 0 \\ 1 & 0 & 0 \\ 0 & 0 & 0 \end{pmatrix} \text{ if } idr = 3 \\ dsdr \leftarrow \frac{-1}{denom3} \begin{bmatrix} 0 & 0 & 0 \\ 0 & -r_2 \cdot r_3 & -(r_3)^2 \\ 0 & (r_2)^2 & r_2 \cdot r_3 \end{bmatrix} + \frac{1}{denom} \cdot \begin{pmatrix} 0 & 0 & 0 \\ 0 & 0 & -1 \\ 0 & 1 & 0 \end{pmatrix} \text{ if } idr = 1 \\ dsdr \leftarrow \frac{-1}{denom3} \begin{bmatrix} r_1 \cdot r_3 & 0 & (r_3)^2 \\ 0 & 0 & 0 \\ -(r_1)^2 & 0 & -r_1 \cdot r_3 \end{bmatrix} + \frac{1}{denom} \cdot \begin{pmatrix} 0 & 0 & 1 \\ 0 & 0 & 0 \\ -1 & 0 & 0 \end{pmatrix} \text{ if } idr = 2 \\ dsdr \cdot drdv \end{bmatrix}$$

Gradient functions for α PODs

$s\_grad\alpha(v, vref, Ip, id, r1) :=$

$r\sigma \leftarrow r\_all(v, vref)_{Ip}$

$mul \leftarrow 1$

$mul \leftarrow -1 \text{ if } r1 \cdot r\sigma < 0$

$r \leftarrow \left(\cos(\alpha_p) \cdot r1 + \sin(\alpha_p) \cdot r\_ortho(r1, r\sigma \cdot mul)\right) \cdot mul$

$drdv \leftarrow drdr_\alpha(r1, r\sigma) \cdot r\_grad(v, vref, Ip) \cdot mul$

$$denom \leftarrow \sqrt{\left[r\left(idx_{id,1}\right)\right]^2 + \left[r\left(idx_{id,2}\right)\right]^2}$$

$dsdr \leftarrow Nul3x3$

$idr \leftarrow id$

if $denom < 10^{-12}$

- $idr \leftarrow id + 1$
- $idr \leftarrow 1 \text{ if } idr > 3$
- $$denom \leftarrow \sqrt{\left[r\left(idx_{idr,1}\right)\right]^2 + \left[r\left(idx_{idr,2}\right)\right]^2}$$

$denom3 \leftarrow denom^3$

$$dsdr \leftarrow \frac{-1}{denom3} \cdot \begin{bmatrix} -r_2 \cdot r_1 & -(r_2)^2 & 0 \\ (r_1)^2 & r_2 \cdot r_1 & 0 \\ 0 & 0 & 0 \end{bmatrix} + \frac{1}{denom} \cdot \begin{pmatrix} 0 & -1 & 0 \\ 1 & 0 & 0 \\ 0 & 0 & 0 \end{pmatrix} \text{ if } idr = 3$$

$$dsdr \leftarrow \frac{-1}{denom3} \cdot \begin{bmatrix} 0 & 0 & 0 \\ 0 & -r_2 \cdot r_3 & -(r_3)^2 \\ 0 & (r_2)^2 & r_2 \cdot r_3 \end{bmatrix} + \frac{1}{denom} \cdot \begin{pmatrix} 0 & 0 & 0 \\ 0 & 0 & -1 \\ 0 & 1 & 0 \end{pmatrix} \text{ if } idr = 1$$

$$dsdr \leftarrow \frac{-1}{denom3} \cdot \begin{bmatrix} r_1 \cdot r_3 & 0 & (r_3)^2 \\ 0 & 0 & 0 \\ -(r_1)^2 & 0 & -r_1 \cdot r_3 \end{bmatrix} + \frac{1}{denom} \cdot \begin{pmatrix} 0 & 0 & 1 \\ 0 & 0 & 0 \\ -1 & 0 & 0 \end{pmatrix} \text{ if } idr = 2$$

$dsdr \cdot drdv$

$t\_grad\alpha(v, vref, Ip, id, r1) :=$

$r\sigma \leftarrow r\_all(v, vref)_{Ip}$

$mul \leftarrow 1$

$mul \leftarrow -1 \text{ if } r1 \cdot r\sigma < 0$

$r \leftarrow \left(\cos(\alpha_p) \cdot r1 + \sin(\alpha_p) \cdot r\_ortho(r1, r\sigma \cdot mul)\right) \cdot mul$

$drdv \leftarrow drdr_\alpha(r1, r\sigma) \cdot r\_grad(v, vref, Ip) \cdot mul$

$drdv \leftarrow drdr_\alpha(r1, r\sigma) \cdot r\_grad(v, vref, Ip) \cdot mul$

$s \leftarrow sloc(id, r)$

$dsdv \leftarrow s\_grad\alpha(v, vref, Ip, id, r1)$

$$dtdr \leftarrow \begin{pmatrix} 0 & s_3 & -s_2 \\ -s_3 & 0 & s_1 \\ s_2 & -s_1 & 0 \end{pmatrix}$$

$$dtds \leftarrow \begin{pmatrix} 0 & -r_3 & r_2 \\ r_3 & 0 & -r_1 \\ -r_2 & r_1 & 0 \end{pmatrix}$$

$dtdr \cdot drdv + dtds \cdot dsdv$

```
dNdv( v , vref, Ip , id) := | r ← r_all( v , vref)_Ip
                            | s ← sloc( id , r)
                            | t ← r × s
                            | drv ← ( r_grad( v , vref, Ip))^T
                            | dsv ← ( s_grad( v , vref, Ip , id))^T
                            | dtv ← t_grad( v , vref, Ip , id)^T
                            |
                            |          [ 2·r_1·drv^⟨1⟩                (s_1·drv^⟨1⟩ + r_1·dsv^⟨1⟩)                (t_1·drv^⟨1⟩ + r_1·dtv^⟨1⟩)                ]^T
                            |          | 2·r_2·drv^⟨2⟩                (s_2·drv^⟨2⟩ + r_2·dsv^⟨2⟩)                (t_2·drv^⟨2⟩ + r_2·dtv^⟨2⟩)                |
                            |          | 2·r_3·drv^⟨3⟩                (s_3·drv^⟨3⟩ + r_3·dsv^⟨3⟩)                (t_3·drv^⟨3⟩ + r_3·dtv^⟨3⟩)                |
                            | dNdv ←   | 2·(r_2·drv^⟨1⟩ + r_1·drv^⟨2⟩)  (s_2·drv^⟨1⟩ + s_1·drv^⟨2⟩ + r_2·dsv^⟨1⟩ + r_1·dsv^⟨2⟩)  (t_2·drv^⟨1⟩ + t_1·drv^⟨2⟩ + r_2·dtv^⟨1⟩ + r_1·dtv^⟨2⟩)  |
                            |          | 2·(r_3·drv^⟨2⟩ + r_2·drv^⟨3⟩)  (s_3·drv^⟨2⟩ + s_2·drv^⟨3⟩ + r_3·dsv^⟨2⟩ + r_2·dsv^⟨3⟩)  (t_3·drv^⟨2⟩ + t_2·drv^⟨3⟩ + r_3·dtv^⟨2⟩ + r_2·dtv^⟨3⟩)  |
                            |          | 2·(r_3·drv^⟨1⟩ + r_1·drv^⟨3⟩)  (s_3·drv^⟨1⟩ + s_1·drv^⟨3⟩ + r_3·dsv^⟨1⟩ + r_1·dsv^⟨3⟩)  (t_3·drv^⟨1⟩ + t_1·drv^⟨3⟩ + r_3·dtv^⟨1⟩ + r_1·dtv^⟨3⟩)  |
                            | dNdv
```

```
dNdv_x_σ( v , vref, Ip , σ_mul , id) := | dNdvar ← dNdv( v , vref, Ip , id)
                                        | for ir ∈ 1 .. 3
                                        |   dN ← 0
                                        |   for is ∈ 1 .. 6
                                        |     dN ← dN + dNdvar_ir,is · σmul_is
                                        |   for js ∈ 1 .. 6
                                        |     dNdv_x_σ_ir,js ← dN_js
                                        | dNdv_x_σ
```

```
dNdv_x_ef( v , vref, Ip , ef, id) := | dNvar ← dNdv( v , vref, Ip , id)
                                     | for is ∈ 1 .. 6
                                     |   dN ← 0
                                     |   for ir ∈ 1 .. 3
                                     |     dN ← dN + dNvar_ir,is · ef_ir
                                     |   for js ∈ 1 .. 6
                                     |     dNdv_x_ef_is,js ← dN_js
                                     | dNdv_x_ef
```

id = POD number

Orthogonal 2nd and 3rd crack variant

$$
\begin{aligned}
&\text{dNdvo}(v, \text{vref}, \text{Ip}, \text{id}, \text{rl}) := \\
&\quad r\sigma \leftarrow \text{r\_all}(v, \text{vref})_{\text{Ip}} \\
&\quad r \leftarrow \text{r\_ortho}(\text{rl}, r\sigma) \\
&\quad s \leftarrow \text{sloc}(\text{id}, r) \\
&\quad t \leftarrow r \times s \\
&\quad dr\sigma v \leftarrow (\text{r\_grad}(v, \text{vref}, \text{Ip})) \\
&\quad drv \leftarrow (\text{drdor}(\text{rl}, r\sigma) \cdot dr\sigma v)^{T} \\
&\quad dsv \leftarrow (\text{s\_grado}(v, \text{vref}, \text{Ip}, \text{id}, \text{rl}))^{T} \\
&\quad dtv \leftarrow \text{t\_grado}(v, \text{vref}, \text{Ip}, \text{id}, \text{rl})^{T} \\
&\quad dNdv \leftarrow \begin{bmatrix}
2 \cdot r_1 \cdot drv^{\langle 1 \rangle} & \left(s_1 \cdot drv^{\langle 1 \rangle} + r_1 \cdot dsv^{\langle 1 \rangle}\right) & \left(t_1 \cdot drv^{\langle 1 \rangle} + r_1 \cdot dtv^{\langle 1 \rangle}\right) \\
2 \cdot r_2 \cdot drv^{\langle 2 \rangle} & \left(s_2 \cdot drv^{\langle 2 \rangle} + r_2 \cdot dsv^{\langle 2 \rangle}\right) & \left(t_2 \cdot drv^{\langle 2 \rangle} + r_2 \cdot dtv^{\langle 2 \rangle}\right) \\
2 \cdot r_3 \cdot drv^{\langle 3 \rangle} & \left(s_3 \cdot drv^{\langle 3 \rangle} + r_3 \cdot dsv^{\langle 3 \rangle}\right) & \left(t_3 \cdot drv^{\langle 3 \rangle} + r_3 \cdot dtv^{\langle 3 \rangle}\right) \\
2 \cdot \left(r_2 \cdot drv^{\langle 1 \rangle} + r_1 \cdot drv^{\langle 2 \rangle}\right) & \left(s_2 \cdot drv^{\langle 1 \rangle} + s_1 \cdot drv^{\langle 2 \rangle} + r_2 \cdot dsv^{\langle 1 \rangle} + r_1 \cdot dsv^{\langle 2 \rangle}\right) & \left(t_2 \cdot drv^{\langle 1 \rangle} + t_1 \cdot drv^{\langle 2 \rangle} + r_2 \cdot dtv^{\langle 1 \rangle} + r_1 \cdot dtv^{\langle 2 \rangle}\right) \\
2 \cdot \left(r_3 \cdot drv^{\langle 2 \rangle} + r_2 \cdot drv^{\langle 3 \rangle}\right) & \left(s_3 \cdot drv^{\langle 2 \rangle} + s_2 \cdot drv^{\langle 3 \rangle} + r_3 \cdot dsv^{\langle 2 \rangle} + r_2 \cdot dsv^{\langle 3 \rangle}\right) & \left(t_3 \cdot drv^{\langle 2 \rangle} + t_2 \cdot drv^{\langle 3 \rangle} + r_3 \cdot dtv^{\langle 2 \rangle} + r_2 \cdot dtv^{\langle 3 \rangle}\right) \\
2 \cdot \left(r_3 \cdot drv^{\langle 1 \rangle} + r_1 \cdot drv^{\langle 3 \rangle}\right) & \left(s_3 \cdot drv^{\langle 1 \rangle} + s_1 \cdot drv^{\langle 3 \rangle} + r_3 \cdot dsv^{\langle 1 \rangle} + r_1 \cdot dsv^{\langle 3 \rangle}\right) & \left(t_3 \cdot drv^{\langle 1 \rangle} + t_1 \cdot drv^{\langle 3 \rangle} + r_3 \cdot dtv^{\langle 1 \rangle} + r_1 \cdot dtv^{\langle 3 \rangle}\right)
\end{bmatrix}^{T} \\
&\quad dNdv
\end{aligned}
$$

$$
\begin{aligned}
&\text{dNdv\_x\_}\sigma\text{o}\left(v, \text{vref}, \text{Ip}, \sigma_{\text{mul}}, \text{id}, \text{rl}\right) := \\
&\quad \text{dNdvar} \leftarrow \text{dNdvo}(v, \text{vref}, \text{Ip}, \text{id}, \text{rl}) \\
&\quad \text{for } ir \in 1..3 \\
&\quad\quad dN \leftarrow 0 \\
&\quad\quad \text{for } is \in 1..6 \\
&\quad\quad\quad dN \leftarrow dN + \text{dNdvar}_{ir, is} \cdot \sigma\text{mul}_{is} \\
&\quad\quad \text{for } js \in 1..6 \\
&\quad\quad\quad \text{dNdv\_x\_}\sigma_{ir, js} \leftarrow dN_{js} \\
&\quad \text{dNdv\_x\_}\sigma
\end{aligned}
$$

$$
\begin{aligned}
&\text{dNdv\_x\_ef}\sigma(v, \text{vref}, \text{Ip}, \text{ef}, \text{id}, \text{rl}) := \\
&\quad \text{dNvar} \leftarrow \text{dNdvo}(v, \text{vref}, \text{Ip}, \text{id}, \text{rl}) \\
&\quad \text{for } is \in 1..6 \\
&\quad\quad dN \leftarrow 0 \\
&\quad\quad \text{for } ir \in 1..3 \\
&\quad\quad\quad dN \leftarrow dN + \text{dNvar}_{ir, is} \cdot \text{ef}_{ir} \\
&\quad\quad \text{for } js \in 1..6 \\
&\quad\quad\quad \text{dNdv\_x\_ef}_{is, js} \leftarrow dN_{js} \\
&\quad \text{dNdv\_x\_ef}
\end{aligned}
$$

$$
\begin{aligned}
&\Delta\text{No}(v, \text{vref}, \text{Ip}, \Delta\sigma, \text{id}, \text{rl}) := \\
&\quad \text{dNdvar} \leftarrow \text{dNdvo}(v, \text{vref}, \text{Ip}, \text{id}, \text{rl}) \\
&\quad \text{for } ir \in 1..3 \\
&\quad\quad \text{for } is \in 1..6 \\
&\quad\quad\quad \Delta N_{ir, is} \leftarrow \text{dNdvar}_{ir, is} \cdot \Delta\sigma \\
&\quad \Delta N
\end{aligned}
$$

For PODs at α_p to existing

$$
\begin{aligned}
&\mathrm{dNdv}\alpha(v, \mathrm{vref}, lp, id, r1) := \\
&\quad r\sigma \leftarrow r\_all(v, \mathrm{vref})_{lp} \\
&\quad mul \leftarrow 1 \\
&\quad mul \leftarrow -1 \quad \text{if } r1 \cdot r\sigma < 0 \\
&\quad r \leftarrow \left(\cos(\alpha_p)\cdot r1 + \sin(\alpha_p)\cdot r\_ortho(r1, r\sigma\cdot mul)\right)\cdot mul \\
&\quad s \leftarrow sloc(id, r) \\
&\quad t \leftarrow r \times s \\
&\quad dr\sigma v \leftarrow (r\_grad(v, \mathrm{vref}, lp)) \\
&\quad drv \leftarrow \left(drdr_\alpha(r1, r\sigma)\cdot dr\sigma v\cdot mul\right)^T \\
&\quad dsv \leftarrow (s\_grad\alpha(v, \mathrm{vref}, lp, id, r1))^T \\
&\quad dtv \leftarrow t\_grad\alpha(v, \mathrm{vref}, lp, id, r1)^T \\
&\quad dNdv \leftarrow \begin{bmatrix}
2\cdot r_1\cdot drv^{\langle 1\rangle} & \left(s_1\cdot drv^{\langle 1\rangle} + r_1\cdot dsv^{\langle 1\rangle}\right) & \left(t_1\cdot drv^{\langle 1\rangle} + r_1\cdot dtv^{\langle 1\rangle}\right) \\
2\cdot r_2\cdot drv^{\langle 2\rangle} & \left(s_2\cdot drv^{\langle 2\rangle} + r_2\cdot dsv^{\langle 2\rangle}\right) & \left(t_2\cdot drv^{\langle 2\rangle} + r_2\cdot dtv^{\langle 2\rangle}\right) \\
2\cdot r_3\cdot drv^{\langle 3\rangle} & \left(s_3\cdot drv^{\langle 3\rangle} + r_3\cdot dsv^{\langle 3\rangle}\right) & \left(t_3\cdot drv^{\langle 3\rangle} + r_3\cdot dtv^{\langle 3\rangle}\right) \\
2\cdot\left(r_2\cdot drv^{\langle 1\rangle} + r_1\cdot drv^{\langle 2\rangle}\right) & \left(s_2\cdot drv^{\langle 1\rangle} + s_1\cdot drv^{\langle 2\rangle} + r_2\cdot dsv^{\langle 1\rangle} + r_1\cdot dsv^{\langle 2\rangle}\right) & \left(t_2\cdot drv^{\langle 1\rangle} + t_1\cdot drv^{\langle 2\rangle} + r_2\cdot dtv^{\langle 1\rangle} + r_1\cdot dtv^{\langle 2\rangle}\right) \\
2\cdot\left(r_3\cdot drv^{\langle 2\rangle} + r_2\cdot drv^{\langle 3\rangle}\right) & \left(s_3\cdot drv^{\langle 2\rangle} + s_2\cdot drv^{\langle 3\rangle} + r_3\cdot dsv^{\langle 2\rangle} + r_2\cdot dsv^{\langle 3\rangle}\right) & \left(t_3\cdot drv^{\langle 2\rangle} + t_2\cdot drv^{\langle 3\rangle} + r_3\cdot dtv^{\langle 2\rangle} + r_2\cdot dtv^{\langle 3\rangle}\right) \\
2\cdot\left(r_3\cdot drv^{\langle 1\rangle} + r_1\cdot drv^{\langle 3\rangle}\right) & \left(s_3\cdot drv^{\langle 1\rangle} + s_1\cdot drv^{\langle 3\rangle} + r_3\cdot dsv^{\langle 1\rangle} + r_1\cdot dsv^{\langle 3\rangle}\right) & \left(t_3\cdot drv^{\langle 1\rangle} + t_1\cdot drv^{\langle 3\rangle} + r_3\cdot dtv^{\langle 1\rangle} + r_1\cdot dtv^{\langle 3\rangle}\right)
\end{bmatrix}^T \\
&\quad dNdv
\end{aligned}
$$

$$
\begin{aligned}
&\mathrm{dNdv\_x\_}\sigma\alpha(v, \mathrm{vref}, lp, \sigma_{mul}, id, r1) := \\
&\quad dNdvar \leftarrow \mathrm{dNdv}\alpha(v, \mathrm{vref}, lp, id, r1) \\
&\quad \text{for } ir \in 1..3 \\
&\quad\quad dN \leftarrow 0 \\
&\quad\quad \text{for } is \in 1..6 \\
&\quad\quad\quad dN \leftarrow dN + dNdvar_{ir, is}\cdot \sigma mul_{is} \\
&\quad\quad \text{for } js \in 1..6 \\
&\quad\quad\quad \mathrm{dNdv\_x\_}\sigma_{ir, js} \leftarrow dN_{js} \\
&\quad \mathrm{dNdv\_x\_}\sigma
\end{aligned}
$$

$$
\begin{aligned}
&\mathrm{dNdv\_x\_ef}\alpha(v, \mathrm{vref}, lp, ef, id, r1) := \\
&\quad dNvar \leftarrow \mathrm{dNdv}\alpha(v, \mathrm{vref}, lp, id, r1) \\
&\quad \text{for } is \in 1..6 \\
&\quad\quad dN \leftarrow 0 \\
&\quad\quad \text{for } ir \in 1..3 \\
&\quad\quad\quad dN \leftarrow dN + dNvar_{ir, is}\cdot ef_{ir} \\
&\quad\quad \text{for } js \in 1..6 \\
&\quad\quad\quad \mathrm{dNdv\_x\_ef}_{is, js} \leftarrow dN_{js} \\
&\quad \mathrm{dNdv\_x\_ef}
\end{aligned}
$$

$$
\begin{aligned}
&\Delta N\alpha(v, \mathrm{vref}, lp, \Delta\sigma, id, r1) := \\
&\quad dNdvar \leftarrow \mathrm{dNdv}\alpha(v, \mathrm{vref}, lp, id, r1) \\
&\quad \text{for } ir \in 1..3 \\
&\quad\quad \text{for } is \in 1..6 \\
&\quad\quad\quad \Delta N_{ir, is} \leftarrow dNdvar_{ir, is}\cdot\Delta\sigma \\
&\quad \Delta N
\end{aligned}
$$

Stress and strain transformation matrices

$$N(r,s,t) := \begin{bmatrix} (r_1)^2 & (r_2)^2 & (r_3)^2 & 2\cdot r_1\cdot r_2 & 2\cdot r_2\cdot r_3 & 2\cdot r_1\cdot r_3 \\ r_1\cdot s_1 & r_2\cdot s_2 & r_3\cdot s_3 & r_2\cdot s_1 + r_1\cdot s_2 & r_3\cdot s_2 + r_2\cdot s_3 & r_1\cdot s_3 + r_3\cdot s_1 \\ r_1\cdot t_1 & r_2\cdot t_2 & r_3\cdot t_3 & r_2\cdot t_1 + r_1\cdot t_2 & r_3\cdot t_2 + r_2\cdot t_3 & r_1\cdot t_3 + r_3\cdot t_1 \end{bmatrix}$$

$$N\varepsilon(r,s,t) := \begin{bmatrix} (r_1)^2 & (r_2)^2 & (r_3)^2 & r_1\cdot r_2 & r_2\cdot r_3 & r_1\cdot r_3 \\ 2\cdot(r_1\cdot s_1) & 2\cdot(r_2\cdot s_2) & 2\cdot(r_3\cdot s_3) & r_2\cdot s_1 + r_1\cdot s_2 & r_3\cdot s_2 + r_2\cdot s_3 & r_1\cdot s_3 + r_3\cdot s_1 \\ 2\cdot(r_1\cdot t_1) & 2\cdot(r_2\cdot t_2) & 2\cdot(r_3\cdot t_3) & r_2\cdot t_1 + r_1\cdot t_2 & r_3\cdot t_2 + r_2\cdot t_3 & r_1\cdot t_3 + r_3\cdot t_1 \end{bmatrix}$$

POD direction

$$\begin{aligned} &PODdir(v, vref, Ip, ipod) := \\ &\quad v_{pr} \leftarrow prl(v) \\ &\quad r\_pod \leftarrow r\_all(v, vref)_{Ip} \\ &\quad s\_pod \leftarrow sloc\left(ns_{ipod}, r\_pod\right) \\ &\quad t\_pod \leftarrow r\_pod \times s\_pod \\ &\quad \begin{pmatrix} v_{pr_1} & r\_pod_1 & s\_pod_1 & t\_pod_1 \\ v_{pr_2} & r\_pod_2 & s\_pod_2 & t\_pod_2 \\ v_{pr_3} & r\_pod_3 & s\_pod_3 & t\_pod_3 \end{pmatrix} \end{aligned}$$

Orthogonal 2nd and 3rd crack variants

$$\begin{aligned} &PODdiro(v, vref, Ip, ipod, rl) := \\ &\quad v_{pr} \leftarrow prl(v) \\ &\quad r\_\sigma \leftarrow r\_all(v, vref)_{Ip} \\ &\quad r\_pod \leftarrow r\_ortho(rl, r\_\sigma) \\ &\quad s\_pod \leftarrow sloc\left(ns_{ipod}, r\_pod\right) \\ &\quad t\_pod \leftarrow r\_pod \times s\_pod \\ &\quad \begin{pmatrix} v_{pr_1} & r\_pod_1 & s\_pod_1 & t\_pod_1 \\ v_{pr_2} & r\_pod_2 & s\_pod_2 & t\_pod_2 \\ v_{pr_3} & r\_pod_3 & s\_pod_3 & t\_pod_3 \end{pmatrix} \end{aligned}$$

Cartesian to direct

Stress transformation matrix

$$Np(r,s,t) := \begin{bmatrix} (r_1)^2 & (r_2)^2 & (r_3)^2 & 2\cdot r_1\cdot r_2 & 2\cdot r_2\cdot r_3 & 2\cdot r_1\cdot r_3 \\ (s_1)^2 & (s_2)^2 & (s_3)^2 & 2\cdot s_1\cdot s_2 & 2\cdot s_2\cdot s_3 & 2\cdot s_1\cdot s_3 \\ (t_1)^2 & (t_2)^2 & (t_3)^2 & 2\cdot t_1\cdot t_2 & 2\cdot t_2\cdot t_3 & 2\cdot t_1\cdot t_3 \end{bmatrix}$$

Strain transformation matrix

Directional transformation matrix of principal axes

$$T_d(rp, sp, tp) := \begin{pmatrix} rp_1 & rp_2 & rp_3 \\ sp_1 & sp_2 & sp_3 \\ tp_1 & tp_2 & tp_3 \end{pmatrix}$$

PODs which form at α_p to existing POD I_p

$$\begin{aligned} &PODdir\alpha(v, vref, Ip, ipod, r_e, \alpha_p) := \\ &\quad v_{pr} \leftarrow prl(v) \\ &\quad r\_\sigma \leftarrow r\_all(v, vref)_{Ip} \\ &\quad mul \leftarrow 1 \\ &\quad mul \leftarrow -1 \text{ if } r\_\sigma\cdot r_e < 0 \\ &\quad r\_orth \leftarrow r\_ortho\left(r_e, r\_\sigma\cdot mul\right) \\ &\quad r\_pod \leftarrow \left(\cos(\alpha_p)\cdot r_e + \sin(\alpha_p)\cdot r\_orth\right)\cdot mul \\ &\quad s\_pod \leftarrow sloc\left(ns_{ipod}, r\_pod\right) \\ &\quad t\_pod \leftarrow r\_pod \times s\_pod \\ &\quad \begin{pmatrix} v_{pr_1} & r\_pod_1 & s\_pod_1 & t\_pod_1 \\ v_{pr_2} & r\_pod_2 & s\_pod_2 & t\_pod_2 \\ v_{pr_3} & r\_pod_3 & s\_pod_3 & t\_pod_3 \end{pmatrix} \end{aligned}$$

Local damage parameter update

$$\text{zeta}(e,\zeta) := \begin{bmatrix} z \leftarrow \zeta f(e) \\ \zeta \leftarrow z \text{ if } z > \zeta \\ \zeta \end{bmatrix}$$

Equivalent strain-local strain rate and local strain related open vector products

$$a_\zeta(\zeta,e,ee) := (ee)\cdot d\phi de(e)^T \qquad a_{eg}(e,ee) := (ee)\cdot de_{gn}(e)^T$$

$$a_g(ee) := \begin{bmatrix} dgde \leftarrow \dfrac{-1}{\sqrt{1+m_g^{\,2}}}\cdot\phi grad(ee) \text{ if } \left(\phi_{inter}(ee) < 0\right)\cdot\left(\phi_{cl}(ee) > 0\right) \\ dgde \leftarrow \dfrac{1}{|ee| + 10^{-10}}\cdot\left(ee_1 \;\; ee_2 \;\; ee_3\right)^T \text{ if } \phi_{cl}(ee) \le 0 \\ dgde \leftarrow (0\;\;0\;\;0)^T \text{ if } \phi_{inter}(ee) \ge 0 \\ (ee)\cdot dgde^T \end{bmatrix}$$

Local loss of contact matrix, in terms of total local strain

$$mx(\zeta,\kappa,e_g,ee) := \begin{bmatrix} \text{"Set proportion function values"} \\ g_b \leftarrow gbar(ee) \\ hc \leftarrow h_c(\zeta,\kappa) \\ hf \leftarrow h_f(\zeta,\kappa,e_g,g_b) \\ \text{"Open"} \\ \Phi_h \leftarrow I_{nul} \text{ if } \left(\phi_{inter}(ee) \ge 0\right) \\ \text{"Interlock"} \\ \Phi_h \leftarrow hf\cdot\Phi g(ee) \text{ if } \phi_{inter}(ee) < 0 \wedge \phi_{cl}(ee) > 0 \\ \text{"Closed"} \\ \Phi_h \leftarrow hf\cdot I_3 \text{ if } \left(\phi_{cl}(ee) \le 0\right) \\ mx \leftarrow hc\cdot I_3 + \Phi_h \\ mx \end{bmatrix}$$

Only employed if on yield surface

$$dm\kappa(\zeta,\kappa,e_g,ee) := \begin{bmatrix} \text{"Set proportion function values"} \\ g_b \leftarrow gbar(ee) \\ hc \leftarrow h_c(\zeta,\kappa) \\ hf \leftarrow h_f(\zeta,\kappa,e_g,g_b) \\ dhcd\kappa \leftarrow dhd\kappa_c(\zeta,\kappa) \\ dhfd\kappa \leftarrow dh_{f\kappa}(\zeta,\kappa,e_g,g_b) \\ \text{"Open"} \\ d\Phi e_{h\kappa} \leftarrow (0\;\;0\;\;0)^T \text{ if } \left(\phi_{inter}(ee) \ge 0\right) \\ \text{"Interlock"} \\ d\Phi e_{h\kappa} \leftarrow dhfd\kappa\cdot\Phi g(ee)\cdot(ee) \text{ if } \left(\phi_{inter}(ee) < 0\right)\cdot\left(\phi_{cl}(ee) > 0\right) \\ \text{"Closed"} \\ d\Phi e_{h\kappa} \leftarrow dhfd\kappa\cdot I_3\cdot(ee) \text{ if } \left(\phi_{cl}(ee) \le 0\right) \\ dhcd\kappa\cdot(ee) + d\Phi e_{h\kappa} \end{bmatrix}$$

Rate of loss of contact matrix, in terms of local strain

$dmx(\zeta, \kappa, e_g, e, ee) :=$

"Set proportion function values"

$g_b \leftarrow gbar(ee)$

$hc \leftarrow h_c(\zeta, \kappa)$

$hf \leftarrow h_f(\zeta, \kappa, e_g, g_b)$

$dhdz_c \leftarrow 0$

$dhdz_c \leftarrow dhd\zeta_c(\zeta, \kappa)$ if $\phi(e, \zeta) > -\varepsilon_{tol}$

$dhf_\zeta \leftarrow 0$

$dhf_\zeta \leftarrow dhf_\zeta(\zeta, \kappa, e_g, g_b)$ if $\phi(e, \zeta) > -\varepsilon_{tol}$

$dhfeg \leftarrow dhf_{eg}(\zeta, \kappa, e_g, g_b)$

$dhfg \leftarrow dhf_g(\zeta, \kappa, e_g, g_b)$

"Open"

if $(\phi_{inter}(ee) \geq 0)$

- $\Phi \leftarrow I_{nul}$
- $\Phi_h \leftarrow I_{nul}$
- $d\Phi_{hz} \leftarrow I_{nul}$
- $d\Phi_{heg} \leftarrow I_{nul}$
- $d\Phi_{hg} \leftarrow I_{nul}$

"Interlock"

if $(\phi_{inter}(ee) < 0) \cdot (\phi_{cl}(ee) > 0)$

- $\Phi \leftarrow \Phi g(ee)$
- $\Phi_h \leftarrow hf \cdot \Phi g(ee)$
- $d\Phi_{hz} \leftarrow dhf_\zeta \cdot \Phi g(ee)$
- $d\Phi_{heg} \leftarrow dhfeg \cdot \Phi g(ee)$
- $d\Phi_{hg} \leftarrow dhfg \cdot \Phi g(ee)$

"Closed"

if $(\phi_{cl}(ee) \leq 0)$

- $\Phi \leftarrow I_3$
- $\Phi_h \leftarrow hf \cdot I_3$
- $d\Phi_{hz} \leftarrow dhf_\zeta \cdot I_3$
- $d\Phi_{heg} \leftarrow dhfeg \cdot I_3$
- $d\Phi_{hg} \leftarrow dhfg \cdot I_3$

$mx \leftarrow hc \cdot I_3 + \Phi_h$

$dmxz \leftarrow (dhdz_c \cdot I_3 + d\Phi_{hz}) \cdot a_\zeta(\zeta, e, ee)$

$dmxe \leftarrow d\Phi_{heg} \cdot a_{eg}(e, ee)$

$dmxg \leftarrow d\Phi_{hg} \cdot a_g(ee)$

$(dmxz + dmxg + dmxe + mx)$

Added flexibility with rfact to avoid 0 added flexibility

$\varepsilon_{tol} := \varepsilon_t \cdot 10^{-6}$

$dmxp(\zeta, \kappa, e_g, e, ee) :=$

"Set proportion function values"

$g_b \leftarrow gbar(ee)$

$hc \leftarrow h_c(\zeta, \kappa)$

$hf \leftarrow h_f(\zeta, \kappa, e_g, g_b)$

$dhdz_c \leftarrow 0$

$dhdz_c \leftarrow dhd\zeta_c(\zeta, \kappa)$ if $\phi(e, \zeta) > -\varepsilon_{tol}$

$dhf_\zeta \leftarrow 0$

$dhf_\zeta \leftarrow dhf_\zeta(\zeta, \kappa, e_g, g_b)$ if $\phi(e, \zeta) > -\varepsilon_{tol}$

$dhfg \leftarrow dhf_g(\zeta, \kappa, e_g, g_b)$

"Open"

if $(\phi_{inter}(ee) \geq 0)$

- $\Phi \leftarrow I_{nul}$
- $\Phi_h \leftarrow I_{nul}$
- $d\Phi_{hg} \leftarrow I_{nul}$

"Interlock"

if $(\phi_{inter}(ee) < 0) \cdot (\phi_{cl}(ee) > 0)$

- $\Phi \leftarrow \Phi g(ee)$
- $\Phi_h \leftarrow hf \cdot \Phi g(ee)$
- $d\Phi_{hg} \leftarrow dhfg \cdot \Phi g(ee)$

"Closed"

if $(\phi_{cl}(ee) \leq 0)$

- $\Phi \leftarrow I_3$
- $\Phi_h \leftarrow hf \cdot I_3$
- $d\Phi_{hg} \leftarrow dhfg \cdot I_3$

$mx \leftarrow hc \cdot I_3 + \Phi_h$

$dmxg \leftarrow d\Phi_{hg} \cdot a_g(ee)$

$(dmxg + mx)$

Local elastic-damage-contact matrices

Flexibility w.r.t e

$$c_{ls}(\zeta,\kappa,e_g,ee) := mx(\zeta,\kappa,e_g,ee)^{-1}\cdot C_L$$

$$c_{lt}(\zeta,\kappa,e_g,e,ee) := \left| \begin{array}{l} dmt \leftarrow dmx(\zeta,\kappa,e_g,e,ee) \\ \text{for } i \in 1..3 \\ \quad dmt_{i,i} \leftarrow 10^{-8} \text{ if } |dmt_{i,i}| < 10^{-8} \\ (dmt)^{-1}\cdot C_L \end{array} \right.$$

$$ea(\zeta,\kappa,e_g,ee,e) := e - mx(\zeta,\kappa,e_g,ee)\cdot(ee)$$

stiffness w.r.t e

$$D_{ls}(\zeta,\kappa,e_g,ee) := D_L\cdot mx(\zeta,\kappa,e_g,ee)$$

$$D_{lt}(\zeta,\kappa,e_g,e,ee) := D_L\cdot dmx(\zeta,\kappa,e_g,e,ee)$$

$$D_{lts}(\zeta,\kappa,e_g,e,ee) := D_L\cdot mx(\zeta,\kappa,e_g,ee)$$

$$D_{lp}(\zeta,\kappa,e_g,e,ee) := D_L\cdot dmxp(\zeta,\kappa,e_g,e,ee)$$

$$M_p(\zeta,\kappa,e_g,e,ee) := dmx(\zeta,\kappa,e_g,e,ee)^{-1}\cdot dmxp(\zeta,\kappa,e_g,e,ee)$$

flexibility w.r.t ef

$$c_{lsf}(\zeta,\kappa,e_g,ee) := c_{ls}(\zeta,\kappa,e_g,ee) - C_L$$

$$c_{ltf}(\zeta,\kappa,e_g,e,ee) := dmx(\zeta,\kappa,e_g,e,ee)^{-1}\cdot C_L - C_L$$

Variation of stiffness with plastic parameter κ

$$D_{l\kappa}(\zeta,\kappa,e_g,ee) := D_L\cdot dm\kappa(\zeta,\kappa,e_g,ee)$$

$$M_\kappa(\zeta,\kappa,e_g,e,ee) := dmx(\zeta,\kappa,e_g,e,ee)^{-1}\cdot dm\kappa(\zeta,\kappa,e_g,ee)$$

Terms in CPP and consistent matrix

Form when damage and local plasticity are active. Ip gives the principal stress direction appropriate for a POD number. Only applied to new PODs

$$A_{dp}(np,\zeta,\kappa,e_g,e,ee,\Delta\mu,sf,r,s,t,Ip) := \left[I_6 + D_{el}\cdot\left[\sum_{j=1}^{np} N(r_j,s_j,t_j)^T\cdot\left(dmxp(\zeta_j,\kappa,eg_j,e_j,ee_j)\cdot d2gds(sf_j)\cdot N(r_j,s_j,t_j)\cdot\Delta\mu_j\right)\right]\right]^{-1}\cdot D_{el}$$

$$N\Delta_{dp}(r,s,t,np,n_{prv},\Delta\mu,\zeta,\kappa,e_g,e,ee,sf,i,Ip) := N(r_i,s_i,t_i) + D_{lp}(\zeta_i,\kappa,eg_i,e_i,ee_i)\cdot d2gds(sf_i)\cdot N(r_i,s_i,t_i)\cdot\Delta\mu_i$$

CPP terms **Damage and local plasticity only**

$$A_{cdp}(np,sf,\Delta\mu,\zeta,\kappa,e_g,e,ee,r,s,t) := \left[I_6 + D_{el}\cdot\left[\sum_{j=1}^{np} N(r_j,s_j,t_j)^T\cdot\left(c_{ltf}(\zeta_j,\kappa,eg_j,e_j,ee_j)\cdot N(r_j,s_j,t_j) + M_p(\zeta_j,\kappa,eg_j,e_j,ee_j)\cdot\Delta\mu_j\cdot d2gds(sf_j)\cdot N(r_j,s_j,t_j)\right)\right]\right]^{-1}\cdot D_{el}$$

$$I_{\Delta Ndp}(np,n_{prv},\sigma_I,\sigma,sf,f_t,\Delta\mu,\zeta,\kappa,e_g,e,ee,r,s,t,Ip,Def) := I_6 - \sum_{j=n_{prv}+1}^{np}\left[N(r_j,s_j,t_j)^T\cdot\left(\begin{array}{l} c_{ltf}(\zeta_j,\kappa,eg_j,e_j,ee_j)\cdot dNdv\_x\_\sigma(\sigma_I,f_t,Ip_j,\sigma,ns_j)\ \ldots \\ +\, M_p(\zeta_j,\kappa,eg_j,e_j,ee_j)\cdot\Delta\mu_j\cdot d2gds(sf_j)\cdot dNdv\_x\_\sigma(\sigma_I,f_t,Ip_j,\sigma,ns_j)\end{array}\right) + dNdv\_x\_ef(\sigma_I,f_t,Ip_j,ea(\zeta_j,\kappa,eg_j,ee_j,e_j),ns_j)\right]\cdot Def$$

$$fn_{dp}(sf,\Delta\mu,\zeta,\kappa,e_g,e,ee) := dfeds(\zeta,\kappa,sf)^T + dfedζ(\zeta,\kappa,sf)\cdot dζde(e)^T\cdot\left(c_{lt}(\zeta,\kappa,e_g,e,ee) + M_p(\zeta,\kappa,e_g,e,ee)\cdot\Delta\mu\cdot d2gds(sf)\right)$$

$$N\Phi_{dp}(sf,\Delta\mu,\zeta,\kappa,e_g,e,ee,r,s,t) := fn_{dp}(sf,\Delta\mu,\zeta,\kappa,e_g,e,ee)\cdot N(r,s,t)$$

Elastic damage matrix for trial stress predicion

$$D_{el}(np,\zeta,\kappa,e_g,ee,r,s,t) := \left[I_6 + D_{el}\cdot\left[\sum_{j=1}^{np} N(r_j,s_j,t_j)^T\cdot\left(c_{lsf}(\zeta_j,\kappa,eg_j,ee_j)\cdot N(r_j,s_j,t_j)\right)\right]\right]^{-1}\cdot D_{el}$$

Secant

Assemble coupled matrix and R.H.S.

Damage and local plasticity only

$$\text{Sol}_{e\mu}(F_E, B_E, P_E, F_\mu, B_\mu, P_\mu, np) :=$$
for $ip \in 1..np$
  $kl \leftarrow 1 + (ip - 1)\cdot 4$
  $R_{kl} \leftarrow F\mu_{ip}$
  for $i \in 1..3$
    $ki \leftarrow 1 + (ip - 1)\cdot 4 + i$
    $R_{ki} \leftarrow (FE_{ip})_i$
  for $jp \in 1..np$
    $irow \leftarrow 1 + (ip - 1)\cdot 4$
    $icol \leftarrow 1 + (jp - 1)\cdot 4$
    $Mat_{irow,icol} \leftarrow P\mu_{(ip-1)\cdot np+jp}$
    for $k \in 1..3$
      $Mat_{irow,icol+k} \leftarrow [B\mu_{(ip-1)\cdot np+jp}]_k$
      $Mat_{irow+k,icol} \leftarrow [PE_{(ip-1)\cdot np+jp}]_k$
    $elm \leftarrow BE_{(ip-1)\cdot np+jp}$
    for $k \in 1..3$
      for $l \in 1..3$
        $Mat_{irow+k,icol+l} \leftarrow elm_{k,l}$
$Mat^{-1}\cdot R$

Total local consistency

$$\text{Frhs}(\zeta, \kappa, eg, ee, e, r, s, t, \varepsilon_e, ip, np) := N(r_{ip}, s_{ip}, t_{ip})\cdot\left[D_{el}\cdot\left[\varepsilon_e - \sum_{j=1}^{np} N(r_j, s_j, t_j)^T\cdot(e_j - mx(\zeta_j, \kappa, eg_j, ee_j)\cdot ee_j)\right]\right] - D_{ls}(\zeta_{ip}, \kappa, eg_{ip}, ee_{ip})\cdot(ee_{ip})$$

$$\text{stress}(\zeta, \kappa, eg, ee, e, r, s, t, \varepsilon_e, np) := D_{el}\cdot\left[\varepsilon_e - \sum_{j=1}^{np} N(r_j, s_j, t_j)^T\cdot(e_j - mx(\zeta_j, \kappa, eg_j, ee_j)\cdot ee_j)\right]$$

Programmes for extracting $d\mu$ and local strains

$$\text{deloc}\varepsilon_{e\mu}(ip, unk) :=$$
for $i \in 1..3$
  $deloc_i \leftarrow unk_{1+(ip-1)\cdot 4+i}$
deloc

$$\text{dmiu}_{e\mu}(ip, unk) :=$$
$dmiu \leftarrow unk_{1+(ip-1)\cdot 4}$
dmiu

Gaussian Reduction with fixities

$n := 4$ $i := 1 .. n$ $ifx_i := 0$ $fx_i := 0$

Input
M = nxn matrix y R.H.S ifx = fixities fx = fixed values

Output
x=unknowns rc=reactions

```
Gaus(n, M, y, ifx, fx) :=
  for i ∈ 1 .. n
    rc_i ← 0
    x_i ← 0
    for j ∈ i .. n                    if ifx_i ≠ 0
      y_j ← y_j − M_j,i · fx_i
    if ifx_i = 0
      piv ← M_i,i
      for j ∈ i + 1 .. n              if i < n
        fac ← M_j,i / piv
        for k ∈ i .. n
          M_j,k ← M_j,k − fac·M_i,k
        y_j ← y_j − fac·y_i
  for i ∈ n .. 1
    piv ← M_i,i
    res ← y_i
    for j ∈ i + 1 .. n                if i < n
      res ← res − M_i,j · x_j
    if ifx_i ≠ 0
      x_i ← fx_i
      rc_i ← −res
    x_i ← res / piv                   if ifx_i = 0
  (x  rc)^T
```

Strain step

Initialise variables

$ne := 10$ $ie := 2 .. ne$ $iset := 1 .. 2$ $elocl_{iset} := \begin{pmatrix} \varepsilon_{ti} \\ 0 \\ 0 \end{pmatrix}$ $r_{iset} := \begin{pmatrix} 1 \\ 0 \\ 0 \end{pmatrix}$ $s_{iset} := \begin{pmatrix} 0 \\ 1 \\ 0 \end{pmatrix}$ $t_{iset} := \begin{pmatrix} 0 \\ 0 \\ 1 \end{pmatrix}$ $ep_{iset} := \begin{pmatrix} 0 \\ 0 \\ 0 \end{pmatrix}$ $dep_{iset} := \begin{pmatrix} 0 \\ 0 \\ 0 \end{pmatrix}$ $delocl_{iset} := \begin{pmatrix} 0 \\ 0 \\ 0 \end{pmatrix}$ $d\mu_{iset} := 0$

$eg_{iset} := 0$ $\kappa := 0$ $rf_{iset} := 1$ $\zeta_{iset} := \varepsilon_{ti} \cdot 1.0000000001$ $\Delta\mu_{iset} := 0$ $\Delta\lambda := 0$ $\Delta\kappa := 0$ $\Delta\varepsilon p := (0\ 0\ 0\ 0\ 0\ 0)^T$ $\Delta ep_{iset} := \begin{pmatrix} 0 \\ 0 \\ 0 \end{pmatrix}$ $sf_{iset} := \begin{pmatrix} 0 \\ 0 \\ 0 \end{pmatrix}$

$\zeta_{prv} := \zeta$ $eg_{iset} := e_{beg} \cdot 0.999999$ $Rep_{iset} := \begin{pmatrix} 0 \\ 0 \\ 0 \end{pmatrix}$ $R\varepsilon := (0\ 0\ 0\ 0\ 0\ 0)^T$ $R\kappa := 0$ $npod := 0$ $ee_{iset} := elocl_{iset} - ep_{iset}$

$\sigma_1 := \begin{pmatrix} 0 \\ 0 \\ 0 \\ 0 \\ 0 \\ 0 \end{pmatrix}$ $\varepsilon_1 := \begin{pmatrix} 0 \\ 0 \\ 0 \\ 0 \\ 0 \\ 0 \end{pmatrix}$ $\Delta\varepsilon := \begin{pmatrix} 0.00015 \\ 0.00001 \\ 0.00001 \\ 0 \\ 0 \\ 0 \end{pmatrix}$ $\varepsilon p := \begin{pmatrix} 0 \\ 0 \\ 0 \\ 0 \\ 0 \\ 0 \end{pmatrix}$ $\varepsilon p\_prv := \begin{pmatrix} 0 \\ 0 \\ 0 \\ 0 \\ 0 \\ 0 \end{pmatrix}$

Stress calculations

$\varepsilon_2 := \varepsilon_1 + \Delta\varepsilon$ $\varepsilon_2^T = (1.5 \times 10^{-4}\ \ 1 \times 10^{-5}\ \ 1 \times 10^{-5}\ \ 0\ \ 0\ \ 0)$

$\sigma tr := D_{el} \cdot \varepsilon_2$ $\sigma tr^T = (6.484472\ \ 1.614907\ \ 1.614907\ \ 0\ \ 0\ \ 0)$ $Z := Zf(\kappa)$

$Ftr := F(\sigma tr, Z)$ $Ftr = -4.680649$ $\kappa prev := \kappa$ $\varepsilon p\_prv := \varepsilon p$ $\sigma I := \sigma tr$ **Set trial stress**

Check if a POD forms and its direction

$pr1(\sigma tr)^T = (6.484472\ \ 1.614907\ \ 1.614907)$ $f_t = 2.9$ **POD forms**

$r\_\sigma := r\_all(\sigma tr, f_t)$ $r\_\sigma^T = \left[\begin{pmatrix} 1 \\ 0 \\ 0 \end{pmatrix}\ \begin{pmatrix} 0 \\ 1 \\ 0 \end{pmatrix}\ \begin{pmatrix} 0 \\ 0 \\ 1 \end{pmatrix}\right]$

$lp_1 := 1$ $\varepsilon e := \varepsilon_2 - \varepsilon p$ $\sigma pr := pr1(\sigma tr)$ $\sigma pr^T = (6.484472\ \ 1.614907\ \ 1.614907)$

$\begin{pmatrix} \sigma pr_1 & rd_1 & sd_1 & td_1 \\ \sigma pr_2 & rd_2 & sd_2 & td_2 \\ \sigma pr_3 & rd_3 & sd_3 & td_3 \end{pmatrix} := PODdir(\sigma I, f_t, lp_1, 1)$ $\sigma pr = \begin{pmatrix} 6.484472 \\ 1.614907 \\ 1.614907 \end{pmatrix}$ **Crack direction based on first trial stress**

$npod_{prv} := 0$ $npod := 1$ $nc_1 := 1$ $ip := 1 .. npod$ $jp := 1 .. npod$ $r_{ip} := rd$ $s_{ip} := sd$ $t_{ip} := tc$

$$r^T = \left[\begin{pmatrix} 0.952295508549404 \\ 0.305177431007984 \\ 5.26835606386175 \times 10^{-9} \end{pmatrix} \begin{pmatrix} 1 \\ 0 \\ 0 \end{pmatrix}\right] \quad s^T = \left[\begin{pmatrix} 0 \\ 1 \\ 0 \end{pmatrix} \begin{pmatrix} 0 \\ 1 \\ 0 \end{pmatrix} \; 0.539859\right] \quad t^T = \left[\begin{pmatrix} 0 \\ 0 \\ 1 \end{pmatrix} \begin{pmatrix} 0 \\ 0 \\ 1 \end{pmatrix} \; -0.83996\right]$$

Record variables before enter stress recovery

$npod := 1$ $ip := 1 .. npod$ $jp := 1 .. npod$ $\zeta rec := \zeta$ $\kappa_{prev} := \kappa$ $\varepsilon p\_prv := \varepsilon p$

$\zeta rec := \zeta$ $\zeta_{prv} := \zeta$ $eg_{prv} := eg$ $elocl_{prv} := elocl$ $ee_{prv} := ee$ $ep_{prv} := ep$ $\Delta\mu_{prv} := \Delta\mu$ $\Delta ep_{prv} := \Delta ep$

Reset all variables

$\Delta\kappa := 0$ $\kappa := 0$ $Z := Zf(\kappa)$ $\Delta\lambda := 0$ $R_\varepsilon := (0\ 0\ 0\ 0\ 0\ 0)^T$ $R_\kappa := 0$ $R_{ep}{}^T = \left[\begin{pmatrix} 0 \\ 0 \\ 0 \end{pmatrix} \begin{pmatrix} 0 \\ 0 \\ 0 \end{pmatrix}\right]$

$\Delta\varepsilon p := (0\ 0\ 0\ 0\ 0\ 0)^T$ $\varepsilon p := (0\ 0\ 0\ 0\ 0\ 0)^T$ $\varepsilon_e := \varepsilon_2 - \varepsilon p$

$\sigma_{tr} := D_{el} \cdot \varepsilon_2$ $\sigma_{tr}{}^T = (6.484472\ \ 1.614907\ \ 1.614907\ \ 0\ \ 0\ \ 0)$

$sf_{ip} := N(r_{ip}, s_{ip}, t_{ip}) \cdot \sigma_{tr}$ $sf_1{}^T = (6.484472\ \ 0\ \ 0)$

Evaluate the POD consistency

$F_{tr} := F(\sigma_{tr}, Z)$ $F_{tr} = -4.680649$

$Fe_{ip} := Frhs(\zeta, \kappa, eg, ee, elocl, r, s, t, \varepsilon_e, ip, npod)$ $Fe_1{}^T = (3.584472\ \ 0\ \ 0)$ $\sum_{j=1}^{npod} |Fe_j| = 3.584472$

$fe_{ip} := f(\zeta_{ip}, \kappa, sf_{ip})$ $fe_1 = 3.584472$

Increment 1 - Iteration 1

$N\Delta e_{ip} := N\Delta_{dp}(r, s, t, npod, npod_{prv}, \Delta\mu, \zeta, \kappa, eg, elocl, ee, sf, ip, Ip)$ $Ae := A_{dp}(npod, \zeta, \kappa, eg, elocl, ee, \Delta\mu, sf, r, s, t, Ip)$

$N\Xi_{ip} := N(r_{ip}, s_{ip}, t_{ip})^T (I_3 - dmx(\zeta_{ip}, \kappa, eg_{ip}, elocl_{ip}, ee_{ip}))$ $N\Psi_{ip} := N(r_{ip}, s_{ip}, t_{ip})^T \cdot dmxp(\zeta_{ip}, \kappa, eg_{ip}, elocl_{ip}, ee_{ip}) \cdot dgds(sf_{ip})$

$dfemod_{ip} := dfeds(\zeta_{ip}, \kappa, sf_{ip})^T \cdot N(r_{ip}, s_{ip}, t_{ip})$ $dfemod_1 = (1\ 0\ 0\ 0\ 0\ 0)$

$R_{\varepsilon m} := R_\varepsilon + d2G\sigma\kappa(\kappa) \cdot \Delta\lambda \cdot a_\kappa(\sigma_{tr}, \kappa, \Delta\lambda) \cdot R_\kappa$

$R_{\varepsilon\kappa} := R_{\varepsilon m} - \sum_{j=1}^{npod} N(r_j, s_j, t_j)^T \cdot (dm\kappa(\zeta_j, \kappa, eg_j, ee_j) \cdot a_\kappa(\sigma_{tr}, \kappa, \Delta\lambda) \cdot R_\kappa)$ $R_{\varepsilon\kappa p} := R_{\varepsilon\kappa} + \sum_{j=1}^{npod} N(r_j, s_j, t_j)^T \cdot dmxp(\zeta_j, \kappa, eg_j, elocl_j, ee_j) \cdot (R_{ep_j})$

Form coupled equations

$F_{\mu_{ip}} := f_{e_{ip}} - dfemod_{ip}^{T} \cdot (Ae \cdot R_{\varepsilon\kappa p})$ $\quad B_{\mu_{(ip-1)\cdot npod+jp}} := \left(dfemod_{ip} \cdot Ae \cdot N\Xi_{jp}\right)^{T}$ $\quad B_{\mu_{(ip-1)\cdot npod+ip}} := B_{\mu_{(ip-1)\cdot npod+ip}} - \left(dfed\zeta\left(\zeta_{ip}, \kappa, sf_{ip}\right) \cdot d\zeta de\left(elocl_{ip}\right)^{T}\right)^{T}$

$P_{\mu_{(ip-1)\cdot npod+jp}} := dfemod_{ip}^{T} \cdot \left(Ae \cdot N\Psi_{jp}\right)$ $\quad FE_{ip} := Fe_{ip} - N\Delta e_{ip} \cdot Ae \cdot R_{\varepsilon\kappa p} - D_{I\kappa}\left(\zeta_{ip}, \kappa, eg_{ip}, ee_{ip}\right) \cdot a_{\kappa}\left(\sigma_{tr}, \kappa, \Delta\lambda\right) \cdot R_{\kappa} + D_{Ip}\left(\zeta_{ip}, \kappa, eg_{ip}, elocl_{ip}, ee_{ip}\right) \cdot Rep_{ip}$

$BE_{(ip-1)\cdot npod+jp} := N\Delta e_{ip} \cdot Ae \cdot N\Xi_{jp}$ $\quad BE_{(ip-1)\cdot npod+ip} := BE_{(ip-1)\cdot npod+ip} + D_{It}\left(\zeta_{ip}, \kappa, eg_{ip}, elocl_{ip}, ee_{ip}\right)$

$PE_{(ip-1)\cdot npod+jp} := N\Delta e_{ip} \cdot Ae \cdot N\Psi_{jp}$ $\quad PE_{(ip-1)\cdot npod+ip} := PE_{(ip-1)\cdot npod+ip} - D_{Ip}\left(\zeta_{ip}, \kappa, eg_{ip}, elocl_{ip}, ee_{ip}\right) \cdot dgds\left(sf_{ip}\right)$

Solve coupled for unknowns

$unknown := Sol_{e\mu}\left(FE, BE, PE, F_{\mu}, B_{\mu}, P_{\mu}, npod\right)$ $\quad d\mu_{ip} := dmiu_{e\mu}(ip, unknown)$ $\quad delocl_{ip} := deloc\zeta_{\mu}(ip, unknown)$ $\quad d\mu_{1} = 8.486765 \times 10^{-6}$ $\quad delocl_{1}^{T} = \left(8.486765 \times 10^{-5} \;\; 0 \;\; 0\right)$

Update state variables

$$d\sigma := -Ae \cdot \left[R_{\varepsilon\kappa p} + \left[\sum_{j=1}^{npod} N\left(r_j, s_j, t_j\right)^{T} \cdot \left[\left(I_3 - dmx\left(\zeta_j, \kappa, eg_j, elocl_j, ee_j\right) \right) \cdot delocl_j + dmxp\left(\zeta_j, \kappa, eg_j, elocl_j, ee_j\right) \cdot dgds\left(sf_j\right) \cdot d\mu_j \right] \right] \right]$$

$d\sigma^{T} = (-4.038106 \;\; -0.712607 \;\; -0.712607 \;\; 0 \;\; 0 \;\; 0)$

$de_{ip} := R_{ep_{ip}} + dgds\left(sf_{ip}\right) \cdot d\mu_{ip} + \Delta\mu_{ip} \cdot d2gds\left(sf_{ip}\right) \cdot N\left(r_{ip}, s_{ip}, t_{ip}\right) \cdot d\sigma$ $\quad de_{1}^{T} = \left(8.486765 \times 10^{-6} \;\; 0 \;\; 0\right)$

$elocl_{ip} := elocl_{ip} + delocl_{ip}$ $\quad \zeta_{ip} := zeta\left(elocl_{ip}, \zeta prv_{ip}\right)$ $\quad \Delta ep_{ip} := \Delta ep_{ip} + de_{ip}$ $\quad ep_{ip} := epprv_{ip} + \Delta ep_{ip}$

$ee_{ip} := elocl_{ip} - ep_{ip}$ $\quad eg_{ip} := egn\left(elocl_{ip}, ee_{ip}\right)$ $\quad eg_{1} = 7.552794 \times 10^{-5}$

$$elocl_{1} = \begin{pmatrix} 1.53529411764706 \times 10^{-4} \\ 0 \\ 0 \end{pmatrix} \quad ep_{1} = \begin{pmatrix} 8.486765 \times 10^{-6} \\ 0 \\ 0 \end{pmatrix} \quad ee_{1} = \begin{pmatrix} 1.450426 \times 10^{-4} \\ 0 \\ 0 \end{pmatrix}$$

$\zeta_{1} = 1.535294 \times 10^{-4}$ $\quad \varepsilon_{ti} = 6.866176 \times 10^{-5}$

$\Delta\mu_{ip} := \Delta\mu_{ip} + d\mu_{ip}$ $\quad \Delta\mu^{T} = \left(8.486765 \times 10^{-6} \;\; 0\right)$ $\quad \varepsilon_{e} := \varepsilon_{2} - \varepsilon_{p}$ $\quad \varepsilon_{e}^{T} = \left(1.5 \times 10^{-4} \;\; 1 \times 10^{-5} \;\; 1 \times 10^{-5} \;\; 0 \;\; 0 \;\; 0\right)$

$\sigma_{tr} := stress\left(\zeta, \kappa, eg, ee, elocl, r, s, t, \varepsilon_{e}, npod\right)$ $\quad \sigma_{tr}^{T} = (2.481054 \;\; 0.908421 \;\; 0.908421 \;\; 0 \;\; 0 \;\; 0)$

$sf_{ip} := N\left(r_{ip}, s_{ip}, t_{ip}\right) \cdot \sigma_{tr}$ $\quad sf_{1}^{T} = (2.481054 \;\; 0 \;\; 0)$

Compute error measures

$Rep_{ip} := -\Delta ep_{ip} + \Delta\mu_{ip} \cdot dgds\left(sf_{ip}\right)$ $\quad Rep_{1}^{T} = (0 \;\; 0 \;\; 0)$ $\quad Fe_{ip} := Frhs\left(\zeta, \kappa, eg, ee, elocl, r, s, t, \varepsilon_{e}, ip, npod\right)$ $\quad \sum_{j=1}^{npod} \left|Fe_{j}\right| = 0$ $\quad f_{e_{ip}} := f\left(\zeta_{ip}, \kappa, sf_{ip}\right)$ $\quad f_{e_{1}} = -1.489893 \times 10^{-10}$

CONVERGED! **Record converged stress** $\sigma_{rec} := \sigma_{tr}$

Form consistent tangent matrix

$Ac\Delta := A_{cdp}(npod, sf, \Delta\mu, \zeta, \kappa, eg, elocl, ee, r, s, t)$ $\quad DI := D_{el}$

$Ic\Delta := I_{\Delta Ndp}(npod, npod_{prv}, \sigma_1, \sigma_{tr}, sf, f_t, \Delta\mu, \zeta, \kappa, eg, elocl, ee, r, s, t, Ip, DI)$ $\quad N\Phi_{ip} := N\Phi_{dp}(sf_{ip}, \Delta\mu_{ip}, \zeta_{ip}, \kappa, eg_{ip}, elocl_{ip}, ee_{ip}, r_{ip}, s_{ip}, t_{ip})$

$fn_{ip} := fn_{dp}(sf_{ip}, \Delta\mu_{ip}, \zeta_{ip}, \kappa, eg_{ip}, elocl_{ip}, ee_{ip})$ $\quad \Gamma_{ip} := N\Phi_{ip} \cdot Ac\Delta \cdot Ic\Delta + fn_{ip} \cdot dNdv\_x\_\sigma(\sigma_1, f_t, Ip_{ip}, \sigma_{tr}, ns_{ip}) \cdot DI$

$\Omega_{ip} := -dfed\zeta(\zeta_{ip}, \kappa, sf_{ip}) \cdot d\zeta de(elocl_{ip}) \cdot (M_p(\zeta_{ip}, \kappa, eg_{ip}, elocl_{ip}, ee_{ip}) \cdot dgds(sf_{ip})) + N\Phi_{ip}^{T} \cdot (Ac\Delta \cdot N(r_{ip}, s_{ip}, t_{ip})^{T} \cdot M_p(\zeta_{ip}, \kappa, eg_{ip}, elocl_{ip}, ee_{ip}) \cdot dgds(sf_{ip}))$

$$Dep := Ac\Delta \cdot \left[Ic\Delta - \sum_{j=1}^{npod} N(r_j, s_j, t_j)^{T} \cdot M_p(\zeta_j, \kappa, eg_j, elocl_j, ee_j) \cdot dgds(sf_j) \cdot (\Omega_j)^{-1} \cdot \Gamma_j \right]$$

$$Dep = \begin{pmatrix} -4.549119 \times 10^{3} & -802.785724 & -802.785724 & 0 & 0 & 0 \\ -802.785724 & 4.077905 \times 10^{4} & 5.996439 \times 10^{3} & 0 & 0 & 0 \\ -802.785724 & 5.996439 \times 10^{3} & 4.077905 \times 10^{4} & 0 & 0 & 0 \\ 0 & 0 & 0 & 5.616546 \times 10^{3} & 0 & 0 \\ 0 & 0 & 0 & 0 & 1.73913 \times 10^{4} & 0 \\ 0 & 0 & 0 & 0 & 0 & 6.87781 \times 10^{3} \end{pmatrix}$$

Add small strain step

$d\varepsilon := (0.00015 \;\; 0.00001 \;\; 0.00001 \;\; 0 \;\; 0 \;\; 0)^{T} \cdot 0.000001$ $\quad d\sigma Dep := Dep \cdot d\varepsilon$ $\quad d\sigma Dep^{T} = (-6.984236 \times 10^{-7} \;\; 3.47337 \times 10^{-7} \;\; 3.47337 \times 10^{-7} \;\; 0 \;\; 0 \;\; 0)$

Reset all to last converged increment

$\Delta\varepsilon_p := (0 \;\; 0 \;\; 0 \;\; 0 \;\; 0 \;\; 0)^{T}$ $\quad \Delta\kappa := 0$ $\quad Z := Zf(\kappa)$ $\quad \Delta\lambda := 0$ $\quad R_\varepsilon := (0 \;\; 0 \;\; 0 \;\; 0 \;\; 0 \;\; 0)^{T}$ $\quad R_\kappa := 0$ $\quad R_{ep_{iset}} := (0 \;\; 0 \;\; 0)^{T}$

$ip := 1 .. npod$ $\quad npod_{prv} := 0$ $\quad npod := 0$ $\quad \zeta := \zeta_{prv}$ $\quad \Delta\mu := \Delta\mu_{prv}$ $\quad elocl := elocl_{prv}$ $\quad ee := ee_{prv}$ $\quad e_p := ep_{prv}$ $\quad \Delta e_p := \Delta ep_{prv}$ $\quad \kappa := \kappa_{prev}$ $\quad \varepsilon_p := \varepsilon p\_prv$

$\varepsilon_2 := \varepsilon_2 + d\varepsilon$ $\quad \varepsilon_2^{T} = (1.500001 \times 10^{-4} \;\; 1.000001 \times 10^{-5} \;\; 1.000001 \times 10^{-5} \;\; 0 \;\; 0 \;\; 0)$

$\sigma_{tr} := D_{el} \cdot \varepsilon_2$ $\quad \sigma_{tr}^{T} = (6.484479 \;\; 1.614908 \;\; 1.614908 \;\; 0 \;\; 0 \;\; 0)$

Check if a POD forms and its direction

$pr1(\sigma_{tr})^T = (6.484479 \quad 1.614908 \quad 1.614908)$ $f_t = 2.9$ **POD forms**

$r\_\sigma := r\_all(\sigma_{tr}, f_t)$ $r\_\sigma^T = \left[\begin{pmatrix}1\\1.053671\times10^{-8}\\1.053671\times10^{-8}\end{pmatrix}\begin{pmatrix}-1.053671\times10^{-8}\\1\\0\end{pmatrix}\begin{pmatrix}-1.053671\times10^{-8}\\0\\1\end{pmatrix}\right]$

$lp_1 := 1$ $\varepsilon_e := \varepsilon_2 - \varepsilon_p$ $\sigma_{pr} := pr1(\sigma_{tr})$ $\sigma_{pr}^T = (6.484479 \quad 1.614908 \quad 1.614908)$

$\begin{pmatrix}\sigma_{pr_1} & rd_1 & sd_1 & td_1\\ \sigma_{pr_2} & rd_2 & sd_2 & td_2\\ \sigma_{pr_3} & rd_3 & sd_3 & td_3\end{pmatrix} := PODdir(\sigma_I, f_t, lp_1, 1)$ $\sigma_{pr} = \begin{pmatrix}6.484472\\1.614907\\1.614907\end{pmatrix}$

Crack direction based on first trial stress

$npod_{prv} := 0$ $npod := 1$ $nc_1 := 1$ $ip := 1..npod$ $jp := 1..npod$ $r_{ip} := rd$ $s_{ip} := sd$ $t_{ip} := td$

$r^T = \left[\begin{pmatrix}1\\0\\0\end{pmatrix}\begin{pmatrix}1\\0\\0\end{pmatrix}\right]$ $s^T = \left[\begin{pmatrix}0\\1\\0\end{pmatrix}\begin{pmatrix}0\\1\\0\end{pmatrix}\ 0.539858635731268\right]$ $t^T = \left[\begin{pmatrix}0\\0\\1\end{pmatrix}\begin{pmatrix}0\\0\\1\end{pmatrix}\ -0.83996\right]$

Record variables before enter stress recovery

$npod := 1$ $ip := 1..npod$ $jp := 1..npod$ $\zeta rec := \zeta$ $\kappa_{prev} := \kappa$ $\varepsilon_{p\_prv} := \varepsilon_p$

$\zeta rec := \zeta$ $\zeta_{prv} := \zeta$ $e_{gprv} := e_g$ $elocl_{prv} := elocl$ $ee_{prv} := ee$ $ep_{prv} := \epsilon_p$ $\Delta\mu_{prv} := \Delta\mu$ $\Delta ep_{prv} := \Delta e_p$

Reset all variables

$\Delta\kappa := 0$ $\kappa := 0$ $Z := Zf(\kappa)$ $\Delta\lambda := 0$ $R_\varepsilon := (0\ 0\ 0\ 0\ 0\ 0)^T$ $R_\kappa := 0$ $Rep_{iset} := (0\ 0\ 0)^T$ $\Delta\varepsilon_p := (0\ 0\ 0\ 0\ 0\ 0)^T$ $\varepsilon_p := (0\ 0\ 0\ 0\ 0\ 0)^T$ $\varepsilon_e := \varepsilon_2 - \varepsilon_p$

$ee_{ip} := elocl_{ip} - e_{p_{ip}}$ $e_{g_{ip}} := e_{gn}(elocl_{ip}, ee_{ip})$ $e_{g_1} = 7.552794\times10^{-5}$

$\sigma_{tr} := D_{el}\cdot\varepsilon_2$ $\sigma_{tr}^T = (6.484479 \quad 1.614908 \quad 1.614908 \quad 0 \quad 0 \quad 0)$

$sf_{ip} := N(r_{ip}, s_{ip}, t_{ip})\cdot\sigma_{tr}$ $sf_1^T = (6.48447853416149 \quad 0 \quad 0)$

Evaluate the POD consistency

$F_{tr} := F(\sigma_{tr}, Z)$ $F_{tr} = -4.680632$

$Fe_{ip} := Frhs(\zeta, \kappa, e_g, ee, elocl, r, s, t, \varepsilon_e, ip, npod)$ $Fe_1^T = (3.584479 \quad 0 \quad 0)$ $\sum_{j=1}^{npod} |Fe_j| = 3.584479$

$f_{e_{ip}} := f_e(\zeta_{ip}, \kappa, sf_{ip})$ $f_{e_1} = 3.584479$

$N\Delta e_{ip} := N\Delta_{dp}(r, s, t, npod, npod_{prv}, \Delta\mu, \zeta, \kappa, e_g, elocl, ee, sf, ip, Ip)$

$Ae := A_{dp}(npod, \zeta, \kappa, e_g, elocl, ee, \Delta\mu, sf, r, s, t, Ip)$

$N\Xi_{ip} := N(r_{ip}, s_{ip}, t_{ip})^T (I_3 - dm\chi(\zeta_{ip}, \kappa, e_{g_{ip}}, elocl_{ip}, ee_{ip}))$

$N\Psi_{ip} := N(r_{ip}, s_{ip}, t_{ip})^T \cdot dmxp(\zeta_{ip}, \kappa, e_{g_{ip}}, elocl_{ip}, ee_{ip}) \cdot dgds(sf_{ip})$

$dfemod_{ip} := dfeds(\zeta_{ip}, \kappa, sf_{ip})^T \cdot N(r_{ip}, s_{ip}, t_{ip})$

$dfemod_1 = (1\ 0\ 0\ 0\ 0\ 0)$

$R_{\varepsilon m} := R_\varepsilon + d2G\sigma\kappa(\kappa) \cdot \Delta\lambda \cdot a_\kappa(\sigma_{tr}, \kappa, \Delta\lambda) \cdot R_\kappa$

$R_{\varepsilon\kappa} := R_{\varepsilon m} - \sum_{j=1}^{npod} N(r_j, s_j, t_j)^T \cdot (dm\kappa(\zeta_j, \kappa, e_{g_j}, ee_j) \cdot a_\kappa(\sigma_{tr}, \kappa, \Delta\lambda) \cdot R_\kappa)$

$R_{\varepsilon\kappa p} := R_{\varepsilon\kappa} + \sum_{j=1}^{npod} N(r_j, s_j, t_j)^T \cdot dmxp(\zeta_j, \kappa, e_{g_j}, elocl_j, ee_j) \cdot (R_{ep_j})$

Form coupled equations

$F\mu_{ip} := fe_{ip} - dfemod_{ip}^T \cdot (Ae \cdot R_{\varepsilon\kappa p})$

$B\mu_{(ip-1)\cdot npod+jp} := (dfemod_{ip} \cdot Ae \cdot N\Xi_{jp})^T$

$B\mu_{(ip-1)\cdot npod+ip} := B\mu_{(ip-1)\cdot npod+ip} - (dfed\zeta(\zeta_{ip}, \kappa, sf_{ip}) \cdot d\zeta de(elocl_{ip})^T)^T$

$P\mu_{(ip-1)\cdot npod+jp} := dfemod_{ip}^T \cdot (Ae \cdot N\Psi_{jp})$

$FE_{ip} := Fe_{ip} - N\Delta e_{ip} \cdot Ae \cdot R_{\varepsilon\kappa p} - D1\kappa(\zeta_{ip}, \kappa, e_{g_{ip}}, ee_{ip}) \cdot a_\kappa(\sigma_{tr}, \kappa, \Delta\lambda) \cdot R_\kappa + D1p(\zeta_{ip}, \kappa, e_{g_{ip}}, elocl_{ip}, ee_{ip}) \cdot Rep_{ip}$

$BE_{(ip-1)\cdot npod+jp} := N\Delta e_{ip} \cdot Ae \cdot N\Xi_{jp}$

$BE_{(ip-1)\cdot npod+ip} := BE_{(ip-1)\cdot npod+ip} + D1t(\zeta_{ip}, \kappa, e_{g_{ip}}, elocl_{ip}, ee_{ip})$

$PE_{(ip-1)\cdot npod+jp} := N\Delta e_{ip} \cdot Ae \cdot N\Psi_{jp}$

$PE_{(ip-1)\cdot npod+ip} := PE_{(ip-1)\cdot npod+ip} - D1p(\zeta_{ip}, \kappa, e_{g_{ip}}, elocl_{ip}, ee_{ip}) \cdot dgds(sf_{ip})$

Solve coupled for unknowns

$unknown := Sol_{e\mu}(FE, BE, PE, F\mu, B\mu, P\mu, npod)$

$d\mu_{ip} := dmiu_{e\mu}(ip, unknown)$

$delocl_{ip} := deloc_{e\mu}(ip, unknown)$

$d\mu_1 = 8.48678 \times 10^{-6}$

$delocl_1^T = (8.48678 \times 10^{-5}\ 0\ 0)$

Update state variables

$d\sigma := -Ae \left[R_{\varepsilon\kappa p} + \left[\sum_{j=1}^{npod} N(r_j, s_j, t_j)^T \left[(I_3 - dm\chi(\zeta_j, \kappa, e_{g_j}, elocl_j, ee_j)) \cdot delocl_j + dmxp(\zeta_j, \kappa, e_{g_j}, elocl_j, ee_j) \cdot dgds(sf_j) \cdot d\mu_j \right] \right] \right]$

$d\sigma^T = (-4.038113\ \ -0.712608\ \ -0.712608\ \ 0\ \ 0\ \ 0)$

$dep_{ip} := Rep_{ip} + dgds(sf_{ip}) \cdot d\mu_{ip} + \Delta\mu_{ip} \cdot d2gds(sf_{ip}) \cdot N(r_{ip}, s_{ip}, t_{ip}) \cdot d\sigma$

$dep_1^T = (8.48678 \times 10^{-6}\ 0\ 0)$

$elocl_{ip} := elocl_{ip} + delocl_{ip}$

$\zeta_{ip} := zeta(elocl_{ip}, \zeta prv_{ip})$

$\Delta ep_{ip} := \Delta ep_{ip} + dep_{ip}$

$ep_{ip} := epprv_{ip} + \Delta ep_{ip}$

$ee_{ip} := elocl_{ip} - ep_{ip}$

$e_{g_{ip}} := e_{gn}(elocl_{ip}, ee_{ip})$

$e_{g_1} = 7.552794 \times 10^{-5}$

$$elocl_1 = \begin{pmatrix} 1.53529565294118 \times 10^{-4} \\ 0 \\ 0 \end{pmatrix} \qquad ep_1 = \begin{pmatrix} 8.48678 \times 10^{-6} \\ 0 \\ 0 \end{pmatrix} \qquad ee_1 = \begin{pmatrix} 1.450428 \times 10^{-4} \\ 0 \\ 0 \end{pmatrix} \qquad \zeta_1 = 1.535296 \times 10^{-4} \qquad \varepsilon_{ti} = 6.866176 \times 10^{-5}$$

$\Delta\mu_{ip} := \Delta\mu_{ip} + d\mu_{ip}$ $\quad \Delta\mu^T = \begin{pmatrix} 8.48678 \times 10^{-6} & 0 \end{pmatrix}$ $\quad \varepsilon_e := \varepsilon_2 - \varepsilon_p$ $\quad \varepsilon_e^T = \begin{pmatrix} 1.500001 \times 10^{-4} & 1.000001 \times 10^{-5} & 1.000001 \times 10^{-5} & 0 & 0 & 0 \end{pmatrix}$

$\sigma_{tr} := stress(\zeta, \kappa, e_g, ee, elocl, r, s, t, \varepsilon_e, npod)$ $\quad \sigma_{tr}^T = (2.481054 \quad 0.908422 \quad 0.908422 \quad 0 \quad 0 \quad 0)$

$sf_{ip} := N(r_{ip}, s_{ip}, t_{ip}) \cdot \sigma_{tr}$ $\quad sf_1^T = (2.481054 \quad 0 \quad 0)$

Compute error measures

$R_{ep_{ip}} := -\Delta e_{p_{ip}} + \Delta\mu_{ip} \cdot dgds(sf_{ip})$ $\quad R_{ep_1}^T = (0 \quad 0 \quad 0)$ $\quad Fe_{ip} := Frhs(\zeta, \kappa, e_g, ee, elocl, r, s, t, \varepsilon_e, ip, npod)$ $\quad \sum_{j=1}^{npod} |Fe_j| = 0$ $\quad fe_{ip} := fe(\zeta_{ip}, \kappa, sf_{ip})$ $\quad fe_1 = -1.489888 \times 10^{-10}$

CONVERGED!

****

Check error

$d\sigma_{chk} := \sigma_{tr} - \sigma_{rec}$ $\quad d\sigma_{chk}^T = \begin{pmatrix} -6.984235 \times 10^{-7} & 3.47337 \times 10^{-7} & 3.47337 \times 10^{-7} & 0 & 0 & 0 \end{pmatrix}$

$d\sigma_{Dep}^T = \begin{pmatrix} -6.984236 \times 10^{-7} & 3.47337 \times 10^{-7} & 3.47337 \times 10^{-7} & 0 & 0 & 0 \end{pmatrix}$

$error := \dfrac{|d\sigma_{chk} - d\sigma_{Dep}|}{|d\sigma_{chk}|}$ $\quad error = 1.242372 \times 10^{-7}$

Appendix II Derivation of Material Parameters

Parameter	Description	Method for obtaining
f_c	Uniaxial compressive strength	From cube ($f_c = 0.8f_{cu}$) or compressive cylinder test ($f_c = f'_c$)
f_t	Uniaxial tensile strength	From peak of softening curve or cylinder splitting test ($0.9f_{cyl}$)
ε_c	Strain at peak of uniaxial compressive strength	$\varepsilon_c = f_c / E$
ε_0	Strain at end of softening curve	$\varepsilon_0 = u_0 / w_c$ w_c = fracture process zone width (3 times maximum aggregate size or gauge length in tests) u_0 = displacement at end of softening curve
G_f	Fracture energy	$G_f = \frac{f_t^2 w_c}{E}$
Z_0	Initial position of yield function	From uniaxial compression test; point at which nonlinearity becomes significant (range 0.4-0.6)
ψ	Dilatancy factor	Calibrated from triaxial test
r_σ	Cohesion to tensile strength ratio	Based upon data which evaluated the shear-normal strength of concrete aggregate interfaces
μ_σ	Residual friction factor	Based upon data which evaluated the shear-normal strength of concrete aggregate interfaces (range 0.5-1.0)
b_r	Biaxial/uniaxial strength ratio	From biaxial and uniaxial tests

m_g	Contact function parameter	From shear-normal curve (range 0.3-0.6 for normal strength concrete)
m_{hi}	Ratio between strains at which shear reduction is significant and end of softening curve	From normal-shear test $m_{hi} = e_{hi} / \varepsilon_0$ $e_{hi} = u_{hi} / w_c$ u_{hi} = opening displacement at which shear stiffness starts to become significant which is associated with the lost of contact of the fine aggregate
m_{ful}	Ratio between the lost of contact and end of softening strains	From shear-tension test $m_{ful} = e_{ful} / \varepsilon_0$ $e_{ful} = u_{ful} / w_c$ u_{ful} = opening displacement beyond which no shear contact can be attained (range 10-20 for aggregate size of 20-30 mm; range 3-5 for aggregate size of 5-8 mm)
α_c	Proportion of coarse component in a representative volume of fully debonded material	Evaluated from the proportion of mortar and coarse aggregate along a crack path (range 0.3-0.4)